Ministero dell'Istruzione, dell'Università e della Ricerca

UNIVERSITY OF SALERNO

Department of Civil Engineering

PhD thesis

in

Risk and Sustainability in Civil, Architectural and Environmental Engineering Systems

Cycle XXXIII (2017-2020)

LOCAL BUCKLING OF ALUMINIUM MEMBERS IN THE ELASTIC-PLASTIC RANGE

Alessandro Pisapia

Tutor

Prof. Vincenzo Piluso

Co-Tutor

Prof. Rosario Montuori

Prof. Elide Nastri

PhD Coordinator

Prof. Fernando Fraternali

RINGRAZIAMENTI

Il presente lavoro è dedicato a tutti i Maestri che ho avuto l'onore di conoscere e che mi hanno accompagnato durante tutto il mio percorso formativo. In particolare, Due sono per me le Colonne portanti della mia formazione: mio Padre Mattia ed il Professore Vincenzo Piluso. Dal Primo, ho ereditato la passione per la Matematica e le Strutture. Il Secondo mi ha trasmesso la passione e la dedizione incondizionata per la Ricerca e la Didattica. A loro va il ringraziamento più grande.

Altresì, è doveroso ringraziare, con grande stima e riconoscenza, il Prof. Montuori, la Prof.ssa Elide Nastri e la mia collega ed amica Simona Streppone, che hanno rappresentato per me un costante punto di riferimento e di sostegno.

Un ringraziamento speciale lo rivolgo a tutta la mia famiglia e, in particolare, a mia Madre Anna, per supportarmi e sopportarmi da tutta la vita e per aver sempre condiviso in maniera incondizionata tutte le mie scelte.

Ringrazio tutti i fantastici colleghi di dottorato del trentatreesimo ciclo e del Lab L2, a Loro rivolgo l'augurio di una vita ricca di successi.

Infine, desidero ringraziare il Prof. Gianvittorio Rizzano, Massimo, Francesco, Antonella, Giovanni, Agostina, Marco, persone fantastiche che ho avuto modo di conoscere e stimare durante questi tre anni.

"Se vuoi essere un cercatore della verità, è necessario

che almeno una volta nella tua vita tu dubiti,

per quanto possibile, di tutte le cose."

René Descartes

Ai miei Maestri

TABLE OF CONTENTS

LIST OF FIGURES

LIST OF TABLES

LIST OF SYMBOLS

γ	Specific weigh.	$\delta V_x, \delta V_y$	Variation of shear actions.
$f_{0.2}$	Conventional elastic limit for aluminium.	$\delta R_x^*, \delta R_y^*$	Variation of equivalent shear actions.
$f_{0.1}$	Stress at a residual strain of 0.1%.	D_s	Flexural rigidity in the elastic-plastic range.
f_u	Maximum stress of aluminium material.	C_i	Plastic coefficients of the buckling criterion; coefficients of EC9 (Chapter 6).
ε_u	Strain corresponding to the maximum stress f_u	ξ	Ratio between the plastic and elastic stresses.
ε_r	Maximum strain of aluminium material.	ϵ	Restraint coefficient.
n	Ramberg-Osgood coefficient.	S_0	the stiffness per unit length of elastic restraining medium (Chapter 2); Internal section area of tensile specimens (Chapter 3).
f_y	Yield stress for steel.	α_i, κ_i	Numerical coefficients.
E, E_s, E_t	Young's modulus, secant modulus, tangent modulus.	e_1, e_2	Functions of ϵ.
ν_e, ν_p	Poisson's ratio in the elastic and plastic region.	$B_{i.nom}, t_{nom}$	Nominal width and thickness of box sections.
α	Thermal coefficient; Shape factor (Chapter 1).	B_i, t_i	Measured width and thickness of box sections.
$N_{u.EC9}$	Maximum load according to EC9.	v_c	Speed tensile testing.
$M_{u.EC9}$	Maximum bending according to EC9.	L_c, L_s, L_{tot}	Lengths of the tensile specimens.
A_{eff}	Effective section area.	$\dot{e}_{L_c}$	Strain rate.
W_{el}	Elastic modulus of cross-section.	S	External section area of tensile specimens.
W_{eff}	Effective modulus of cross-section.	E_{exp}	Experimental Young's modulus.
W_{pl}	Plastic modulus of cross-section.	$\overline{N}_u$	Nondimensional value of the compressive action.
γ_{M1}	Safety coefficient according to EC9.	$\delta_{u.exp}$	Experimental displacements corresponding to $N_{u.exp}$.
$N_{u.th}$	Theoretical maximum load.	$\delta_{0.2}$	Conventional displacement according to the conventional strain ε_0
$M_{u.th}$	Theoretical maximum bending.	$\bar{\delta}_u$	Nondimensional value of the displacement.
$N_{u.exp}$	Experimental maximum load.	ε_0	Conventional strain equal to $f_{0.2}/E$.
$M_{u.exp}$	Experimental maximum bending.	$\bar{\varepsilon}_u$	Normalised buckling strain.
D_e	Elastic flexural stiffness.	L, L_i	Beam length.

$w(x,y)$	Displacement function.	v_i, v_f	Initial and final speeds of bending tests.
b	Width of a single plate.	δ^*	Limit displacement of bending tests.
t	Thickness of a single plate.	$\theta_{u.exp}$	Experimental chord rotation corresponding to $M_{u.exp}$.
a	Length of a single plate (Chapter 2); Length of aluminium members (Chapters 3,4).	$\chi_{u.exp}$	Experimental curvature corresponding to the maximum bending.
N_x, N_y, N_{xy}	Normal and shearing forces per unit distance in middle surface of the plate	$M_{0.2}$	Bending moment at the conventional yield stress $f_{0.2}$.
x, y, z	Cartesian axes.	$\theta_{0.2}$	Rotation at the conventional yield stress $f_{0.2}$.
N	Normal action.	$\chi_{0.2}$	Curvature at the conventional yield stress $f_{0.2}$.
$\sigma_x, \sigma_y, \sigma_z$	Unit normal stresses in x, y and z directions.	$\bar{M}_u$	Nondimensional flexural strength.
U	Strain energy of a system.	$\bar{\theta}_u$	Nondimensional rotational capacity.
P	Work done by the applied loads.	$\bar{\chi}_u$	Nondimensional curvature.
w_{mn}	Unknown coefficients.	I	Inertia moment of cross-section.
m, n	Number of half waves in x and y directions.	$A_i^{(j)}$	Integration coefficients (Chapter 4).
$N_{cr.e}$	Elastic critical load.	$N_{u.DTP}$	Ultimate buckling load obtained by the deformation theory of plasticity.
k	Buckling factor	$\bar{\varepsilon}_{u.DTP}$	Normalised strain corresponding to $N_{u.DTP}$.
$\sigma_{cr.e}, \sigma_{cr.p}$	Elastic critical stress, elastic-plastic critical stress.	$N_{u.ETM}$	Ultimate buckling load obtained by the effective thickness method.
$f(y)$	Generic Function in y-direction.	$\bar{\varepsilon}_{u.ETM}$	Normalised strain corresponding to $N_{u.ETM}$.
a_i	Integration coefficients (Chapter 2).	Y_0	Conventional elastic limit strength.
λ, ψ	Generic coefficients.	Q, C	Curve fitting parameters of Hopperstad model.
α, β	Functions of λ, N	ε_p	Plastic strain.
M_x, M_y, M_{xy}	Bending and twisting moments per unit distance in plate.	L_s	Shear length.
V_x, V_y	Shearing forces per unit distance in plate.	b_f, t_f	Flange width, flange thickness (Chapter 5).
R_x^*, R_y^*	Equivalent shearing forces per unit distance in plate.	h, t_w	Web length, web thickness (Chapter 5).
$\phi_\alpha, \phi_\beta, \psi_\alpha, \psi_\beta$	Functions of α, β and λ.	λ_f	Flange slenderness.
φ_x, φ_y	Rotations around x and y axes.	α_s	Flange-to-web slenderness ratio.

σ_1, σ_2	Normal stresses along x-direction.	$\bar{L}_s$	Normalised shear length.
ω	Function of σ_1 and σ_2	R_0	Stable part of rotation.
$\tau_{xy}, \tau_{xz}, \tau_{yz}$	Unit shear stresses in the planes x-y, x-z and y-z.	R	Total rotation capacity.
σ, σ_i	Standard deviation; Stress intensity (Chapter 2).	c_i	Regression coefficients.
$\varepsilon_x, \varepsilon_y, \varepsilon_z$	Unit normal strains in x, y and z directions.	$M_{u.ER}$	Ultimate flexural strength provided by the mathematical relation.
γ_{xy}	Shearing unit strain in the plane x-y.	$\bar{\theta}_{u.ER}$	Normalised rotation provided by the mathematical relation.
ε_i	Strain intensity.	$M_{u.ETM}$	Ultimate flexural strength provided by the effective thickness method.
ν	Function of Poisson's ratio provided by Gerard and Wildhorn.	$\bar{\theta}_{u.ETM}$	Normalised rotation provided by the effective thickness method.
$\delta\varepsilon_{x.0}, \delta\varepsilon_{y.0}, \delta\varepsilon_{xy.0}$	The strain variations at the mid-thickness line of the plate.	ζ	Factor accounting for plate interactions.
$\delta\chi_x, \delta\chi_y, \delta\chi_{xy}$	The variations of curvatures and twisting.	α_{LS}	Factor accounting for the influence of longitudinal stress.
$\delta\sigma_x, \delta\sigma_y, \delta\tau_{xy}$	The normal and tangential stress variations	μ	Mean value; Factor accounting for the inelastic behaviour of aluminium material (Chapter 6).
Φ, ψ_i	Functions of the strain level	b_{eff}, t_{eff}	Effective width; effective thickness.
$\delta\nu$	Variation of the Poison's function.	ϵ_0	Coefficient of EC9 equal to $\sqrt{250/f_{0.2}}$
δE_s	Variation of the secant modulus.	$\bar{\lambda}_p$	Normalised slenderness
$H, \Psi, S_x, S_y, S_{xy}, K_\varepsilon, K_\chi, k_x, k_y, k_{xy}$	Functions of the stress level and the mechanical properties of material.	ψ	Factor accounting for strain distribution along the loaded edge of the plate (EC9).
A_{ij}	Plastic functions of $H, \Psi, S_x, S_y, S_{xy}, K_\varepsilon, K_\chi, k_x, k_y, k_{xy}$.	β	Slenderness parameter equal to the ratio between the width and the thickness of a single plate (Chapter 6).
$\delta M_x, \delta M_y, \delta M_{xy}$	Variation of bending moments.	L_p	Length of plastic hinge.

CHAPTER 1
INTRODUCTION

1.1. Aluminium as a Structural Material

The success of aluminium alloys as constructional material in civil engineering structural applications is based on some prerequisites. They are connected with the physical and mechanical properties, the production process and the technological features. In particular, the main properties of this material are: the lightness, its specific weight γ is 2700 kg/m^3 equal to one-third that of steel, the corrosion resistance (except for some specific alloys) thanks to the formation of a thin inert aluminium oxide film which blocks further oxidation, the functionality of the structural shapes, due to the extrusion fabrication process, allowing the design of tailor-made shapes for specific applications. Figure 1.1 shows the main cross-sectional shapes employed in the structural applications, while the main mechanical properties of aluminium and steel materials are summarised in Figure 1.2.

Moreover, the favorable life-cycle cost given by the sum of the initial cost of the product, the cost of operating and maintaining and the cost of disposing or recycling it after its life [1.1],[1.2].

For these reasons, the 25% of the global aluminium production is currently used in the structural sector [1.3]. Aluminium is used in external facades, roofs and walls, in windows and doors, in staircases, railings, shelves, and other several applications. Deteriorated bridge decks replacements, residential area bridges and structures situated in inaccessible places far from the fabrication shop [1.1],[1.2] are also typical applications. Moreover, in the seismic applications aluminium alloys can assume different tasks being used as fuses, dissipative shear walls or seismic links [1.5]-[1.7]. Recently, columns made of an aluminium alloy have also been used for the construction of a residential building in a seismic area [1.8]. Typical structural aluminium applications along with brief information are depicted in Figure 1.3, Figure 1.4.

The aluminium alloys are also characterized by some structural disadvantages: the thermal coefficient α is twice the one of steel, consequently, it is more sensitive to thermal variations; the initial cost is very high, so that other metals are selected instead of aluminium. Another disadvantage is related to the strain-hardening behaviour. Figure 1.2 shows the qualitative trends of the steel and aluminium. From the comparison of two typical stress-strain curves, it can be observed that: both materials present a linear elastic behaviour with a different slope up to the yield stress f_y for steel and the conventional limit $f_{0.1}$ for aluminium, corresponding to the residual strain of 0.1%. After the elastic region, aluminium alloys provide a continuous strain-hardening behaviour which is not preceded by

a perfectly plastic branch corresponding to yielding plateau as for steel material. In particular, up to $f_{0.1}$, the aluminium behaviour presents a non-linear "knee" up to the conventional yielding of $f_{0.2}$, the stress corresponding to the residual strain of 0.2%, and subsequently, the plastic behaviour occurs. The "knee" shape of $\sigma - \varepsilon$ curve depends on the ratio $f_{0.2}/f_{0.1}$. Moreover, the ultimate deformation ε_r is about 8-12%, while that of steel is greater than 20% [1.2].

However, the main problem of the aluminium structures is referred to the instability phenomena. In fact, because of the small value of Young's modulus E, the instability phenomenon is more likely to occur than in steel structures and, besides, the increase of the deformability gives rise to additional drawbacks in checking serviceability limit states. As will been seen below, the focus of the present work is related to the study of the instability phenomenon at the sectional level and the influence of strain-hardening behaviour of aluminium alloys.

Aluminium is not just one material, but it gives rise to a wide family of different groups of alloys whose mechanical properties vary from one group to another and within each group itself. The Aluminum Association Inc. divides the aluminium alloys into 9 series using a four-digit system and each series includes different combinations of alloying additions. The first digit (Xxxx) provides the principal constituent alloy, while the second digit (xXxx) indicates the modifications made in the original alloy. The last two digits (xxXX) represent arbitrary numbers so that the specific alloy can be identified in the series. Research on aluminium alloys has focused on wrought alloys belonging to 5000,6000 and 7000 which are the most attractive for structural applications due to their mechanical properties [1.9]. The alloy classification is also obtained as a function of the temper designation in order to provide more information about the fabrication treatment. It is possible to define five basic tempers; F, O, H, W, or T, accompanied by additional digits for more details about the fabrication treatment:

- **F** (fabricated): The thermal conditions during working or strain-hardening process to obtain specific material properties do not demand any special control.
- **O** (annealed): Treatment under high-temperature conditions in order to achieve maximum workability, toughness and ductility.
- **H** (strain-hardened): Used for non-heat-treatable alloys cold worked by strain-hardening method in order to stabilise their strength.
- **W** (solution heat treated): Applied to alloys subjected to natural aging after the solution heat treatment.
- **T** (thermally treated): Used for heat-treatable alloys subjected to natural or artificial aging in order stable tempers different than F, O, or H to be elaborated.

In the present work, the aluminium alloys belong to 2000, 6000 and 7000 thermally treated (temper T) have been considered, because they represent the most widespread alloys in Europe and they are the most used in the civil engineering. As for any structural material, structural design codes are present for aluminum alloy structures. Currently there are four international design specifications for the structural design of aluminum alloys:

- **European Committee for Standardization: BS EN 1999:2007**, "Design of Aluminium Structures" [1.10]
- **The Aluminium Association: AA 2020**, "Aluminium Design Manual" [1.11]
- **Australian/New Zealand Standard: AS/NZS 1664: 1997**, "Aluminium Structures" [1.12]
- **Chinese Standard: GB 50429: 2007**, "Code for design of Aluminium Structures" [1.13]

All future references will be made to the Eurocode 9 which is currently under review.

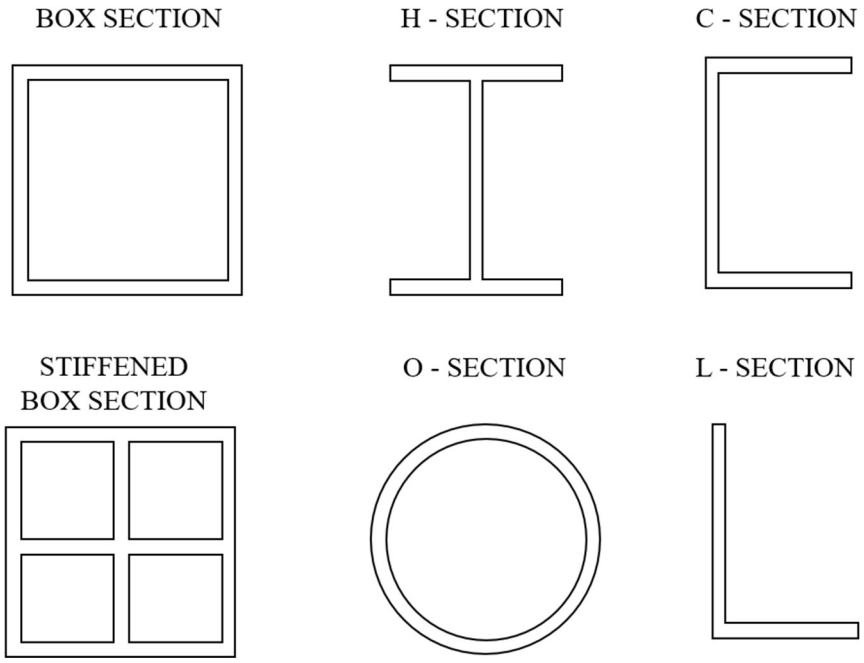

Figure 1.1. Main cross-sectional shapes employed in the structural applications.

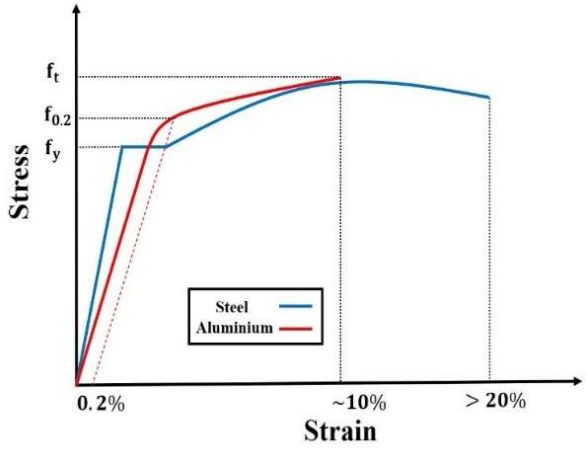

	Aluminium	**Steel**
$\boldsymbol{\gamma}$ **[kg/m³]**	~2700	~7860
$\boldsymbol{\alpha}$ [−]	$2.4\text{x}10^{-5}$	$1.2\text{x}10^{-5}$
$\boldsymbol{E}$ **[GPa]**	70	210
$\boldsymbol{\nu_e}$ [−]	0.30	0.30
$\boldsymbol{\varepsilon_r}$ [%]	$8 - 12$	> 20

Figure 1.2. Comparison between aluminium alloy and mild steel.

Retrofitting of the “Real Ferdinando” bridge (1990)
Prof. F.M. Mazzolani

Truss aluminium roof of Ferrari’s stand (2010)
Prof. V. Piluso

The iceberg Skating Palace (2012)
UP MNIIP mosproject-4 group
“The aluminium is one of the key materials in the structure of this building.”

The Crystal (2012)
Wilkinson Eyre Architects
“The roof is made from recycled aluminium”

St. Mary Axe (2003)
Foster’s group
“the aluminium was used to integrate the raking columns with the curved façade”

Casablanca Finance City Tower (2019)
Morphosis Architects
“for cost reasons, the modular façade elements are made out from aluminium”

Figure 1.3. Examples of aluminium alloy buildings.

Aluminium Heliport in Singapore (2015)

A tower for parabolic antennas

A rotating bridge crane

Aluminium pedestrian bridge

Figure 1.4. Examples of aluminium alloy structures.

1.2. State of Art

The physical phenomenon occurring when the deformed configuration of a structure undergoes a sudden shape variation accompanied by a significant increase of displacements and strains is usually referred to as buckling. The most well-known example is that of column buckling under axial compression. Buckling phenomena constitute a widespread field involving a wide category of civil and mechanical engineering problems.

The occurrence of buckling leads to a sudden loss of strength due to second-order effects rising from the deformed configuration resulting from buckling itself. In the case of metal structures, depending on the overall slenderness and on the local slenderness of the structural elements, buckling can be of concern for the structure as a whole (global level), the individual structural elements (member level) or the plate elements constituting the member section (sectional level), [Figure 1.5]. Besides, it can occur either in the elastic or in the plastic range.

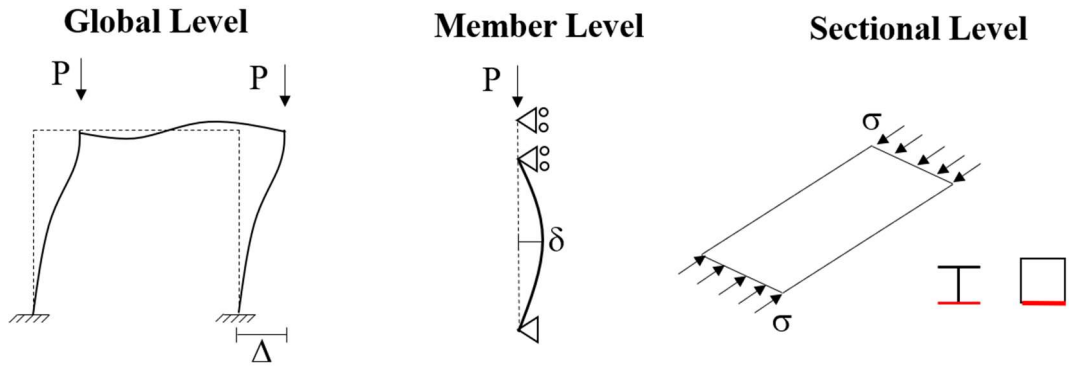

Figure 1.5. Instability phenomena on the metal structures.

At sectional level, the occurrence of the local buckling in the compressed part elements of section influences the ultimate behaviour of metal members in terms of ultimate resistance and deformation capacity. The occurrence of local buckling depends on the width-to-thickness ratios of the plate elements constituting the cross-section. For this reason, elastic bifurcation and post-buckling behaviour of thin plates have been extensively studied and well documented in standard texts [1.14], [1.15]. The need for reducing the width-to-thickness ratios to improve the ductile deformation of metal members is well known and codified [1.10], [1.16]. However, for small values of the width-to-thickness ratio, typically lower than 20, the use of thick plate theories such as the plate theory of *Mindlin* [1.17] is needed to calculate the buckling load; otherwise, the buckling load will be overestimated. Moreover, elastic/plastic theories are required for a more advanced bifurcation buckling analysis. The first researcher who arrived at a satisfactory theoretical solution for inelastic buckling was *Bijlaard* [1.18]. His work considered both incremental and deformation theories. It has been pointed out that deformation theory predicts buckling loads that are smaller than those obtained with flow theory [1.19]. During the last decade, analytical elastic/plastic stability criteria have been

derived for rectangular plates [1.20]. In particular, the *Mindlin* plate theory and two plasticity theories have been investigated. The application of both the incremental theory, also named the flow theory of plasticity, with the *Prandtl-Reuss* constitutive equations and the deformation theory of plasticity with the *Hencky* stress-strain relation has pointed out discrepancies in critical load predictions. Such differences obtained from the two plasticity theories are known as the plastic buckling paradox. However, even though there is a general agreement among researchers that the deformation theory is physically less correct than flow theory [1.21], experimental evidence has proved the better accuracy of the results obtained from the deformation theory (see Section 2.3.1).

The aforementioned theoretical works concern isolated plates subjected to different boundary conditions at their edges. However, a more complex behaviour occurs because most of the local buckling phenomena occurring in metal structures involve interactive buckling between the plate elements constituting the structural members. In addition, the occurrence of bifurcation does not necessarily represent the limit of the load carrying capacity. Obviously, the occurrence of local buckling phenomena influences greatly the ultimate resistance and the deformation ability of the cross-sections. Consequently, accounting for the effects of local buckling, the current Eurocode 9 [1.10] provides an approach similar to the one used for the steel [1.16]. In particular, the cross-sections may be classified according to the width-to-thickness ratio of the individual plate elements composing the section and the conventional yield strength of the material. So that, four classes are considered.

First-class sections can develop their whole plastic resistance with a high plastic deformation capacity. The whole plastic resistance can be also attained in the case of **second-class** sections, but with a limited plastic deformation capacity. **Third-class** sections locally buckle before the complete development of the plastic sources, so their plastic deformation capacity is very limited. Finally, in the case of **fourth-class** sections, local buckling occurs in the elastic range [1.22]-[1.25]. This classification allows to evaluate the ultimate resistance of a generic cross-section, taking into account the local buckling effects. So that, in the case of uniform compression, the maximum load can be computed according to the Section 6.2.4 of EN 1999-1-1:

$$N_{u.EC9} = \frac{A_{eff} f_{0.2}}{\gamma_{M1}} \tag{1.1}$$

where A_{eff} represents the effective section area based on the reduced thickness allowing for local buckling, $f_{0.2}$ is the conventional yield stress and γ_{M1} is the safety coefficient equal to 1.10. While the maximum bending moment is evaluated according to Section 6.2.5 of EN 1999-1-1:

$$M_{u.EC9} = \frac{\alpha W_{el} f_{0.2}}{\gamma_{M1}} \tag{1.2}$$

where W_{el} is the elastic modulus of section, while α is the shape factor provided by:

$$\alpha = \begin{cases} W_{pl}/W_{el} \ for\ class\ 1\ and\ 2 \\ 1 \quad for\ the\ class\ 3 \\ W_{eff}/W_{el} \ for\ the\ class\ 4 \end{cases} \tag{1.3}$$

where W_{pl} is the plastic modulus and W_{eff} represents the effective elastic section modulus, obtained using a reduced thickness for the fourth-class sections. Obviously, this approach represents a conservative method, however the Eqns. (1.1) and (1.2) often provide the values of the maximum resistances far from the real behaviour of aluminium members. So that, many research works have been devoted to improvement the accuracy in the prediction of the inelastic response of the aluminium alloy sections.

In order to increase the knowledge of the aluminium column under uniform compression, many stub column tests have been performed on a wide range of cross-sectional shapes: *Faella et al.* [1.23] tested SHS and RHS sections and they proposed an empirical equation about the local buckling resistance.

Mazzolani et al. [1.26] tested angles and they evaluated the ultimate resistance by means of the effective width approach, currently adopted for steel sections. *Liu et al.* [1.27] investigated the behaviour of stiffened and irregular-shaped cross-sections and they compared the experimental results with those obtained by the Direct Strength Method (DSM) originally developed for the cold-formed steel [1.34],[1.35] . *Yuan et al.* [1.28] evaluated experimentally the post-buckling behaviour of slender H-sections and *Wang et al.* [1.29] and *Feng and Young* [1.30] conducted stub columns tests on CHSs.

Through the experimental campaign on the cross-sections in compression, *Su et al.* [1.31] highlighted the contribution of the material strain-hardening on the cross-section capacity and evaluated the applicability of the Continuous Strength Method (CSM), that was originally developed for stainless steel stocky (i.e. small width to thickness ratio) cross-sections [1.32],[1.33].

In the case of the prediction of aluminium beams under uniform and non-uniform bending, the first experimental work is carried out by *Panlio* in 1947, which investigated the behaviour of two-span statically indeterminated beams [1.36]. Subsequently, *Welo* performed tests under uniform moment for determining the moment–curvature behaviour [1.37]. In the last thirty years, many experimental and numerical investigations have been carried out on aluminium beams under three, four and five bending conditions. *Opheim* [1.38] performed four point bending tests and demonstrated that there is no significant difference between tensile and compressive behaviour of 6060-T4 beams. *Moen et al.* [1.39],[1.40] carried out three- and four-point bending tests and numerical studies, demonstrating that the rotational capacity is dependent on the strain-hardening of aluminium material and the magnitude

of the moment gradient. *Zhu and Young* [1.41] modified the current Direct Strength Method (DSM) to achieve more accurate design provisions for flexural SHS members, while *Kim and Peköz* [1.42] presented a simplified design approach called Numerical Slenderness Approach (NSA) for determining the nominal stresses of each plate element of a complex section under flexure. *Feng et al.* [1.43], [1.44] performed many experimental and numerical studies on perforated CHS beams subjected to gradient and constant moments, while *Wang et al.* [1.45] led recently the experiments on H-shaped beams with and without intermediate stiffeners subjected to concentrated loads. Finally, *Su et al.* [1.31], [1.46], [1.47] performed an extensive experimental campaign on the SHS and RHS sections with and without internal stiffeners. Numerous experimental and numerical investigations have been carried out on aluminium beams under three, four- and five-point bending conditions.

It is important to underline that some experimental and numerical data have been collected by *Georgantzia et al.* [1.48] which have recently developed a review of research on the use of aluminium alloys as structural material.

The results of these studies are summarised in Table 1.1 and Table 1.2, where the comparison between the experimental results and those obtained by the theoretical approaches is shown. The mean values μ and standard deviations σ of ratios of the predicted strength, $N_{u.th}(M_{u.th})$, to the reported experimental strength, $N_{u.exp}$ $(M_{u.exp})$, are provided. For mean ratios $N_{u.th}/N_{u.exp}$ $(M_{u.th}/M_{u.exp})$ lower than 1.00, the predictions are conservative, for higher than 1.00 they are unsafe and for close to 1.00 they are accurate.

Table 1.1. Summary of main numerical and experimental results for aluminium members in compression.

Authors	**Aluminium alloys**	**cross section**	**No of tests**	**Design codes**	$N_{u.th}/N_{u.exp}$	
					Mean [μ]	**standard deviation [σ]**
Faella et al.	6060 T6 6061T6 6082 T6 6082 TF	RHS, SHS	39	EWM	1.00	0.11
Mazzolani et al.	6060 T6 6061 T6 6082 T6 6082 TF	L	64	EWM	1.012	0.10
Liu et al.	6063 T5	Stiffened irregular cross-section	17	GB 50429	1.04	0.05
				EN 1999-1-1	0.99	0.04
				AA	1.06	0.08
				DSM	1.20	0.05
Yuan et al.	6061 T6 6063 T5	I, H	15	GB 50429	0.88	0.11
				EN 1999-1-1	0.89	0.11
				AA	0.94	0.08
				AS/NZS	0.91	0.08
Wang et al.	6082 T6	CHS	9	-	-	-
Feng and Young	6061 T6	Perforated SHS	28	AA	1.05	0.35
Su et al.	6061 T6 6063 T5	SHS, RHS (with and without stiffeners)	15	EN 1999-1-1	0.93	0.09
				AS/NZS	0.75	0.12
				AA	0.84	0.16
				CSM	0.96	0.06
Heimerl et al.	2014 T6 7178 T6 7075 T6	I,H	139	-	-	-

Table 1.2. Summary of main numerical and experimental results for aluminium members in bending.

Authors	Aluminium alloys	cross section	Type of tests	No of tests	Design codes	$M_{u.th}/M_{u.exp}$	
						Mean [μ]	standard deviation [σ]
Opheim	6060 T4 6064 T6	SHS	4-point	-	-	-	-
Moen et al.	6082 T4 6082 T6 7108 T7	SHS, RHS H (welded and unwelded)	3-point	37	EN 1999-1-1	0.87	0.10
Zhu and Young	6061 T6 6063 T5	SHS	4-point	70	EN 1999-1-1	0.80	0.09
					AS/NZS	0.70	0.10
					AA	0.74	0.15
					DSM	0.83	0.06
Kim and Peköz	6063 T6	I, H	4-point	3	AA	0.83	0.05
Feng et al.	6061 T6 6063 T5	Perforated CHS	3-point 4-point	416	AA	0.83	0.19
Wang et al.	6061 T6 6063 T5	I, H	3-point	40	EN 1999-1-1	1.08	0.14
Su et al.	6061 T6 6063 T5	SHS, RHS	3-point 4-point	161	EN 1999-1-1	0.85	0.09
					AS/NZS	0.65	0.16
					AA	0.72	0.14
					CSM	0.90	0.09
Su et al.	6061 T6 6063 T5	SHS, RHS	5-point	147	EN 1999-1-1	0.55	0.13
					AS/NZS	0.44	0.10
					AA	0.50	0.26
					CSM	0.72	0.12
Su et al.	6063 T6 6063 T5	SHS, RHS (with and without stiffeners)	3-point 4-point 5-point	180	EN 1999-1-1	0.71	0.08
					AS/NZS	0.50	0.05
					AA	0.60	0.11
					CSM	0.77	0.08

1.3. Motivation of Work

The difficulties on the assessment of inelastic response of aluminium alloys is related to the occurrence of local buckling phenomena, which can be presented in the elastic-plastic region. It is well known that the local buckling depends on the geometrical width-to-thickness ratios of the plate elements constituting the section, but a generic member is an assembly of plates interacting on each other, so that also the plate interaction plays a fundamental role on the inelastic response. Another aspect concerns the effect of the different material properties, such as the strain-hardening behaviour and the plastic anisotropy on the local buckling.

Nowadays, a substantial gap of knowledge regarding the ultimate behaviour of aluminium sections is recognised. In fact, according to the results provided in the previous section, the numbers of experimental tests and the numerical investigations are still not exhaustive respect to those regarding to steel members. Moreover, the design codes often provide the ultimate strength values excessively conservative than the experimental data, especially in the case of the flexural resistance. Only a few studies indicated accurate cross-sectional strength predictions. Obviously, this aspect is opposed to an economic design process. Another main aspect is related to the prediction of the deformation capacity of aluminium cross-sections. In fact, both stub and bending tests, provided in the scientific literature, have shown that the aluminium members have a good ductility, but which is still difficult to accurately determine with the current methodologies available. The lack of accuracy is also related to the fact that the design formulations for aluminium are often adopted in a similar manner to the steel members, without sufficient consideration of the differences between the two materials. It is clear that a substantial gap of knowledge is related to the high variety of aluminium alloy tempers and section shapes which would require a large number of experimental tests.

For these reasons, the present research work is devoted to increase the knowledge of the ultimate behaviour of aluminium members under uniform compression and non-uniform bending. Starting from the main plate stability theories, both in elastic and plastic range, and through the experimental results, different methodologies are proposed to predict the ultimate resistances and the deformation capacities of box-shaped and H-shaped sections in compression or in bending.

In particular, Starting from the J_2 deformation theory of plasticity, which are extended to include the variability of the Poisson's ratio depending on the stress levels (Chapter 2), a fully theoretical approach for predicting the ultimate resistance of aluminium alloy members subjected to local buckling under uniform compression is presented, taking into account the interaction of the plate element constituting the cross-sections by means of the boundary conditions along the common edges (Chapter 4).

The second issue is related to the study on the ultimate flexural resistance and rotation capacity of aluminium alloy members under non-uniform bending. To this scope, a wide parametric analysis has been performed by the ABAQUS computer program to investigate the response parameters characterising the ultimate behaviour of I-beams. The parameters affecting the ultimate performances of aluminium alloy I-beams subject to local buckling under non-uniform bending are the flange slenderness, the flange-to-web slenderness ratio and the non-dimensional shear length. Based on this analysis, the mathematical formulations are proposed to predict both the maximum bending resistance and the rotation capacity of aluminium beams (Chapter 5).

Then, an extension of the effective thickness approach, currently adopted Eurocode 9, is herein presented. In particular, the new version of this method represents a simplified approach which allows to estimate the load-strain and the moment-curvature of each aluminium cross-section (Chapter 6).

The results obtained by the previous methodologies are compared with the experimental data provided in technical literature and in Chapter 3 describing both compression and bending tests.

Finally, it is important to underline that the present research work is supportive within the activities of CEN-TC250/SC9 the technical committee encharged of the revision of Eurocode 9. In fact, the empirical regressions, provided in Chapter 5 and the extension of effective thickness method (ETM) are currently adopted in the new proposed Annex L of EN1999-1-1.

1.4. Organization of Work

The present work is divided in seven Chapters and it is included five Appendices and two Annex:

- **CHAPTER 1** provides the background and motivation, objective and scope, and organization of the work.
- **CHAPTER 2** preliminarily reports the main results of the elastic stability theory of a single plate under uniform and non-uniform compression. Subsequently, starting from the J2 deformation theory of plasticity, the theory of plastic buckling of plates is presented including also the variability of the Poisson's ratio depending on the stress levels. This chapter includes the Appendices A, B and C, where some intermediate steps are reported.
- **CHAPTER 3** presents the experimental tests performed at the Structural Engineering Testing Hall Laboratory (STRENGTH Lab) of the Department of Civil Engineering of Salerno University. In particular, 9 stub column tests and 12 three point bending tests have been carried out on four SHS sections made of EN AW 6060 with temper T6.
- **CHAPTER 4** provides a fully theoretical approach for predicting the ultimate resistance of aluminium alloy members subjected to local buckling under uniform compression. In

particular, starting from the buckling differential equation of a single plate, derived under the assumption that the Poisson's ratio is variable in the elastic-plastic range (Chapter 2), the plastic critical stress and the corresponding deformation have been predicted by imposing the boundary conditions accounting for the interaction between the plate elements constituting the section resulting from the edge's connection between adjacent plates.

- **CHAPTER 5** is dedicated to evaluation of aluminium beams under non-uniform bending. the finite element analyses have been performed on the four different aluminium alloys belonging to 6000 series, in order to evaluate the influence of the strain-hardening on the inelastic response of the aluminium beams. Subsequently, an extensive parametric analysis has been performed by varying the main mechanical and geometrical non-dimensional parameters. Finally, the four mathematical formulations are derived to estimate the flexural overstrength and the rotation capacity of aluminium beams in the post elastic range. This chapter includes the Appendix D, where the normalised moment-rotation curves, provided by the finite element simulations, are reported.
- **CHAPTER 6** provides an extension of the effective thickness approach properly modified to account for the occurrence of buckling in the plastic range, as it occurs in the case of sections whose plate elements are characterised by small values of the width-to-thickness ratio. This method has been applied both on compressed columns and on beams in bending. It includes the Appendix E, where the program scripts of the previous procedure are reported.
- **CHAPTER 7** presents the summary of the work with some suggestions for future research.
- **ANNEX A** shows the numerical comparison between the experimental results of the stub column tests, provided in Chapter 3 and in scientific literature, with those obtained by means of the theoretical approach, presented in Chapter 4, and of the effective thickness method.
- **ANNEX B** shows the numerical comparison between the experimental results of the three point bending tests, provided in Chapter 3 and in scientific literature, with those obtained by means of the mathematical formulations, presented in Chapter 5, and of the effective thickness method.

1.5. References

[1.1] **F.M. Mazzolani**: "Structural applications of aluminium in civil engineering", Structural Engineering International: Journal of the International Association for Bridge and Structural Engineering, 16(4), pp. 280-285, 2006.

[1.2] **F.M. Mazzolani**: "3D aluminium structures", Thin-Walled Structures, 61, pp. 258-266, 2012.

[1.3] **E. Georgantzia, M. Gkantou, G.S. Kamaris:** “Aluminium alloys as structural material: A review of research”, Engineering Structures, 227, art. no. 111372, 2021.

[1.4] **E. Georgantzia, M. Gkantou, G.S. Kamaris:** “Aluminium alloys as structural material: A review of research”, Engineering Structures, 227, art. no. 111372, 2021.

[1.5] **G. De Matteis, G. Brando, F.M. Mazzolani:** "Hysteretic behaviour of bracing-type pure aluminium shear panels by experimental tests", Earthquake Engineering and Structural Dynamics, 40 (10), pp.1143-1162, 2011.

[1.6] **G. Brando, G. De Matteis:** "Design of low strength-high hardening metal multi-stiffened shear plates", Engineering Structures, 60, pp. 2-10, 2014.

[1.7] **G. Brando, G. Sarracco, G. De Matteis:** “Strength of an aluminum column web in tension”, Journal of Structural Engineering, 141(7), no. 4014180, 2015.

[1.8] **C.C. Spyrakos, J. Ermopoulos:** “Development of aluminum load-carrying space frame for building structures”, Engineering Structures, 27, pp. 1942-1950, 2005.

[1.9] **J.G. Kaufman:** “Introduction to aluminium alloys and tempers”, Materials Park (OH): ASM International, 2000.

[1.10] **EN1999-1-1:** “Eurocode 9: Design of aluminium structures - Part 1-1: General structural rules”, European Committee for Standardization, 2007.

[1.11] **The Aluminium Association:** “Aluminium Design Manual”, Washington, 2020.

[1.12] **Australian/New Zealand Standard (AS/NZS):** “Aluminium Structures part 1: Limit Stade Design”, Sydney, 1997.

[1.13] **GB 50429:** “Code for Design of Aluminium Structures”, Ministry of Construction of the People’s Republic of China, 2007.

[1.14] **S. Timoshenko:** “Theory of Elastic Stability”, McGraw-Hill Book Co., Inc., 1936.

[1.15] **Z. P. Bazant, L. Cedolin:** “Stability of Structures”, Oxford University Press, New York, 1991.

[1.16] **EN 1993-1-1**: “Eurocode 3: Design of steel structures - Part 1-1: General rules and rules for buildings”, European Committee for Standardization, 2005.

[1.17] **R.D. Mindlin**: “Influence of rotatory inertia and shear on flexural motions of isotropic, elastic plates”, ASME Trans. J. Appl. Mech., 18, pp. 31-38, 1951.

[1.18] **P.P. Bijlaard**: “Theory and Tests on the Plastic Stability of Plates and Shells”, Journal of the Aeronautical Science, 16(9), pp. 529.541, 1949.

[1.19] **G. Gerard and H. Becker**: “Handbook of structural stability. I: Buckling of flat plate”, National Advisory Council for Aeronautics (NACA), Washington, D.C., 1957.

[1.20] **C.M. Wang, Y. Xiang, J. Chakrabarty**: “Elastic/plastic buckling of thick plates”, International Journal of Solids and Structures, 38, pp. 8617-8640, 2001.

[1.21] **D. Durban and Z. Zuckerman**: "Elastoplastic buckling of rectangular plates in biaxial compression/tension", International Journal of Mechanical Sciences, 41, pp. 751-756, 1999.

[1.22] **F.M. Mazzolani, V. Piluso:** "Prediction of the rotation capacity of aluminium alloy beams", Thin-Walled Structures, **27** (1), pp. 103-116, 1997.

[1.23] **C. Faella, F.M. Mazzolani, V. Piluso, G. Rizzano:** "Local buckling of aluminium members: testing and classification", Journal of Structural Engineering, ASCE 2000, 126 (3), pp.353–60, 2000.

[1.24] **G. De Matteis, L.A. Moen, M. Langseth, R. Landolfo, O.S. Hopperstad, F.M. Mazzolani**: "Cross-sectional classification for aluminium beams: a parametric study", Journal of Structural Engineering, 127 (3), pp. 271-279, 2001.

[1.25] **G. De Matteis, R. Landolfo, M. Manganiello, F.M. Mazzolani:** "Inelastic behaviour of I-shaped aluminium beams: Numerical analysis and cross-sectional classification", Computers and Structures, 82, pp. 2157-2171, 2004.

[1.26] **F.M. Mazzolani, V. Piluso, G. Rizzano:** "Local buckling of aluminum alloy angles under uniform compression", Journal of Structural Engineering, 137(2), pp. 173-184, 2011.

[1.27] **M. Liu, L. Zhang, P. Wang, Y. Chang:** "Experimental investigation on local buckling behaviors of stiffened closed-section thin-walled aluminum alloy columns under compression", Thin-Walled Structure, 94, pp. 188-198, 2015.

[1.28] **H.X. Yuan, Y.Q. Wang, T. Chang, X.X. Du, Y.D. Bu, Y.J. Shi:** "Local buckling and post buckling strength of extruded aluminium alloy stub columns with slender I-sections", Thin-Walled Structures, 90, pp.140-149, 2015.

[1.29] **Y. Wang, F. Fan, S. Lin:** "Experimental investigation on the stability of aluminium alloy 6082 circular tubes in axial compression", Thin-Walled Structures, 89, pp.54-66, 2015.

[1.30] **R. Feng and B. Young:** "Experimental investigation of aluminum alloy stub columns with circular openings", Journal of Structural Engineering, 141(11), pp. 1-10, 2015.

[1.31] **M.N. Su, B. Young, L. Gardner:** "The continuous strength method for the design of aluminium alloy structural elements", Engineering Structures, 122, pp.338–348, 2016.

[1.32] **L. Gardner and M. Ashraf:** "Structural design for non-linear metallic materials", Engineering Structures, 28(6), pp.926-934, 2006.

[1.33] **M. Ashraf and B. Young:** "Design formulations for non-welded and welded aluminium columns using continuous strength method", Engineering Structures, 33(12), pp.3197-3207, 2011.

[1.34] **B.W. Schafer and T. Peköz:** "Direct Strength prediction of cold-formed steel members using numerical elastic buckling solutions, International Specialty Conference on Cold-Formed Steel Structures: Recent Research and Developments in Cold-Formed Steel Design and Construction, pp. 69-76, 1998.

[1.35] **C.D. Moen and B.W. Schafer:** "Direct strength method for design of cold-formed steel columns with holes", Journal of Structural Engineering, 137(5), pp. 559-570, 2011.

[1.36] **F. Panlio:** "The theory of limit design applied to magnesium alloy and aluminium alloy structures", R Aerinaut Soc, pp. 534-571, 1947.

[1.37] **T. Welo:** "Inelastic deformation capacity of flexurally-loaded aluminium alloy structures", Norwegian University of Science and Technology, 1990.

[1.38] **B.S. Opheim:** "Bending of thin-walled aluminium extrusions", Norwegian University of Science and Technology, 1996.

[1.39] **L.A. Moen, O.S. Hopperstad, M. Langseth:** "Rotational capacity of aluminum beams under moment gradient. I: Experiments", Journal of Structural Engineering, 125 (8), pp. 910-920, 1999.

[1.40] **L.A. Moen, G. De Matteis, O.S. Hopperstad, M. Langseth, R. Landolfo, F.M. Mazzolani**: "Rotational capacity of aluminum beams under moment gradient. II: numerical simulation", Journal of Structural Engineering, 125 (8), pp. 921-929, 1999.

[1.41] **J.H. Zhu and B. Young**: "Design of aluminum alloy flexural members using direct strength method", Journal of Structural Engineering, 135 (5), pp. 558-566, 2009.

[1.42] **Y. Kim and T. Peköz:** "Numerical Slenderness Approach for design of complx aluminium extrusion subjected to flexural loading", Thin-Walled Structures, 127, pp. 62-75, 2018.

[1.43] **R. Feng, C. Shen, J. Lin:** "Finite element analysis and design of aluminium alloy CHSs with circular through-holes in bending", Thin-Walled Structures, 144, 2019.

[1.44] **R. Feng, Z. Chen, C. Shen, K. Roy, B. Chen, J.B.P. Lim:** "Flexural capacity of perforated aluminium CHS tubes–An experimental study", Structures, 25, pp. 463-480, 2020.

[1.45] **Y.Q. Wang, Z.X. Wang, F.X. Yin, L. Yang, Y.J. Shi, J. Yin:** ". Experimental study and finite element analysis on the local buckling behavior of aluminium alloy beams under concentrated loads", Thin-Walled Structures, 105, pp. 105-144, 2016.

[1.46] **M.N. Su, B. Young, L. Gardner:** "Deformation-based design of aluminum alloy beams" Engineering Structures, 80, pp. 339-349, 2014.

[1.47] **M.N. Su, B. Young, L. Gardner:** ". Flexural response of aluminium alloy SHS and RHS with internal stiffeners", Engineering Structures, 121, pp. 170-180, 2016.

[1.48] **E. Georgantzia, M. Gkantou, G.S. Kamaris:** "Aluminium alloys as structural material: A review of research", Engineering Structures, 227, art. no. 111372, 2021.

CHAPTER 2
STABILITY OF PLATES

2.1. Introduction

The structural behaviour of aluminium thin-walled sections is strongly affected by local buckling phenomena, which arise in the compressed part of the members. Considering the cross-section composed by a finite number of plates, the theory of stability of a single plate under uniform and non-uniform compression represents an aspect of primary importance to analyze the influence of the local instability on the sectional behaviour. Obviously, the study of the plate subjected to the actions in his middle-plane is extremely complex, because geometrical and mechanical non-linearity effects occur. For this reason, the main results of the elastic buckling theory are reported in the case of a single plate under uniform and non-uniform compression for different boundary conditions, neglecting the geometrical imperfections.

Subsequently, including the mechanical nonlinearity of material, the critical load of a single plate under compression is derived in the elastic-plastic region. Starting from the fundamental relationships in J_2 deformation theory, the theory of plastic buckling of plates is presented also including the variability of the Poisson's ratio depending on the stress levels. The differential equation of the plates at the onset of buckling is developed and the corresponding solution is provided. This is an innovative step compared to the theoretical solutions currently existing in the technical literature because the variability of the Poisson's ratio in the elastic-plastic range is commonly neglected.

2.2. Elastic Buckling

2.2.1. Second order differential equation

It is well known that the second order differential equation which describes the behaviour of a thin plate under uniform compression in its middle plane was derived for the first time in 1807 from *De Saint Venant* [2.1]. According to Figure 2.1, where the infinitesimal plate element under the membrane actions of the middle plane is depicted, the basic assumptions of the elastic buckling criterion are:

a. The material is perfectly elastic according to the *Hooke*'s law;
b. The material is homogenous and isotropic, for this reason the mechanical properties are independent of the direction of the applied stresses;

c. The thickness of plate is constant and small compared to the two dimensions of the plate in plane;
d. The segments which are orthogonal to the middle-plane of the plate remain orthogonal to the middle-plane also after the deformations;
e. The plate is incompressible in the direction orthogonal to the middle plane, so the stresses in the same direction are negligible;
f. The displacements $w(x, y)$ orthogonal to the middle plane have an order of magnitude less than the thickness of the plate, consequently, the curvature can be assumed as the second derivatives of $w(x, y)$;

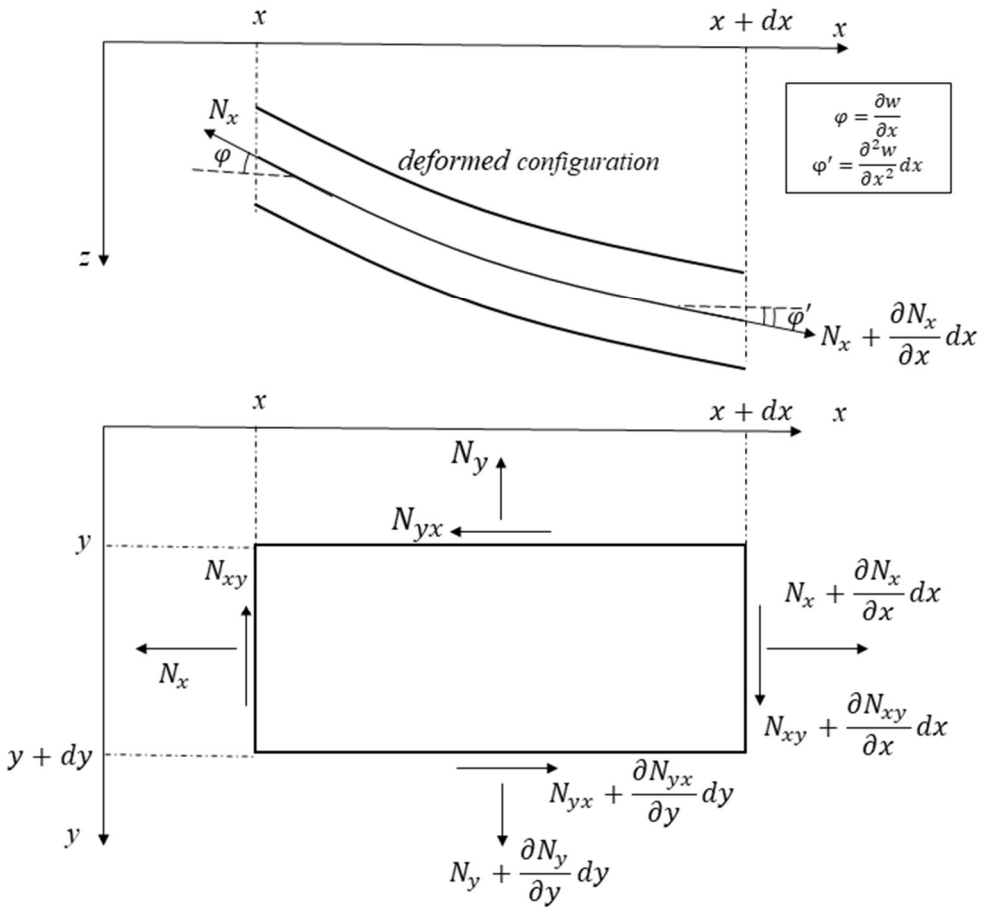

Figure 2.1. Infinitesimal plate element subjected to the membrane actions in the plane $x - z$ and $x - y$.

It is important to underline that the same assumptions are the basis of the first order differential equation of a single plate under uniform load, provided by *Sophie German and Lagrange* [2.1].

The elastic buckling criterion is expressed by Eq.(2.1), where D_e represents the elastic flexural stiffness of the plate and it is expressed in (2.2):

$$\frac{\partial^4 w}{\partial x^4} + 2\frac{\partial^4 w}{\partial x^2 \partial y^2} + \frac{\partial^4 w}{\partial y^4} = -\frac{1}{D_e}\left(N_x \frac{\partial^2 w}{\partial x^2} + 2N_{xy}\frac{\partial^2 w}{\partial x \partial y} + N_y \frac{\partial^2 w}{\partial y^2}\right) \tag{2.1}$$

and:

$$D_e = \frac{Et^3}{12(1-\nu_e^2)} \tag{2.2}$$

where E and ν_e are, respectively, the Young's modulus and the Poisson's ratio in the elastic region of metal materials and t represents the plate thickness.

In the simple case of only uniform compression along $x - direction$, as depicted in Figure 2.2, the second order differential equation becomes:

$$\frac{\partial^4 w}{\partial x^4} + 2\frac{\partial^4 w}{\partial x^2 \partial y^2} + \frac{\partial^4 w}{\partial y^4} = -\frac{N}{D_e}\frac{\partial^2 w}{\partial x^2} \tag{2.3}$$

From a mathematical point of view, the previous relation represents a homogeneous linear differential equation of the fourth order with partial differential, which can be solved taking into account the specific boundary conditions. A trivial solution, corresponding to undeformed configuration of the plate, is the displacement function equal to zero ($w = 0$). The buckling condition is achieved for infinite values of compressed load N (eigenvalues) for which a non-trivial displacement solution (eigenvector) correspond. The smallest eigenvalue represents the critical load.

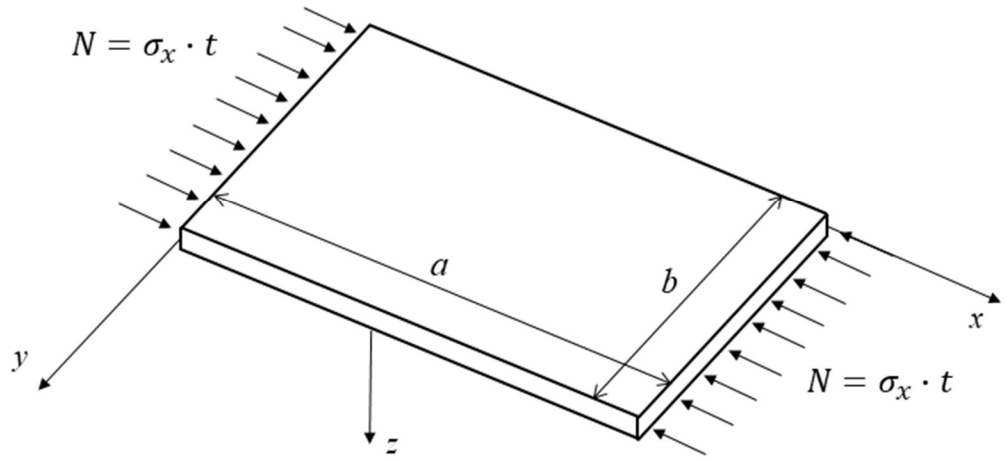

Figure 2.2. Single plate under uniform compression along $x - direction$.

2.2.2. Solutions Methods of the Buckling Equation

The solution of Eq.(2.3) can be solved by means of different approaches [2.2]. The main solution methods are, briefly, described:

Eulerian approach. It consists in the integration of the differential equation starting from a general solution, which satisfies the constraint and loading conditions along the sides of the plate. In the following, this method is applied to determine the elastic critical load of a single plate under uniform compression along x direction and for different edge condition along unloaded sides.

Energy approaches. These methods are all based on the definition of the strain energy produced by the internal stresses (U) and the potential energy of external actions (P) [2.3]. In particular, it is possible to apply two different methods:

- *The principle of energy conservation* states that the sum of the strain energy of system and the work done by the applied loads during the loading process is equal to zero:

$$U + P = 0 \tag{2.4}$$

  This method can be applied when the deflected shape w is known. For this reason, the final value of the elastic critical stress is not approximated.

- *The minimum potential energy (Rayleigh-Ritz method)* [2.4], [2.5]. When the plate reaches the buckling point, it is in neutral equilibrium and in this state the total potential energy ($U + P$) is always a minimum. So, it is necessary to satisfy the following relationship:

$$\delta U + \delta P = 0 \tag{2.5}$$

  The importance of this method consists of choosing arbitrarily a deflected shape and, consequently, the final solution the buckling stress is approximated and, in particular, this value is higher than the true critical stress. Obviously, if the shape chosen for the deflection is exact, this method provides the same result as the previous approach.

Galerkin's method [2.6]**.** It is an alternative to the *Rayleigh-Ritz* solution. In this case, an approximate shape is assumed for the deflection surface, however the expression for $w(x, y)$ is directly substituted in the differential equation. After replacement, a waste is provided, and the *Galerkin*'s method is necessary to minimize this error. Obviously, if the deflection shape is exact and, consequently the previous waste is equal to zero, so this method perfectly coincides with the eulerian approach.

The finite difference method. It represents an approximate numerical procedure, based on the use of the expressions of the *Taylor* series to describe the derivatives of the deflection, which appear in the fundamental differential equation. In particular, the technique is to subdivide the plate longitudinally and transversely by a grid system, so that the spacing between the intersection points

is sufficiently small. In this way, the first derivative at a point can be expressed as the difference between adjacent deflections divided by the distance between them. Similarly, the second derivatives can be obtained as the difference between the first derivatives divided by distance between adjacent points. The fourth derivatives can be expressed by deducing the second derivatives of the second derivatives. Then, substituting these expressions in the differential equation, an algebraic equation is obtained in terms of the deflections at the surrounding points. Applying this equation to each point of the grid, a simple system of linear equations in the unknown deflections can be derived. Obviously, the points near the sides of the plate are influenced by the boundary conditions.

The finite elements method. Also, this approach represents a simplified numerical procedure, and it consists of cutting the plate into a finite number of flat elements joined only at specified nodes and the continuity and equilibrium are established at these nodes only. These elements are connected to each other to their corners. In order to respect the continuity, the deflection of adjacent elements has to be the same and the rotations of adjacent elements orthogonal to the axes x and y must be equal. The most important advantage of this method is the widespread implementation to the software program, which allows to solve the plates with mixed boundary and loading conditions.

2.2.3. Buckling Factor of a Single Plate under Uniform Compression

Following the eulerian approach, the elastic buckling stress of a thin plate under uniform compression is derived for different edge conditions and without initial geometrical imperfections. According to Figure 2.2, the edges $x = 0$ and $x = a$ are considered simply supported, so the solutions of Eq. (2.3) depends on the edge conditions along the other sides ($y = 0$; $y = b$). In the following, the different conditions for unloaded edges are considered to estimate the critical stress under uniform compression.

Free edges for unloaded sides. The simplest case of buckling is verified when the uniform compression is applied to simply supported edges, while the other sides are free. In this configuration, the plate behaves in the same way as a column subjected to the normal force, so the critical load is provided by the *Euler* theory [2.1].

All edges are simply supported. In the case of the simply supported along all four edges, the unknown function $w(x, y)$ is searched in the form of the infinite double trigonometrical series (Fourier series):

$$(x, y) = \sum_{m=1}^{\infty} \sum_{n=1}^{\infty} w_{mn} sin\left(\frac{m\pi x}{a}\right) sin\left(\frac{n\pi y}{b}\right) \tag{2.6}$$

where m and n are, respectively, the number of half waves in x and y directions, while w_{mn} are the unknown coefficients, satisfying the differential equation reported in (2.3) and they represent the

amplitudes of function $w(x,y)$. Substituting the Eq.(2.6) into Eq.(2.3), the following relationship is obtained:

$$\sum_{m=1}^{\infty}\sum_{n=1}^{\infty} w_{mn}\left[\left(\frac{m^4\pi^4}{a^4}+2\frac{m^2n^2\pi^4}{a^2b^2}+\frac{n^4\pi^4}{b^4}\right)-\frac{N}{D_e}\frac{m^2\pi^2}{a^2}\right]sin\left(\frac{m\pi x}{a}\right)sin\left(\frac{n\pi y}{b}\right)=0 \tag{2.7}$$

The first term of the above equation is made by the sum of the infinite number of the independent functions. So that the Eq.(2.7) is satisfied when all coefficients are equal to zero and with reference to the single component of the double Fourier series, it means:

$$w_{mn}\left[\left(\frac{m^4\pi^4}{a^4}+2\frac{m^2n^2\pi^4}{a^2b^2}+\frac{n^4\pi^4}{b^4}\right)-\frac{N}{D_e}\frac{m^2\pi^2}{a^2}\right]=0 \tag{2.8}$$

Obviously, $w_{mn}=0$ represents a trivial solution to which corresponds an undeformed configuration of the plate, so it is neglected. Conversely, a nontrivial solution can be obtained in closed form, by assuming $n=1$, i.e. the plate buckles forming only one half-wave in the $y-direction$; and it represents the expression of the buckling load in the elastic region:

$$N_{cr.e}=k\frac{\pi^2 D_e}{b^2} \tag{2.9}$$

where k is the buckling factor and it depends on the number of half-waves in $x-direction$ (m) and the ratio between the geometrical dimension of the plate (a/b) by means of the following relationship:

$$k=\frac{b^2}{a^2}\left(m+\frac{1}{m}\frac{a^2}{b^2}\right)^2 \tag{2.10}$$

Figure 2.3 shows the trend of the buckling factor. The minimum value of k is achieved for integer values of the ratio a/b and it is equal to 4. Moreover, for the plates with $a/b>4$, it results that $k\rightarrow 4$ because the variation of the buckling factor respect to the minimum value can be neglected. Theoretically, this procedure should be repeated for each component of double series and the final result is the sum of all components, however it is well known that it is possible to consider the component of the series which is related to the main buckling mode and in this specific case to the ratio between the geometrical dimensions of the plate (a/b). As an example, the buckling shape of the plate with $a/b=2$ is reported in Figure 2.4. By dividing the first and second members of Eq. (2.9) and taking into account Eq. (2.2), the critical stress in the elastic range can be expressed as:

$$\sigma_{cr.e}=k\frac{\pi^2 E}{12(1-v_e^2)(b/t)^2} \tag{2.11}$$

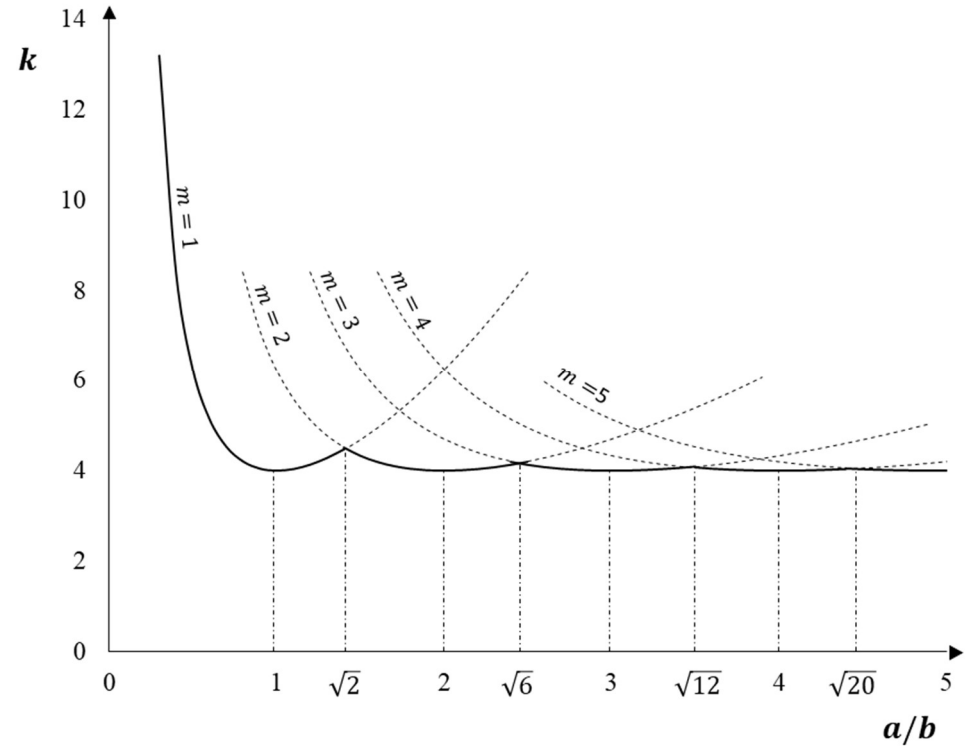

Figure 2.3. Buckling factor k for simply supported plates.

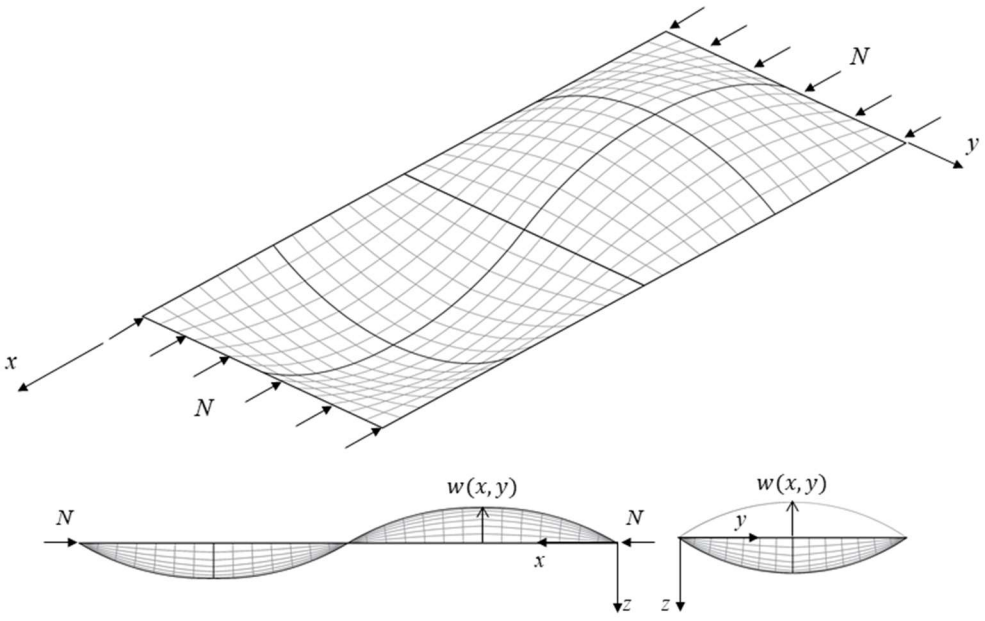

Figure 2.4. Buckling shape for plate with simply supported edges and for $m = 2$.

When the plate under uniform compression is not simply supported along the unloaded sides, the buckling load cannot be determined in the closed form, but it is necessary to define an iterative procedure, as shown in the following cases. Moreover, the deflected function $w(x,y)$ cannot be searched by means of Fourier series (2.6), but it is possible to use the Levy's general solution in the following form [2.1]:

$$w(x,y) = f(y)sin\left(\frac{m\pi x}{a}\right) \tag{2.12}$$

where $f(y)$ represents an unknown function of y. The Eq. (2.12) satisfies the boundary conditions along the loaded sides, in particular the displacements and the bending moments for $x = 0$ and $x = a$ are equal to zero:

$$w(x,y)|_{x=0;x=a} = 0$$
$$M_x|_{x=0;x=a} = 0 => \left\{D_e sin\left(\frac{m\pi x}{a}\right)\left[f(y)\left(\frac{m\pi}{a}\right)^2 - \nu_e \frac{\partial^2 f}{\partial y^2}\right]\right\}\Bigg|_{x=0;x=a} = 0 \tag{2.13}$$

By substituting the general solution (2.12) into Eq.(2.3) and replaced $\lambda = m\pi/a$, the following homogenous fourth order differential equation is obtained:

$$\frac{d^4 f}{dy^4} - 2\lambda^2 \frac{d^2 f}{dy^2} + f\lambda^2\left(\lambda^2 - \frac{N}{D_e}\right) = 0 \tag{2.14}$$

the corresponding algebraic characteristic equation of previous relationship is equal to:

$$\psi^4 - 2\lambda^2\psi^2 + f\lambda^2\left(\lambda^2 - \frac{N}{D_e}\right) = 0 \tag{2.15}$$

Through some mathematical steps, the general solution of Eq. (2.14) is equal to:

$$w(x,y) = (a_1 cosh\alpha y + a_2 sinh\alpha y + a_3 cos\beta y + a_4 sin\beta y)sin\lambda x \tag{2.16}$$

where a_i represent the constants of integrations and they can be determined by means of the boundary conditions, while the coefficients α and β are expressed by following relationships:

$$\alpha = \sqrt{\lambda^2 + \lambda\sqrt{\frac{N}{D_e}}}$$
$$\beta = \sqrt{-\lambda^2 + \lambda\sqrt{\frac{N}{D_e}}} \tag{2.17}$$

The edge $y = 0$ is simply supported - the edge $y = b$ is free. According to the conditions of constraints, the deflection w and the bending moment M_y are zero along the side $y = 0$, while the side $y = b$ is free and, consequently, the bending moment M_y, the twisting moment M_{xy} and the shearing force V_y are equal to zero. However, it is possible to reduce the boundary conditions along

the free edge, in particular the twisting moment and the shearing action can be replaced by one boundary condition R_y^* defined equivalent shearing force [2.1]:

$$R_y^* = V_y + \frac{\partial M_{xy}}{\partial x} \tag{2.18}$$

So, the boundary conditions along the unloaded edges are:

$$\begin{aligned}
&1)\ \ w|_{y=0} = 0 \\
&2)\ \ M_y\big|_{y=0} = 0 \Rightarrow \left(\frac{\partial^2 w}{\partial y^2} + \nu_e \frac{\partial^2 w}{\partial x^2}\right)\Big|_{y=0} = 0 \\
&3)\ \ M_y\big|_{y=b} = 0 \Rightarrow \left(\frac{\partial^2 w}{\partial y^2} + \nu_e \frac{\partial^2 w}{\partial x^2}\right)\Big|_{y=b} = 0 \\
&4)\ \ R_y^*\big|_{y=b} = 0 \Rightarrow \left(\frac{\partial^3 w}{\partial y^3} + (2-\nu_e)\frac{\partial^3 w}{\partial x^2 \partial y}\right)\Big|_{y=b} = 0
\end{aligned} \tag{2.19}$$

By substituting Eq.(2.16) into previous relations, it results:

$$\begin{aligned}
&1)\ \ a_1 + a_3 = 0 \\
&2)\ \ a_1\phi_\alpha + a_3\phi_\beta = 0 \\
&3)\ \ a_2\phi_\alpha sinh\alpha b - a_4\phi_\beta sin\beta b = 0 \\
&4)\ \ a_2\psi_\alpha cosh\alpha b - a_4\psi_\beta cos\beta b = 0
\end{aligned} \tag{2.20}$$

where ϕ_α, ϕ_β, ψ_α and ψ_β are equal to:

$$\begin{aligned}
\phi_\alpha &= \alpha^2 - \nu_e\lambda^2 \\
\phi_\beta &= \beta^2 + \nu_e\lambda^2 \\
\psi_\alpha &= \alpha(\alpha^2 - \nu_e\lambda^2) \\
\psi_\beta &= \beta(\beta^2 + \nu_e\lambda^2)
\end{aligned} \tag{2.21}$$

From the first two boundary conditions, $a_1 = a_3 = 0$, consequently, by neglecting the trivial solution $a_2 = a_4 = 0$ corresponding to the unbuckled configuration, the solution can be performed by imposing the following determinant of coefficients equal to zero:

$$\begin{vmatrix} \phi_\alpha sinh\alpha b & -\phi_\beta sin\beta b \\ \psi_\alpha cosh\alpha b & -\psi_\beta cos\beta b \end{vmatrix} = 0 \Rightarrow \phi_\beta\psi_\alpha sin\beta b cosh\alpha b = \phi_\alpha\psi_\beta sinh\alpha b cos\beta b \tag{2.22}$$

As depicted in Eq.(2.17) , the coefficients α and β are dependent on the load level, so the elastic critical stress $\sigma_{cr.e}$ can be provided by means of an iterative procedure by satisfying the previous condition. The smallest value of the buckling load corresponds to $m = 1$, i.e., by assuming that the buckled plate has only one half-wave. Moreover, in the scientific literature and according to Eq.(2.9), the expression of buckling factor can be expressed, with a good approximation, by means of the following relationship:

$$k \cong \left(0.456 + \frac{b^2}{a^2}\right) \tag{2.23}$$

The comparison between the previous relation and the trend of buckling factor obtained by an iterative procedure is shown in Figure 2.5, while the buckling shape of a plate under uniform compression with an unloaded edge simply supported and the other free is reported in Figure 2.6.

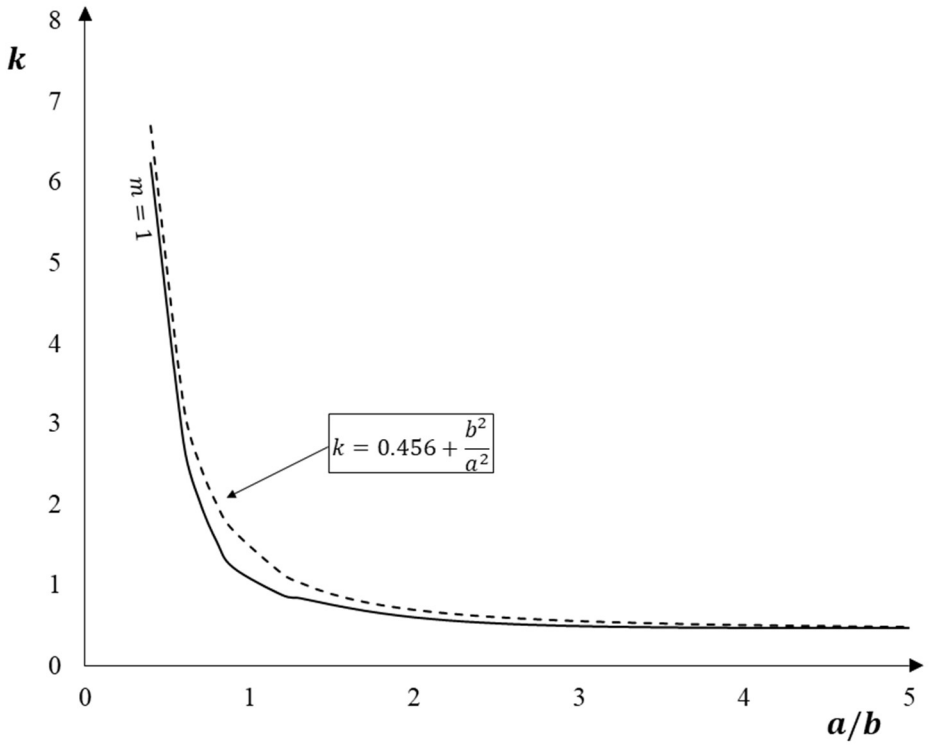

Figure 2.5. Buckling factor k for a plate with one free edge and the other simply supported.

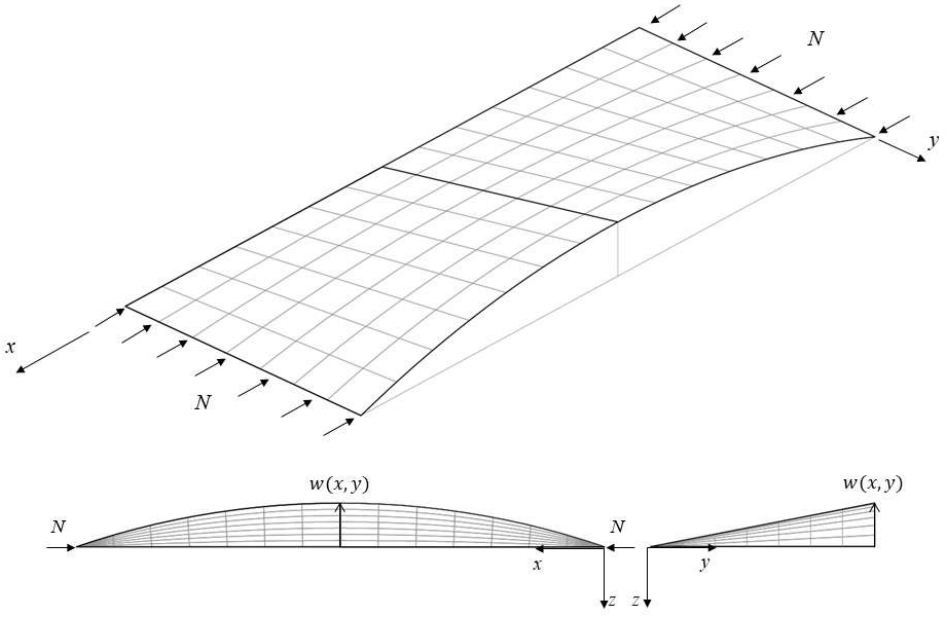

Figure 2.6. The buckling shape of a plate with one free edge and the other simply supported.

Similar considerations can be repeated for the other following boundary conditions:

The unloaded edges are clamped. In this case, the deflection w and the rotation φ_y are equal to zero along the unloaded sides, while the bending moments M_y and the equivalent shearing forces Q_y have non-zero values:

$$\begin{aligned} &1)\ w|_{y=0} = 0 \\ &2)\ \varphi_y\big|_{y=0} = 0 => \frac{\partial w}{\partial y}\Big|_{y=0} = 0 \\ &3)\ w|_{y=b} = 0 \\ &4)\ \varphi_y\big|_{y=b} = 0 => \frac{\partial w}{\partial y}\Big|_{y=b} = 0 \end{aligned} \tag{2.24}$$

According to the Levy's solution (2.16) into previous conditions, it results:

$$\begin{aligned} &1)\ a_1 + a_3 = 0 => a_3 = -a_1 \\ &2)\ a_2\alpha + a_4\beta = 0 => a_4 = -(\alpha/\beta)a_2 \\ &3)\ a_1 cosh\alpha b + a_2 sinh\alpha b + a_3 cos\beta b + a_4 sin\beta b = 0 \\ &4)\ a_1\alpha sinh\alpha b + a_2\alpha cosh\alpha b - a_3\beta sin\beta b + a_4\beta cos\beta b = 0 \end{aligned} \tag{2.25}$$

By substituting the results of the first two relations into into the other equations and neglecting the trivial solution $a_1 = a_2 = 0$, the elastic critical stress can be derived by imposing the determinant of the following matrix is equal to zero:

$$\begin{vmatrix} (cosh\alpha b - cos\beta b) & \left(sinh\alpha b - \frac{\alpha}{\beta} sin\beta b\right) \\ (\alpha sinh\alpha b + \beta sin\beta b) & \alpha(cosh\alpha b - cos\beta b) \end{vmatrix} = 0 \tag{2.26}$$

In this case, according to Eq.(2.9), the minimum value of elastic critical stress can be achieved when the buckling factor is equal to 7, as depicted in Figure 2.7. The values of the critical load are about twice the one of those obtained for the same plate but with the unloaded edges simply supported. This result is justified by the presence of the clamp constraints which provide the greater resistance to the instability phenomena. In Figure 2.8, the buckling shape of a single plate with the clamped unloaded edges is shown in the case of $a/b = 2$ and, consequently, with three half-waves along x ($m = 3$).

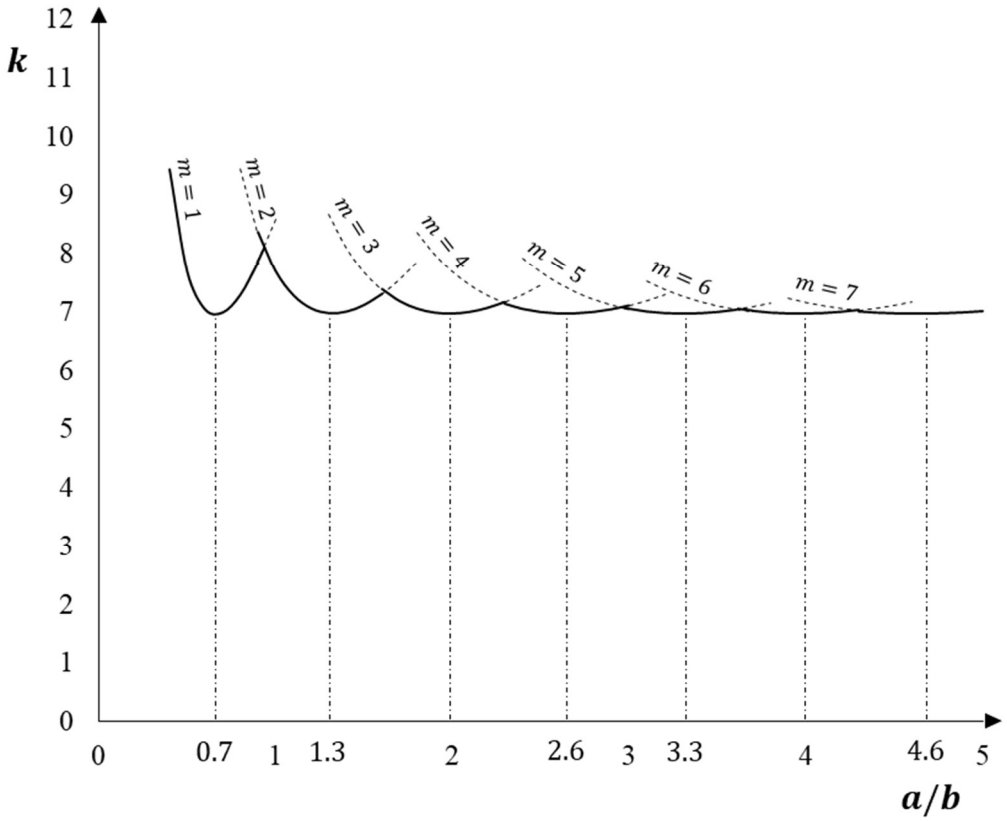

Figure 2.7. Buckling factor k for a plate with clamped edges.

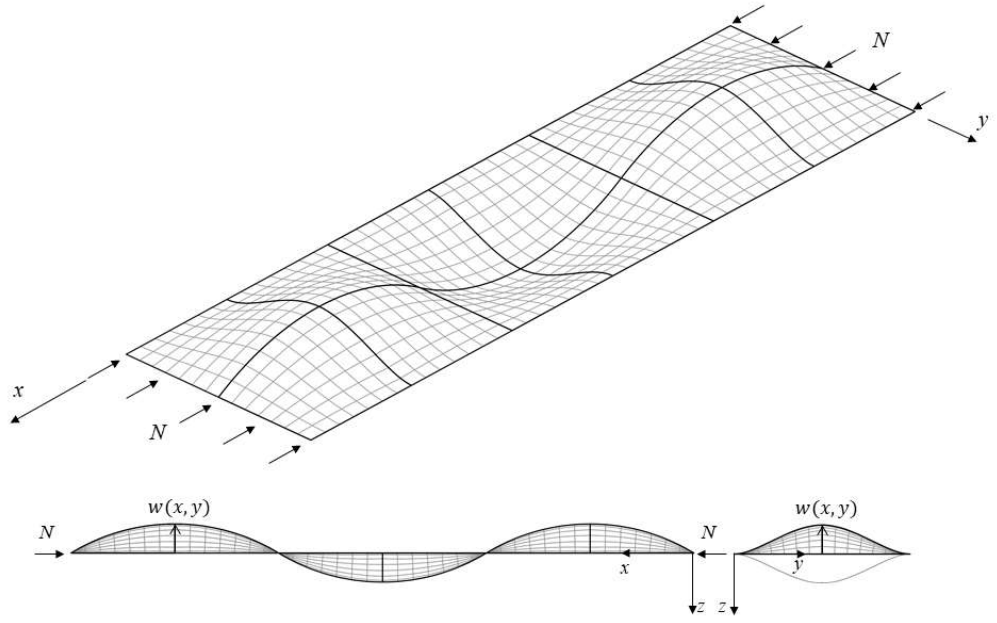

Figure 2.8. Buckling shape of a plate with clamped edges.

The edge $y = 0$ is clamped - the edge $y = b$ is free. The displacement w and the rotation φ_y are equal to zero for the edge $y = 0$, while along the other side $y = b$ the bending moments M_y and the equivalent shearing forces R_y^* are zero:

$$\begin{aligned}
&1)\ \ w|_{y=0} = 0 \\
&2)\ \ \varphi_y\big|_{y=0} = 0 \Rightarrow \frac{\partial w}{\partial y}\Big|_{y=0} = 0 \\
&3)\ \ M_y\big|_{y=b} = 0 \Rightarrow \left(\frac{\partial^2 w}{\partial y^2} + \nu_e \frac{\partial^2 w}{\partial x^2}\right)\Big|_{y=b} = 0 \\
&4)\ \ R_y^*\big|_{y=b} = 0 \Rightarrow \left(\frac{\partial^3 w}{\partial y^3} + (2-\nu_e)\frac{\partial^3 w}{\partial x^2 \partial y}\right)\Big|_{y=b} = 0
\end{aligned} \tag{2.27}$$

By substituting the Eq.(2.16) into previous conditions, it results:

$$\begin{aligned}
&1)\ \ a_1 + a_3 = 0 \Rightarrow a_3 = -a_1 \\
&2)\ \ a_2\alpha + a_4\beta = 0 \Rightarrow a_4 = -(\alpha/\beta)a_2 \\
&3)\ \ a_1\phi_\alpha cosh\alpha b + a_2\phi_\alpha sinh\alpha b - a_3\phi_\beta cos\beta b - a_4\phi_\beta sin\beta b = 0 \\
&4)\ \ a_1\psi_\alpha sinh\alpha b + a_2\psi_\alpha cosh\alpha b + a_3\psi_\beta sin\beta b - a_4\psi_\beta cos\beta b = 0
\end{aligned} \tag{2.28}$$

The elastic critical stress can be estimated by imposing the determinant of following matrix equal to zero:

$$\begin{vmatrix} \left(\phi_\alpha cosh\alpha b + \phi_\beta cos\beta b\right) & \left(\phi_\alpha sinh\alpha b + \dfrac{\alpha}{\beta}\phi_\beta sin\beta b\right) \\ \left(\psi_\alpha sinh\alpha b - \psi_\beta sin\beta b\right) & \left(\psi_\alpha cosh\alpha b + \dfrac{\alpha}{\beta}\psi_\beta cos\beta b\right) \end{vmatrix} = 0 \tag{2.29}$$

As depicted in Figure 2.9, for increasing of the ratio a/b, the value of $k \to 1.25$ and, consequently, the smallest value of critical stress is achieved. the buckling shape of a single plate with two half-waves in $x - direction$ is reported in Figure 2.10.

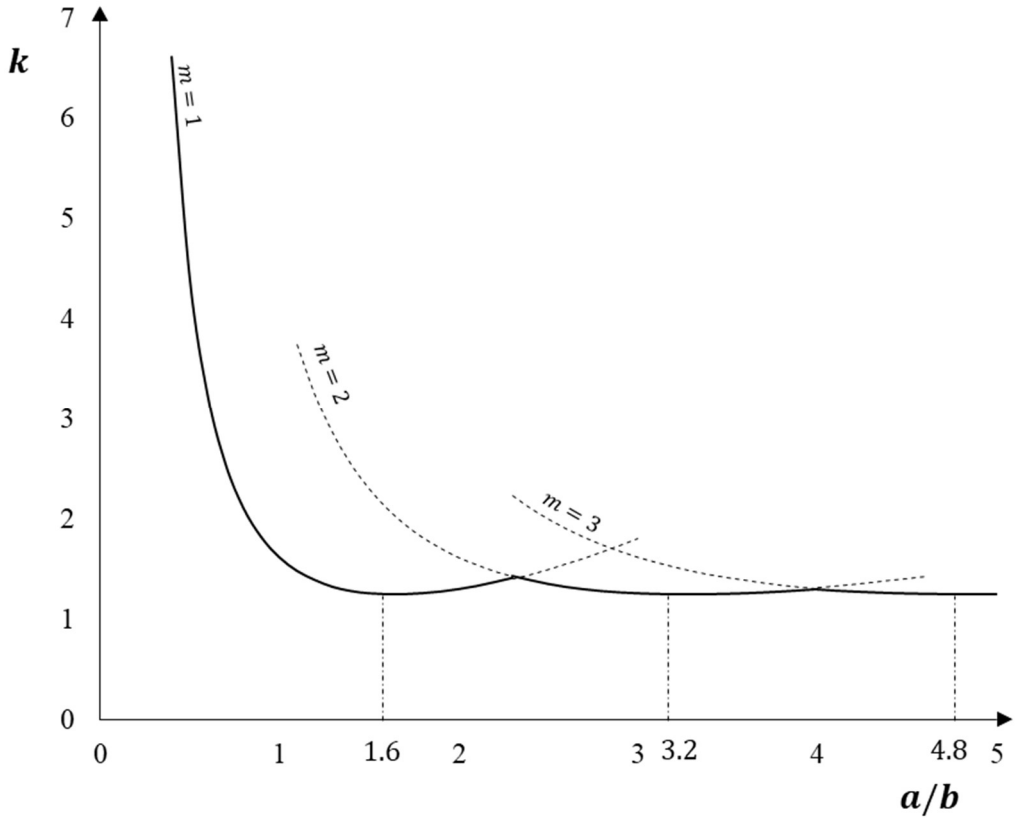

Figure 2.9. Buckling factor k for a plate with one free edge and the other clamped.

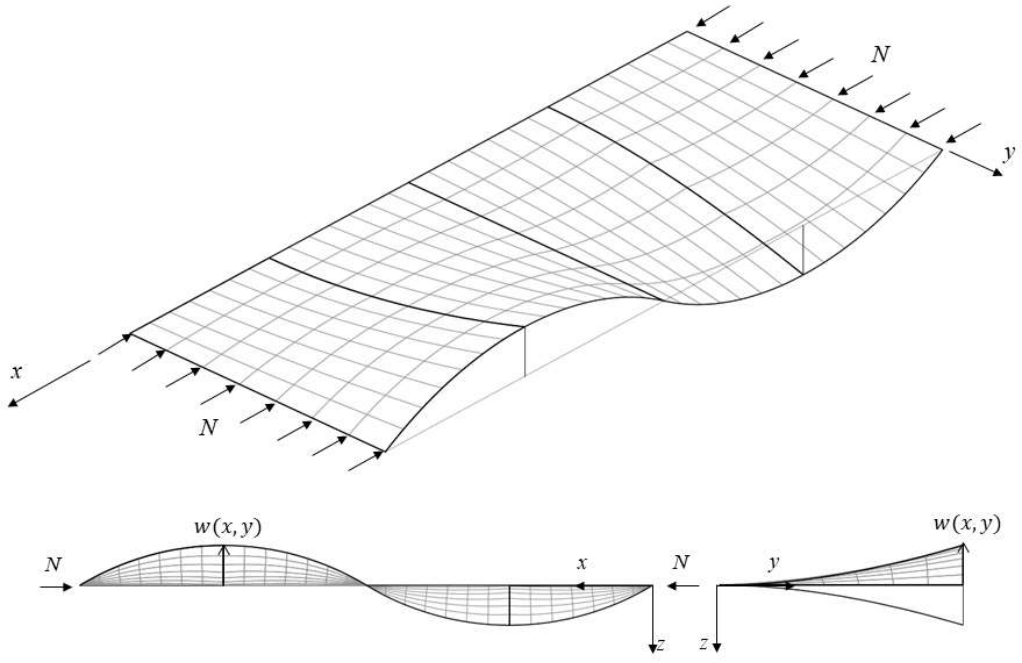

Figure 2.10. Buckling shape of a plate with one free edge and the other clamped.

The edge $y = 0$ is clamped - the edge $y = b$ is simply supported. The restraints of this scheme are characterized by two kinematic conditions for $y = 0$, in particular and, specifically, the displacement w and the rotation φ_y are zero, while the displacement w and the bending moment M_y are equal to zero for $y = b$:

$$\begin{aligned} &1)\ w|_{y=0} = 0 \\ &2)\ \varphi_y\big|_{y=0} = 0 => \frac{\partial w}{\partial y}\Big|_{y=0} = 0 \\ &3)\ w|_{y=b} = 0 \\ &4)\ M_y\big|_{y=b} = 0 => \left(\frac{\partial^2 w}{\partial y^2} + \nu_e \frac{\partial^2 w}{\partial x^2}\right)\Big|_{y=b} = 0 \end{aligned} \tag{2.30}$$

By developing the previous boundary conditions according to the Levy's solution, the following relationships are obtained:

$$\begin{aligned} &1)\ a_1 + a_3 = 0 => a_3 = -a_1 \\ &2)\ a_2\alpha + a_4\beta = 0 => a_4 = -(\alpha/\beta)a_2 \\ &3)\ a_1 cosh\alpha b + a_2 sinh\alpha b + a_3 cos\beta b + a_4 sin\beta b = 0 \\ &4)\ a_1\phi_\alpha cosh\alpha b + a_2\phi_\alpha sinh\alpha b - a_3\phi_\beta cos\beta b - a_4\phi_\beta sin\beta b = 0 \end{aligned} \tag{2.31}$$

By substituting $a_3 = -a_1$ and $a_4 = -(\alpha/\beta)a_2$ in the other relations, the elastic critical stress can be determined by imposing the following determinant equal to zero:

$$\begin{vmatrix} (cosh\alpha b - cos\beta b) & \left(sinh\alpha b - \frac{\alpha}{\beta} sin\beta b\right) \\ \left(\phi_\alpha cosh\alpha b + \phi_\beta cos\beta b\right) & \left(\phi_\alpha sinh\alpha b + \frac{\alpha}{\beta}\phi_\beta sin\beta b\right) \end{vmatrix} = 0 \tag{2.32}$$

According to Eq. (2.9), the minimum value of the elastic critical stress $\sigma_{cr.e}$ is achieved for $k \cong 5.40$, as depicted in Figure 2.11. The buckling shape of a single plate with two half-waves in $x - direction$ is depicted in Figure 2.12.

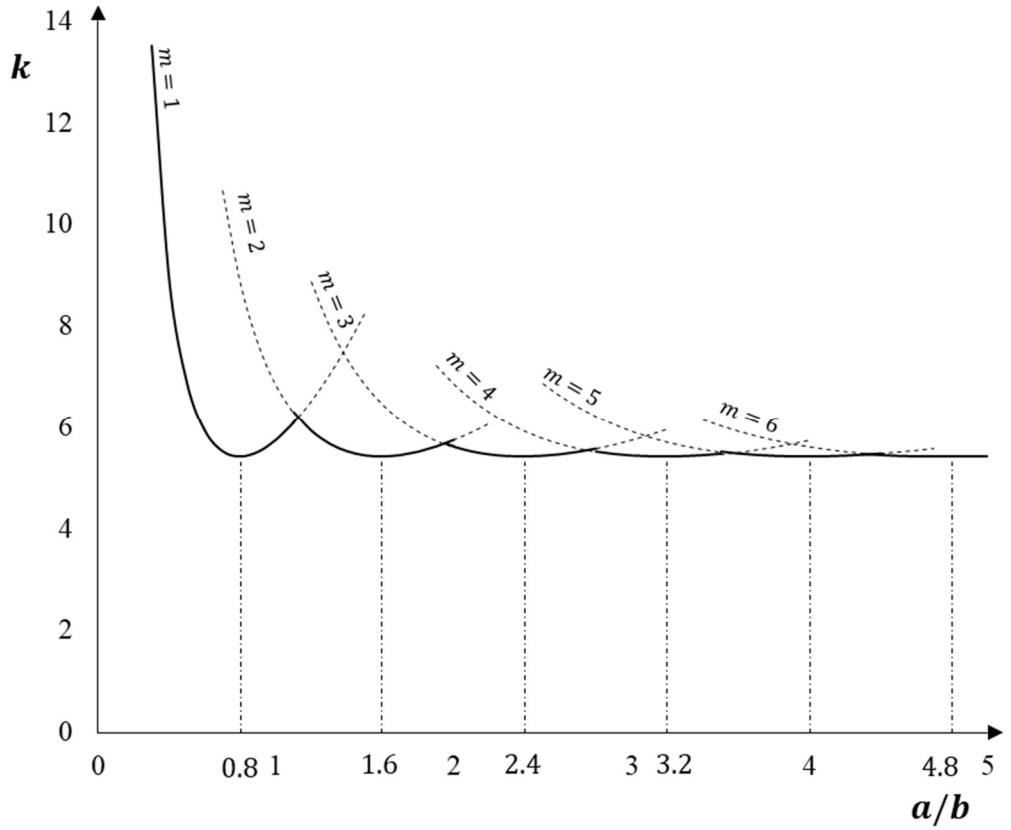

Figure 2.11. Buckling factor k for a plate with one edge simply supported and the other clamped.

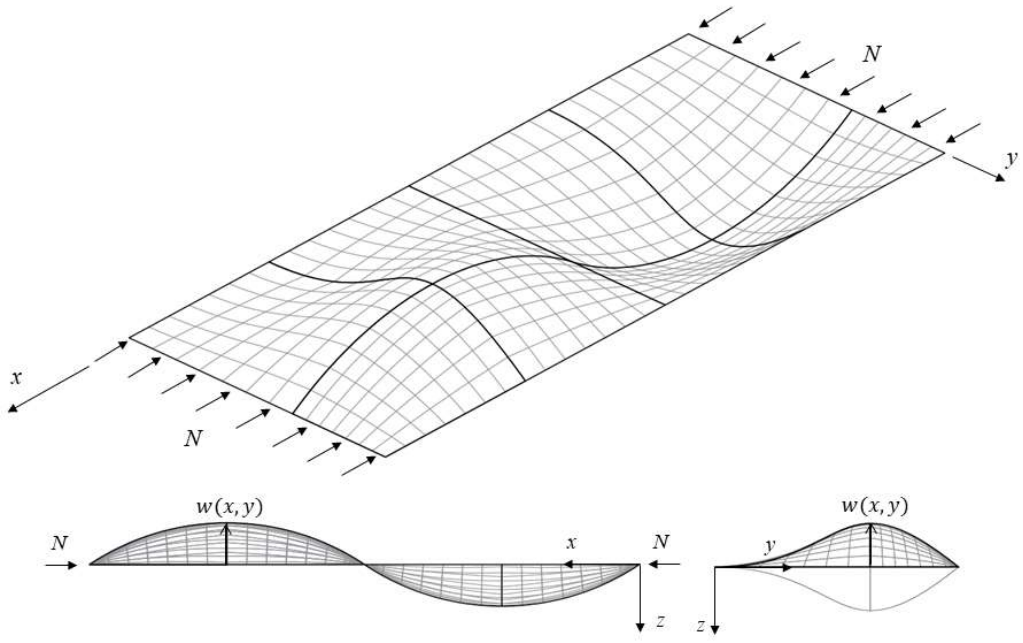

Figure 2.12. Buckling shape of a plate with one edge simply supported and the other clamped.

2.2.4. Buckling Factor of a Single Plate under Non-uniform Compression

When the plate is subjected to non-uniform compression, as in the case of web plates of aluminium members in bending, the solution of differential equation can not be solved by following the eulerian approach, but it is necessary to apply the energy or similar method, based on an assumed deflected form. The main results, reported in the scientific literature, are discussed for the same boundary conditions of the previous cases. According to Figure 2.13, the expression of the linearly variable stress is assumed as:

$$\sigma_x = \sigma_1 \left(1 + \frac{\omega - 1}{b} y\right) \tag{2.33}$$

where the coefficient ω as the ratio between σ_2 and σ_1 which represent the stresses at the end of the plate. When ω is equal to 1, the plate is subjected under uniform compression, while the plate is only in bending for $\omega = -1$.

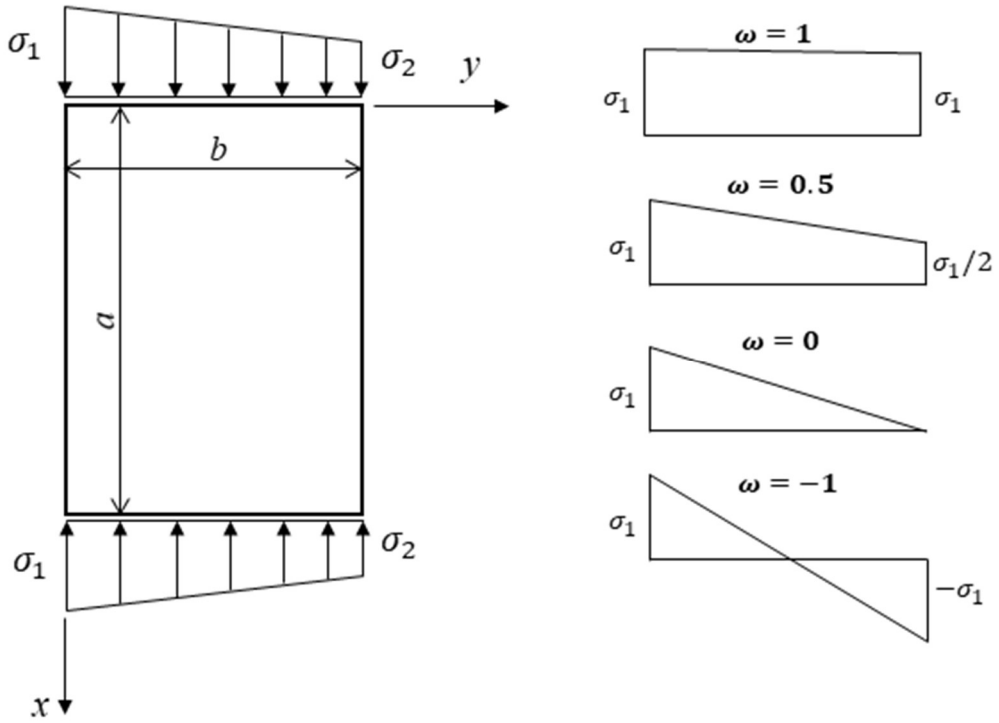

Figure 2.13. The single plate under non-uniform compression.

In the case of simply supported plates, *Timoshenko* provided the solution by means of the principle of conservation of energy [2.1], while *Nölke* solved the plate under non-uniform compression when the unloaded sides are clamped [2.7]. In Figure 2.14, the main results of the above solutions are shown in terms of the minimum buckling factor k as function of ω. It is possible to observe that the buckling factor and, consequently, the value of elastic buckling stress $\sigma_{cr.e}$, increases from $\omega = 1$, i.e., the state of uniform compression, to $\omega = -1$, i.e., pure bending loading. For every value of ω, the ratio between the buckling factor of a plate with edges clamped and those derived by a simply

supported plate is included in the range $1.66 - 1.88$, so the variation of buckling factor as function of the loading variability is almost the same for both cases. Finally, it is possible to verify that the approximate values of the minimum buckling factor can be obtained, considering the mean value of the distributed stress σ_x , but only for $\omega \in [0,1]$.

Kollbrunner and Hermann provided the minimum value of the buckling factor, when the plate is characterized by the clamped edge in $y = 0$ and the simply supported edge in $y = b$ [2.8]. The boundary conditions along the two unloaded sides are different, for this reason the value of k varies depending on the orientation of the edge stress to $y = 0$, as shown in Figure 2.15. When the simply supported edge is in tension side of the plate for $\omega = -1$, the value of k is 39.52 and it does not differ greatly from that with both clamped edges ($k = 39.60$). Conversely, when the fixed edge is in tension, the minimum buckling factor is about 24.48 and it is not very different from that with both edges simply supported ($k = 23.90$).

Figure 2.16 shows the trend of the buckling factor as function of the stress distribution for a plate with the clamped edge in $y = 0$, while the edge $y = b$ is free. Also in this case, the value of k again depends on the orientation of the edge forces to $y = 0$.

Finally, in Figure 2.17, the case of the plate with one edge simply supported and the otherside free is depicted. Moreover, when in the case of pure bending ($\omega = -1$), the relationship between the buckling factor and the ratio of the geometric dimensions of the plate is equal to:

$$k \cong 2\left[\frac{b^2}{a^2} + \frac{6}{\pi^2}(1 - \nu_e)\right] \tag{2.34}$$

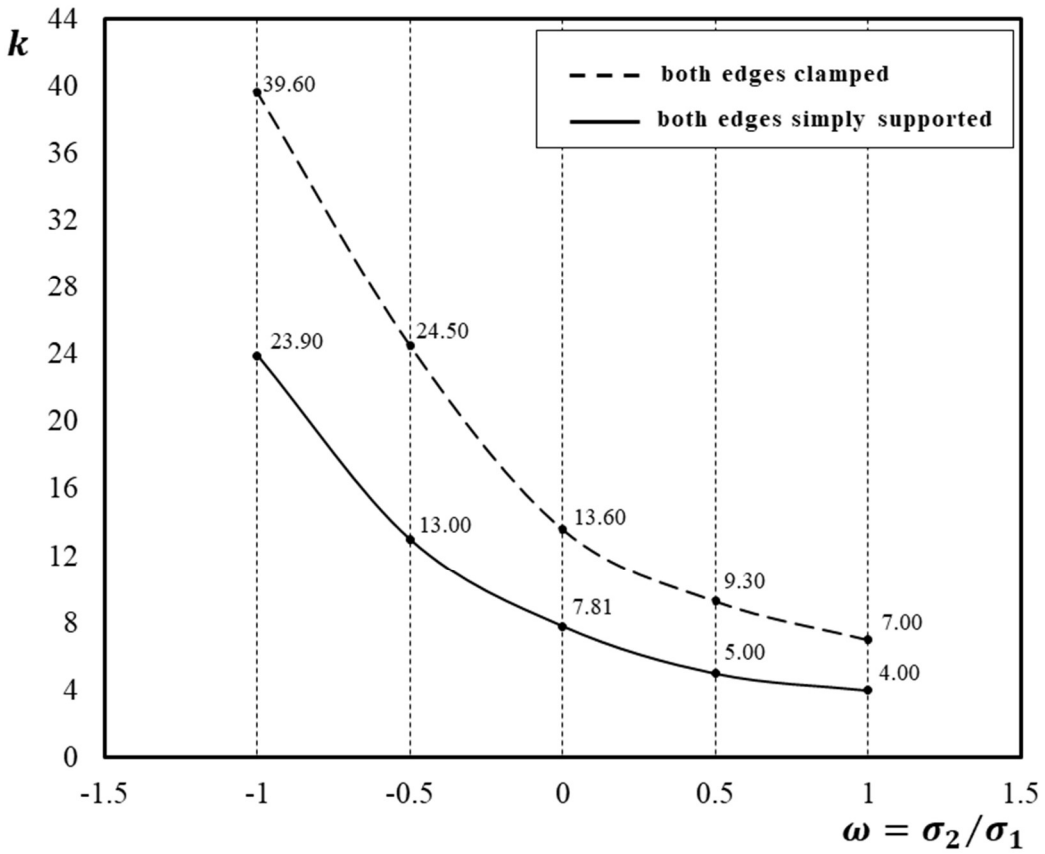

Figure 2.14. The minimum values of buckling factor k for plates with simply supported and clamped edges.

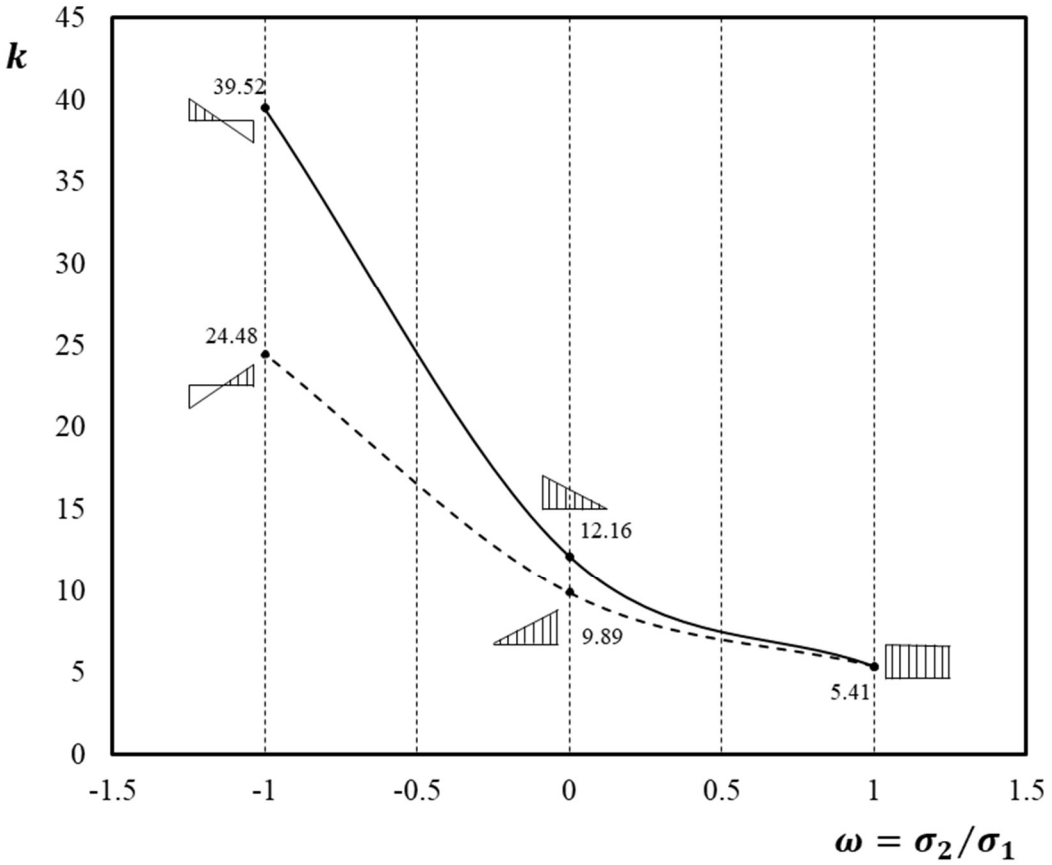

Figure 2.15. The minimum values of buckling factor k when the edge $y = 0$ is clamped and the other is supported.

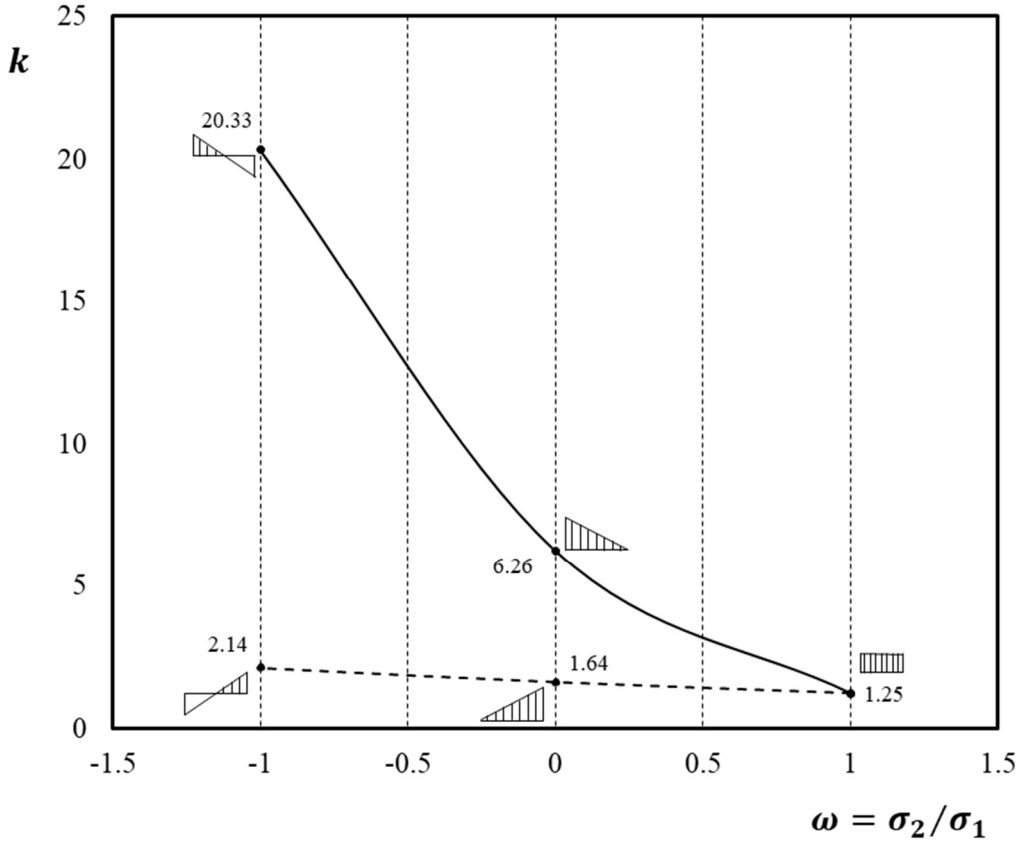

Figure 2.16. The minimum values of buckling factor k when the edge $y = 0$ is clamped and the edge $y = b$ is free.

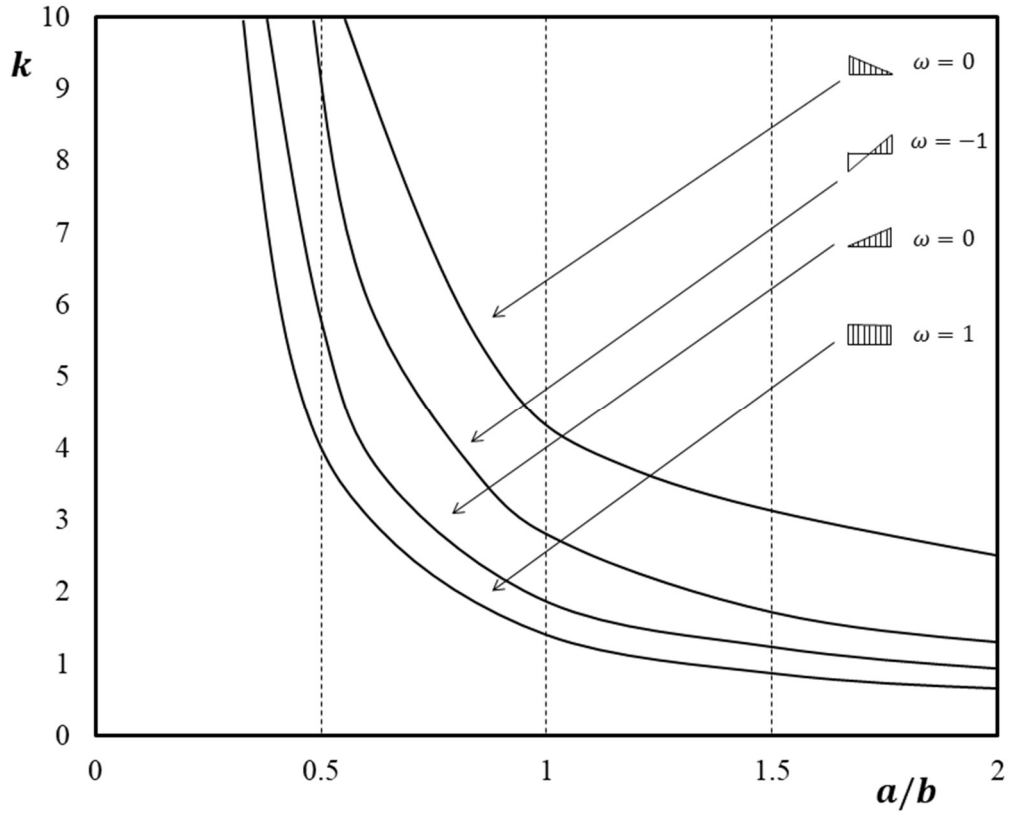

Figure 2.17. The minimum values of buckling factor k when the edge $y = 0$ is supported and the edge $y = b$ is free.

2.3. Plastic Buckling

2.3.1. Plastic buckling paradox

In this section, with reference to a single plate under uniform compression, an extension of the buckling criterion in the elastic-plastic range is provided.

When the instability phenomena occur after the yielding of the material, the mechanical nonlinearity has to be taken into account in the buckling analysis, for this reason, it is necessary to introduce a new model for describing the inelastic response of material.

Since the beginning of the twentieth century, many developments in the study of elastic-plastic behaviour of structures gave rise to a large improvement in the theory of plasticity, leading to the identification of different models for engineering materials based on whether path-dependence is accounted for or not. In particular, the plasticity models currently adopted for metal structures can be divided into two main groups: 1) the deformation theory of plasticity (*Hencky-Nadai*); 2) the flow theory of plasticity (*Lévy-Mises*). A common issue in these theories is that the plastic deformation does not allow any volume change. As this issue is ruled by the second invariant of the stress deviator, under this point of view, both the flow and the deformation theories are called J_2 theories of plasticity. However, the flow theory of plasticity leads to a path-dependent relationship in which the current strain depends not only on the value of the current total stress but also on how the actual stress value has been reached. The flow theory of plasticity assumes that an infinitesimal increment of strain is determined by the current stress and its increment. In particular, it is worthwhile mentioning that according to J_2 flow theory of plasticity the unloading takes place along a line parallel to the initial elastic path. This is in agreement with the experimental behaviour of most metals. Conversely, the deformation theory of plasticity is based on the assumption that the state of strain is uniquely determined by the state of stress. Therefore, it is essentially a special path-independent nonlinear constitutive law. In particular, loading and unloading take place along the same non-linear stress-strain path. However, even though the deformation theory lacks physical rigour compared to the flow theory of plasticity, in many engineering problems involving the inelastic buckling of structures, the deformation theory seems to be more in agreement with the experimental results. This phenomenon is usually referred to as the "plastic buckling paradox" [2.9]-[2.11]. Despite the more satisfactory theoretical framework, the use of the J_2 flow theory of plasticity leads to overestimated predictions of the critical load. Conversely, the application of the J_2 deformation theory of plasticity has proved its ability to lead to more accurate results when theoretical predictions are compared to available experimental data. This paradox has existed for many years leading to a multitude of controversies, many of them are still to be solved. For this reason, many numerical, analytical, and experimental investigations have involved many researchers in the attempt of solving the plastic paradox since the

early 40s. According to some studies, the possible reason for the discrepancies in the results obtained with the two plasticity theories was likely due either to the assumption of small deformation or the exclusion of transverse shear deformation in buckling analysis. Conversely, other studies concluded that a reduction of the discrepancies in the results between the flow and the deformation theory can be obtained provided that imperfections are included in the application of the flow theory. Moreover, other researchers pointed out that the deformation theory predicts a lower plastic shear modulus as the plasticity level increases and, as a consequence, this is the reason why deformation theory tends to predict lower buckling loads when compared to those obtained by applying the flow theory [2.12]. According to *Yun and Kyriakides* [2.13], the plastic buckling paradox has to be still considered "unresolved". This position is agreed by other researchers stating the available explanations are still to be judged "inconclusive".

This work is not aimed to contribute to solving the controversies resulting from the plastic buckling paradox. For this reason, flow theory of plasticity is not applied because the use of the deformation theory of plasticity is still recommended for practical applications concerning the investigation of the inelastic buckling of plates and shells. Research studies have confirmed once again that the deformation theory predictions are more in-line with experimental results than those of flow theory. This fact can be accepted in practical applications, so that reference can be made only to the deformation theory [2.9]. Therefore, the analytical study herein presented will refer to the deformation theory of plasticity. The original contribution of the analytical approach herein presented is given by the introduction of the variability of the Poisson's ratio in the elastic-plastic range, i.e., as dependent on the stress intensity measure, in the evaluation of the plate buckling differential equation.

2.3.2. Fundamental Relations in J_2 Deformation Theory of Plasticity

The simple J_2 deformation theory of plasticity is herein used aiming to relate the biaxial stresses to the plastic deformation [2.14]. According to the J_2 deformation theory of plasticity for isotropic materials under biaxial plane stress state $(\sigma_z = \tau_{xz} = \tau_{yz} = 0)$, the stress intensity is given by:

$$\sigma_i = \sqrt{\sigma_x^2 + \sigma_y^2 - \sigma_x\sigma_y + 3\tau_{xy}^2} \tag{2.35}$$

The corresponding strain intensity, as a function of the biaxial strains, is given by:

$$\varepsilon_i = \frac{1}{1-\nu^2}\sqrt{(1-\nu+\nu^2)(\varepsilon_x^2+\varepsilon_y^2) - (1-4\nu+\nu^2)\varepsilon_x\varepsilon_y + \frac{3}{4}(1-\nu)^2\gamma_{xy}^2} \tag{2.36}$$

According to Eq. (2.36), developed by *Lunchick* [2.15], the strain intensity is a continuous function of the biaxial strains and of the Poisson's ratio which varies from the elastic value $\nu_e = 0.30$ to the plastic value $\nu_p = 0.50$.

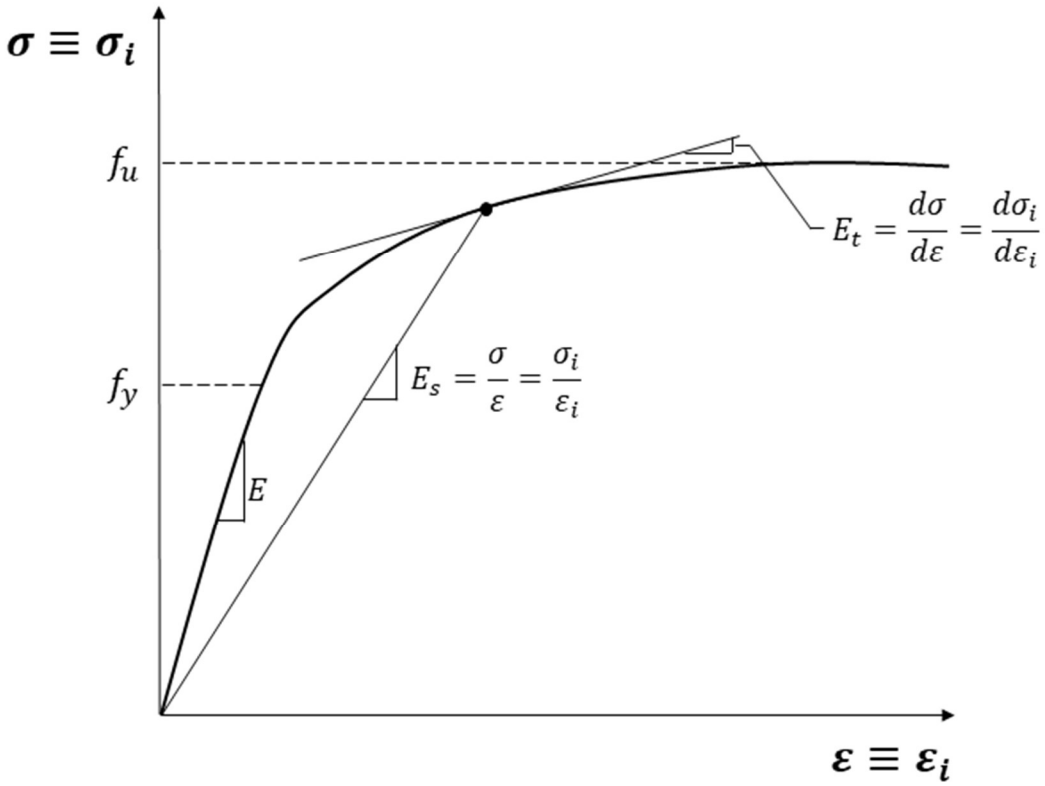

Figure 2.18. A generic universal stress-strain curve.

According to the deformation theory, the stress-strain relations with general non-linear material properties are given by:

$$\sigma_x = \frac{E_s}{1-\nu^2}\left(\varepsilon_x + \nu\varepsilon_y\right)$$

$$\sigma_y = \frac{E_s}{1-\nu^2}\left(\varepsilon_y + \nu\varepsilon_x\right) \tag{2.37}$$

$$\tau_{xy} = \frac{E_s}{2(1+\nu)}\gamma_{xy}$$

According to Figure 2.18, E_s is the secant modulus. A fundamental assumption of the J_2 Theory is that the universal stress-strain curve $\sigma_i - \varepsilon_i$ is perfectly identical to the uniaxial stress-strain curve $\sigma - \varepsilon$ and, consequently, the secant modulus E_s is simply the ratio between σ and ε and it coincides with the secant modulus of the multiaxial stress state:

$$E_s = \frac{\sigma}{\varepsilon} = \frac{\sigma_i}{\varepsilon_i} \tag{2.38}$$

This important identity allows to determine the main properties of an isotropic material under multiaxial stress state through the uniaxial stress-strain curve. For linear elastic materials, this relation is trivial because the material properties are independent of the stress level, conversely it is fundamental when the behaviour of material is non-linear, because the material properties are non-linear function of the acting stress state. Moreover, ν is the Poisson's ratio which, according to *Gerard and Wildhorn* [2.16], given by:

$$\nu = \nu_p - (\nu_p - \nu_e)\frac{E_s}{E} = \frac{1}{2} - \left(\frac{1}{2} - \nu_e\right)\frac{E_s}{E} \tag{2.39}$$

Therefore, in this paper, a smooth transition is obtained between the elastic compressible state and the plastic incompressible state. Conversely, the classical *Stowell*'s [2.17] and *Ilyushin*'s [2.18] assumption is $\nu = \nu_e = \nu_p = 0.50$, i.e. a plastically incompressible state. From Eq.(2.37), it is well known that the strain-stress relations are given by:

$$\begin{aligned} \varepsilon_x &= \frac{\sigma_x - \nu\sigma_y}{E_s} \\ \varepsilon_y &= \frac{\sigma_y - \nu\sigma_x}{E_s} \\ \gamma_{xy} &= \frac{2(1+\nu)}{E_s}\tau_{xy} \end{aligned} \tag{2.40}$$

2.3.3. Variation of Stresses during Buckling

The assumption *d*, introduced in the section 2.2.1, is considered valid also in the elastic-plastic buckling criterion so that, according to Figure 2.1, the segments which are orthogonal to the mid-plane of the plate remain orthogonal also in the deformed configuration. Therefore, the variation of strains can be expressed by the following relationships:

$$\begin{aligned} \delta\varepsilon_x &= \delta\varepsilon_{x.0} - z\delta\chi_x \\ \delta\varepsilon_y &= \delta\varepsilon_{y.0} - z\delta\chi_y \\ \delta\gamma_{xy} &= 2\delta\varepsilon_{xy.0} - 2z\delta\chi_{xy} \\ \left[\varepsilon_{xy} &= \gamma_{xy}/2\right] \end{aligned} \tag{2.41}$$

where $\delta\varepsilon_{x.0}$, $\delta\varepsilon_{y.0}$ and $2\delta\varepsilon_{xy.0}$ are the strain variations at the mid-thickness line of the plate; $\delta\chi_x$, $\delta\chi_y$ and $2\delta\chi_{xy}$ are the variations of curvatures and twisting, respectively; z is the distance of the generic fibre from the mid-thickness line of the plate. The stresses during buckling vary from their

pre-buckling values. Considering the variability of E_s and ν with the stress levels, the variation of the normal stress $\delta\sigma_x$ can be derived from the first of Eqns.(2.37) as follows:

$$\delta\sigma_x = \frac{E_s}{1-\nu^2}\left[\delta(\varepsilon_x) + \nu\delta(\varepsilon_y)\right] + \frac{\delta(E_s)}{1-\nu^2}(\varepsilon_x + \nu\varepsilon_y) + E_s\varepsilon_x\delta\left[\frac{1}{1-\nu^2}\right] + E_s\varepsilon_y\delta\left[\frac{\nu}{1-\nu^2}\right] \tag{2.42}$$

It is worthwhile noting that:

$$\delta(E_s) = \delta\left(\frac{\sigma_i}{\varepsilon_i}\right) = \frac{\delta(\sigma_i)\varepsilon_i - \delta(\varepsilon_i)\sigma_i}{\varepsilon_i^2} = \frac{\delta(\sigma_i)}{\varepsilon_i} - \frac{\delta(\varepsilon_i)\sigma_i}{\varepsilon_i^2} = \frac{\delta(\varepsilon_i)}{\varepsilon_i}(E_t - E_s) \tag{2.43}$$

Where, according to Figure 2.18, E_t is the tangent modulus. Eq.(2.43) can be rearranged as:

$$\delta(E_s) = -\frac{E_s}{\varepsilon_i}\left(1 - \frac{E_t}{E_s}\right)\delta(\varepsilon_i) = -\frac{E_s^2}{\sigma_i}\left(1 - \frac{E_t}{E_s}\right)\delta(\varepsilon_i) \tag{2.44}$$

Besides:

$$\delta\left[\frac{1}{1-\nu^2}\right] = \frac{2\nu}{(1-\nu^2)^2}\delta\nu \tag{2.45}$$

$$\delta\left[\frac{\nu}{1-\nu^2}\right] = \frac{\delta\nu(1-\nu^2) + 2\nu^2\delta\nu}{(1-\nu^2)^2} = \frac{1+\nu^2}{(1-\nu^2)^2}\delta\nu \tag{2.46}$$

$$\delta\nu = \delta\left[\frac{1}{2} - \frac{E_s}{E}\left(\frac{1}{2} - \nu_e\right)\right] = -\left(\frac{1}{2} - \nu_e\right)\frac{\delta(E_s)}{E} = \left(\frac{1/2 - \nu_e}{E}\right)\left(1 - \frac{E_t}{E_s}\right)\frac{E_s^2}{\sigma_i}\delta\varepsilon_i \tag{2.47}$$

By substituting the Eqns.(2.44)-(2.47) into Eq.(2.42), $\delta\sigma_x$ can be expressed as:

$$\delta\sigma_x = \frac{E_s}{1-\nu^2}\left\{\begin{array}{c}(\delta\varepsilon_x + \nu\delta\varepsilon_y) + \frac{1}{2H\sigma_i^2}\left(1 - \frac{E_t}{E_s}\right)\left[\frac{1-2\nu}{2(1-\nu^2)}(\sigma_y + \nu\sigma_x) - \sigma_x\right] \\ \left\{\left[(2-\nu)\sigma_x - (1-2\nu)\sigma_y\right]\delta\varepsilon_x + \left[(2-\nu)\sigma_y - (1-2\nu)\sigma_x\right]\delta\varepsilon_y + \left[3(1-\nu)\tau_{xy}\right]\delta\gamma_{xy}\right\}\end{array}\right\} \tag{2.48}$$

where H is equal to:

$$H = 1 - \frac{1-2\nu}{2(1-\nu^2)}\left(1 - \frac{E_t}{E_s}\right)\left\{2\nu + \frac{1}{2\sigma_i^2}\left[2(\nu+2)\sigma_x\sigma_y - (2\nu+1)\left(\sigma_x^2 + \sigma_y^2\right) - 6(1+\nu)\tau_{xy}^2\right]\right\} \tag{2.49}$$

Similarly, by exchanging x with y and the other way around:

$$\delta\sigma_y = \frac{E_s}{1-\nu^2}\left\{\begin{array}{c}(\delta\varepsilon_y + \nu\delta\varepsilon_x) + \frac{1}{2H\sigma_i^2}\left(1 - \frac{E_t}{E_s}\right)\left[\frac{1-2\nu}{2(1-\nu^2)}(\sigma_x + \nu\sigma_y) - \sigma_y\right] \\ \left\{\left[(2-\nu)\sigma_y - (1-2\nu)\sigma_x\right]\delta\varepsilon_y + \left[(2-\nu)\sigma_x - (1-2\nu)\sigma_y\right]\delta\varepsilon_x + \left[3(1-\nu)\tau_{xy}\right]\delta\gamma_{xy}\right\}\end{array}\right\} \tag{2.50}$$

Starting from Eqns.(2.37) (third):

$$\delta\tau_{xy} = \frac{E_s}{2(1+\nu)}\delta\gamma_{xy} + \gamma_{xy}\left[\frac{\delta(E_s)}{2(1+\nu)} + \frac{E_s}{2}\frac{\delta\nu}{(1+\nu)^2}\right] \tag{2.51}$$

After a few algebraic passages, the variation of the shear stress is given by:

$$\delta\tau_{xy} = \frac{E_s}{2(1-\nu^2)}\left\{\begin{array}{c}(1-\nu)\delta\gamma_{xy} - \frac{3}{2H\sigma_i^2}\left(1 - \frac{E_t}{E_s}\right)\left(\frac{\tau_{xy}}{1+\nu}\right) \\ \left\{\left[(2-\nu)\sigma_x - (1-2\nu)\sigma_y\right]\delta\varepsilon_x + \left[(2-\nu)\sigma_y - (1-2\nu)\sigma_x\right]\delta\varepsilon_y + \left[3(1-\nu)\tau_{xy}\right]\delta\gamma_{xy}\right\}\end{array}\right\} \tag{2.52}$$

Moreover, by combining the variations of strains, provided in Eq.(2.41), with Eqns. (2.48),(2.50),(2.51) and (2.52) , the final expressions of variations of stresses are obtained:

$$\delta\sigma_x = \frac{E_s}{1-\nu^2}\left[\left(\delta\varepsilon_{x.0} + \nu\delta\varepsilon_{y.0}\right) - z\left(\delta\chi_x + \nu\delta\chi_y\right) - \Psi\sigma_x S_x(\mathrm{K}_\varepsilon - z\mathrm{K}_\chi)\right] \tag{2.53}$$

$$\delta\sigma_y = \frac{E_s}{1-\nu^2}\left[\left(\delta\varepsilon_{y.0} + \nu\delta\varepsilon_{x.0}\right) - z\left(\delta\chi_y + \nu\delta\chi_x\right) - \Psi\sigma_y S_y(\mathrm{K}_\varepsilon - z\mathrm{K}_\chi)\right] \tag{2.54}$$

$$\delta\tau_{xy} = \frac{E_s}{2(1-\nu^2)}\left[2(1-\nu)(\delta\varepsilon_{xy.0} - z\delta\chi_{xy}) - \Psi\tau_{xy} S_{xy}(\mathrm{K}_\varepsilon - z\mathrm{K}_\chi)\right] \tag{2.55}$$

where the coefficients Ψ, S_x, S_y, S_{xy}, K_ε and K_χ are expressed as:

$$\begin{aligned}
\Psi &= \frac{1}{2H\sigma_i^2}\left(1 - \frac{E_t}{E_s}\right) \\
S_x &= 1 - \frac{1-2\nu}{2(1-\nu^2)}\frac{\left(\sigma_y + \nu\sigma_x\right)}{\sigma_x} \\
S_y &= 1 - \frac{1-2\nu}{2(1-\nu^2)}\frac{\left(\sigma_x + \nu\sigma_y\right)}{\sigma_y} \\
S_{xy} &= \frac{3}{(1+\nu)}
\end{aligned} \tag{2.56}$$

$$\mathrm{K}_\varepsilon = k_x\sigma_x\delta\varepsilon_{x.0} + k_y\sigma_y\delta\varepsilon_{y.0} + k_{xy}\tau_{xy}\delta\varepsilon_{xy.0}$$

$$\mathrm{K}_\chi = k_x\sigma_x\delta\chi_x + k_y\sigma_y\delta\chi_y + k_{xy}\tau_{xy}\delta\chi_{xy}$$

while k_x, k_y and k_{xy} are equal to:

$$\begin{aligned}
k_x &= (2-\nu) - (1-2\nu)\frac{\sigma_y}{\sigma_x} \\
k_y &= (2-\nu) - (1-2\nu)\frac{\sigma_x}{\sigma_y} \\
k_{xy} &= 6(1-\nu)
\end{aligned} \tag{2.57}$$

The intermediate steps to determine the final expressions of Eqns.(2.53),(2.54) and (2.55) are provided in the Appendix A.

2.3.4. Variation of Internal Actions in Thin Plates

The variations of the bending moments and the twisting moment due to buckling are given by:

$$\delta M_x = \int_{-t/2}^{+t/2} \delta\sigma_x \cdot z dz \qquad \delta M_y = \int_{-t/2}^{+t/2} \delta\sigma_y \cdot z dz \qquad \delta M_{xy} = \int_{-t/2}^{+t/2} \delta\tau_{xy} \cdot z dz \tag{2.58}$$

By substituting Eq. (2.53) into Eq.(2.58) (first), the variation δM_x is equal to:

$$\delta M_x = -\frac{E_s t^3}{12(1-\nu^2)}\left[\delta\chi_x + \nu\delta\chi_y - \Psi\sigma_x S_x \mathrm{K}_\chi\right] \tag{2.59}$$

By explaining the quantity K_χ, through the relation provided in (2.56), it results:

$$\begin{aligned}\delta M_x &= -\frac{E_s t^3}{12(1-\nu^2)}\left[\delta\chi_x + \nu\delta\chi_y - \Psi\sigma_x S_x(k_x\sigma_x\delta\chi_x + k_y\sigma_y\delta\chi_y + k_{xy}\tau_{xy}\delta\chi_{xy})\right] \\ \delta M_x &= -\frac{E_s t^3}{12(1-\nu^2)}\left[\delta\chi_x(1-\Psi\sigma_x^2 k_x S_x) + \delta\chi_y\left(\nu - \Psi\sigma_x\sigma_y k_y S_x\right) - \delta\chi_{xy}\Psi\sigma_x\tau_{xy}k_{xy}S_x\right]\end{aligned} \tag{2.60}$$

Finally, the previous relationship can be rearranged as:

$$\delta M_x = -D_s\left[A_{11}\delta\chi_x + A_{12}\delta\chi_y + A_{13}\delta\chi_{xy}\right] \tag{2.61}$$

where D_s represents the flexural rigidity in the elastic-plastic region and it is equal to:

$$D_s = \frac{E_s t^3}{12(1-\nu^2)} \tag{2.62}$$

while the coefficients A_{ij} are equal to:

$$\begin{aligned}A_{11} &= 1 - \Psi\sigma_x^2 k_x S_x = 1 - \frac{\sigma_x^2}{2H\sigma_i^2}\left(1 - \frac{E_t}{E_s}\right)k_x S_x \\ A_{12} &= \nu - \Psi\sigma_x\sigma_y k_y S_x = \nu - \frac{\sigma_x\sigma_y}{2H\sigma_i^2}\left(1 - \frac{E_t}{E_s}\right)k_y S_x \\ A_{13} &= -\Psi\sigma_x\tau_{xy}k_{xy}S_x = -\frac{\sigma_x\tau_{xy}}{2H\sigma_i^2}\left(1 - \frac{E_t}{E_s}\right)k_{xy}S_x\end{aligned} \tag{2.63}$$

Similarly, the variation δM_y can be defined as:

$$\delta M_y = -D_s\left[A_{21}\delta\chi_x + A_{22}\delta\chi_y + A_{23}\delta\chi_{xy}\right] \tag{2.64}$$

where the coefficients A_{ij} are equal to:

$$\begin{aligned}A_{21} &= \nu - \Psi\sigma_x\sigma_y k_x S_y = \nu - \frac{\sigma_x\sigma_y}{2H\sigma_i^2}\left(1 - \frac{E_t}{E_s}\right)k_x S_y \\ A_{22} &= 1 - \Psi\sigma_y^2 k_y S_y = 1 - \frac{\sigma_y^2}{2H\sigma_i^2}\left(1 - \frac{E_t}{E_s}\right)k_y S_y \\ A_{23} &= -\Psi\sigma_y\tau_{xy}k_{xy}S_y = -\frac{\sigma_y\tau_{xy}}{2H\sigma_i^2}\left(1 - \frac{E_t}{E_s}\right)k_{xy}S_y\end{aligned} \tag{2.65}$$

Finally, by substituting Eq. (2.55) into Eq. (2.58) (third), the variation δM_{xy} is provided:

$$\delta M_{xy} = -\frac{E_s t^3}{24(1-\nu^2)}\left[2(1-\nu)\delta\chi_{xy} - \Psi S_\tau^* \tau_{xy}\mathrm{K}_\chi\right] \tag{2.66}$$

By explaining the quantity K_{χ}, it results:

$$\delta M_{xy} = -\frac{D_s}{2}\left[2(1-\nu)\delta\chi_{xy} - \Psi S_{xy}\tau_{xy}(k_x\sigma_x\delta\chi_x + k_y\sigma_y\delta\chi_y + k_{xy}\tau_{xy}\delta\chi_{xy})\right]$$
$$\delta M_{xy} = -\frac{D_s}{2}\left\{-\Psi S_{xy}\tau_{xy}\sigma_x k_x\delta\chi_x - \Psi S_{xy}\tau_{xy}\sigma_y k_y\delta\chi_y + \left[2(1-\nu) - \Psi S_{xy}\tau_{xy}^2 k_{xy}\right]\delta\chi_{xy}\right\} \quad (2.67)$$

Then, the previous equation can be expressed as:

$$\delta M_{xy} = -\frac{D_s}{2}\left[A_{31}\delta\chi_x + A_{32}\delta\chi_y + A_{33}\delta\chi_{xy}\right] \quad (2.68)$$

where the coefficients A_{ij} are equal to:

$$A_{31} = -\Psi\sigma_x\tau_{xy}k_x S_{xy} = -\frac{\sigma_x\tau_{xy}}{2H\sigma_i^2}\left(1-\frac{E_t}{E_s}\right)k_x S_{xy}$$
$$A_{32} = -\Psi\sigma_y\tau_{xy}k_y S_{xy} = -\frac{\sigma_y\tau_{xy}}{2H\sigma_i^2}\left(1-\frac{E_t}{E_s}\right)k_y S_{xy} \quad (2.69)$$
$$A_{33} = 2(1-\nu) - \Psi S_{xy}\tau_{xy}^2 k_{xy} = 2(1-\nu) - \frac{\tau_{xy}^2}{2H\sigma_i^2}\left(1-\frac{E_t}{E_s}\right)k_{xy}S_{xy}$$

2.3.5. Equilibrium Equation at the onset of Buckling

If the plate is subjected to membrane forces only, in the pre-buckling stage, the bending deflection of the plate is equal to zero. Therefore, by denoting with $w = w(x,y)$ the bending deflection of the plate at buckling, the changes in curvatures are given by:

$$\delta\chi_x = \frac{\partial^2 w}{\partial x^2} \qquad \delta\chi_y = \frac{\partial^2 w}{\partial y^2} \qquad \delta\chi_{xy} = \frac{\partial^2 w}{\partial x\partial y} \quad (2.70)$$

In the pre-buckling stage, the plate is in equilibrium under the membrane actions N_x, N_y and N_{xy}. At buckling, the variations of the bending moments and the twisting moments have to assure the equilibrium under the actions resulting from the second-order effects due to the changes in curvatures. Therefore, the differential equation of the plate under in-plane loading at buckling can be written as:

$$\frac{\partial^2(\delta M_x)}{\partial x^2} + 2\frac{\partial^2(\delta M_{xy})}{\partial x\partial y} + \frac{\partial^2(\delta M_y)}{\partial y^2} = N_x\frac{\partial^2 w}{\partial x^2} + 2N_{xy}\frac{\partial^2 w}{\partial x\partial y} + N_y\frac{\partial^2 w}{\partial y^2} \quad (2.71)$$

By substituting Eqns.(2.61), (2.64) and (2.68) into Eq. (2.71) , the plate differential equation becomes:

$$C_1\frac{\partial^4 w}{\partial x^4} - C_2\frac{\partial^4 w}{\partial x^3\partial y} + 2C_3\frac{\partial^4 w}{\partial x^2\partial y^2} - C_4\frac{\partial^4 w}{\partial x\partial y^3} + C_5\frac{\partial^4 w}{\partial y^4} = -\frac{1}{D_s}\left(N_x\frac{\partial^2 w}{\partial x^2} + 2N_{xy}\frac{\partial^2 w}{\partial x\partial y} + N_y\frac{\partial^2 w}{\partial y^2}\right) \quad (2.72)$$

Where the coefficients C_i are equal to:

$$C_1 = A_{11} \quad C_2 = -(A_{13} + A_{31}) \quad 2C_3 = A_{12} + A_{21} + A_{33} \quad C_4 = -(A_{23} + A_{32}) \quad C_5 = A_{22} \quad (2.73)$$

Eq. (67) is an original contribution because, to the best of the author's knowledge, provides the plate buckling differential equation accounting for the variability of the Poisson's ratio in the elastic-plastic range, i.e. as dependent on the stress and strain intensity measure.

Taking into account Eqns. (2.63), (2.65) and (2.69) , accounting for Eq. (2.57), after few passages the following relations are obtained:

$$C_1 = 1 - \frac{1}{4H\sigma_i^2(1-\nu^2)}\left(1-\frac{E_t}{E_s}\right)\left[(2-\nu)\sigma_x - (1-2\nu)\sigma_y\right]^2$$

$$C_2 = \frac{3\tau_{xy}}{H\sigma_i^2(1+\nu)}\left(1-\frac{E_t}{E_s}\right)\left[(2-\nu)\sigma_x - (1-2\nu)\sigma_y\right]$$

$$C_3 = 1 - \frac{1}{4H\sigma_i^2}\left(1-\frac{E_t}{E_s}\right)\left\{\frac{\left[(2-\nu)\sigma_x - (1-2\nu)\sigma_y\right]\left[(2-\nu)\sigma_y - (1-2\nu)\sigma_x\right] + 18\tau_{xy}^2(1-\nu)^2}{1-\nu^2}\right\} \quad (2.74)$$

$$C_4 = \frac{3\tau_{xy}}{H\sigma_i^2(1+\nu)}\left(1-\frac{E_t}{E_s}\right)\left[(2-\nu)\sigma_y - (1-2\nu)\sigma_x\right]$$

$$C_5 = 1 - \frac{1}{4H\sigma_i^2(1-\nu^2)}\left(1-\frac{E_t}{E_s}\right)\left[(2-\nu)\sigma_y - (1-2\nu)\sigma_x\right]^2$$

Aiming to the analysis of aluminium alloy members subjected to local buckling under uniform compression, in the following reference is made to the case of plate uniaxial compression as depicted in Figure 2.2:

$$\begin{aligned}\sigma_x &= \sigma_i \\ \sigma_y &= \tau_{xy} = 0\end{aligned} \quad (2.75)$$

Under uniaxial compression, by substituting Eq. (2.75) into Eq. (2.74) the coefficients C_i are simplified as follows:

$$C_1 = 1 - \frac{(2-\nu)^2}{4H(1-\nu^2)}\left(1-\frac{E_t}{E_s}\right)$$

$$C_2 = 0$$

$$C_3 = 1 + \frac{(2-\nu)(1-2\nu)}{4H(1-\nu^2)}\left(1-\frac{E_t}{E_s}\right) \quad (2.76)$$

$$C_4 = 0$$

$$C_5 = 1 - \frac{(1-2\nu)^2}{4H(1-\nu^2)}\left(1-\frac{E_t}{E_s}\right)$$

Besides, Eq. (2.49) provides:

$$H = 1 + \frac{(1-2\nu)^2}{4(1-\nu^2)}\left(1-\frac{E_t}{E_s}\right) \quad (2.77)$$

So, the differential equation of a single plate under uniform compression in the elastic-plastic range is equal to:

$$C_1 \frac{\partial^4 w}{\partial x^4} + 2C_3 \frac{\partial^4 w}{\partial x^2 \partial y^2} + C_5 \frac{\partial^4 w}{\partial y^4} = -\frac{N}{D_s} \frac{\partial^2 w}{\partial x^2} \tag{2.78}$$

In Table 2.1, a comparison of the final expressions of coefficients C_i is reported in the different theories of the plate stability. Starting from the relationships in the elastic-plastic range, it is easy to observe that, by imposing $\nu = \nu_e = 0.30$ and $E_s = E_t = E$, the buckling differential equation represents the elastic buckling criterion proposed by De Saint Venant [2.1]; while fixed $\nu = \nu_p = 0.50$, the Eq. (2.78) returns the well-known plastic buckling equation provided by *Yliushin and Stowell* in [2.17], [2.18].

Table 2.1.Comparison of expressions of coefficients C_i in the elastic, plastic and elastoplastic regions.

ELASTIC REGION (***De Saint Venant***) $\nu = 0.30 - E_s = E_t = E$	**ELASTIC-PLASTIC REGION** $\nu = variable$	**PLASTIC REGION** (***Yliushin-Stowell***) $\nu = 0.50$
$C_1 = 1$	$C_1 = 1 - \left[\frac{(2-\nu)^2}{4H(1-\nu^2)}\right]\left(1 - \frac{E_t}{E_s}\right)$	$C_1 = \frac{1}{4} + \frac{3}{4}\left(\frac{E_t}{E_s}\right)$
$C_2 = 0$	$C_2 = 0$	$C_2 = 0$
$C_3 = 1$	$C_3 = 1 + \left[\frac{(1-2\nu)(2-\nu)}{4H(1-\nu^2)}\right]\left(1 - \frac{E_t}{E_s}\right)$	$C_3 = 1$
$C_4 = 0$	$C_4 = 0$	$C_4 = 0$
$C_5 = 1$	$C_5 = 1 - \left[\frac{(1-2\nu)^2}{4H(1-\nu^2)}\right]\left(1 - \frac{E_t}{E_s}\right)$	$C_5 = 1$
$H = 1$	$H = 1 + \frac{(1-2\nu)^2}{4(1-\nu^2)}\left(1 - \frac{E_t}{E_s}\right)$	$H = 1$

The solution of the differential equation (2.78) can be found according to Levy's form presented in Section 2.2.3. In particular, by substituting Eq.(2.12) into Eq. (2.78), it results:

$$\frac{d^4 f}{dy^4} - \frac{2C_3\lambda^2}{C_5}\frac{d^2 f}{dy^2} + \left(\frac{C_1\lambda^4}{C_5} - \frac{N\lambda^2}{D_s C_5}\right) f(y) = 0 \tag{2.79}$$

where $\lambda = m\pi/a$ and the trivial solution $sin\lambda x = 0$ has been neglected. The solution of the differential equation (2.79) can be easily found through the same general solution, presented in the only elastic range, specifically in Eq. (2.16), where a_i always represent the unknown constants of integration, while α and β are expressed as:

$$\alpha = \sqrt{\frac{C_3\lambda^2}{C_5} + \sqrt{\left(\frac{C_3}{C_5}\right)^2 \lambda^4 - \lambda^2\left(\lambda^2\frac{C_1}{C_5} - \frac{N}{D_s C_5}\right)}}$$

$$\beta = \sqrt{-\frac{C_3\lambda^2}{C_5} + \sqrt{\left(\frac{C_3}{C_5}\right)^2 \lambda^4 - \lambda^2\left(\lambda^2\frac{C_1}{C_5} - \frac{N}{D_s C_5}\right)}} \tag{2.80}$$

The integration constants have to be derived accounting for the boundary conditions. The writing of the boundary conditions can concern kinematic conditions (i.e. displacements and rotations) and static conditions (i.e. internal actions). Regarding the internal actions, the variation of the bending moments and the twisting moment are simplified as follows:

$$\delta M_x = -D_s\left[C_1\frac{\partial^2 w}{\partial x^2} + (\nu + C_3 - 1)\frac{\partial^2 w}{\partial y^2}\right]$$

$$\delta M_y = -D_s\left[C_5\frac{\partial^2 w}{\partial y^2} + (\nu + C_3 - 1)\frac{\partial^2 w}{\partial x^2}\right] \tag{2.81}$$

$$\delta M_{xy} = -D_s(1-\nu)\frac{\partial^2 w}{\partial x \partial y}$$

Therefore, the variations of the shear actions are given by:

$$\delta V_x = \frac{\partial(\delta M_x)}{\partial x} + \frac{\partial(\delta M_{xy})}{\partial y} = -D_s\left[C_1\frac{\partial^3 w}{\partial x^3} + C_3\frac{\partial^3 w}{\partial x \partial y^2}\right]$$

$$\delta V_y = \frac{\partial(\delta M_y)}{\partial y} + \frac{\partial(\delta M_{xy})}{\partial x} = -D_s\left[C_5\frac{\partial^3 w}{\partial y^3} + C_3\frac{\partial^3 w}{\partial x^2 \partial y}\right] \tag{2.82}$$

Finally, the edge equivalent shear actions are given by:

$$\delta R_x^* = \delta V_x + \frac{\partial(\delta M_{xy})}{\partial y} = -D_s\left[C_1\frac{\partial^3 w}{\partial x^3} + (C_3 + 1 - \nu)\frac{\partial^3 w}{\partial x \partial y^2}\right]$$

$$\delta R_y^* = \delta V_y + \frac{\partial(\delta M_{xy})}{\partial x} = -D_s\left[C_5\frac{\partial^3 w}{\partial y^3} + (C_3 + 1 - \nu)\frac{\partial^3 w}{\partial x^2 \partial y}\right] \tag{2.83}$$

2.3.6. Correction Factor of Plastic Buckling

As described previously, following an eulerian approach, the solution of the elastic-plastic buckling equation can only be solved by means of an iterative procedure, taking into account that the mechanical properties (Poisson's ratio, secant and tangent moduli) depend on the stress level.

Conversely, the energy method allows to obtain a solution in closed form but approximate. The accuracy of which depends upon how closely the assumed deflection surface describes the true deflection surface. However, by using this approach, it is possible to define a correction factor ξ which taking into account the mechanical nonlinearity and it depends on the boundary conditions along the unloaded sides. This factor can be obtained as:

$$\xi = \frac{\sigma_{cr.p}}{\sigma_{cr.e}} \tag{2.84}$$

where $\sigma_{cr.e}$ and $\sigma_{cr.p}$ represent, respectively, the elastic and the elastic-plastic critical stress of a single plate under compression. Obviously, if ξ and $\sigma_{cr.e}$ are known, remembering Eq. (2.11), the elastic-plastic buckling stress can be expressed as:

$$\sigma_{cr.p} = \xi\sigma_{cr.e} = \xi k \frac{\pi^2 E}{12(1-\nu_e^2)(b/t)^2} \tag{2.85}$$

Starting from the results provided by *Stowell* in [2.17], the formulation of ξ is provided in the elastic-plastic region and for different boundary conditions. In particular, two cases are considered: the plate supported along three sides while the last edge is free, and the rectangular plate supported along edges. In addition, the formulations are derived under the assumption that the unloaded sides are elastically restrained. The restraint coefficient ϵ depends upon the relative stiffness of the plate and the restraining element along the side edge of the plate. The simplest relation of ϵ is obtained when the restraining element, or stiffness, is assumed to be replaced by an elastic medium in which rotation at one point does not influence rotation at another point [2.19], [2.20]. For this type of restraining medium along the edge of the plate, ϵ can be expressed as:

$$\epsilon = \frac{4S_0 b}{D_e} \tag{2.86}$$

where S_0 is the stiffness per unit length of elastic restraining medium or moment required to rotate a unit length of elastic medium through one-fourth radian; D_e represents the elastic flexural rigidity of the plate provided in Eq. (2.2) while b is the width of the plate. So, according to energy method, the critical stress in the elastic region, in the case of uniform compression, can be expressed as:

$$\sigma_{cr.e} = \frac{D_e}{t} \frac{\iint \left[\left(\frac{\partial^2 w}{\partial x^2}\right)^2 + \left(\frac{\partial^2 w}{\partial x \partial y}\right)^2 + \left(\frac{\partial^2 w}{\partial x^2}\frac{\partial^2 w}{\partial y^2}\right) + \left(\frac{\partial^2 w}{\partial y^2}\right)^2\right] dxdy + \frac{\epsilon}{b}\int \left[\left(\frac{\partial w}{\partial y}\right)_{y=y_0}\right]^2 dx}{\iint \left(\frac{\partial w}{\partial x}\right)^2 dxdy} \tag{2.87}$$

The quantity $\frac{\epsilon}{b}\int \left[\left(\frac{\partial w}{\partial y}\right)_{y=y_0}\right]^2 dx$ represents the strain energy due to the elastically restraining side, while y_0 is the edge coordinate. By replacing D_e with flexural rigidity in elastoplastic region D_s and

taking into account the coefficients C_i provided in the previous section, the elastoplastic critical stress can be expressed by the following energy integrals:

$$\sigma_{cr.p} = \frac{D_s}{t}\frac{\iint\left[C_1\left(\frac{\partial^2 w}{\partial x^2}\right)^2 + C_3\left(\frac{\partial^2 w}{\partial x \partial y}\right)^2 + C_3\left(\frac{\partial^2 w}{\partial x^2}\frac{\partial^2 w}{\partial y^2}\right) + C_5\left(\frac{\partial^2 w}{\partial y^2}\right)^2\right]dxdy + \frac{\epsilon}{b}\int\left[\left(\frac{\partial w}{\partial y}\right)_{y=y_0}\right]^2 dx}{\iint\left(\frac{\partial w}{\partial x}\right)^2 dxdy} \quad (2.88)$$

Assuming a specific deflection $w(x, y)$, the coefficient ξ can be defined by means of Eqns. (2.86), (2.87) and (2.88).

Case I: the edge $y = 0$ is elastically restrained - the edge $y = b$ is free

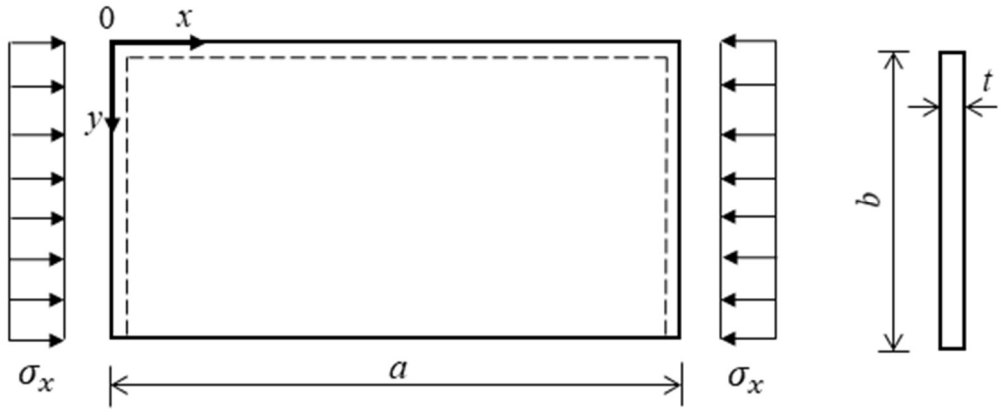

Figure 2.19. Scheme of a plate with one free edge and the other elastically restrained under uniform compression.

According to Figure 2.19, if $y = 0$ is the elastically restrained edge and $y = b$ is the free edge, a deflection surface, satisfying these conditions with a good accuracy, is provided by *Lundquist and Stowell* in [2.19]:

$$w(x, y) = \left\{\frac{y}{b} + \frac{\epsilon}{2\alpha_3}\left[\left(\frac{y}{b}\right)^5 + \alpha_1\left(\frac{y}{b}\right)^4 + \alpha_2\left(\frac{y}{b}\right)^3 + +\alpha_3\left(\frac{y}{b}\right)^2\right]\right\} cos\lambda x \quad (2.89)$$

where $\lambda = m\pi/a$ while α_i represent the fitting coefficients and they are equal to:

$$\alpha_1 = -4.963 \qquad \alpha_2 = 9.852 \qquad \alpha_1 = -9.778 \quad (2.90)$$

By substituting Eq. (2.89) into Eq. (2.88), and taking into account that $y_0 = 0$, the elastoplastic critical stress can be expressed as:

$$\sigma_{cr.p} = \frac{D_s}{t}\left[\frac{\lambda^2 C_1\left(\frac{1}{6} + \kappa_1\frac{\epsilon}{2} + \kappa_2\frac{\epsilon^2}{2}\right) + \frac{C_3}{b^2}\left(\frac{1}{2} + (\kappa_3 - \kappa_5)\frac{\epsilon}{2} + (\kappa_4 - \kappa_6)\frac{\epsilon^2}{2}\right) + \frac{1}{2\lambda^2 b^4}(C_5\kappa_7\epsilon^2 + \epsilon)}{\frac{1}{6} + \kappa_8\frac{\epsilon}{2} + \kappa_9\frac{\epsilon^2}{2}}\right] \quad (2.91)$$

where the coefficients κ_i are equal to:

$$\begin{aligned} \kappa_1 &= 0.11847 & \kappa_4 &= 0.04391 & \kappa_7 &= 0.14178 \\ \kappa_2 &= 0.010715 & \kappa_5 &= 0.04924 & \kappa_8 &= 0.11847 \\ \kappa_3 &= 0.3977 & \kappa_5 &= 0.005429 & \kappa_9 &= 0.01072 \end{aligned} \tag{2.92}$$

The intermediate steps to define Eq. (2.91) are reported in Appendix B. In order to find the minimum value of $\sigma_{cr.p}$, it is necessary to impose the variation of stress with respect to that of λ^2 equal to zero:

$$\frac{\partial \sigma_{cr.p}}{\partial \lambda^2} = 0 \tag{2.93}$$

which gives:

$$\lambda^2 = \frac{1}{b^2}\sqrt{\frac{\frac{1}{2b^4}(C_5\kappa_7\epsilon^2+\epsilon)}{C_1\left(\frac{1}{6}+\kappa_1\frac{\epsilon}{2}+\kappa_2\frac{\epsilon^2}{2}\right)}} \tag{2.94}$$

By substituting Eq. (2.94) into Eq. (2.91), it results:

$$\sigma_{cr.p} = \frac{D_s}{tb^2}\left[\frac{2\sqrt{\frac{C_1}{2}\left(\frac{1}{6}+\kappa_1\frac{\epsilon}{2}+\kappa_2\frac{\epsilon^2}{2}\right)(C_5\kappa_7\epsilon^2+\epsilon)}+C_3\left(\frac{1}{2}+(\kappa_3-\kappa_5)\frac{\epsilon}{2}+(\kappa_4-\kappa_6)\frac{\epsilon^2}{2}\right)}{\frac{1}{6}+\kappa_8\frac{\epsilon}{2}+\kappa_9\frac{\epsilon^2}{2}}\right] \tag{2.95}$$

For the elastic case, the same expression is obtained with $C_1 = C_3 = C_5 = 1$ and D_s replaced by D_e:

$$\sigma_{cr.e} = \frac{D_e}{tb^2}\left[\frac{2\sqrt{\frac{1}{2}\left(\frac{1}{6}+\kappa_1\frac{\epsilon}{2}+\kappa_2\frac{\epsilon^2}{2}\right)(\kappa_7\epsilon^2+\epsilon)}+\left(\frac{1}{2}+(\kappa_3-\kappa_5)\frac{\epsilon}{2}+(\kappa_4-\kappa_6)\frac{\epsilon^2}{2}\right)}{\frac{1}{6}+\kappa_8\frac{\epsilon}{2}+\kappa_9\frac{\epsilon^2}{2}}\right] \tag{2.96}$$

By substituting Eqns. (2.95) and (2.96) into Eq. (2.84), the final expression of ξ is given by:

$$\xi = \frac{D_s}{D_e}\left[\frac{2\sqrt{\frac{C_1}{2}\left(\frac{1}{6}+\kappa_1\frac{\epsilon}{2}+\kappa_2\frac{\epsilon^2}{2}\right)(C_5\kappa_7\epsilon^2+\epsilon)}+C_3\left(\frac{1}{2}+(\kappa_3-\kappa_5)\frac{\epsilon}{2}+(\kappa_4-\kappa_6)\frac{\epsilon^2}{2}\right)}{2\sqrt{\frac{1}{2}\left(\frac{1}{6}+\kappa_1\frac{\epsilon}{2}+\kappa_2\frac{\epsilon^2}{2}\right)(\kappa_7\epsilon^2+\epsilon)}+\left(\frac{1}{2}+(\kappa_3-\kappa_5)\frac{\epsilon}{2}+(\kappa_4-\kappa_6)\frac{\epsilon^2}{2}\right)}\right] \tag{2.97}$$

According to level of elastic constraint, expressed by ϵ, it is possible to identify two limit schemes:

a. $\boldsymbol{\epsilon = 0 \Rightarrow y = 0}$ ***is hinged***

From the condition a. and remembering the expression of the flexural rigidities and the values of coefficients κ_i, the Eq. (2.97) becomes:

$$\xi = C_3 \left(\frac{1 - \nu_e^2}{1 - \nu^2} \right) \frac{E_s}{E} \tag{2.98}$$

b. $\boldsymbol{\epsilon \to \infty \Rightarrow y = 0}$ ***is clamped***

From the condition b. and remembering the expression of the flexural rigidities and the values of coefficients κ_i, the Eq. (2.97) becomes:

$$\xi = \left[0.33 C_3 + 0.67 \sqrt{C_1 C_5} \right] \left(\frac{1 - \nu_e^2}{1 - \nu^2} \right) \frac{E_s}{E} \tag{2.99}$$

The expressions of ξ are functions of the variability of Poisson's ratio and the secant and tangent moduli through the elastoplastic coefficients C_i.

Moreover, it is easy to observe that these relationships return the final expressions provided by *Stowell* in [2.17] under the assumption of only plastic case. In fact, by fixing the Poisson's ratio equal to 0.50 and remembering the values of plastic coefficients C_i reported in Table 2.1, it results:

$$\begin{gathered} \xi = \frac{E_s}{E} \; if \; y = 0 \; is \; hinged \\ \xi = \left[0.33 + 0.67 \sqrt{\frac{1}{4} + \frac{3}{4} \left(\frac{E_t}{E_s} \right)} \right] \frac{E_s}{E} \; if \; y = 0 \; is \; clamped \end{gathered} \tag{2.100}$$

Figure 2.20 shows a comparison between Eq.(2.98) and (2.99). In particular, according to the nominal mechanical properties of EN-AW 6082 aluminium alloy [$f_{0.2} = 260$ MPa; $n = 25$], the trend between the stress values and the values obtained by the previous formulations are reported. It is possible to observe that, for a fixed value of stress, the coefficient referring to a plate with the hinged edge is greater than the coefficient referring to a plate with clamped edge. All others intermediate conditions are included between the previous boundary schemes and they are expressed by the general relationship, Eq. (2.97), depending on the level of elastic constraint ϵ.

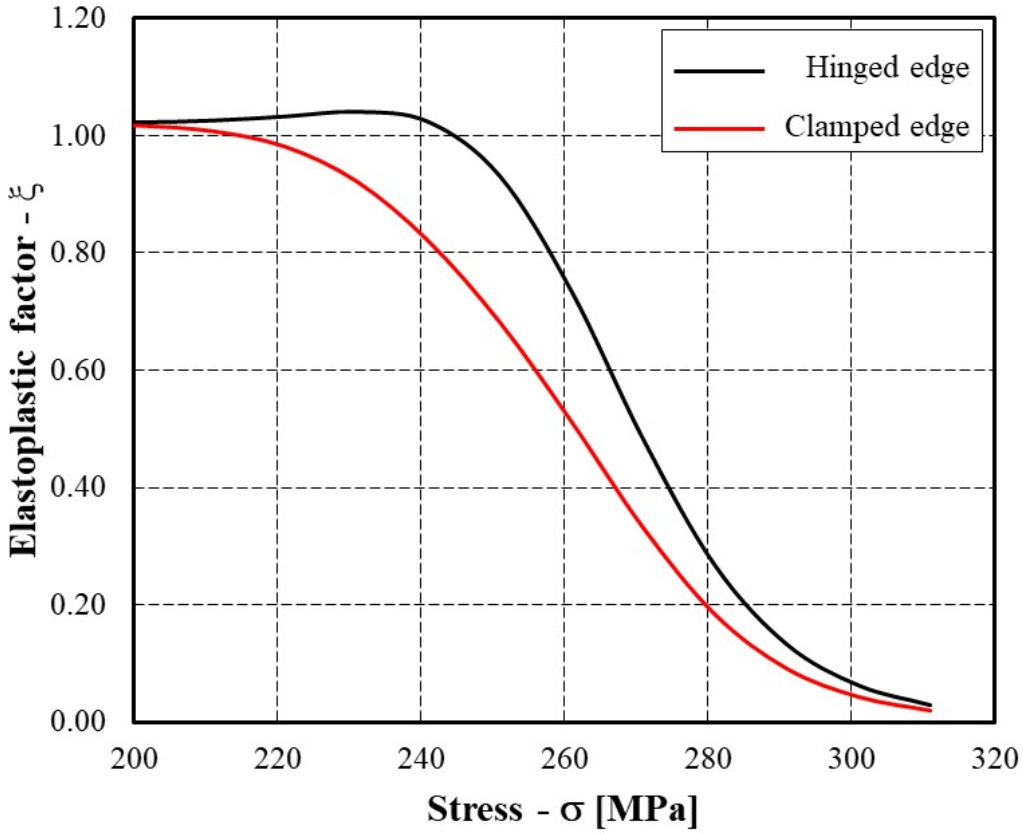

Figure 2.20. Elastoplastic coefficient-stress curves referring to a single plate with one free edge and the other restrained.

Case II: Plate elastically restrained along two unloaded sides ($y = \pm b/2$)

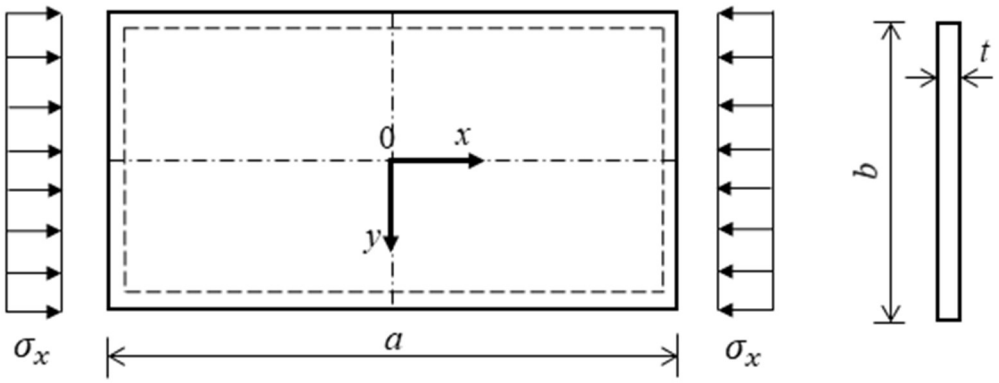

Figure 2.21. Scheme of a plate with unloaded edges elastically restrained under uniform compression.

According to Figure 2.21, if $y = \pm b/2$ are the elastically restrained, a deflection surface, satisfying these conditions with a good accuracy, is provided by *Lundquist and Stowell* in [2.20]:

$$w(x,y) = \left[e_1\left(\frac{y}{b}\right)^2 + e_2 cosBy - \frac{e_1}{4}\right] cos\lambda x \tag{2.101}$$

where:

$$e_1 = \frac{\pi\epsilon}{2} \qquad e_2 = 1 + \frac{\epsilon}{2} \qquad B = \frac{\pi}{b} \tag{2.102}$$

By substituting Eq. (2.101) into Eq. (2.88), and taking into account that $y_0 = -b/2$, the elastoplastic critical stress can be expressed as:

$$\sigma_{cr.p} = \frac{D_s}{t}\left[\frac{\frac{a\lambda^4 C_1}{2}\left(\frac{e_1^2 b}{30} - \frac{8e_1e_2}{b^2B^3} + \frac{e_2^2 b}{2}\right) + a\lambda^2 C_3\left(\frac{e_1^2}{3b} - \frac{8e_1e_2}{b^2B} + \frac{e_2^2 bB^2}{2}\right) + \frac{aC_5}{2}\left(\frac{4e_1^2}{b^3} - \frac{8e_1e_2}{b^2} + \frac{e_2^2 bB^4}{2}\right) + \frac{a\epsilon}{2b}\left(\frac{e_1^2}{b^2} - \frac{2e_1e_2B}{b^2} + e_2^2B^2\right)}{\frac{a\lambda^2}{2}\left(\frac{e_1^2 b}{30} - \frac{8e_1e_2}{b^2B^3} + \frac{e_2^2 b}{2}\right)}\right] \tag{2.103}$$

The intermediate steps to define Eq. (2.103) are reported in Appendix C. In order to find the minimum value of $\sigma_{cr.p}$, it is necessary to impose the variation of stress with respect to that of λ^2 equal to zero from which λ^2 can be expressed as:

$$\lambda^2 = \sqrt{\frac{\frac{aC_5}{2}\left(\frac{4e_1^2}{b^3} - \frac{8e_1e_2}{b^2} + \frac{e_2^2 bB^4}{2}\right) + \frac{\epsilon}{2b}\left(\frac{e_1^2}{b^2} - \frac{2e_1e_2B}{b^2} + e_2^2B^2\right)}{\frac{C_1}{2}\left(\frac{e_1^2 b}{30} - \frac{8e_1e_2}{b^2B^3} + \frac{e_2^2 b}{2}\right)}} \tag{2.104}$$

By substituting Eq. (2.104)into Eq. (2.103), it results:

$$\sigma_{cr.p} = \frac{D_s}{t}\left\{2\sqrt{\frac{C_1\left[C_5\left(\frac{4e_1^2}{b^3} - \frac{8e_1e_2}{b^2} + \frac{e_2^2 bB^4}{2}\right) + \frac{\epsilon}{b}\left(\frac{e_1^2}{b^2} - \frac{2e_1e_2B}{b^2} + e_2^2B^2\right)\right]}{\left(\frac{e_1^2 b}{30} - \frac{8e_1e_2}{b^2B^3} + \frac{e_2^2 b}{2}\right)}} + 2C_3\frac{\left(\frac{e_1^2}{3b} - \frac{8e_1e_2}{b^2B} + \frac{e_2^2 bB^2}{2}\right)}{\left(\frac{e_1^2 b}{30} - \frac{8e_1e_2}{b^2B^3} + \frac{e_2^2 b}{2}\right)}\right\} \tag{2.105}$$

For the elastic case, the same expression is obtained with $C_1 = C_3 = C_5 = 1$ and D_s replaced by D_e:

$$\sigma_{cr.e} = \frac{D_e}{t}\left\{2\sqrt{\frac{\left[\left(\frac{4e_1^2}{b^3} - \frac{8e_1e_2}{b^2} + \frac{e_2^2 bB^4}{2}\right) + \frac{\epsilon}{b}\left(\frac{e_1^2}{b^2} - \frac{2e_1e_2B}{b^2} + e_2^2B^2\right)\right]}{\left(\frac{e_1^2 b}{30} - \frac{8e_1e_2}{b^2B^3} + \frac{e_2^2 b}{2}\right)}} + 2\frac{\left(\frac{e_1^2}{3b} - \frac{8e_1e_2}{b^2B} + \frac{e_2^2 bB^2}{2}\right)}{\left(\frac{e_1^2 b}{30} - \frac{8e_1e_2}{b^2B^3} + \frac{e_2^2 b}{2}\right)}\right\} \tag{2.106}$$

By substituting Eqns. (2.105)and (2.106) into Eq. (2.84), the final expression of ξ is given by:

$$\xi = \frac{D_s}{D_e}\frac{\left\{2\sqrt{\frac{C_1\left[C_5\left(\frac{4e_1^2}{b^3} - \frac{8e_1e_2}{b^2} + \frac{e_2^2 bB^4}{2}\right) + \frac{\epsilon}{b}\left(\frac{e_1^2}{b^2} - \frac{2e_1e_2B}{b^2} + e_2^2B^2\right)\right]}{\left(\frac{e_1^2 b}{30} - \frac{8e_1e_2}{b^2B^3} + \frac{e_2^2 b}{2}\right)}} + 2C_3\frac{\left(\frac{e_1^2}{3b} - \frac{8e_1e_2}{b^2B} + \frac{e_2^2 bB^2}{2}\right)}{\left(\frac{e_1^2 b}{30} - \frac{8e_1e_2}{b^2B^3} + \frac{e_2^2 b}{2}\right)}\right\}}{\left\{2\sqrt{\frac{\left[\left(\frac{4e_1^2}{b^3} - \frac{8e_1e_2}{b^2} + \frac{e_2^2 bB^4}{2}\right) + \frac{\epsilon}{b}\left(\frac{e_1^2}{b^2} - \frac{2e_1e_2B}{b^2} + e_2^2B^2\right)\right]}{\left(\frac{e_1^2 b}{30} - \frac{8e_1e_2}{b^2B^3} + \frac{e_2^2 b}{2}\right)}} + 2\frac{\left(\frac{e_1^2}{3b} - \frac{8e_1e_2}{b^2B} + \frac{e_2^2 bB^2}{2}\right)}{\left(\frac{e_1^2 b}{30} - \frac{8e_1e_2}{b^2B^3} + \frac{e_2^2 b}{2}\right)}\right\}} \tag{2.107}$$

According to level of elastic constraint, expressed by ϵ, it is possible to identify two limit schemes:

a. $\epsilon = 0 \Rightarrow y = \pm b/2$ *are simply supported*

From the condition a. and remembering the expression of the flexural rigidities and the values of coefficients e_i and B, the Eq. (2.107) becomes:

$$\xi = \left[\frac{C_3 + \sqrt{C_1 C_5}}{2}\right]\left(\frac{1-\nu_e^2}{1-\nu^2}\right)\frac{E_s}{E} \tag{2.108}$$

b. $\epsilon \to \infty \Rightarrow y = b/2$ *are clamped*

From the condition b. and remembering the expression of the flexural rigidities and the values of coefficients e_i and B, the Eq. (2.107) becomes:

$$\xi = \left[0.34C_3 + 0.66\sqrt{C_1 C_5}\right]\left(\frac{1-\nu_e^2}{1-\nu^2}\right)\frac{E_s}{E} \tag{2.109}$$

Also in this case, Moreover, it is easy to observe that these relationships return the final expressions provided by *Stowell* in [2.17] under the assumption of only plastic case. In fact, by fixing the Poisson's ratio equal to 0.50 and remembering the values of plastic coefficients C_i reported in Table 2.1, it results:

$$\begin{aligned} \xi &= \left[\frac{1}{2} + \frac{1}{2}\sqrt{\frac{1}{4} + \frac{3}{4}\left(\frac{E_t}{E_s}\right)}\right]\frac{E_s}{E} \; if \; y = \pm\frac{b}{2} are \; simply \; supported \\ \xi &= \left[0.34 + 0.66\sqrt{\frac{1}{4} + \frac{3}{4}\left(\frac{E_t}{E_s}\right)}\right]\frac{E_s}{E} \; if \; y = \pm\frac{b}{2} are \; clamped \end{aligned} \tag{2.110}$$

All previous considerations will be resumed in Chapter 6, where an extension of the effective thickness method is provided for aluminium members under uniform and non-uniform compression in the elastic-plastic range. In particular, by combining Eqns. (2.108) and (2.109) a new formulation will be adopted for deriving a simplified method to evaluate the ultimate behaviour of a generic aluminium members in compression and in bending, taking into account the plastic local buckling and the interaction between the plate elements constituting the cross-section. In particular, the Formulation 1, defined as the average of two previous relationships, is equal to:

$$\xi = \left[0.42C_3 + 0.58\sqrt{C_1 C_5}\right]\left(\frac{1-\nu_e^2}{1-\nu^2}\right)\frac{E_s}{E} \tag{2.111}$$

The trends of previous formulations, Eqns. (2.108), (2.109) and (2.111), depending on the stress level, are depicted in Figure 2.22. The considerations made to the previous condition are also valid in this case. However, in the last one, there is not much difference between the hinged edges and the clamped edges.

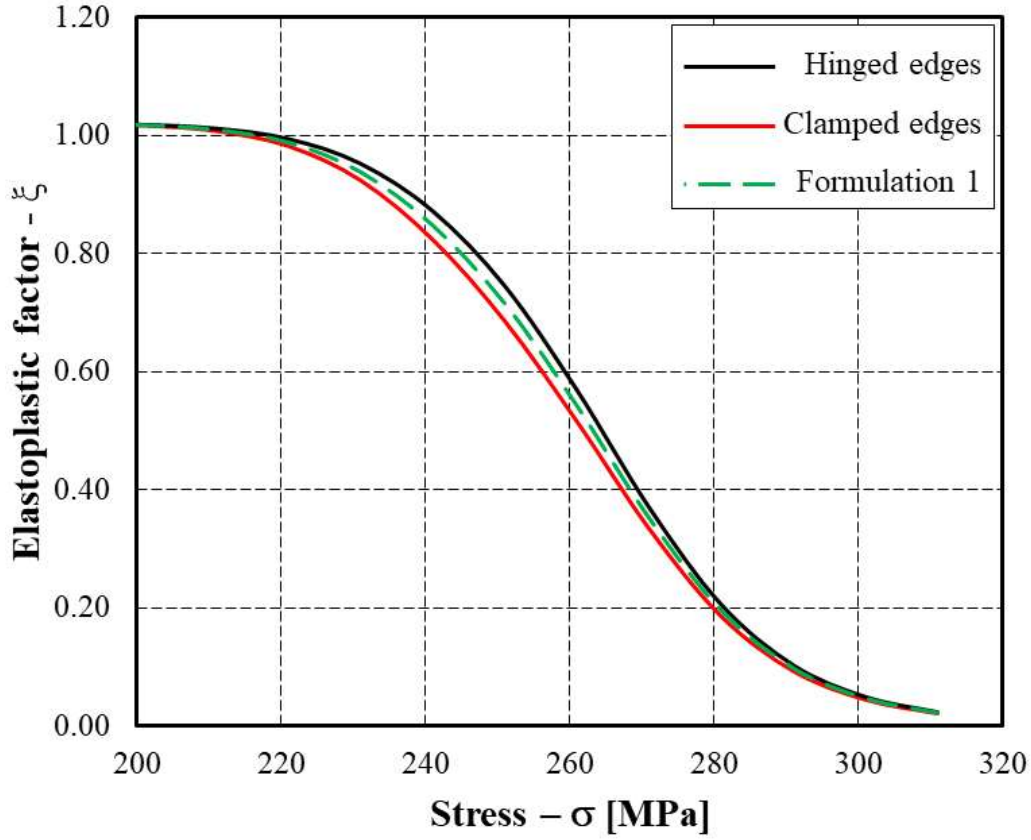

Figure 2.22. Elastoplastic coefficient-stress curves referring to a single plate unloaded restrained edges.

2.4. References

[2.1] **S. Timoshenko:** "Theory of Elastic Stability", McGraw-Hill Book Co., Inc., 1936.

[2.2] **P.S. Bulson:** "The Stability of Flat Plates", Chatto and Windsu, London, 1970.

[2.3] **T.H.G. Megson**: "An introduction to aircraft structural analysis", Butterworth-Heinemann, UK, 2007.

[2.4] **Lord Rayleigh**: "Theory of Sound", 1877.

[2.5] **W. Ritz:** "Journal für Reine und Angewandte Mathematik", vol.135, No. 1, p.1, 1909.

[2.6] **V.G. Galerkin:** "Rods and Plates", Vestnik Ingeneroff, p.897, 1915.

[2.7] **K. Nölke:** "Der Baningenieur", Vol.17, p.111, 1936.

[2.8] **C.F. Kollbrunner, G. Hermann:** "Elastike Beulung von auf einseitgen ungleichunbigen Druk beanspruchten platen. Mitte der T.K.V.S.B.", H.I., p.28, Zurich:Leeman, 1948.

[2.9] **R.M. Jones:** "Deformation Theory of Plasticity", Bull Ridge Publishing, Blacksburg (Virginia) 2009.

[2.10] **J. Blachut, G.D. Galletly and S. James:** "On the plastic buckling paradox for cylindrical shells", Proc. Inst. Mech. Eng. Part C 210, 477–488, 1996.

[2.11] **R. Shamass, G. Alfano, and F. Guarracino:** "A numerical investigation into the plastic buckling paradox for circular cylindrical shells under axial compression", Engineering Structures, Vol.75, pp.429–447, 2014.

[2.12] **R. Shamass:** "Plastic Buckling Paradox: An Updated Review", Frontiers in Built Environment, Vol.6(35), 2020.

[2.13] **H. Yun, and S. Kyriakides:** "On the beam and shell modes of buckling of buried pipelines", Soil Dynamics and Earthquake Engineering, Vol.9, pp.179–193.

[2.14] **A. Nadai:** "Theory of flow and fracture of solids", Volume I, McGraw Hill, New York, 1950.

[2.15] **M.E. Lunchick:** "Plasticity Research on Submarine Pressure Hulls Conducted at the David Taylor Basin", Proceedings of the Second Symposium on Naval Structural Mechanics, Edited by E.H. Lee and P.S. Symonds, Pergamon Press, pp. 347-368, 1960.

[2.16] **G. Gerard and S. Wildhorn:** "A Study of Poisson's Ratio in the Yield Region", NACA Technical Note 2561, National Advisory Committee on Aeronautics, Washington, D.C., 1952.

[2.17] **E.Z. Stowell**: "A Unified Theory of Plastic Buckling of Columns and Plates", National Advisory Committee for Aeronautics, NACA Technical Note n. 1556, Washington, 1948.

[2.18] **A.A. Ilyushin:** "The Elasto-Plastic Stability of Plates", NACA Technical Memorandum 1188, National Advisory Committee on Aeronautics, Washington, D.C., 1946.

[2.19] **E.E. Lundquist and E.Z. Stowell**: "Critical Compressive Stress for Outstanding Flanges", National Advisory Committee for Aeronautics, NACA Technical Note n. 734, Washington, 1942.

[2.20] **E.E. Lundquist and E.Z. Stowell**: "Critical Compressive Stress for Flat Rectangular Plates Supported along All Edges and Elastically Restrained against Rotation along the Unloaded Edges", National Advisory Committee for Aeronautics, NACA Technical Note n. 733, Washington, 1942.

Appendix A

Intermediate Steps for Determining the Final Expressions of $\delta\sigma_x$,$\delta\sigma_y$ and $\delta\tau_{xy}$

By substituting Eqns. (2.44)-(2.47) into Eq.(2.42), the following relation for $\delta\sigma_x$ is obtained:

$$\delta\sigma_x = \frac{E_s}{1-\nu^2}\left\{ (\delta\varepsilon_x + \nu\delta\varepsilon_y) - \frac{E_s}{\sigma_i}\left(1-\frac{E_t}{E_s}\right)\left[(\varepsilon_x + \nu\varepsilon_y) - \left(\frac{1/2 - \nu_e}{E}\right)\left(\frac{2\nu E_s\varepsilon_x + (1+\nu^2)E_s\varepsilon_y}{1-\nu^2}\right)\right]\delta\varepsilon_i\right\} \quad \text{(A.1)}$$

To apply Eq. (A.1), the variation of the strain intensity has to be expressed as a function of the stress levels and the variation of the strains. To this scope, it is convenient to rearrange Eq.(2.36) as follows:

$$\varepsilon_i = \frac{1}{1-\nu^2}\sqrt{\Phi} \quad \text{(A.2)}$$

where:

$$\Phi = (1-\nu+\nu^2)\left(\varepsilon_x^2 + \varepsilon_y^2\right) - (1-4\nu+\nu^2)\varepsilon_x\varepsilon_y + \frac{3}{4}(1-\nu)^2\gamma_{xy}^2 \quad \text{(A.3)}$$

so that:

$$\delta\varepsilon_i = \delta\left(\frac{1}{1-\nu^2}\right)\sqrt{\Phi} + \frac{1}{1-\nu^2}\frac{\delta\Phi}{2\sqrt{\Phi}} \quad \text{(A.4)}$$

From Eq. (A.3):

$$\delta\Phi = \psi_1\delta\nu + \psi_2 \quad \text{(A.5)}$$

where:

$$\psi_1 = 2(2-\nu)\varepsilon_x\varepsilon_y - (1-2\nu)\left(\varepsilon_x^2 + \varepsilon_y^2\right) - \frac{3}{2}(1-\nu)\gamma_{xy}^2 \quad \text{(A.6)}$$

and:

$$\psi_2 = 2(1-\nu+\nu^2)\left(\varepsilon_x\delta\varepsilon_x + \varepsilon_y\delta\varepsilon_y\right) - (1-4\nu+\nu^2)\left(\varepsilon_y\delta\varepsilon_x + \varepsilon_x\delta\varepsilon_y\right) + \frac{3}{2}(1-\nu)^2\gamma_{xy}\delta\gamma_{xy} \quad \text{(A.7)}$$

By combining Eq. (2.45) and (A.5) with Eq. (A.6), the variation of the strain intensity can be expressed as:

$$\delta\varepsilon_i = \left[\frac{2\nu\sqrt{\Phi}}{(1-\nu^2)^2} + \frac{\psi_1}{2(1-\nu^2)\sqrt{\Phi}}\right]\delta\nu + \frac{\psi_2}{2(1-\nu^2)\sqrt{\Phi}} \quad \text{(A.8)}$$

Combining Eq. (2.47) and Eq. (A.4), the following relation is obtained:

$$\delta\varepsilon_i\left\{1 - \left(\frac{1/2 - \nu_e}{E}\right)\left(1-\frac{E_t}{E_s}\right)\frac{E_s^2}{\sigma_i}\left[\frac{2\nu\sqrt{\Phi}}{(1-\nu^2)^2} + \frac{\psi_1}{2(1-\nu^2)\sqrt{\Phi}}\right]\right\} = \frac{\psi_2}{2(1-\nu^2)\sqrt{\Phi}} \quad \text{(A.9)}$$

From Eq. (A.2), $\sqrt{\Phi} = \varepsilon_i(1-\nu^2)$, so that, taking into account that $E_s = \sigma_i/\varepsilon_i$, Eq. (A.9) can be rewritten as:

$$\delta\varepsilon_i\left\{1-\left(\frac{1/2-\nu_e}{1-\nu^2}\right)\frac{E_s}{E}\left(1-\frac{E_t}{E_s}\right)\left[2\nu+\frac{\psi_1 E_s^2}{2(1-\nu^2)\sigma_i^2}\right]\right\} = \frac{\psi_2}{2(1-\nu^2)^2\varepsilon_i} \tag{A.10}$$

From Eq. (2.39):

$$\left(\frac{1}{2}-\nu_e\right)\frac{E_s}{E} = \frac{1}{2}-\nu = \frac{1-2\nu}{2} \tag{A.11}$$

Therefore, Eq. (A.10) becomes:

$$\delta\varepsilon_i\left\{1-\frac{1-2\nu}{2(1-\nu^2)}\left(1-\frac{E_t}{E_s}\right)\left[2\nu+\frac{\psi_1 E_s^2}{2(1-\nu^2)\sigma_i^2}\right]\right\} = \frac{\psi_2}{2(1-\nu^2)^2\varepsilon_i} \tag{A.12}$$

By denoting with:

$$H = 1-\frac{1-2\nu}{2(1-\nu^2)}\left(1-\frac{E_t}{E_s}\right)\left[2\nu+\frac{\psi_1 E_s^2}{2(1-\nu^2)\sigma_i^2}\right] \tag{A.13}$$

The variation of the strain intensity can be written as:

$$\delta\varepsilon_i = \frac{\psi_2}{2H(1-\nu^2)^2\varepsilon_i} \tag{A.14}$$

By combining Eqns. (2.40) and (A.6), the parameter ψ_1 can be expressed as a function of stress levels. After some few passages, the following relation is obtained:

$$\psi_1 = \frac{1-\nu^2}{E_s^2}\left\{2(\nu+2)\sigma_x\sigma_y - (2\nu+1)\left(\sigma_x^2+\sigma_y^2\right) - 6(1+\nu)\tau_{xy}^2\right\} \tag{A.15}$$

By substituting Eq. (A.15) into Eq. (A.13), the parameter H is expressed as:

$$H = 1-\frac{1-2\nu}{2(1-\nu^2)}\left(1-\frac{E_t}{E_s}\right)\left\{2\nu+\frac{1}{2\sigma_i^2}\left[2(\nu+2)\sigma_x\sigma_y - (2\nu+1)\left(\sigma_x^2+\sigma_y^2\right) - 6(1+\nu)\tau_{xy}^2\right]\right\} \tag{A.16}$$

Besides, by combining Eq. (A.14) with Eq. (A.7), the strain intensity is given by:

$$\delta\varepsilon_i = \frac{1}{2H\varepsilon_i(1-\nu^2)^2}\left\{2(1-\nu+\nu^2)\left(\varepsilon_x\delta\varepsilon_x+\varepsilon_y\delta\varepsilon_y\right) - (1-4\nu+\nu^2)\left(\varepsilon_y\delta\varepsilon_x+\varepsilon_x\delta\varepsilon_y\right) + \frac{3}{2}(1-\nu)^2\gamma_{xy}\delta\gamma_{xy}\right\} \tag{A.17}$$

Taking into account Eq. (A.11), the stress variation $\delta\sigma_x$, Eq. (A.1), can be written as:

$$\delta\sigma_x = \frac{E_s}{1-\nu^2}\left\{\left(\delta\varepsilon_x+\nu\delta\varepsilon_y\right) - \frac{E_s}{\sigma_i}\left(1-\frac{E_t}{E_s}\right)\left[\left(\varepsilon_x+\nu\varepsilon_y\right) - \frac{1-2\nu}{2(1-\nu^2)}\left(2\nu\varepsilon_x+(1+\nu^2)\varepsilon_y\right)\right]\delta\varepsilon_i\right\} \tag{A.18}$$

By substituting Eqns. (2.40) into Eq. (A.17)(A.17) and taking into account that $E_s = \sigma_i/\varepsilon_i$, after few algebraic passages, the final expression for the strain intensity as a function of the stress levels and strain variations is obtained:

$$\delta\varepsilon_i = \frac{1}{2H\sigma_i(1-\nu^2)}\left\{\left[(2-\nu)\sigma_x - (1-2\nu)\sigma_y\right]\delta\varepsilon_x + \left[(2-\nu)\sigma_y - (1-2\nu)\sigma_x\right]\delta\varepsilon_y + \left[3(1-\nu)\tau_{xy}\right]\delta\gamma_{xy}\right\} \tag{A.19}$$

The stress variation $\delta\sigma_x$, Eq. (A.18), taking into account Eq. (2.37) (first) and Eqns. (2.40), after a few algebraic passages, is given by:

$$\delta\sigma_x = \frac{E_s}{1-\nu^2}\left(\delta\varepsilon_x + \nu\delta\varepsilon_y\right) - \frac{E_s}{\sigma_i}\left(1-\frac{E_t}{E_s}\right)\left[\sigma_x - \frac{1-2\nu}{2(1-\nu^2)}\left(\sigma_y + \nu\sigma_x\right)\right]\delta\varepsilon_i \tag{A.20}$$

Finally, by substituting Eq. (A.19) into Eq. (A.20), the stress variation is expressed as a function of the stress levels and strain variations:

$$\delta\sigma_x = \frac{E_s}{1-\nu^2}\left\{\begin{array}{c}\left(\delta\varepsilon_x + \nu\delta\varepsilon_y\right) + \frac{1}{2H\sigma_i^2}\left(1-\frac{E_t}{E_s}\right)\left[\frac{1-2\nu}{2(1-\nu^2)}\left(\sigma_y+\nu\sigma_x\right) - \sigma_x\right] \\ \left\{\left[(2-\nu)\sigma_x - (1-2\nu)\sigma_y\right]\delta\varepsilon_x + \left[(2-\nu)\sigma_y - (1-2\nu)\sigma_x\right]\delta\varepsilon_y + \left[3(1-\nu)\tau_{xy}\right]\delta\gamma_{xy}\right\}\end{array}\right\} \tag{A.21}$$

Similarly, by exchanging x with y and the other way around:

$$\delta\sigma_y = \frac{E_s}{1-\nu^2}\left\{\begin{array}{c}\left(\delta\varepsilon_y + \nu\delta\varepsilon_x\right) + \frac{1}{2H\sigma_i^2}\left(1-\frac{E_t}{E_s}\right)\left[\frac{1-2\nu}{2(1-\nu^2)}\left(\sigma_x+\nu\sigma_y\right) - \sigma_y\right] \\ \left\{\left[(2-\nu)\sigma_y - (1-2\nu)\sigma_x\right]\delta\varepsilon_y + \left[(2-\nu)\sigma_x - (1-2\nu)\sigma_y\right]\delta\varepsilon_x + \left[3(1-\nu)\tau_{xy}\right]\delta\gamma_{xy}\right\}\end{array}\right\} \tag{A.22}$$

From Eqns. (2.37) (third):

$$\delta\tau_{xy} = \frac{E_s}{2(1+\nu)}\delta\gamma_{xy} + \gamma_{xy}\left[\frac{\delta(E_s)}{2(1+\nu)} + \frac{E_s}{2}\frac{\delta\nu}{(1+\nu)^2}\right] \tag{A.23}$$

Accounting for Eq. (2.44), (2.47) and (A.11), after a few algebraic passages, the variation of the shear stress is given by:

$$\delta\tau_{xy} = \frac{E_s}{2(1-\nu^2)}\left\{(1-\nu)\delta\gamma_{xy} - \frac{E_s}{2\sigma_i}\left(1-\frac{E_t}{E_s}\right)\left[\frac{3(1-\nu^2)}{(1+\nu)^2}\right]\gamma_{xy}\delta\varepsilon_i\right\} \tag{A.24}$$

and accounting for Eqns. (2.40) (third):

$$\delta\tau_{xy} = \frac{E_s}{2(1-\nu^2)}\left\{(1-\nu)\delta\gamma_{xy} - \frac{1}{2\sigma_i}\left(1-\frac{E_t}{E_s}\right)6(1-\nu)\tau_{xy}\delta\varepsilon_i\right\} \tag{A.25}$$

By substituting Eq. (A.11) into Eq. (A.25), also the variation of the shear stress is expressed as a function of the stress levels and strain variations:

$$\delta\tau_{xy} = \frac{E_s}{2(1-\nu^2)}\left\{\begin{array}{c}(1-\nu)\delta\gamma_{xy} - \frac{3}{2H\sigma_i^2}\left(1-\frac{E_t}{E_s}\right)\left(\frac{\tau_{xy}}{1+\nu}\right)\cdot \\ \left\{\left[(2-\nu)\sigma_x - (1-2\nu)\sigma_y\right]\delta\varepsilon_x + \left[(2-\nu)\sigma_y - (1-2\nu)\sigma_x\right]\delta\varepsilon_y + \left[3(1-\nu)\tau_{xy}\right]\delta\gamma_{xy}\right\}\end{array}\right\} \tag{A.26}$$

By denoting with:

$$\begin{aligned} k_x &= (2-\nu) - (1-2\nu)\frac{\sigma_y}{\sigma_x} \Rightarrow k_x\sigma_x = (2-\nu)\sigma_x - (1-2\nu)\sigma_y \\ k_y &= (2-\nu) - (1-2\nu)\frac{\sigma_x}{\sigma_y} \Rightarrow k_y\sigma_y = (2-\nu)\sigma_y - (1-2\nu)\sigma_x \\ k_{xy} &= 6(1-\nu) \end{aligned} \tag{A.27}$$

The expressions of $\delta\sigma_x$, $\delta\sigma_y$ and $\delta\tau_{xy}$ can be rearranged, by substituting Eqns. (2.41) and (A.27) into Eqns. (A.21), (A.22) and (A.26):

$$\delta\sigma_x = \frac{E_s}{1-\nu^2}\begin{Bmatrix}(\delta\varepsilon_{x.0} + \nu\delta\varepsilon_{y.0}) - z(\delta\chi_x + \nu\delta\chi_y) + \frac{1}{2H\sigma_i^2}\left(1-\frac{E_t}{E_s}\right)\left[\frac{1-2\nu}{2(1-\nu^2)}(\sigma_y + \nu\sigma_x) - \sigma_x\right]\cdot \\ \left[k_x\sigma_x\delta\varepsilon_{x.0} + k_y\sigma_y\delta\varepsilon_{y.0} + k_{xy}\tau_{xy}\delta\varepsilon_{xy.0} - z(k_x\sigma_x\delta\chi_x + k_y\sigma_y\delta\chi_y + k_{xy}\tau_{xy}\delta\chi_{xy})\right]\end{Bmatrix} \tag{A.28}$$

$$\delta\sigma_y = \frac{E_s}{1-\nu^2}\begin{Bmatrix}(\delta\varepsilon_{y.0} + \nu\delta\varepsilon_{x.0}) - z(\delta\chi_y + \nu\delta\chi_x) + \frac{1}{2H\sigma_i^2}\left(1-\frac{E_t}{E_s}\right)\left[\frac{1-2\nu}{2(1-\nu^2)}(\sigma_x + \nu\sigma_y) - \sigma_y\right]\cdot \\ \left[k_x\sigma_x\delta\varepsilon_{x.0} + k_y\sigma_y\delta\varepsilon_{y.0} + k_{xy}\tau_{xy}\delta\varepsilon_{xy.0} - z(k_x\sigma_x\delta\chi_x + k_y\sigma_y\delta\chi_y + k_{xy}\tau_{xy}\delta\chi_{xy})\right]\end{Bmatrix} \tag{A.29}$$

$$\delta\tau_{xy} = \frac{E_s}{2(1-\nu^2)}\begin{Bmatrix}2(1-\nu)(\delta\varepsilon_{xy.0} - z\delta\chi_{xy}) - \frac{3\tau_{xy}}{2H\sigma_i^2(1+\nu)}\left(1-\frac{E_t}{E_s}\right)\cdot \\ \left[k_x\sigma_x\delta\varepsilon_{x.0} + k_y\sigma_y\delta\varepsilon_{y.0} + k_{xy}\tau_{xy}\delta\varepsilon_{xy.0} - z(k_x\sigma_x\delta\chi_x + k_y\sigma_y\delta\chi_y + k_{xy}\tau_{xy}\delta\chi_{xy})\right]\end{Bmatrix} \tag{A.30}$$

By substituting the relations reported in (2.56) into previous equations, it results:

$$\delta\sigma_x = \frac{E_s}{1-\nu^2}\left[\left(\delta\varepsilon_{x.0} + \nu\delta\varepsilon_{y.0}\right) - z\left(\delta\chi_x + \nu\delta\chi_y\right) - \Psi\sigma_x S_x(\mathrm{K}_\varepsilon - z\mathrm{K}_\chi)\right] \tag{A.31}$$

$$\delta\sigma_y = \frac{E_s}{1-\nu^2}\left[\left(\delta\varepsilon_{y.0} + \nu\delta\varepsilon_{x.0}\right) - z\left(\delta\chi_y + \nu\delta\chi_x\right) - \Psi\sigma_y S_y(\mathrm{K}_\varepsilon - z\mathrm{K}_\chi)\right] \tag{A.32}$$

$$\delta\tau_{xy} = \frac{E_s}{2(1-\nu^2)}\left[2(1-\nu)(\delta\varepsilon_{xy.0} - z\delta\chi_{xy}) - \Psi\tau_{xy} S_{xy}(\mathrm{K}_\varepsilon - z\mathrm{K}_\chi)\right] \tag{A.33}$$

Appendix B

Intermediate Steps for Determining the Eq. (2.91)

Taking into account the Eq. (2.89), the final expressions of derivatives, presented in Eqns. (2.87) and (2.88), are provided in the following equation:

$$\frac{\partial w}{\partial x} = -\lambda sin\lambda x\left\{\frac{y}{b} + \frac{\epsilon}{2\alpha_3}\left[\left(\frac{y}{b}\right)^5 + \alpha_1\left(\frac{y}{b}\right)^4 + \alpha_2\left(\frac{y}{b}\right)^3 + \alpha_3\left(\frac{y}{b}\right)^2\right]\right\} \tag{B.1}$$

$$\frac{\partial^2 w}{\partial x^2} = -\lambda^2 cos\lambda x\left\{\frac{y}{b} + \frac{\epsilon}{2\alpha_3}\left[\left(\frac{y}{b}\right)^5 + \alpha_1\left(\frac{y}{b}\right)^4 + \alpha_2\left(\frac{y}{b}\right)^3 + \alpha_3\left(\frac{y}{b}\right)^2\right]\right\} \tag{B.2}$$

$$\frac{\partial w}{\partial y} = cos\lambda x\left\{\frac{1}{b} + \frac{\epsilon}{2\alpha_3 b}\left[5\left(\frac{y}{b}\right)^4 + 4\alpha_1\left(\frac{y}{b}\right)^3 + 3\alpha_2\left(\frac{y}{b}\right)^2 + 2\alpha_3\left(\frac{y}{b}\right)\right]\right\} \tag{B.3}$$

$$\frac{\partial^2 w}{\partial y^2} = cos\lambda x\left\{\frac{\epsilon}{2\alpha_3 b^2}\left[20\left(\frac{y}{b}\right)^3 + 12\alpha_1\left(\frac{y}{b}\right)^2 + 6\alpha_2\left(\frac{y}{b}\right) + 2\alpha_3\right]\right\} \tag{B.4}$$

$$\frac{\partial^2 w}{\partial x \partial y} = -\lambda sin\lambda x \left\{\frac{1}{b} + \frac{\epsilon}{2\alpha_3 b}\left[5\left(\frac{y}{b}\right)^4 + 4\alpha_1\left(\frac{y}{b}\right)^3 + 3\alpha_2\left(\frac{y}{b}\right)^2 + 2\alpha_3\left(\frac{y}{b}\right)\right]\right\} \tag{B.5}$$

By substituting the previous relations into the integrals presented in Eqns. (2.87) and (2.88), the final expressions are obtained:

$$\iint \left(\frac{\partial^2 w}{\partial x^2}\right)^2 dxdy = \lambda^4 ab\left(\frac{1}{6} + \kappa_1\frac{\epsilon}{2} + \kappa_2\frac{\epsilon^2}{2}\right) \tag{B.6}$$

$$\iint \left(\frac{\partial^2 w}{\partial x \partial y}\right)^2 dxdy = \frac{\lambda^2 a}{b}\left(\frac{1}{2} + \kappa_3\frac{\epsilon}{2} + \kappa_4\frac{\epsilon^2}{2}\right) \tag{B.7}$$

$$\iint \left[\frac{\partial^2 w}{\partial x^2}\frac{\partial^2 w}{\partial y^2}\right] dxdy = -\frac{\lambda^2 a}{b}\left(\kappa_5\frac{\epsilon}{2} + \kappa_6\frac{\epsilon^2}{2}\right) \tag{B.8}$$

$$\iint \left(\frac{\partial^2 w}{\partial y^2}\right)^2 dxdy = \frac{\kappa_7 a}{2b^3}\epsilon^2 \tag{B.9}$$

$$\int \left[\left(\frac{\partial w}{\partial y}\right)_{y=0}\right]^2 dx = \frac{a}{2b^2} \tag{B.10}$$

$$\iint \left(\frac{\partial w}{\partial x}\right)^2 dxdy = \lambda^2 ab\left(\frac{1}{6} + \kappa_8\frac{\epsilon}{2} + \kappa_9\frac{\epsilon^2}{2}\right) \tag{B.11}$$

where the values of coefficients α_i and κ_i are reported, respectively, in Eq. (2.90) and Eq. (2.92). By substituting Eqns. (B.6)-(B.11) into Eq. (2.88), the final expression of $\sigma_{cr.p}$ is defined and provided in Eq. (2.91)

Appendix C

Intermediate steps for determining the Eq. (2.103)

Taking into account the Eq.(2.101), the final expressions of derivatives, presented in Eqns. (2.87) and (2.88), are provided in the following equation:

$$\frac{\partial w}{\partial x} = -\lambda sin\lambda x\left[e_1\left(\frac{y}{b}\right)^2 + e_2 cosBy - \frac{e_1}{4}\right] \tag{C.1}$$

$$\frac{\partial^2 w}{\partial x^2} = -\lambda^2 cos\lambda x\left[e_1\left(\frac{y}{b}\right)^2 + e_2 cosBy - \frac{e_1}{4}\right] \tag{C.2}$$

$$\frac{\partial w}{\partial y} = cos\lambda x\left[\frac{2e_1}{b}\left(\frac{y}{b}\right) - e_2 B sinBy\right] \tag{C.3}$$

$$\frac{\partial^2 w}{\partial y^2} = cos\lambda x\left[\frac{2e_1}{b^2} - e_2 B^2 cosBy\right] \tag{C.4}$$

$$\frac{\partial^2 w}{\partial x \partial y} = -\lambda sin\lambda x\left[\frac{2e_1}{b}\left(\frac{y}{b}\right) - e_2 B sinBy\right] \tag{C.5}$$

By substituting the previous relations into the integrals presented in Eqns. (2.87) and (2.88), the final expressions are obtained:

$$\iint \left(\frac{\partial^2 w}{\partial x^2}\right)^2 dxdy = \frac{\lambda^4 a}{2}\left(\frac{e_1^2}{30} - \frac{8e_1 e_2}{b^2 B^3} + \frac{e_2^2 b}{2}\right) \tag{C.6}$$

$$\iint \left(\frac{\partial^2 w}{\partial x \partial y}\right)^2 dxdy = \frac{\lambda^2 a}{2}\left(\frac{e_1^2 b}{3b} - \frac{8e_1 e_2}{b^2 B} + \frac{e_2^2 b B^2}{2}\right) \tag{C.7}$$

$$\iint \left[\frac{\partial^2 w}{\partial x^2}\frac{\partial^2 w}{\partial y^2}\right] dxdy = \frac{\lambda^2 a}{2}\left(\frac{e_1^2 b}{3b} - \frac{8e_1 e_2}{b^2 B} + \frac{e_2^2 b B^2}{2}\right) \tag{C.8}$$

$$\iint \left(\frac{\partial^2 w}{\partial y^2}\right)^2 dxdy = \frac{a}{2}\left(\frac{4e_1^2}{b^3} - \frac{8e_1 e_2 B}{b^2} + \frac{e_2^2 b B^4}{2}\right) \tag{C.9}$$

$$\int \left[\left(\frac{\partial w}{\partial y}\right)_{y=-\frac{b}{2}}\right]^2 dx = \frac{a}{2}\left(\frac{e_1^2}{b^2} - \frac{2e_1 e_2 B}{b} + e_2^2 B^2\right) \tag{C.10}$$

$$\iint \left(\frac{\partial w}{\partial x}\right)^2 dxdy = \frac{\lambda^2 a}{2}\left(\frac{e_1^2 b}{30} - \frac{8e_1 e_2}{b^2 B^3} + \frac{e_2^2 b}{2}\right) \tag{C.11}$$

where the values of coefficients e_i and B are reported in Eq. (2.101). By substituting Eqns. (C.6)-(C.11) into Eq. (2.88), the final expression of $\sigma_{cr.p}$ is defined and provided in Eq. (2.103).

CHAPTER 3
EXPERIMENTAL TESTS

3.1. Previous experimental works

The study of inelastic behaviour of aluminium members, in terms of resistance and capacity of deformation, must necessarily start from the experimental tests. However, due to the low spread of aluminium compared to steel material in the structural applications, experimental activities are currently not very widespread in the scientific literature. With reference to the SHS,RHS and I,H shaped sections subjected to uniform and non-uniform compression, a summary of the main experimental campaigns is provided below.

In the early 2000s, within the activities of CEN-TC250/SC9 [3.1], *Faella et al.* [3.2] carried out an experimental program devoted to the evaluation of the ultimate resistance of aluminium alloy hollow members subjected to local buckling under uniform compression. Successively, *Feng et al.* [3.3] have tested a total of 44 perforated box-section specimens of different aluminium grade. Instead, *Su et al.* [3.4] evaluated the performance of SHS-RHS aluminium members with and without internal stiffeners. As regards the I,H shaped sections under uniform compression, the most recent contribution is provided by *Yuan et al.* [3.5] in the 2015, however the most of the investigated specimens are characterized by the high width-to-thickness ratios, consequently these members are affected by the elastic local buckling, by neglecting the influence of inelastic behaviour. An extensive experimental campaign was carried out to the second half of the 20th century and it is provided in the NACA reports, however the results are reported only in terms of ultimate resistance [3.6]-[3.8].

As regards the aluminium beams under bending, the main experimental campaign has been carried out by *Moen et al.* [3.9] in 1999. In particular, three and four-point bending tests have been performed on box-shaped and H-sections, with and without stiffeners, made of alloys 6082-T4, T6 and 7108-T7. Successively, other 4-point tests have been carried out on SHS sections by *Zhu and Young*, while *Kim and Peköz* analyzed the I-shaped sections [3.10],[3.11]. Lately, *Su et al.* performed three, four and five point bending tests on box sections made of 6061-T6, 6063-T5,T6 aluminium alloys, with and without internal stiffeners [3.12],[3.13]; while *Wang et al.* performed only three point bending tests on the unwelded I-shaped aluminium beams made of the same previous aluminium alloys [3.14].

A summary of the main stub tests and the bending tests, presented in the scientific literature, is reported in Table 3.1.

In the present Chapter, for increasing known out of aluminium members under compression and bending, 9 stub columns tests and 12 three-point bending tests have been carried out on 4 different SHS sections made of alloys 6060. Obviously, the main aim of these experiments is the evaluation local buckling effects on the ultimate behaviour of aluminium members, in terms of resistance and capacity of deformation. The tests have been performed at the Structural Engineering Testing Hall Laboratory (STRENGTH Lab) of the Department of Civil Engineering of Salerno University. It is important to underline that no specific standards have been adopted in the stub and bending tests, but the test speeds are defined in order to accurately evaluate the main mechanical properties in the elastic and post-elastic regions, avoiding speed variations that could influence the experimental results.
Moreover, the results provided here were used to compare and validate the methodological approaches presented in the following chapters. In particular, the results of stub column tests have been compared with those obtained by a theoretical approach (DTP) and the effective thickness method (ETM), provided, respectively, in Chapter 4 and Chapter 6. While the experimental curves obtained by three-point bending tests have been used to calibrate a finite element model presented in the Chapter 5 and, also in this case, the results, in terms of the flexural resistance and the capability of rotation, have been compared with those provided by the effective thickness method (ETM).

Table 3.1. Summary of stub column tests and bending tests.

Authors	Date	Alloy	Type of test	Shape	No of tests
Faella et al. [3.2]	2000	6060 T6 6061 T6 6082 T6 6082 TF	Stub column test	RHS,SHS	39
Feng et al. [3.3]	2018	6061 T6 6063 T5	Stub column test	Perforated RHS,SHS	16
Su et al. [3.4]	2014	6061 T6 6063 T5	Stub column test	RHS,SHS (with and without stiffeners)	15
Yuan et al. [3.5]	2015	6061 T6 6063 T5	Stub column test	I,H	15
Heimerl & Niles [3.6]	1946	2014 T6	Stub column test	I,H	48
Heimerl & Roy [3.7]	1945	7178 T6	Stub column test	I,H	40
Heimerl & Fay [3.8]	1945	7075 T6	Stub column test	I,H	51
Moen et al. [3.9]	1999	6082 T4,T6 7108 T7	3-point bending test	RHS,SHS,H (welded and unwelded)	37
Zhu & Young [3.10]	2009	6061 T6 6063 T5	4-point bending test	SHS	70
Kim and Peköz [3.11]	2010	6063 T6	4-point bending test	I,H	3
Su et al. [3.12],[3.13]	2015-16	6061 T6 6063 T5	3,4,5-point bending test	RHS,SHS (with and without stiffeners)	327
Wang et al. [3.14]	2016	6061 T6 6063 T5	3-point bending test	I,H	34

3.2. Geometrical and Mechanical Properties

The aluminium members investigated in the current experimental tests are extruded profiles made of EN-AW 6060 T6 with the SHS section. Temper T6 is the treatment corresponding to EN-AW6082 aluminium alloy and it identifies a material artificially aged at a prescribed low temperature (100-200ºC) until the metal reaches a stable condition. It is suitable for structural applications because of its high resistance but shows lower ductility than the naturally aged tempers.

Four types of section are considered for both stub and bending tests, characterized by nominal width of 40,60,80,100 mm and with the same nominal thickness equal to 2 mm. According to Figure 3.1, the nominal and measured geometrical properties of specimens are reported in Table 3.2.

Table 3.2. Nominal and measured geometrical properties of tested specimens.

Section	$B_{1.nom}$ [mm]	$B_{2.nom}$ [mm]	t_{nom} [mm]	A_{nom} [mm²]	B_1 [mm]	B_2 [mm]	t_1 [mm]	t_2 [mm]	t_3 [mm]	t_4 [mm]	A [mm²]
SHS40	40.00	40.00	2.00	304	40.18	40.11	1.99	2.20	2.09	2.00	315.26
SHS60	60.00	60.00	2.00	464	60.31	60.40	2.00	2.16	2.00	2.09	480.92
SHS80	80.00	80.00	2.00	624	80.17	80.06	2.00	1.98	1.90	1.89	607.40
SHS100	100.00	100.00	2.00	784	100.30	100.30	2.24	2.04	2.12	2.37	860.40

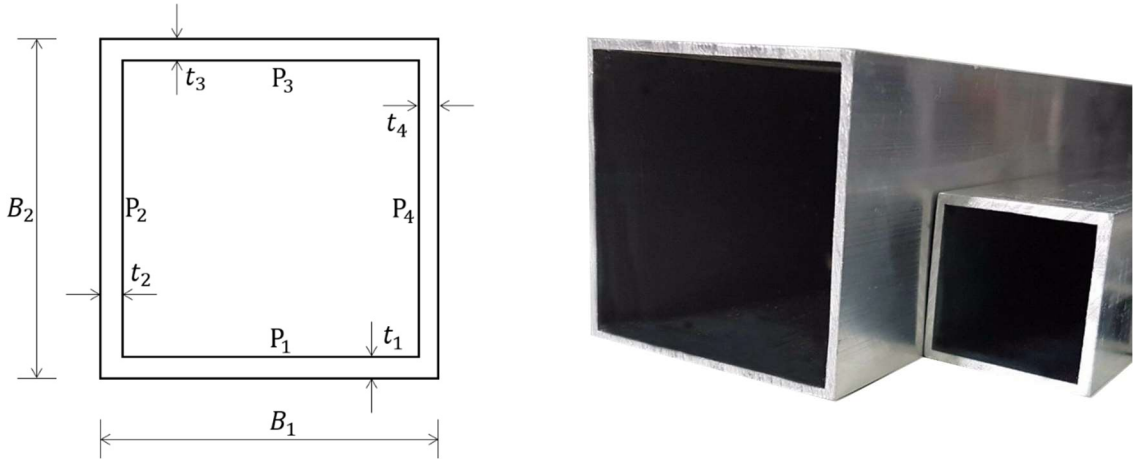

Figure 3.1. Geometrical scheme of box section.

Standard tensile testing was performed on specimens cut from each type of section, according to UNI-EN-ISO 6892-1-1 [3.15]. In particular, the specimens P_i were cut from each plate constituting the section according to the shape depicted in Figure 3.2, while the dimensions of the specimens are reported in Table 3.3. The monotonic tests have been carried out under displacement control according to the Method A2 as described in the aforementioned standard. So, the speed test has been computed as a function of the length L_c and the estimated strain rate $\dot{e}_{L_c}$:

$$v_c = L_c \cdot \dot{e}_{L_c} \tag{3.1}$$

With reference to the scheme depicted in Figure 3.3, four intervals of speed have been considered for predicting accurately the elastic and inelastic property of aluminium material. For each interval is reported the corresponding strain rate, while in the speed tests are reported for each section according to the Eq. (3.1), as shown in Table 3.3.

Table 3.3. Geometrical properties and displacement speed of tensile testing.

Section	S_0 [mm]	S [mm]	L_c [mm]	L_s [mm]	L_{tot} [mm]	$v_c^{(I)}$ [mm/s]	$v_c^{(II)}$ [mm/s]	$v_c^{(III)}$ [mm/s]	$v_c^{(IV)}$ [mm/s]
SHS40	15	30	80	90	275	0.0056	0.020	0.16	0.54
SHS60	15	30	80	90	275	0.0056	0.020	0.16	0.54
SHS80	20	40	100	100	320	0.0070	0.030	0.20	0.67
SHS100	20	40	100	100	320	0.0070	0.030	0.20	0.67

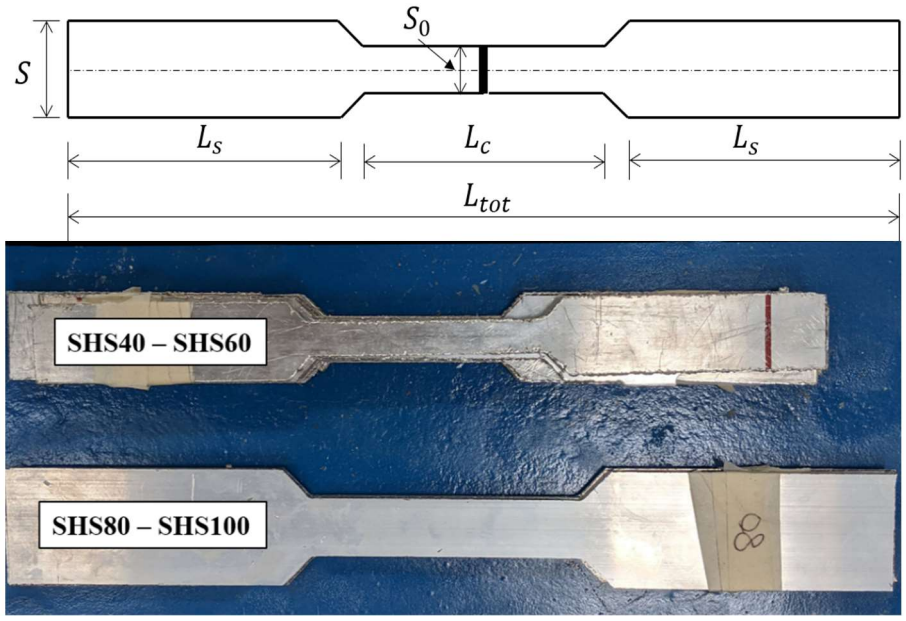

Figure 3.2. Geometrical scheme of material specimen.

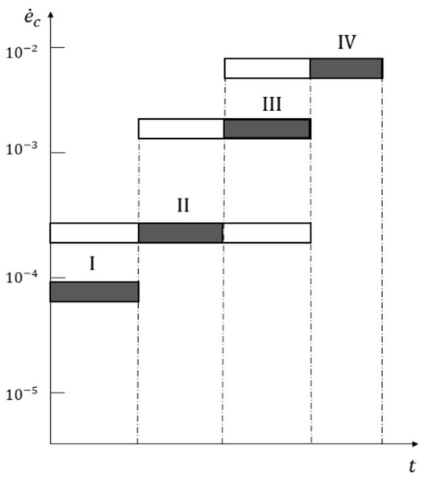

Interval	$\dot{e}_{L_c}$
I	$7.00\text{x}10^{-5}$
II	$2.50\text{x}10^{-4}$
III	$2.00\text{x}10^{-3}$
IV	$6.70\text{x}10^{-3}$

Figure 3.3. strain rate for each interval provided by UNI-EN-ISO 6892-1 [3.15].

The experimental stress-strain curves are depicted in Figure 3.5-Figure 3.8, while the summary of tensile tests is shown for each plate constituting each tested section in Table 3.4. In particular, the following measured properties are provided:

- The experimental Young's modulus $[E_{exp}]$
- The stress at a residual strain of 0.1% $[f_{0.1}]$
- The stress at a residual strain of 0.2% $[f_{0.2}]$
- The engineering maximum stress $[f_u]$
- The engineering strain corresponding to the maximum stress $[\varepsilon_u]$
- The ultimate strain $[\varepsilon_r]$
- The Ramberg-Osgood coefficient $[n]$ given by:

$$n = \frac{ln2}{ln\left(\frac{f_{0.2}}{f_{0.1}}\right)} \tag{3.2}$$

Moreover, the experimental curves have also been described according to the Ramberg-Osgood law expressed by the following relationship [3.16]:

$$\varepsilon = \frac{\sigma}{E} + 0.002\left(\frac{\sigma}{f_{0.2}}\right)^n \tag{3.3}$$

The Ramberg-Osgood curves are always reported in Figure 3.5-Figure 3.8, while Figure 3.4 shows the real specimens after the tensile testing. By analyzing the results of the tensile testing, it can be observed that after the elastic range, for each test, aluminium alloy presents the typical strain-hardening behaviour which is not preceded by a perfectly plastic branch corresponding to yielding plateau as for steel material. The ultimate deformation ε_r is around 6-10%, while the maximum stress f_u varies between 187.38 to 255.41 MPa, while the yield stress $f_{0.2}$ never assumes values lower than 152 MPa. Moreover, it is interesting to observe that the coefficient n, which influences the shape and the strain hardening behaviour of the stress-strain curves, even the single section has very different values. It is well known that if $n \to \infty$, the Ramberg-Osgood law represents the mild steel behaviour, conversely for low values of the exponent, the relationship tends to linear elastic behaviour. This is clearly evident by observing the Ramberg-Osgood model curves. Finally, the break line at 45^o,characterizing almost all the specimens, generally indicate good ductility of aluminium alloy.

Table 3.4. Mechanical properties of tested specimens.

Specimen		E_{exp} [MPa]	$f_{0.1}$ [MPa]	$f_{0.2}$ [MPa]	f_u [MPa]	ε_u [-]	ε_r [-]	n [-]
SHS 40	P_1	73054	171.00	181.75	207.85	0.055	0.075	11.34
	P_2	75767	176.70	182.59	203.03	0.046	0.062	21.14
	P_3	71465	160.83	174.03	202.17	0.053	0.074	8.78
	P_4	66793	154.92	166.92	192.36	0.057	0.072	9.29
SHS 60	P_1	65669	210.11	227.32	252.65	0.054	0.064	8.80
	P_2	61254	207.09	215.00	238.83	0.065	0.088	18.49
	P_3	65277	224.68	231.39	252.22	0.065	0.082	23.55
	P_4	72674	213.20	226.59	253.58	0.069	0.095	11.38
SHS 80	P_1	69665	210.82	224.17	246.02	0.039	0.064	11.29
	P_2	75975	199.00	211.00	253.41	0.061	0.068	11.84
	P_3	65174	226.46	236.92	255.41	0.042	0.050	15.35
	P_4	63341	217.45	231.12	253.71	0.070	0.091	11.37
SHS 100	P_1	71564	168.65	174.75	199.10	0.060	0.088	19.51
	P_2	70044	165.38	175.61	201.80	0.060	0.098	11.55
	P_3	66906	140.02	152.86	187.38	0.080	0.103	7.90
	P_4	69317	155.32	169.36	195.79	0.060	0.085	8.00

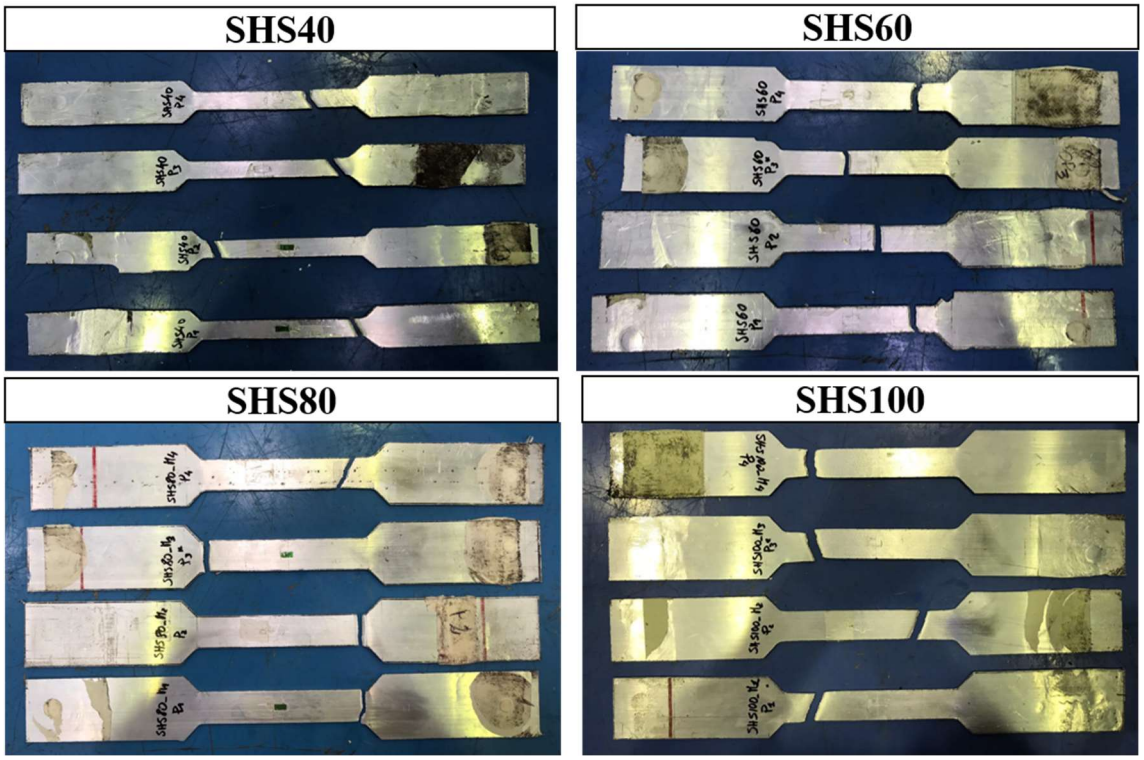

Figure 3.4. The specimens after the tensile testing.

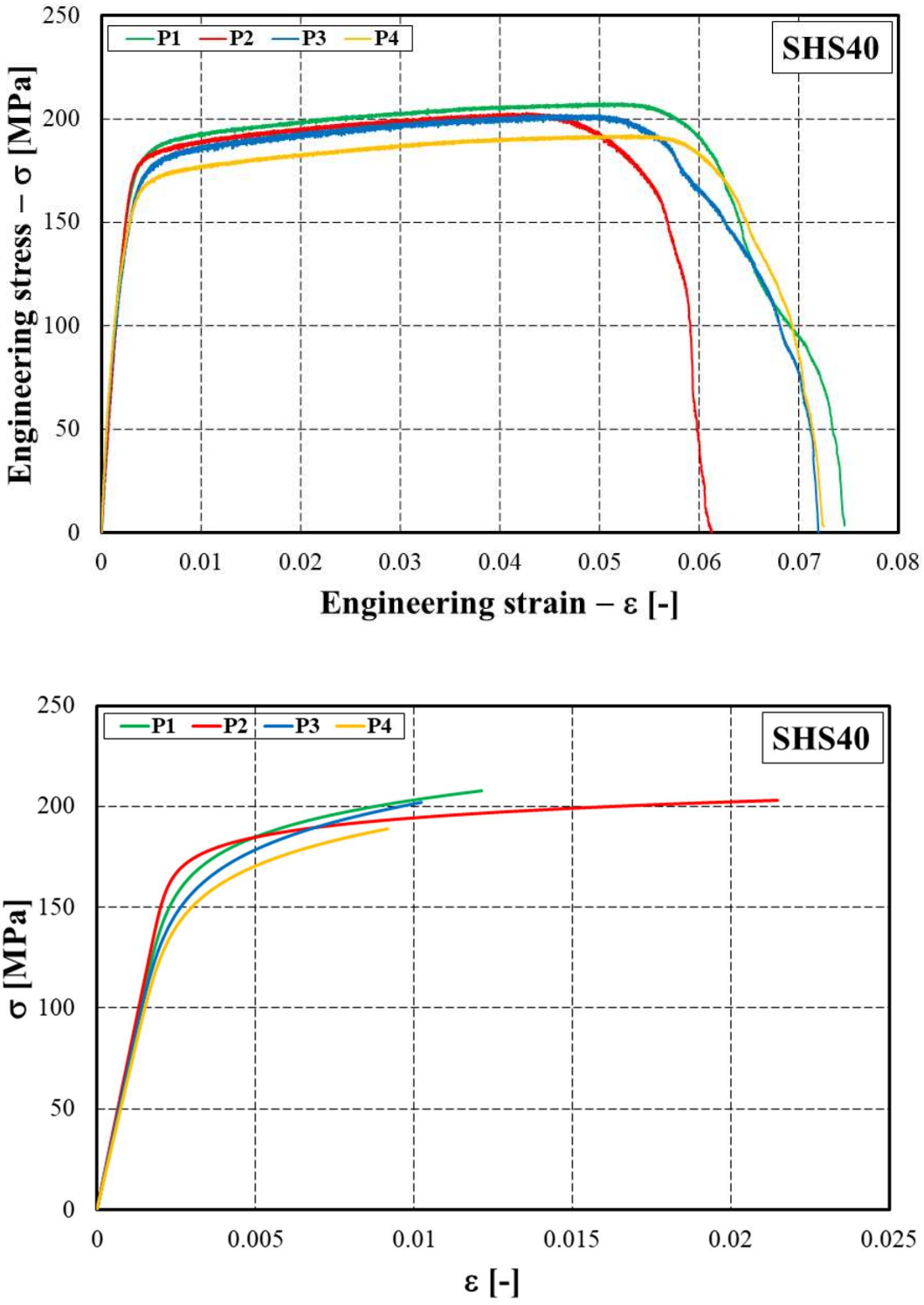

Figure 3.5. Experimental curves(top) and Ramberg-Osgood models(bottom) for SHS40.

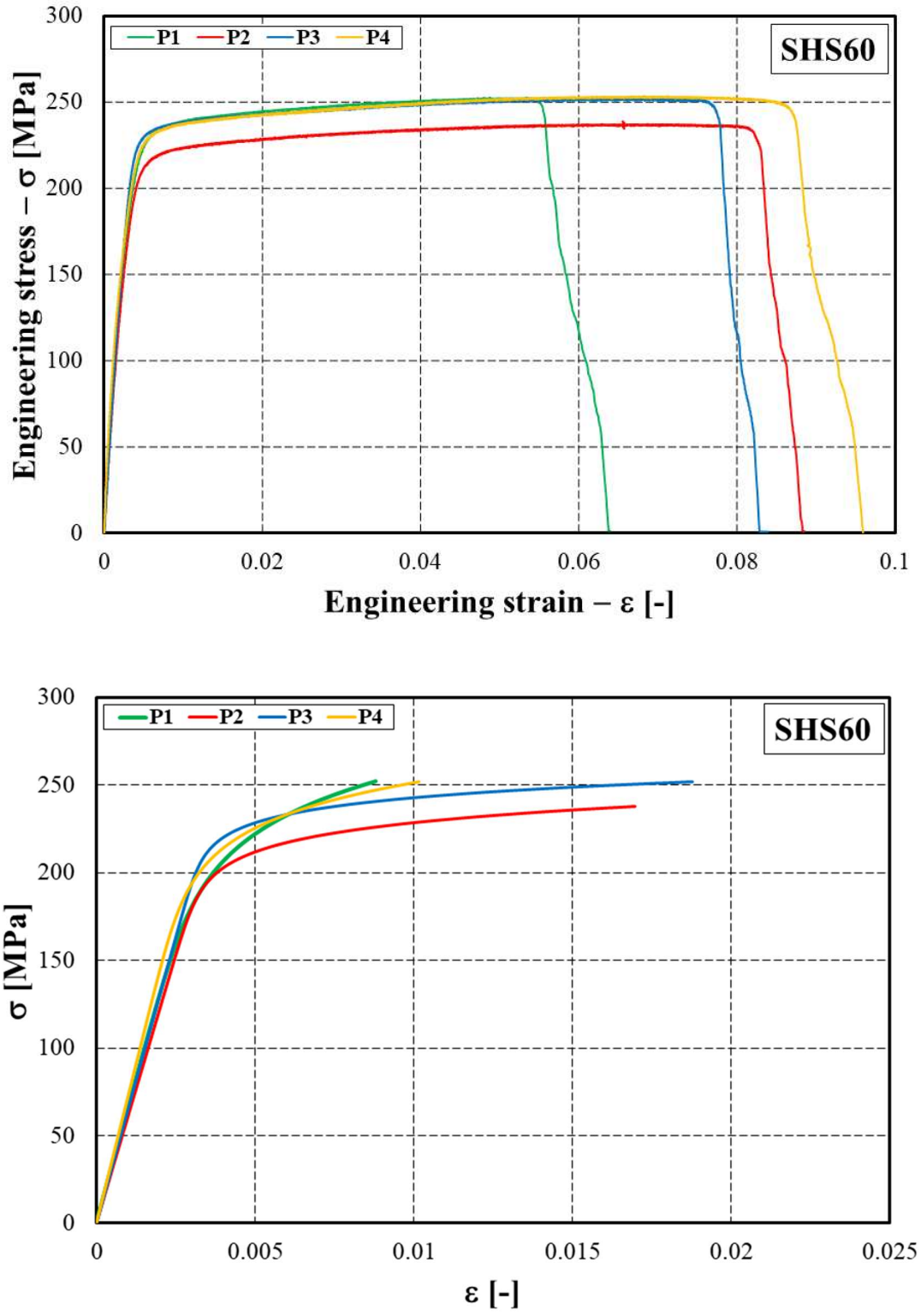

Figure 3.6. Experimental curves(top) and Ramberg-Osgood models(bottom) for SHS60.

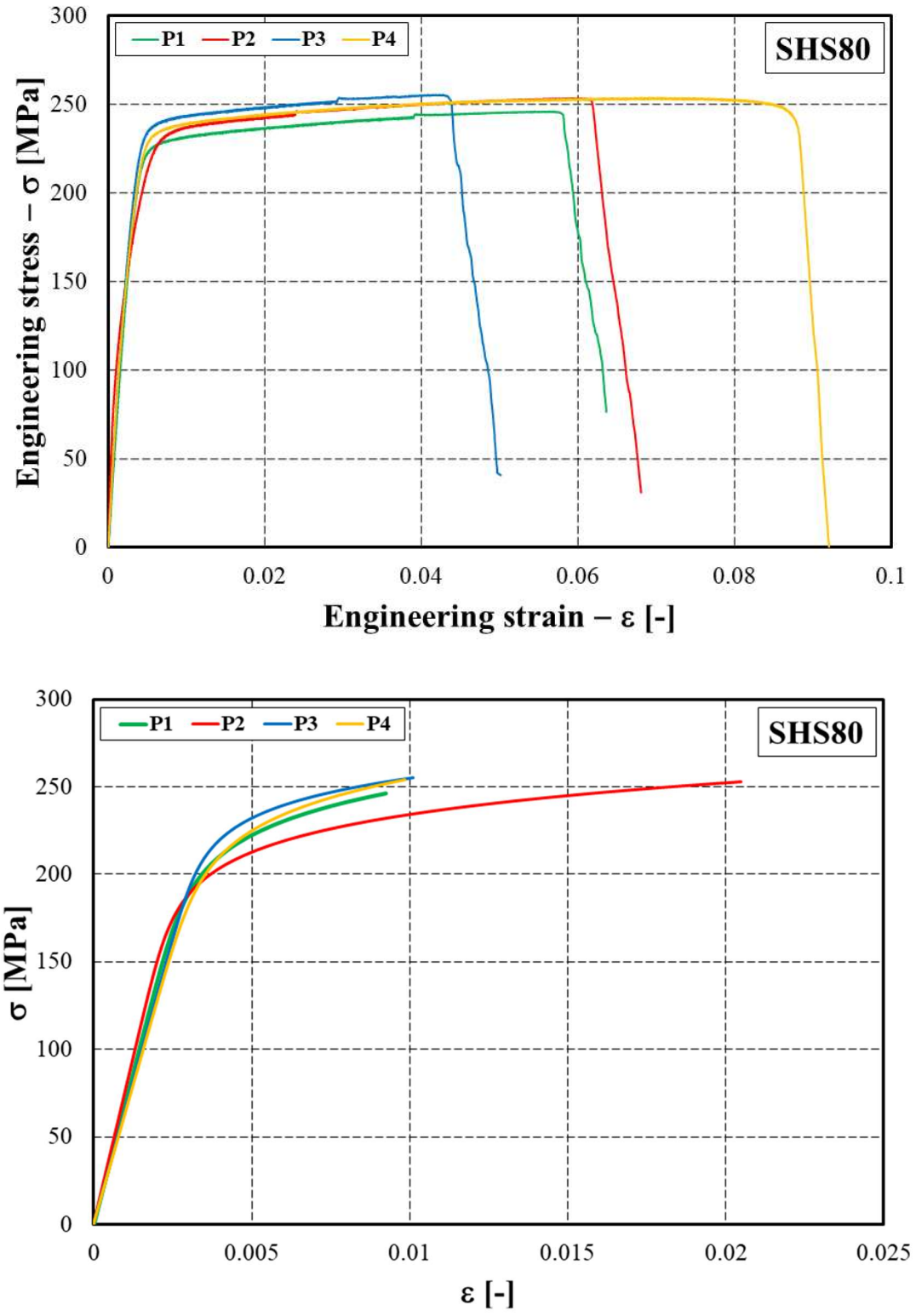

Figure 3.7. Experimental curves(top) and Ramberg-Osgood models(bottom) for SHS80.

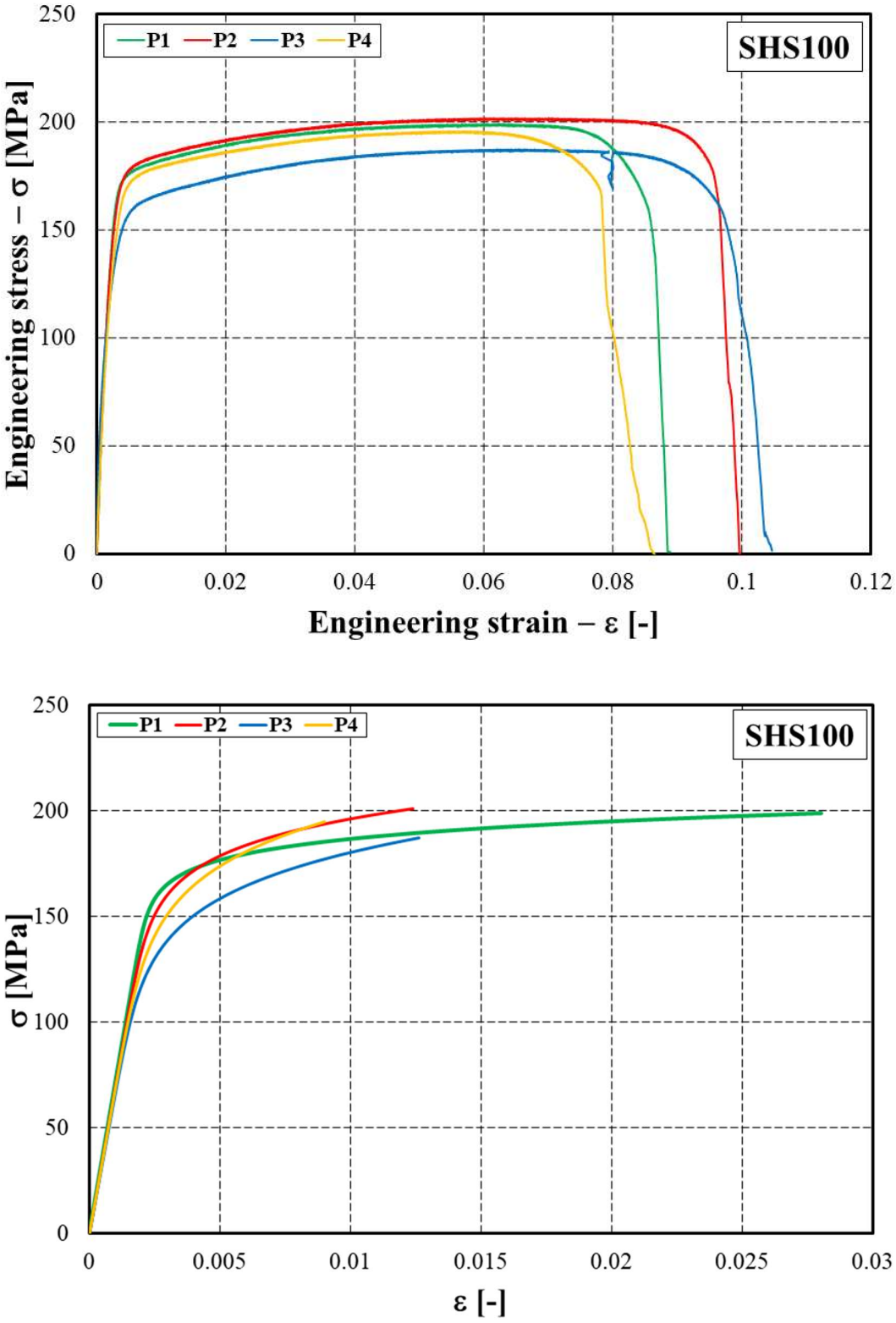

Figure 3.8. Experimental curves(top) and Ramberg-Osgood models(bottom) for SHS100.

3.3. Stub Column Tests

With reference to the SHS aluminium members previously described, the stub column tests have been carried out in order to evaluate the maximum load $N_{u.exp}$ and the corresponding displacement $\delta_{u.exp}$. Figure 3.9 shows the setup of compression tests, in particular, they have been performed with a Schenck Hydropuls S56 testing machine (maximum load 630 kN, piston stroke $\pm$ 125 mm). For each profile, a minimum of two stub tests have been carried out under displacement control. The test speed was not defined by any standard protocol, the choice is based on the application of two different test speeds, equal for each specimen: an initial low speed v_i equal to 0.42 mm/min up to post elastic level and, successively, a final speed v_f equal to 1.20 mm/min. The speed change was set for each specimen according to the theoretical yield displacement $\delta_{0.2}$ mentioned below. The reasons are related to test under displacement control and for evaluating accurately the main mechanical properties in the elastic region. The axial displacements have been measured by means of three inductive transducers (LDT). The mean value of the three measures have been considered. Almost all the specimens have failed due to pure local buckling without any coupling phenomenon, except the tests referring to SHS100 (test a, test b) and SHS80 (test a) where the instability phenomenon occurred, preliminarily, of a single plate due to the geometrical imperfections of sections and as can also be depicted by observing the shapes of $N-\delta$ curves provided in Figure 3.10-Figure 3.13. The test results are summarized in Table 3.5, where the specimen height a, the ultimate resistance $N_{u.exp}$, its nondimensional value $\bar{N}_u$, the maximum displacement $\delta_{u.exp}$ are given. In particular, the nondimensional values are expressed as:

$$\bar{N}_u = \frac{N_{u.exp}}{A \cdot f_{0.2}} \tag{3.4}$$

and:

$$\bar{\delta}_u = \frac{\delta_{u.exp}}{\delta_{0.2}} \tag{3.5}$$

where A represents the section area of each section reported in Table 3.3, $f_{0.2}$ is the mean value of the four measures provided in Table 3.4 for each section, while $\delta_{0.2}$ corresponds to the displacement according to the conventional strain $\varepsilon_0 = f_{0.2}/E$. So, taking into account that $\delta = \varepsilon \cdot a$, the previous relationship can be expressed as the normalised buckling strain:

$$\bar{\varepsilon}_u = \frac{\varepsilon_u}{\varepsilon_0} \tag{3.6}$$

By defining ε_u as the strain corresponding to the occurrence of local buckling. The results highlight that for SHS40 the occurrence of local buckling occurs in the inelastic region, in fact the nondimensional values $\bar{N}_u$ slightly exceed 1.00; conversely the other cases are strongly affected by

the elastic local buckling. It is obviously depended on the with-to-thickness ratios which increase from SHS40 to SHS100. Figure 3.14 shows the specimens after stub column tests which present the typical formation of local buckles.

Table 3.5. Results of stub column tests.

Specimen	***Test***	a [mm]	$N_{u.exp}$ [kN]	$\bar{N}_u$ [-]	$\delta_{u.exp}$ [mm]	$\bar{\delta}_u(\bar{\varepsilon}_u)$ [-]
SHS40	a	120.05	58.30	1.05	0.87	2.96
	b	120.12	57.53	1.04	0.86	2.92
	c	130.43	55.55	1.01	0.51	1.60
SHS60	a	181.10	92.26	0.85	0.59	0.96
	b	180.80	85.62	0.79	0.61	0.99
SHS80	a	240.12	79.50	0.58	0.60	0.76
	b	240.32	87.18	0.63	0.64	0.81
SHS100	a	300.10	90.22	0.62	0.62	0.58
	b	299.00	80.85	0.55	0.61	0.75

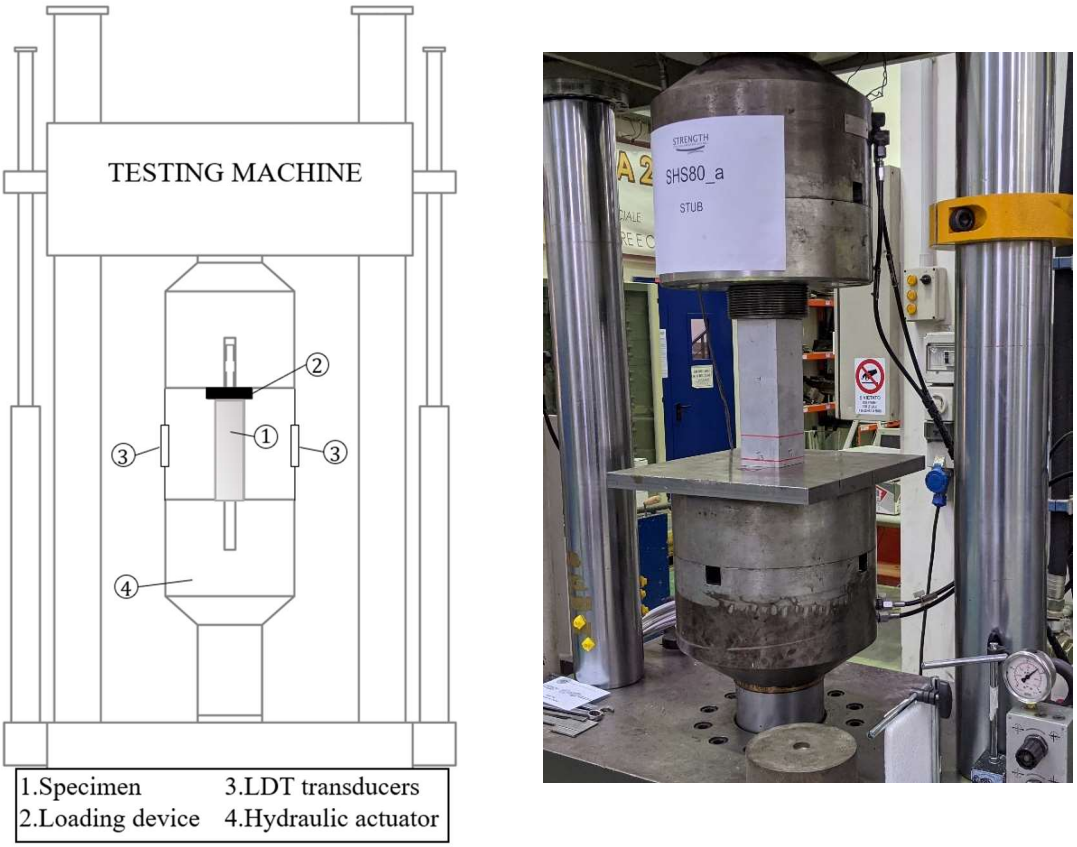

Figure 3.9. Setup of stub column test.

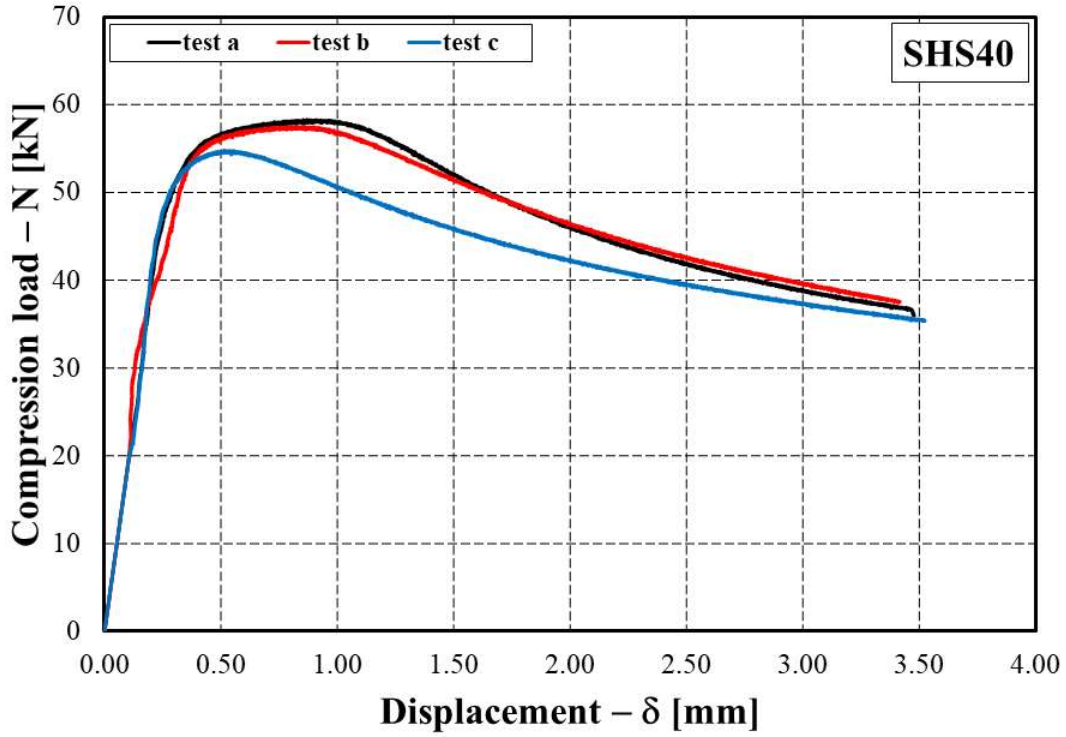

Figure 3.10. Experimental curve relating compression load N to displacement δ for SHS40.

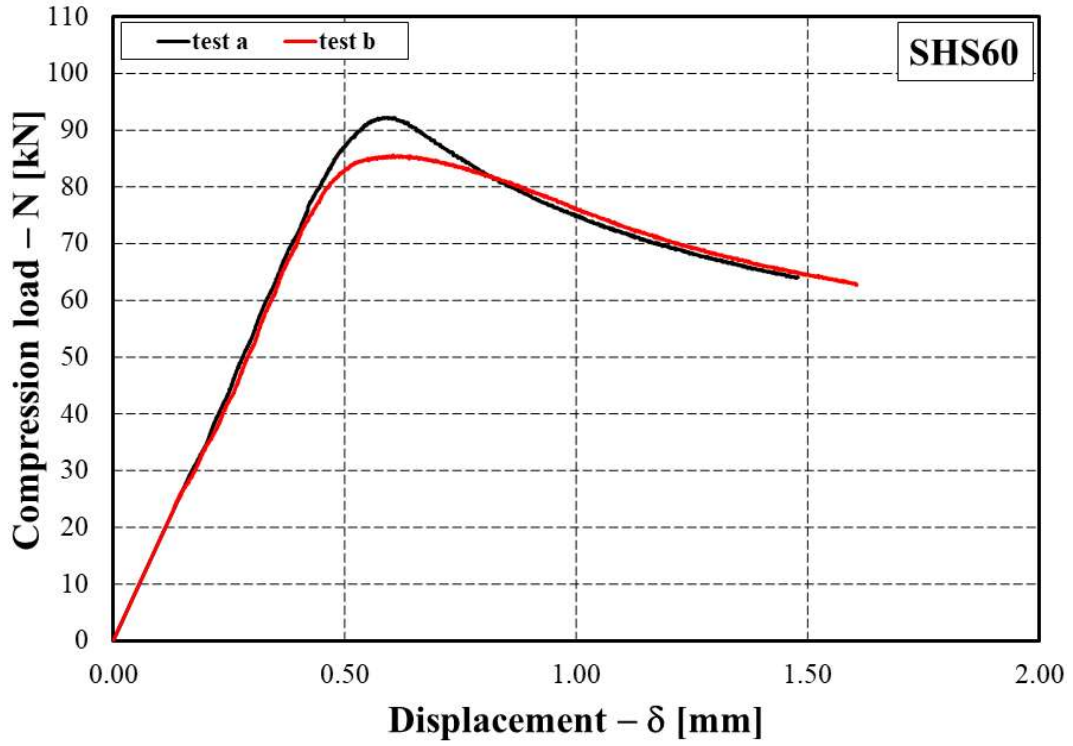

Figure 3.11. Experimental curve relating compression load N to displacement δ for SHS60.

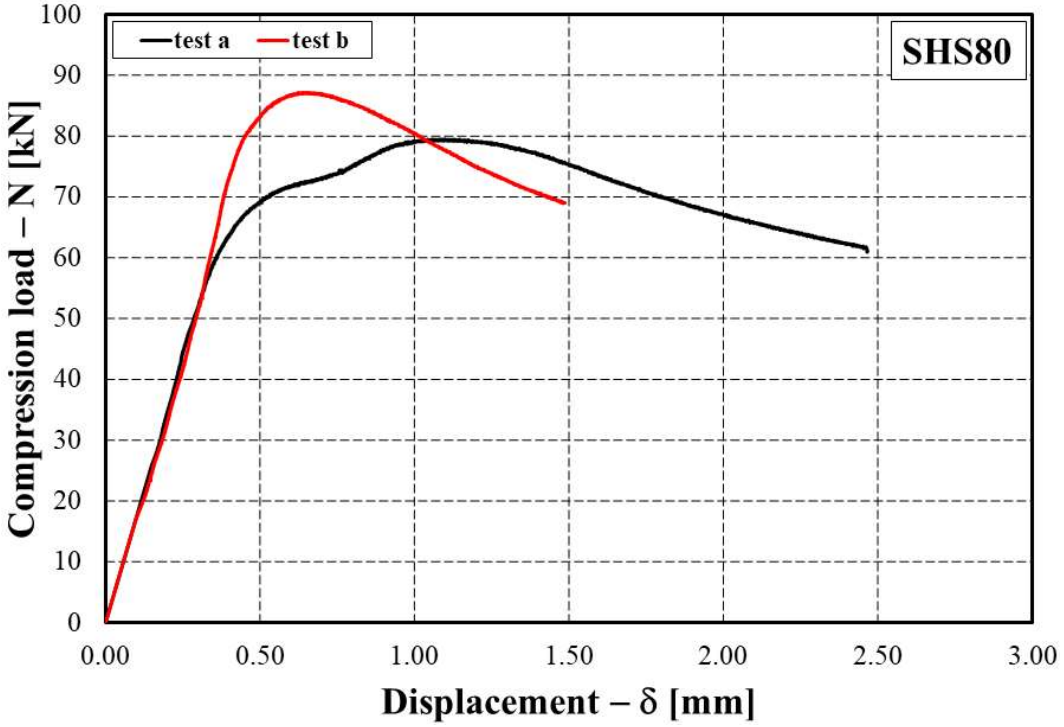

Figure 3.12. Experimental curve relating compression load N to displacement δ for SHS80.

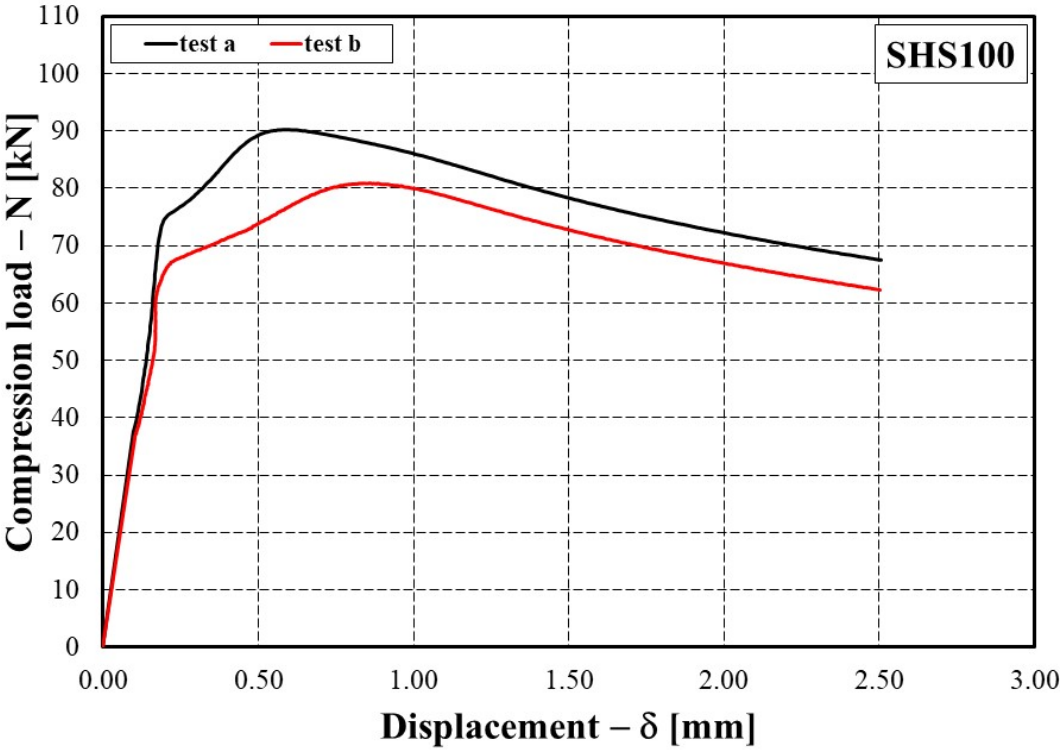

Figure 3.13. Experimental curve relating compression load N to displacement δ for SHS100.

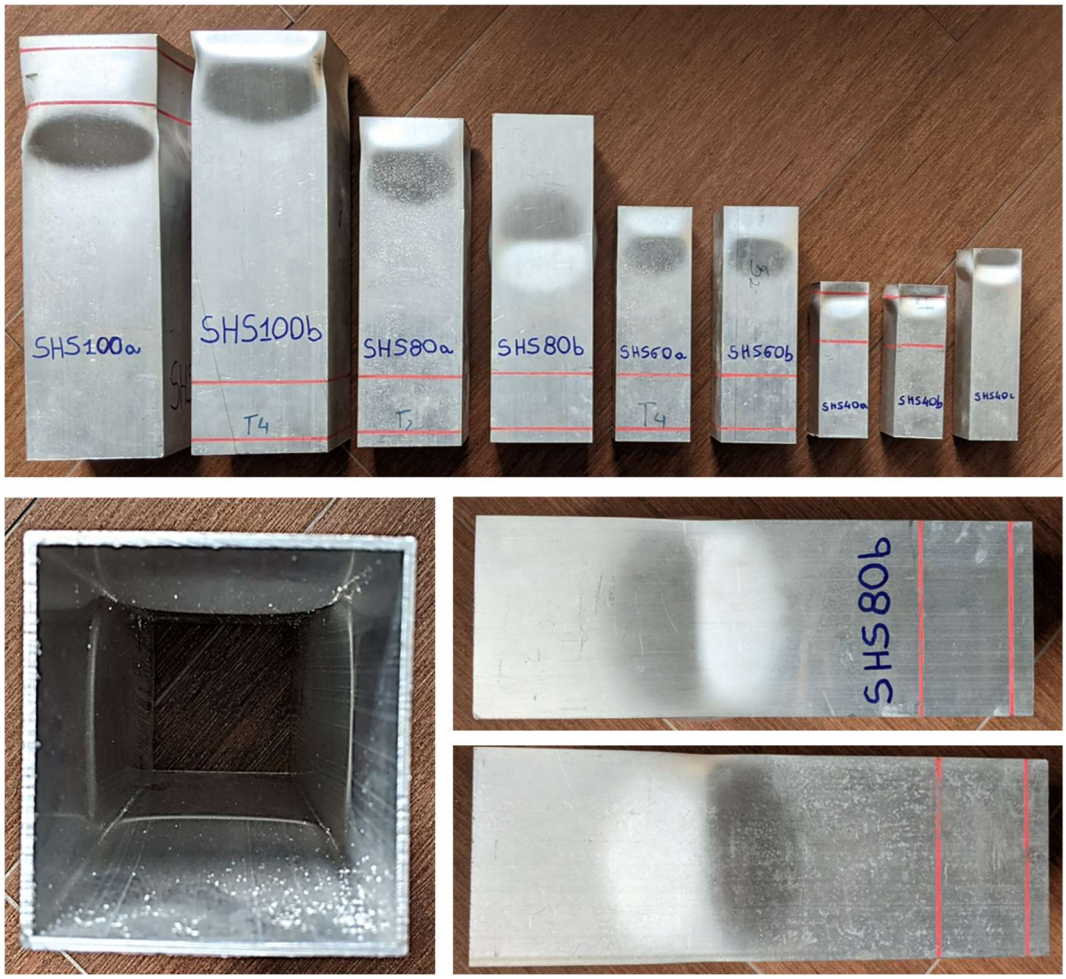

Figure 3.14. Specimens after stub column tests showing typical buckling shape for box section.

3.4. Three Point Bending Tests

In order to evaluate the maximum flexural resistance and the corresponding rotational capacity, three-point bending tests have been carried out on the same box-shaped beams for three different length: $L_1 = 1300\ mm$, $L_2 = 800\ mm$ and $L_2 = 500\ mm$; giving a total of 12 reported tests.

The test rig is depicted in Figure 3.16. A simply supported beam is vertically loaded at the midspan through the same hydraulic actuator used in the stub tests. The load is measured by a load cell on top of the loading device which consists of a compact steel half cylinder with diameter of 50 mm. The beam is placed on top of the other half cylindrical supports which are fixed on top of a stiff supporting steel beam HEA 220, consequently, the support system may be considered stiff compared the test specimen. In order to neglect any displacements and rotations out of the plane, two transducers (LDT-S; LDT-D) are placed at the supports, while others two transducers (LDT-C_1; LDT-C_2) are placed at the midspan for computing the displacements during the tests. In particular, the displacements were measured as the distance between loading device and the support system. Moreover, four one-dimensional strain gauges were fixed to the web plates of each specimens for evaluating the maximum

curvature under bending tests. The adopted strain gauge is FLAB-3-23 produced by Tokyo Instruments Lab and its main properties are summarized in Figure 3.15.

Also in the case of three point bending tests, the test speeds were not defined by any specific standard protocol. The tests have been carried out under displacement control and the speed rate has been calibrated as a function of the length of beams. In particular, for each length, two displacement speeds are defined: an initial speed v_i up to a limit displacement δ^*, successively a final speed v_f until the beam collapses. The values of speed adopted for each length are reported in Table 3.6.

Table 3.6. Speed rate of Three Point Bending Test.

$\boldsymbol{Length}$ [mm]	$\boldsymbol{v_i}$ [mm/min]	$\boldsymbol{\delta^*}$ [mm]	$\boldsymbol{v_f}$ [mm/min]
$L_1 = 1300$	5	20	15
$L_2 = 800$	3	12	9
$L_3 = 500$	1	4	3

Figure 3.17-Figure 3.20 show the experimental curves $F - \delta$ of each section and for the three tested lengths, while the main results are summarized in Table 3.7. In particular, the maximum load $F_{u.exp}$ and the corresponding displacements $\delta_{u.exp}$ are given. Moreover, with reference to the middle section and according to the geometrical scheme, the maximum bending moment $M_{u.esp}$ has been expressed as:

$$M_{u.exp} = \frac{F_{u.exp} L}{4} \tag{3.7}$$

While the corresponding chord rotation $\theta_{u.exp}$ has been computed as:

$$\theta_{u.exp} = \frac{2\delta_u}{L} \tag{3.8}$$

where L represents the generic length of the tested beams. Moreover, the nondimensional flexural overstrength $\bar{M}_u$ and the rotational capacity $\bar{\theta}_u$ are computed as:

$$\begin{aligned} \bar{M}_u &= \frac{M_{u.exp}}{M_{0.2}} \\ \bar{\theta}_u &= \frac{\theta_{u.exp}}{\theta_{0.2}} \end{aligned} \tag{3.9}$$

where $M_{0.2}$ and $\theta_{0.2}$ are, respectively, the bending moment and the rotation at the conventional yield stress $f_{0.2}$ and they are expressed as:

$$\begin{aligned} M_{0.2} &= W_e f_{0.2} \\ \theta_{0.2} &= \frac{M_{0.2} L}{4EI} \end{aligned} \tag{3.10}$$

where W_e is the elastic moment resistance, I represents the inertia moment of geometrical section and E is the Young's modulus of aluminium material. Finally, by means of the experimental data obtained by the strain gauges, it was possible to determine the maximum curvature $\chi_{u.exp}$ in the middle section and, consequently, its nondimensional value $\bar{\chi}_u$ given by:

$$\bar{\chi}_u = \frac{\chi_{u.exp}}{\chi_{0.2}} \tag{3.11}$$

where $\chi_{0.2}$ represents the curvature at the conventional yield stress, so it is expressed as:

$$\chi_{0.2} = \frac{M_{0.2}}{EI} \tag{3.12}$$

The experimental results show that the SHS40 aluminium beams and the SHS60 beams with L_1 and L_2 present the flexural overstrength, in fact both $\bar{M}_u$ and $\bar{\theta}_u$ exceed 1.00. Conversely, in the other cases, the local buckling occurs in the elastic range. For each section, the maximum vertical load and, consequently, the maximum bending moment enhances by decreasing the length of the beam while, conversely, the corresponding maximum chord rotation reduces. The same observation is valid when the beam section increases with the fixed length.

During testing, the specimens SHS100 and SHS80 with lengths L_2 and L_3 achieved the collapse due to the transversal concentrated load which provided, prematurely, the local buckling of the web plates. So, these cases are not governed by the flexural behaviour, but the crisis is related to the transverse load, as described in Section 6.7.5 of Eurocode 9 [3.1]. For this reason, the previous specimens will be neglected during the discussion of the following chapters.

Finally, as an example, the typical buckling shape of hollow section beam under bending is reported in Figure 3.21, where it is evident that the instability phenomena occur in the upper plate in compression and in the compression parts of the web plates.

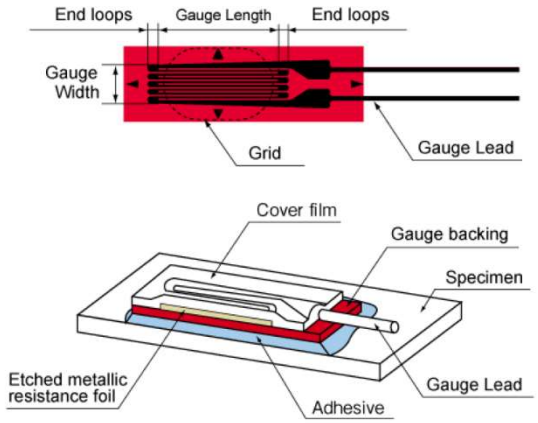

Type	FLAB-3-23
Test condition	$23°C - 50\%$ RH
Gauge Length	3 mm
Gauge Width	1.70 mm
Backing Length	8.80 mm
Backing Width	3.50 mm
Gauge Resistance	$120 \pm 0.3\Omega$
Gauge Factor	$2.09 \pm 1\%$

Figure 3.15. The main properties of FLAB-3-23 strain gauge.

Table 3.7. Results of Three Point Bending Tests.

Section	L [mm]	$F_{u.exp}$ [kN]	$\delta_{u.exp}$ [mm]	$M_{u.exp}$ [kNm]	$\bar{M}_u$ [−]	$\theta_{u.exp}$ [rad]	$\bar{\theta}_u$ [−]	$\chi_{u.exp}$ [m^{-1}]	$\bar{\chi}_u$ [−]
SHS40	1300	2.50	35.17	0.81	1.23	0.054	1.73	0.503	3.44
	800	4.04	11.46	0.81	1.19	0.029	1.59	0.320	2.23
	500	6.56	5.19	0.82	1.21	0.021	1.94	0.362	2.34
SHS60	1300	6.71	18.99	2.18	1.08	0.027	1.07	0.167	1.32
	800	10.40	7.17	2.08	1.03	0.018	1.03	0.163	1.33
	500	15.31	3.03	1.91	0.95	0.012	0.79	0.122	0.99
SHS80	1300	9.18	10.54	2.98	0.86	0.016	0.56	0.096	1.08
	800	13.05	3.89	2.61	0.76	0.010	0.55	0.084	0.94
	500	17.07	1.67	2.13	0.62	0.007	0.60	0.098	1.09
SHS100	1300	11.24	6.42	3.65	0.80	0.010	0.60	0.076	1.52
	800	14.57	2.76	2.91	0.65	0.007	0.69	0.046	0.94
	500	18.20	1.41	2.28	0.51	0.006	0.90	0.062	1.24

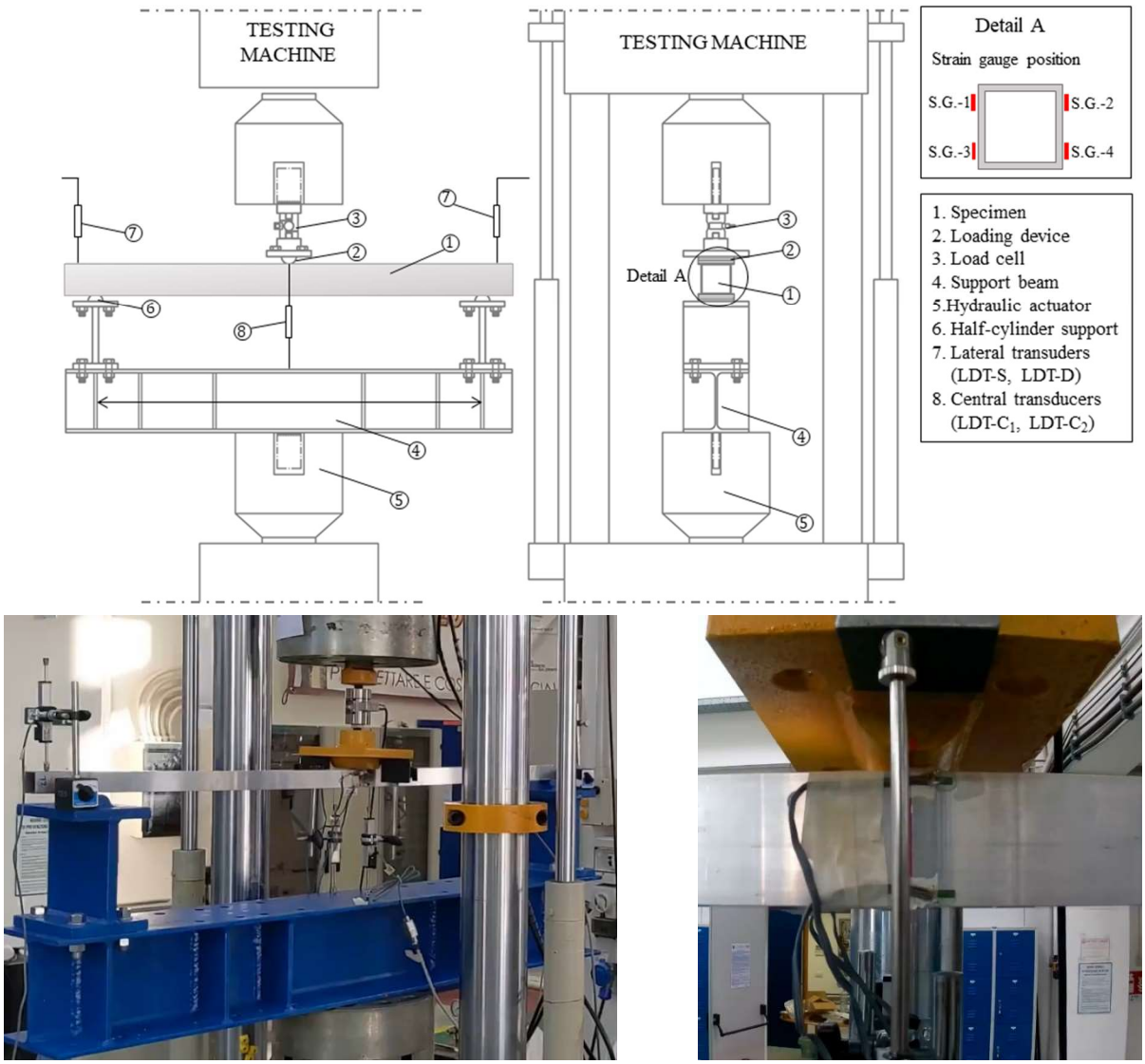

Figure 3.16. Setup of Three Point Bending Test.

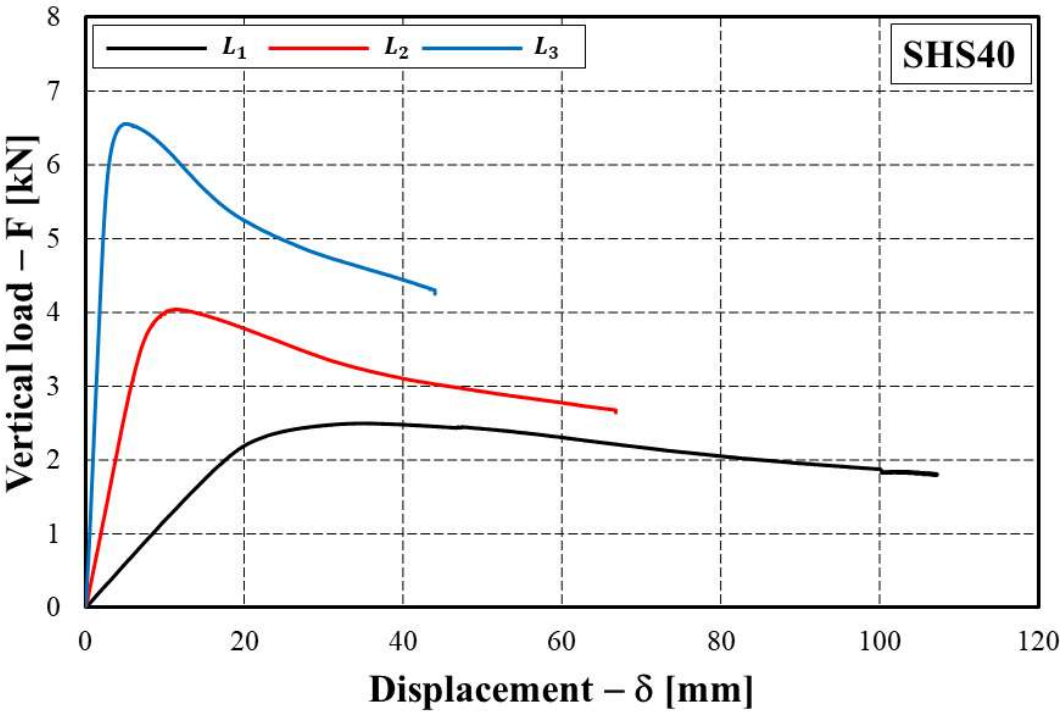

Figure 3.17. Experimental curve $F - \delta$ for SHS40.

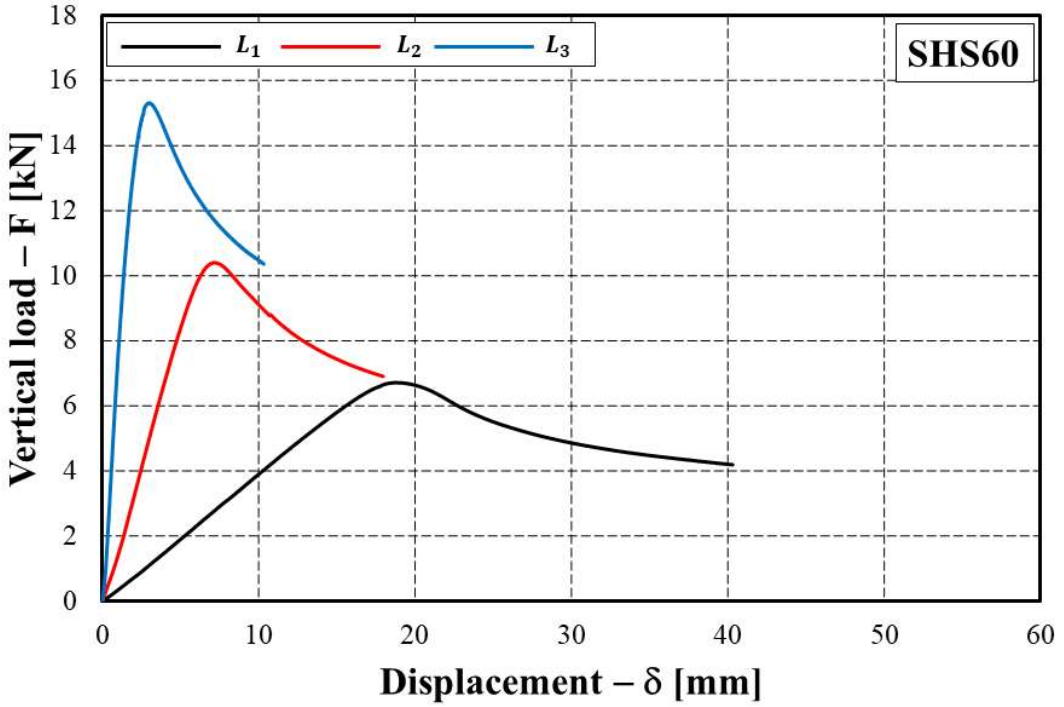

Figure 3.18. Experimental curve $F - \delta$ for SHS60.

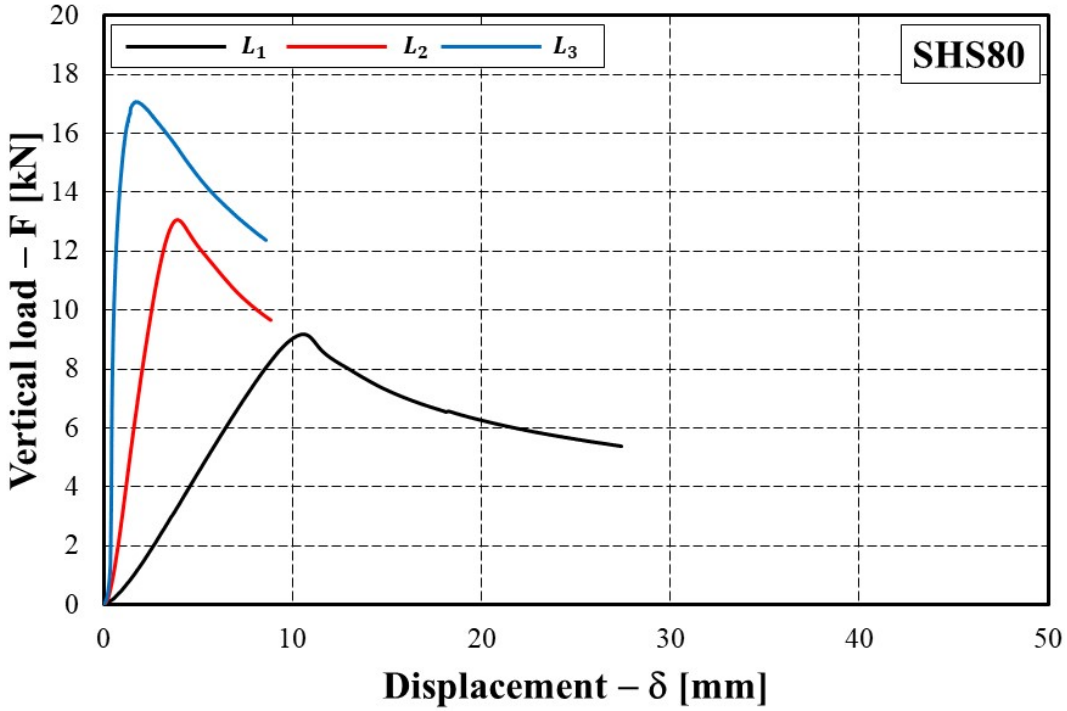

Figure 3.19. Experimental curve F − δ for SHS80.

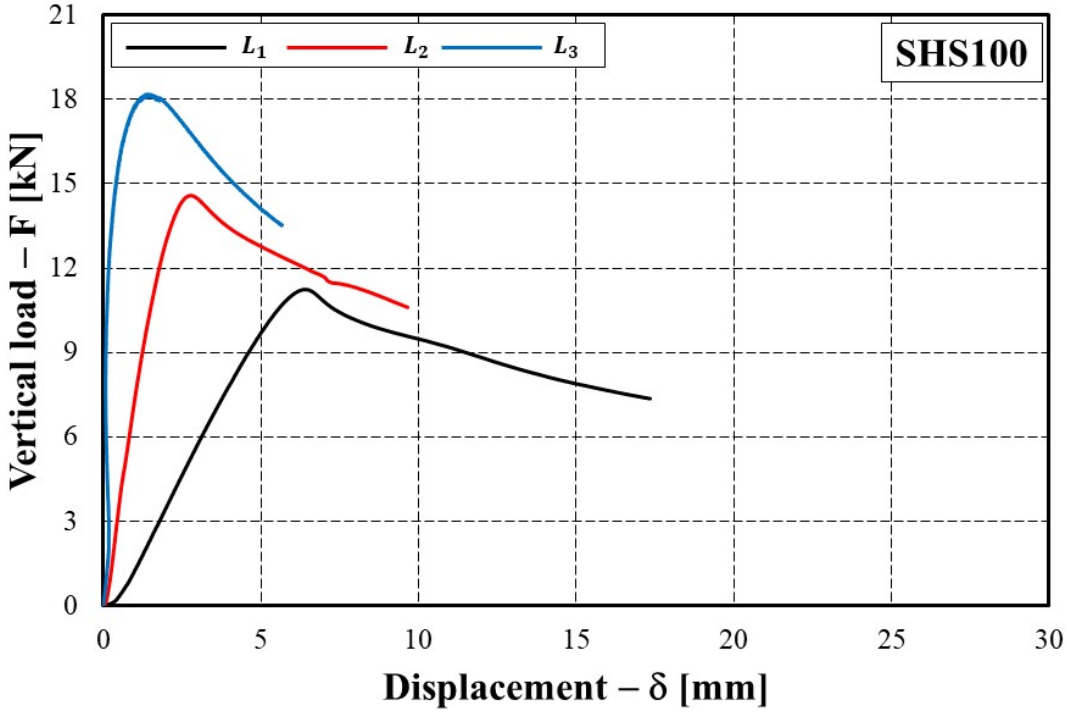

Figure 3.20. Experimental curve F − δ for SHS100.

Figure 3.21. Close-up of beam after testing showing typical formation of local buckles.

3.5. References

[3.1] **EN1999-1-1:** "Eurocode 9: Design of aluminium structures - Part 1-1: General structural rules", European Committee for Standardization, 2007.

[3.2] **C. Faella, F.M. Mazzolani, V. Piluso, G. Rizzano:** "Local buckling of aluminium members: testing and classification", Journal of Structural Engineering, ASCE 2000, 126 (3), pp.353–60, 2000.

[3.3] **R. Feng, W. Zhu, H. Wan, A. Chen, Y. Chen:** "Tests of perforated aluminium alloy SHSs and RHSs under axial compression", Thin-Walled Structures, 130, pp.194–212, 2018.

[3.4] **M.N. Su, B. Young, L. Gardner:** "Testing and design of aluminum alloy cross sections in compression", Journal of Structural Engineering, 140(9), 2014.

[3.5] **H.X. Yuan, Y.Q. Wang, T. Chang, X.X. Du, Y.D. Bu, Y.J. Shi:** "Local buckling and post buckling strength of extruded aluminium alloy stub columns with slender I-sections", Thin-Walled Structures, 90, pp.140-149, 2015.

[3.6] **G.J. Heimerl and D.E. Niles:** "Column and plate compressive strengths of aircraft structural materials extruded 14S-T aluminium alloys", NACA Technical Note L6c19, National Advisory Committee on Aeronautics, Washington, D.C., 1946.

[3.7] **G.J. Heimerl and J.A. Roy:** "Column and plate compressive strengths of aircraft structural materials extruded 75S-T aluminium alloys", NACA Technical Note L5F08a, National Advisory Committee on Aeronautics, Washington, D.C., 1945.

[3.8] **G.J. Heimerl and D.P. Fay:** "Column and plate compressive strengths of aircraft structural materials extruded R303S-T aluminium alloys", NACA Technical Note L5H04, National Advisory Committee on Aeronautics, Washington, D.C., 1945.

[3.9] **L.A. Moen, O.S. Hopperstad, M. Langseth:** "Rotational capacity of aluminum beams under moment gradient. I: Experiments", Journal of Structural Engineering, 125 (8), pp. 910-920, 1999.

[3.10] **J.H. Zhu and B. Young:** "Design of aluminum alloy flexural members using direct strength method", Journal of Structural Engineering, 135(5), pp.558–566, 2009.

[3.11] **Y. Kim and T. Peköz:** "Ultimate flexural strength of aluminum sections". Thin-Walled Structures, 48, pp.857–865, 2010.

[3.12] **M.N. Su, B. Young, L. Gardner:** "Continuous beams of aluminum alloy tubular cross sections. I: Tests and FE model validation", Journal of Structural Engineering, 141(9), 2015.

[3.13] **M.N. Su, B. Young, L. Gardner:** ". Flexural response of aluminium alloy SHS and RHS with internal stiffeners", Engineering Structures, 121, pp. 170-180, 2016.

[3.14] **Y.Q. Wang, Z.X. Wang, F.X. Yin, L. Yang, Y.J. Shi, J. Yin:** "Experimental study and finite element analysis on the local buckling behavior of aluminium alloy beams under concentrated loads". Thin-Walled Structures, 105, pp. 44–56, 2016.

[3.15] **UNI-EN-ISO 6892-1:** "Metallic materials – Tensile testing – Part 1: Method of test at room temperature", European Standard, 2020.

[3.16] **F.M. Mazzolani:** "Aluminium Alloy Structure", E&FN SPON. An imprint of Chapman & Hall, London, 1994.

CHAPTER 4
INTERACTIVE LOCAL BUCKLING UNDER UNIFORM COMPRESSION

4.1. Introduction

The ultimate resistance and the plastic deformation capacity of metal members are strongly affected by the local slenderness of the plate elements constituting the member section, i.e., the width-to-thickness ratios of the plate elements. The occurrence of local buckling, either in the elastic or in the plastic range, is the phenomenon governing the ultimate behaviour of metal members. In particular, ductile behaviour can be obtained provided that the occurrence of local buckling in the elastic range is prevented by properly limiting the width-to-thickness ratios of the plate elements [4.1],[4.2]. Therefore, the study of plastic local buckling has paramount importance in the investigation of the ultimate resistance and plastic deformation capacity of metal members [4.3]-[4.5].

For this reason, many research activities have been carried out to predict the ultimate resistance and the plastic deformation of metal members, considering the occurrence of local buckling in the plastic range [4.6]-[4.10]. However, as illustrated by *Georgantzia et al.* [4.11], the current methodologies, aiming the evaluation the inelastic response of aluminium members, provide the predictional values of ultimate compressive resistance which are excessively conservative in comparison with the experimental results, presented in the technical literature.

So, in order to improve the accuracy in the evaluation of the ultimate behaviour of aluminium profiles under uniform compression, a fully theoretical approach has been developed for hollow sections and H-shaped sections, taking into account the instability phenomena in the plastic range. In particular, starting from the buckling differential equation of a single plate, derived under the assumption that the Poisson's ratio is variable in the elastic-plastic range (Chapter 2), the plastic critical stress and the corresponding deformation have been predicted by imposing the boundary conditions accounting for the interaction between the plate elements constituting the section resulting from the edge's connection between adjacent plates. Specifically, the plastic critical stress is obtained by looking for the stress value leading to a non-trivial solution of the equation's system resulting from the boundary conditions.

Finally, the accuracy of the theoretical approach, based on the J_2 deformation theory of plasticity, is pointed out by the comparison with available experimental data. In particular, in the case of hollow

sections, the comparison has been made with the experimental results presented in Chapter 3 (Table 3.5) and with those provided by *Su et al.* [4.8] and *Faella et al.* [4.12]. In the case of H-shaped sections, the results of the stub column test have been extracted from the NACA reports [4.13]-[4.15] and from the experimental campaign carried out by *Yuan et al.* [4.16]. The main mechanical and geometrical properties of the experimental data are reported in Annex A at the end of this work.

4.2. Interactive Local Buckling of Aluminium Members

4.2.1. Theoretical Procedure for Box Section

In the section 2.3.5, the solution of the differential equation of the plate at buckling under uniaxial compression has been derived for the single plate element, Eq. (2.78) . To investigate the interactive local buckling of box-sections in either the elastic or the plastic range the solution of the plate differential equation, Eq. (2.16), has to be applied to the two plate elements (plate 1 and plate 2 in Figure 4.1) constituting the member section. Therefore, 8 integration constants have to be derived to get:

Plate 1

$$w_1(x,y) = \left(A_1^{(1)} cosh\alpha_1 y_1 + A_2^{(1)} sinh\alpha_1 y_1 + A_3^{(1)} cos\beta_1 y_1 + A_4^{(1)} sin\beta_1 y_1\right) sin\lambda x \qquad (4.1)$$

Plate 2

$$w_2(x,y) = \left(A_1^{(2)} cosh\alpha_2 y_2 + A_2^{(2)} sinh\alpha_2 y_2 + A_3^{(2)} cos\beta_2 y_2 + A_4^{(2)} sin\beta_2 y_2\right) sin\lambda x \qquad (4.2)$$

By remembering that m is the number of half-waves along $x - direction$ and a the height of aluminium member, according to Figure 4.1, the coefficient λ is equal to $m\pi/a$. The coefficients α_1,β_1, α_2 and β_2 are expressed in (2.80) and they are dependent on the plastic coefficients C_i and, consequently, the stress level and the mechanical non-linearity of aluminium material. Finally, the coefficients $A_i^{(1)}$ and $A_i^{(2)}$ are, respectively, the unknown integration coefficients of the plate 1 and the plate 2.

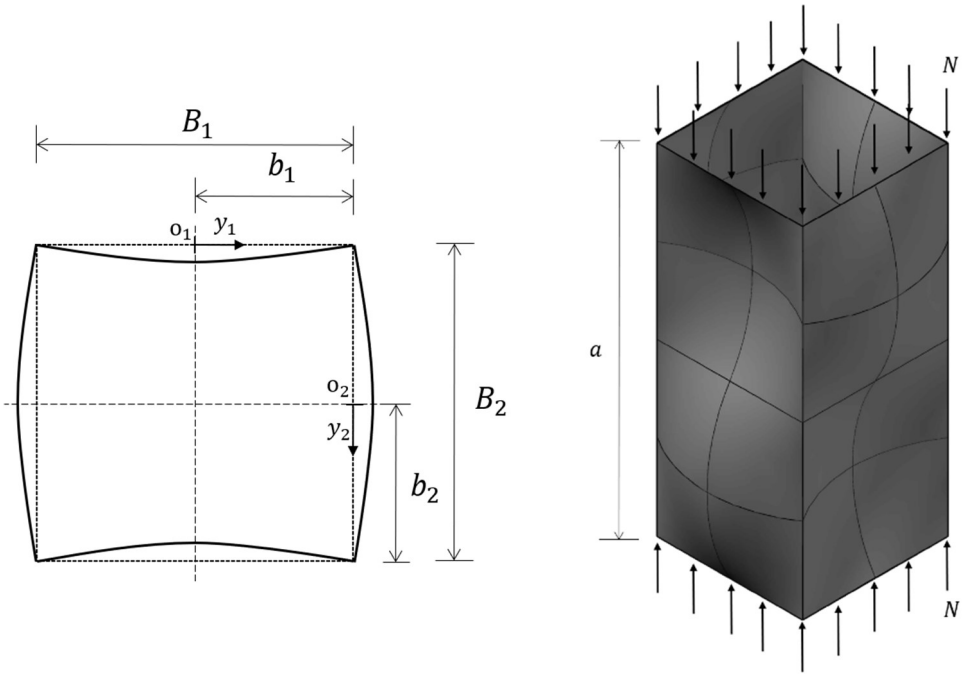

Figure 4.1. Geometrical scheme of a stub column under uniform compression having box-section.

According to Figure 4.1, in the middle of each plate the rotations and the equivalent shear actions are equal to zero:

Plate 1

$$1)\left.\frac{\partial w_1}{\partial y_1}\right|_{y_1=0} = 0 \Rightarrow A_2^{(1)}\alpha_1 + A_4^{(1)}\beta_1 = 0$$

$$2)\ R_{x.1}^*|_{y_1=0} = 0 \Rightarrow C_5\left.\frac{\partial^3 w_1}{\partial y_1^3}\right|_{y_1=0} + (C_3 + 1 - \nu)\left.\frac{\partial^3 w_1}{\partial x_1^3 \partial y_1}\right|_{y_1=0} = 0 \Rightarrow \tag{4.3}$$

$$\Rightarrow C_5\left(A_2^{(1)}\alpha_1^3 - a_4^{(1)}\beta_1^3\right) - \lambda^2(C_3 + 1 - \nu)\left(A_2^{(1)}\alpha_1 + A_4^{(1)}\beta_1\right) = 0$$

Plate 2

$$1)\left.\frac{\partial w_2}{\partial y_2}\right|_{y_2=0} = 0 \Rightarrow A_2^{(2)}\alpha_2 + A_4^{(2)}\beta_2 = 0$$

$$2)\ R_{x.2}^*|_{y_2=0} = 0 \Rightarrow C_5\left.\frac{\partial^3 w_2}{\partial y_2^3}\right|_{y_2=0} + (C_3 + 1 - \nu)\left.\frac{\partial^3 w_2}{\partial x_2^3 \partial y_2}\right|_{y_2=0} = 0 \Rightarrow \tag{4.4}$$

$$\Rightarrow C_5\left(A_2^{(2)}\alpha_2^3 - A_4^{(2)}\beta_2^3\right) - \lambda^2(C_3 + 1 - \nu)\left(A_2^{(2)}\alpha_1 + A_4^{(2)}\beta_2\right) = 0$$

Because of double symmetry, it is easy to recognize that:

$$A_2^{(1)} = A_4^{(1)} = A_2^{(2)} = A_4^{(2)} = 0 \tag{4.5}$$

Consequently, there are only four unknown integration coefficients which can be collected in the transpose vector $\underline{A}$:

$$\underline{A} = \left[A_1^{(1)} \quad A_3^{(1)} \quad A_1^{(2)} \quad A_3^{(2)}\right]^T \tag{4.6}$$

So that. The Eqns. (4.1) and (4.2) becomes:

$$w_1(x,y) = \left(A_1^{(1)} cosh\alpha_1 y_1 + A_3^{(1)} cos\beta_1 y_1\right) sin\lambda x \tag{4.7}$$

and:

$$w_2(x,y) = \left(A_1^{(2)} cosh\alpha_2 y_2 + A_3^{(2)} cos\beta_2 y_2\right) sin\lambda x \tag{4.8}$$

The remaining boundary conditions along the common side are:

- *Displacement condition for* $y_1 = b_1$

$$1)\ w_1|_{y_1=b_1} = 0 \Rightarrow A_1^{(1)} cosh\alpha_1 b_1 + A_3^{(1)} cos\beta_1 b_1 = 0 \tag{4.9}$$

- *Displacement condition* $y_2 = -b_2$

$$2)\ w_2|_{y_2=-b_2} = 0 \Rightarrow A_1^{(2)} cosh\alpha_2 b_2 + A_3^{(2)} cos\beta_2 b_2 = 0 \tag{4.10}$$

- *Rotation condition at the common edge*

$$3)\ \left.\frac{\partial w_1}{\partial y_1}\right|_{y_1=b_1} = \left.\frac{\partial w_2}{\partial y_2}\right|_{y_2=-b_2} \Rightarrow$$
$$\Rightarrow A_1^{(1)}\alpha_1 sinh\alpha_1 b_1 - A_3^{(1)}\beta_1 sin\beta_1 b_1 + A_1^{(2)}\alpha_2 sinh\alpha_2 b_2 - A_3^{(2)}\beta_2 sin\beta_2 b_2 = 0 \tag{4.11}$$

- *Bending moment condition at the common edge*

$$4)\ M_y\big|_{y_1=b_1} = M_y\big|_{y_2=-b_2} \Rightarrow$$
$$\Rightarrow D_s^{(1)}\left[C_5\frac{\partial^2 w_1}{\partial y_1^2} + (\nu + C_3 - 1)\frac{\partial^2 w_1}{\partial x^2}\right]\Bigg|_{y_1=b_1} = D_s^{(2)}\left[C_5\frac{\partial^2 w_2}{\partial y_2^2} + \nu(\nu + C_3 - 1)\frac{\partial^2 w_2}{\partial x^2}\right]\Bigg|_{y_2=-b_2} \tag{4.12}$$

where $D_s^{(1)}$ and $D_s^{(2)}$ are, respectively, the secant flexural rigidities of the plate 1 and the plate 2 and their expressions are provided in (2.62). By noting that:

$$\left.\frac{\partial^2 w_1}{\partial x^2}\right|_{y_1=b_1} = -\lambda^2 sinkx\left[A_1^{(1)} cosh\alpha_1 b_1 + A_3^{(1)} cos\beta_1 b_1\right]$$
$$\left.\frac{\partial^2 w_2}{\partial x^2}\right|_{y_2=-b_2} = -\lambda^2 sinkx\left[A_1^{(2)} cosh\alpha_2 b_2 + A_3^{(2)} cos\beta_2 b_2\right] \tag{4.13}$$

and taking into account the Eqns. (4.9) and (4.10), it results:

$$\left.\frac{\partial^2 w_1}{\partial x^2}\right|_{y_1=b_1} = 0$$
$$\left.\frac{\partial^2 w_2}{\partial x^2}\right|_{y_2=-b_2} = 0 \tag{4.14}$$

So, Eq. (4.12) can be written as:

$$4)\ D_s^{(1)}\left.\frac{\partial^2 w_1}{\partial y_1^2}\right|_{y_1=b_1} = D_s^{(2)}\left.\frac{\partial^2 w_2}{\partial y_2^2}\right|_{y_2=-b_2} \Rightarrow \tag{4.15}$$
$$\Rightarrow D_s^{(1)}A_1^{(1)}\alpha_1^2 cosh\alpha_1 b_1 - D_s^{(1)}A_3^{(1)}\beta_1^2 cos\beta_1 b_1 = D_s^{(2)}A_1^{(2)}\alpha_2^2 cosh\alpha_2 b_2 - D_s^{(2)}A_3^{(2)}\beta_2^2 sin\beta_2 b_2$$

The four boundary conditions along the common edge lead to a system of four equations, which can be expressed under matrix form, as follows:

$$\begin{bmatrix} cosh\alpha_1 b_1 & cos\beta_1 b_1 & 0 & 0 \\ 0 & 0 & cosh\alpha_2 b_2 & cos\beta_2 b_2 \\ \alpha_1 sinh\alpha_1 b_1 & -\beta_1 sin\beta_1 b_1 & \alpha_2 sinh\alpha_2 b_2 & -\beta_2 sin\beta_2 b_2 \\ D_s^{(1)}\alpha_1^2 cosh\alpha_1 b_1 & -D_s^{(1)}\beta_1^2 cos\beta_1 b_1 & -D_s^{(2)}\alpha_2^2 cosh\alpha_2 b_2 & D_s^{(2)}\beta_2^2 cos\beta_2 b_2 \end{bmatrix} \begin{Bmatrix} A_1^{(1)} \\ A_3^{(1)} \\ A_1^{(2)} \\ A_3^{(2)} \end{Bmatrix} = \begin{Bmatrix} 0 \\ 0 \\ 0 \\ 0 \end{Bmatrix} \tag{4.16}$$

A trivial solution $\underline{A} = 0$ represents the unbuckled configuration. A nontrivial solution, corresponding to the occurrence of buckling, is obtained when the membrane axial force reaches a value such that the determinant of the coefficient matrix is equal to zero:

$$\begin{vmatrix} cosh\alpha_1 b_1 & cos\beta_1 b_1 & 0 & 0 \\ 0 & 0 & cosh\alpha_2 b_2 & cos\beta_2 b_2 \\ \alpha_1 sinh\alpha_1 b_1 & -\beta_1 sin\beta_1 b_1 & \alpha_2 sinh\alpha_2 b_2 & -\beta_2 sin\beta_2 b_2 \\ D_s^{(1)}\alpha_1^2 cosh\alpha_1 b_1 & -D_s^{(1)}\beta_1^2 cos\beta_1 b_1 & -D_s^{(2)}\alpha_2^2 cosh\alpha_2 b_2 & D_s^{(2)}\beta_2^2 cos\beta_2 b_2 \end{vmatrix} = 0 \tag{4.17}$$

The buckling stress corresponding to the solution of Eq. (4.17) can be easily found employing a numerical procedure working for increasing values of the axial stress in the plate elements up to the identification of the value satisfying Eq. (4.17).

4.2.2. Theoretical procedure for H-shaped section

The same considerations and, consequently the same steps, can be repeated to evaluate the ultimate behaviour of H-shaped aluminium members under uniform compression. Therefore, in order to investigate the interactive local buckling of box-sections in either the elastic or the plastic range the solution of the plate differential equation, Eq. (2.16), has to be applied to the flanges and the web plates constituting the member section.

However, because the double symmetry, it is possible to consider only one half of web and one half of flange, as shown in Figure 4.2 (plate 1, plate 2):

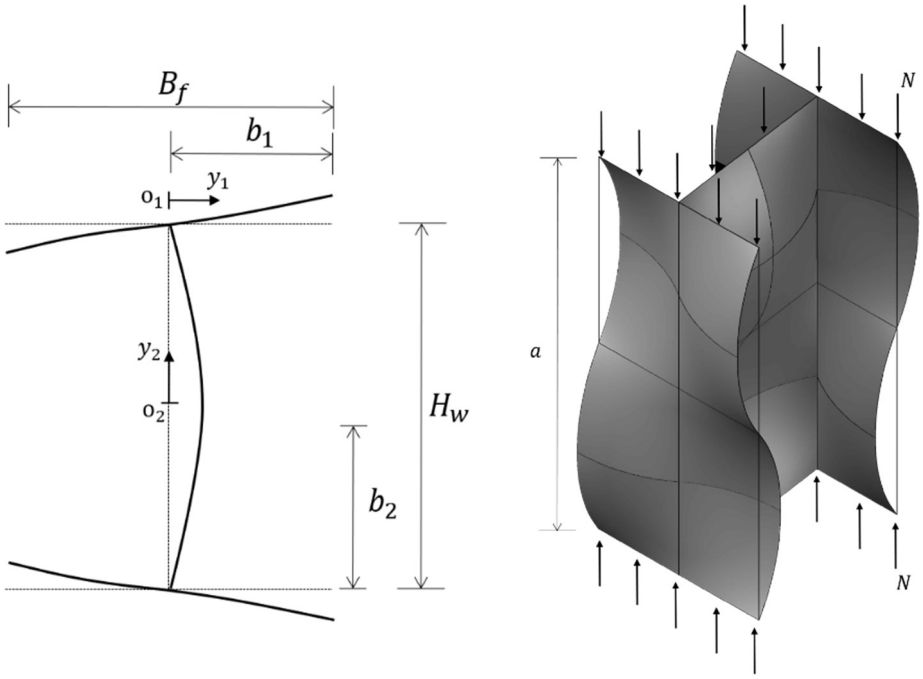

Figure 4.2. Geometrical scheme of a stub column under uniform compression having H-section.

In this case, the unknown integration coefficients are six: four for plate 1 and two for plate 2. In particular, it results:

Plate 1

$$w_1(x,y) = \left(A_1^{(1)} cosh\alpha_1 y_1 + A_2^{(1)} sinh\alpha_1 y_1 + A_3^{(1)} cos\beta_1 y_1 + A_4^{(1)} sin\beta_1 y_1\right) sin\lambda x \qquad (4.18)$$

Plate 2

$$w_2(x,y) = \left(A_1^{(2)} cosh\alpha_2 y_2 + A_3^{(2)} cos\beta_2 y_2\right) sin\lambda x \qquad (4.19)$$

The plate 2 is an internal element and, consequently, it is possible to carry out the same considerations made for the hollow sections [See Eqns. (4.3) and (4.4)]. The unknown vector $\underline{A}$ is equal to:

$$\underline{A} = \left[A_1^{(1)} \quad A_2^{(1)} \quad A_3^{(1)} \quad A_4^{(1)} \quad A_1^{(2)} \quad A_3^{(2)}\right]^T \qquad (4.20)$$

By neglecting the trivial solution $sin\lambda x = 0$, the boundary conditions along the common edge are:

- *Displacement condition for* $y_1 = 0$

1) $w_1|_{y_1=0} = 0 \Rightarrow A_1^{(1)} + A_3^{(1)} = 0$ (4.21)

- *Displacement condition for* $y_2 = b_2$

2) $w_2|_{y_2=b_2} = 0 \Rightarrow A_1^{(2)} cosh\alpha_2 b_2 + A_3^{(2)} cos\beta_2 b_2 = 0$ (4.22)

- *Rotation condition at the common edge*

$$3)\ \left.\frac{\partial w_1}{\partial y_1}\right|_{y_1=0} = \left.\frac{\partial w_2}{\partial y_2}\right|_{y_2=b_2} \Rightarrow A_2^{(1)}\alpha_1 + A_4^{(1)}\beta_1 - A_1^{(2)}\alpha_2 sinh\alpha_2 b_2 + A_3^{(2)}\beta_2 sin\beta_2 b_2 = 0 \tag{4.23}$$

- *Bending moment at the common edge* [see Eqns. (4.14) and (4.15)]

$$4)\ M_y\big|_{y_1=0} = M_y\big|_{y_2=b_2} \Rightarrow D_s^{(1)}\left.\frac{\partial^2 w_1}{\partial y_1^2}\right|_{y_1=0} = D_s^{(2)}\left.\frac{\partial^2 w_2}{\partial y_2^2}\right|_{y_2=b_2} \Rightarrow$$

$$\Rightarrow A_1^{(1)}D_s^{(1)}\alpha_1^2 - A_3^{(1)}D_s^{(1)}\beta_1^2 - A_1^{(2)}D_s^{(2)}\alpha_2^2 cosh\alpha_2 b_2 + A_3^{(2)}D_s^{(2)}\beta_2^2 cos\beta_2 b_2 = 0 \tag{4.24}$$

The boundary condition along the free edge ($y_1 = b_1$) are:

- *Bending moment for* $y_1 = b_1$

$$5)\ M_y\big|_{y_1=b_1} = 0 \Rightarrow D_s^{(1)}\left[C_5\frac{\partial^2 w_1}{\partial y_1^2} + (\nu + C_3 - 1)\frac{\partial^2 w_1}{\partial x^2}\right]\Bigg|_{y_1=b_1} = 0 \Rightarrow$$

$$\Rightarrow A_1^{(1)}\phi_\alpha cosh\alpha_1 b_1 + A_2^{(1)}\phi_\alpha sinh\alpha_1 b_1 - A_3^{(1)}\phi_\beta cos\beta_1 b_1 - A_4^{(1)}\phi_\beta sin\beta_1 b_1 = 0 \tag{4.25}$$

- *Equivalent shear action for* $y_1 = b_1$

$$6)\ R_{x.1}^*\big|_{y_1=0} = 0 \Rightarrow C_5\left.\frac{\partial^3 w_1}{\partial y_1^3}\right|_{y_1=0} + (C_3 + 1 - \nu)\left.\frac{\partial^3 w_1}{\partial x_1^3 \partial y_1}\right|_{y_1=0} = 0 \Rightarrow$$

$$\Rightarrow A_1^{(1)}\psi_\alpha sinh\alpha_1 b_1 + A_2^{(1)}\psi_\alpha cosh\alpha_1 b_1 + A_3^{(1)}\psi_\beta sin\beta_1 b_1 - A_4^{(1)}\psi_\beta cos\beta_1 b_1 = 0 \tag{4.26}$$

where the expressions of the coefficients ϕ_α, ϕ_β, ψ_α and ψ_β are reported in Eq. (4.27) and they are perfectly analogous to the expressions provided for only the elastic region and reported in Eq. (2.21).

$$\begin{aligned}
\phi_\alpha &= C_5\alpha_1^2 - (\nu + C_3 - 1)\lambda^2 \\
\phi_\beta &= C_5\beta_1^2 + (\nu + C_3 - 1)\lambda^2 \\
\psi_\alpha &= C_5\alpha_1^3 - (C_3 + 1 - \nu)\alpha_1^2\lambda^2 \\
\psi_\beta &= C_5\beta_1^3 + (C_3 + 1 - \nu)\beta_1^2\lambda^2
\end{aligned} \tag{4.27}$$

By expressing $A_3^{(1)} = -A_1^{(1)}$, the unknown coefficients can be further reduced to five and, consequently, the critical stress can be obtained by solving the following system:

$$\begin{bmatrix}
0 & 0 & 0 & cosh\alpha_2 b_2 & cos\beta_2 b_2 \\
0 & \alpha_1 & \beta_1 & -\alpha_2 sinh\alpha_2 b_2 & \beta_2 sin\beta_2 b_2 \\
D_s^{(1)}(\alpha_1^2 + \beta_1^2) & 0 & 0 & -D_s^{(2)}\alpha_2^2 cosh\alpha_2 b_2 & D_s^{(2)}\beta_2^2 cos\beta_2 b_2 \\
\phi_\alpha cosh\alpha_1 b_1 + \phi_\beta cos\beta_1 b_1 & \phi_\alpha sinh\alpha_1 b_1 & -\phi_\beta sin\beta_1 b_1 & 0 & 0 \\
\psi_\alpha sinh\alpha_1 b_1 - \psi_\beta sin\beta_1 b_1 & \psi_\alpha cosh\alpha_1 b_1 & -\psi_\beta cos\beta_1 b_1 & 0 & 0
\end{bmatrix}
\begin{Bmatrix} A_1^{(1)} \\ A_2^{(1)} \\ A_4^{(1)} \\ A_1^{(2)} \\ A_3^{(2)} \end{Bmatrix} = \begin{Bmatrix} 0 \\ 0 \\ 0 \\ 0 \\ 0 \end{Bmatrix} \tag{4.28}$$

A nontrivial solution, corresponding to the occurrence of buckling, is obtained when the membrane axial force reaches a value such that the determinant of the coefficient matrix is equal to zero:

$$\begin{vmatrix} 0 & 0 & 0 & cosh\alpha_2 b_2 & cos\beta_2 b_2 \\ 0 & \alpha_1 & \beta_1 & -\alpha_2 sinh\alpha_2 b_2 & \beta_2 sin\beta_2 b_2 \\ D_s^{(1)}(\alpha_1^2+\beta_1^2) & 0 & 0 & -D_s^{(2)}\alpha_2^2 cosh\alpha_2 b_2 & D_s^{(2)}\beta_2^2 cos\beta_2 b_2 \\ \phi_\alpha cosh\alpha_1 b_1 + \phi_\beta cos\beta_1 b_1 & \phi_\alpha sinh\alpha_1 b_1 & -\phi_\beta sin\beta_1 b_1 & 0 & 0 \\ \psi_\alpha sinh\alpha_1 b_1 - \psi_\beta sin\beta_1 b_1 & \psi_\alpha cosh\alpha_1 b_1 & -\psi_\beta cos\beta_1 b_1 & 0 & 0 \end{vmatrix} = 0 \qquad (4.29)$$

It is worthwhile mentioning that the parameters α_1, β_1, α_2, and β_2 in the previous equations are dependent on the stress level according to Eq. (2.80), where also the coefficients of the plate stability differential equation (C_1, C_3 and C_5) are dependent on the stress level. Therefore, the buckling stress corresponding to the solution of Eq. (4.29) can be easily found employing a numerical procedure working for increasing values of the axial stress in the plate elements up to the identification of the value satisfying Eq. (4.29).

4.3. Numerical Procedure by means of MATLAB

As mentioned previously, the solutions of the Eqns. (4.17) and (4.29) can not be reached in closed form, because the parameters, presented in these relationships, are dependent on the stress level and, consequently, on the value of the critical stress to be determined. For this reason, a numerical procedure has been developed through the MATLAB program [4.17]. In particular, the critical value of the stress in the plastic region, corresponding to the bifurcation point of equilibrium, can be found for increasing values of the axial stress in the plate elements until the determinant of the coefficient matrix is equal to zero, as depicted in Figure 4.3.

As an example, the program script is reported in reference only to the hollow section. It is divided in three main parts:

- *Section 1.* The main mechanical e geometrical properties are reported in this part. In particular, the stress-strain relationship of aluminium material is described according to Ramberg-Osgood law [Eq. (3.3)].

```
%ELASTIC-PLASTIC BUCKLING FOR BOX SECTION UNIFORM COMPRESSION
clear all
close all
clc

%MECHANICAL PROPERTIES
E=70000; %Young's modulus [MPa]
n=25; %Ramberg-Osgood exponent
f02=260; %Yield stress [MPa]
fu=310; %Ultimate stress [MPa]
s= [0: fu]; % Stress vector [MPa]
e =s./E+0.002*(s./f02). ^n; %Strain vector
ne=0.33; %Poisson's ratio
np=0.5; %Plastic Poisson's ratio
```

```
%GEOMETRIC DATA
m=[1:8]; %Number of buckling half-waves along the loading direction
a=300; % Plate length [mm]
%PLATE 1
b1=100; %width plate 1 [mm]
t1=5; %thickness plate 1 [mm]
%PLATE 2
b2=100; %width plate 2 [mm]
t2=5; %thickness plate 2 [mm]
%%
```

- *Section 2.* The secant and tangent moduli, the Poisson's ratio and, consequently, the elastic-plastic coefficient H and C_i are determined as a function of the stress vector, according to the relationships provided in Section 2.3. Moreover, the vectors of coefficients α_i and β_i are computed according to Eq. (2.80).

```
%DEFINITION OF ELASTIC-PLASTIC COEFFICIENTS
for i=2: length(e)
  Es(i)=s(i). /e(i); %Secant modulus vector
  Et(i)=(s(i)-s(i-1)). /(e(i)-e(i-1)); %Tangent modulus vector
  ni(i)=np-(Es(i). /E) *(np-ne); %Poisson' ratio according to Gerard and Wildhorn
  H(i)=1+(((1-2*ni(i)). ^2). /4*(1-ni(i). ^2)). *(1-Et(i)./Es(i));
  C1(i)=1-(((2-ni(i)). ^2). /(4*H(i). *(1-ni(i). ^2))) .*(1-Et(i)./Es(i)); % Coefficient C1
  C3(i)=1+(((2-ni(i)). *(1-2*ni(i))). /(4*H(i). *(1-ni(i). ^2))).*(1-Et(i)./Es(i)); % Coefficient C3
  C5(i)=1-(((1-2*ni(i)). ^2). /(4*H(i). *(1-ni(i).^2))).*(1-Et(i)./Es(i)); %Coefficient C5
  D1(i)=Es(i)*(t1^3/(12*(1-ni(i)^2))); %Flexural rigidity of the plate 1
  D2(i)=Es(i)*(t2^3/(12*(1-ni(i)^2))); %Flexural rigidity of the plate 2
end

%DEFINITION OF COEFFICIENTS ALPHA AND BETA
%Plate 1
k1=(m*pi)/a; %Buckling factor for plate 1
N1=t1*s;
A1=sqrt((C3*(k1^2) +k1*sqrt((C3*k1). ^2-C5. *(C1*(k1^2)-N1./D1))./C5);
B1=sqrt((-C3*(k1^2) +k1*sqrt((C3*k1). ^2-C5. *(C1*(k1^2)-N1./D1))./C5);

%Plate 2
k2=(m*pi)/a; %Buckling factor for plate 2
N2=t2*s;
A2=sqrt((C3*(k2^2) +k2*sqrt((C3*k2). ^2-C5. *(C1*(k2^2)-N2. /D2))). /C5);
B2=sqrt((-C3*(k2^2) +k2*sqrt((C3*k2). ^2-C5. *(C1*(k2^2)-N2. /D2))). /C5);
%%
```

- *Section 3.* In the last part, the determinant of coefficient matrix is computed by increasing the load applied to the plates constituting the box section. Finally, the elastic-plastic buckling stress is evaluated as the value corresponding to a determinant equal to zero. However, this will never be exactly zero, for this reason, the final result can be obtained by means of a linear interpolation.

```
%DEFINITION OF DETERMINANT OF COEFFICIENT MATRIX
for i=1:length(e)
Det(i)=det([cosh(A1(i)*b1),cos(B1(i)*b1),0,0;0,0,cosh(A2(i)*b2),cos(B2(i)*b2);A1(i)*sinh(A1(i)*b1),-
B1(i)*sin(B1(i)*b1),A2(i)*sinh(A2(i)*b2),-B2(i)*sin(B2(i)*b2);D1(i)*(A1(i)^2)*cosh(A1(i)*b1),-
D1(i)*(B1(i)^2)*cos(B1(i)*b1),-D2(i)*(A2(i)^2)*cosh(A2(i)*b2),D2(i)*(B2(i)^2)*cos(B2(i)*b2)]);
end
```

```
%COMPUTATION OF ELASTIC-PLASTIC CRITICAL STRESS
p=find(Det<=0);
Scr=(-Det(p(1)-1)*((s(p(1))-s((p(1)-1)))/(Det(p(1))-Det(p(1)-1))))+s(p(1)-1);
%%
```

Obviously, this procedure has to be repeated for increasing the number buckling half-waves along the loading direction. The final value of the buckling stress will be the smallest among those computed. The ultimate resistance $N_{u.th}$ is provided by the product of the critical stress $\sigma_{cr.p}$ and the geometric area of aluminium member A. With reference to aluminium alloy 6082-T6, characterized by a nominal conventional stress $f_{0.2} = 260\ MPa$ and the Ramberg-Osgood coefficient $n = 25$, the relationship between the width-to-thickness ratio and the interactive critical stress in the elastic-plastic range is reported in Figure 4.4. for a square hollow section and a H-shaped section. It is possible to observe that, for a fixed value of the slenderness ratio $\mathrm{b/t}$, the critical stress of box section is greater than that of H-section. This is obvious because, under the same conditions, the occurrence of the local buckling occurs earlier in the outstand parts, constituting the H-section, than in the flat internal parts constituting the hollow sections. Moreover, by observing the shape of curves, the transition between the only elastic region and the post elastic region is provided by the change in curvature of the curves.

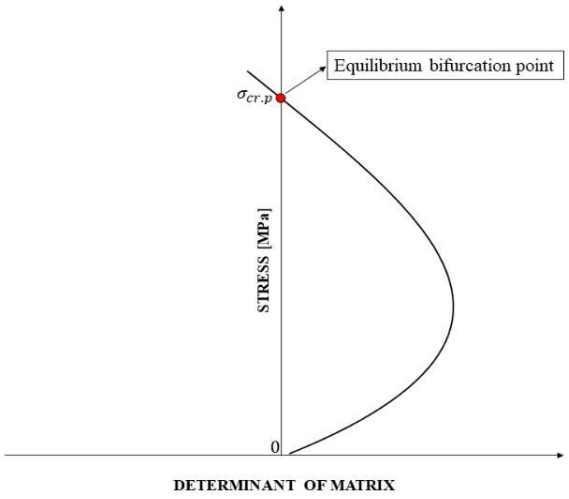

Figure 4.3. A generic trend between the determinant of matrix and the stress level in compression.

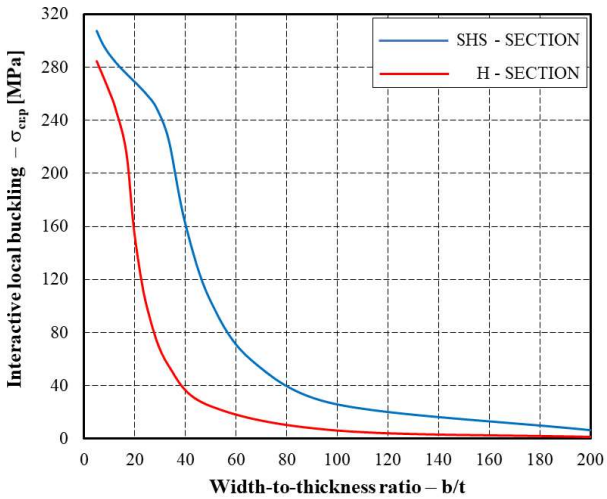

Figure 4.4. Relationship between the width-to-thickness ratio and the interactive critical stress.

4.4. Comparison with Stub Tests

The accuracy of the theoretical procedure can be investigated by comparing the theoretical results with the values of the ultimate resistance obtained by stub column tests. To this scope, in the case of hollow section, reference is made to the stub column tests provided in Chapter 3, the stub tests recently performed by *Su et al.* [4.8] at the Structural Laboratory at the University of Hong Kong and the experimental campaign carried out by *Faella et al.* [4.12] at the beginning of the new millennium at the University of Salerno. As regards the H-shaped section, the comparison is referred to the experimental campaign performed by *Heimerl et al.* [4.13]-[4.15] in 1945 and whose results are collected NACA Technical Reports (National Advisory Committee on Aeronautics) and, more recently, the stub column tests carried out by *Yuan et al.* [4.16] at the school of Civil Engineering of Wuhan University. Most of the specimens are made of aluminium alloys belonging to the 6000 series, as it represents the series most used in civil structural applications. However, there are some specimens belonging to the 2000 and 7000 series, especially for the H-shaped sections.

The geometrical and mechanical properties of all specimens, considered for comparison with the theoretical results, are collected in Annex A. In the case of the stub column tests, described in the Section 3.3, reference is made to the mean values of the mechanical and geometrical properties, provided in Table 3.2 and Table 3.3.

In Figure 4.5-Figure 4.8, the comparison between the theoretical procedure and the experimental tests is provided. In particular, in Figure 4.5 and Figure 4.7, the theoretical buckling loads $N_{u.DTP}$, obtained by the procedure based on the deformation theory of plasticity, are compared with the experimental results $N_{u.exp}$. While Figure 4.6 and Figure 4.8 show the comparison between the theoretical normalised strains $\bar{\varepsilon}_{u.DTP}$, corresponding to the theoretical buckling load $N_{u.DTP}$, and the experimental normalised strains $\bar{\varepsilon}_{u.exp}$. The normalization of the strain, corresponding to the occurrence of local buckling, is defined according to Eq. *(3.6)*. The accuracy of the prediction of the ultimate behaviour of aluminium members is very high, especially, as regards the ultimate resistance. In fact, the average value of the ratio $N_{u.DTP}/N_{u.exp}$ is equal to 1.02 for hollow sections and 1.01 for H-shaped sections, while the standard deviation is, respectively, equal to 0.089 and 0.080. Instead, the prediction of the deformation capacity is less accurate. In fact, the average value of the ratio $\bar{\varepsilon}_{u.DTP}/\bar{\varepsilon}_{u.exp}$. is equal to 0.99 for hollow sections and 0.97 for H-shaped sections, while the standard deviation is, respectively, equal to 0.176 and 0.173. However, the theoretical approach is a safety procedure, because, in most cases, the experimental values are greater than those provided by DTP Method. For the sake of completeness, the numerical results are given in Annex A.

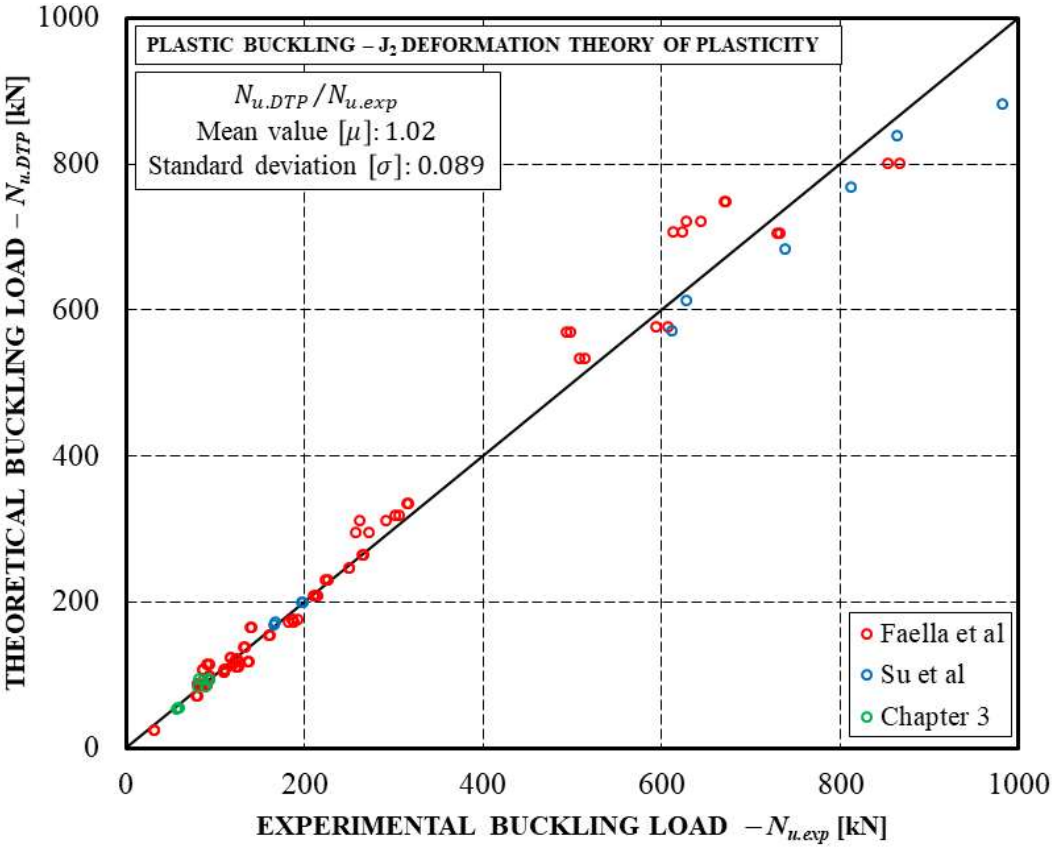

Figure 4.5. Comparison of the theoretical ultimate resistances with experimental results for box sections.

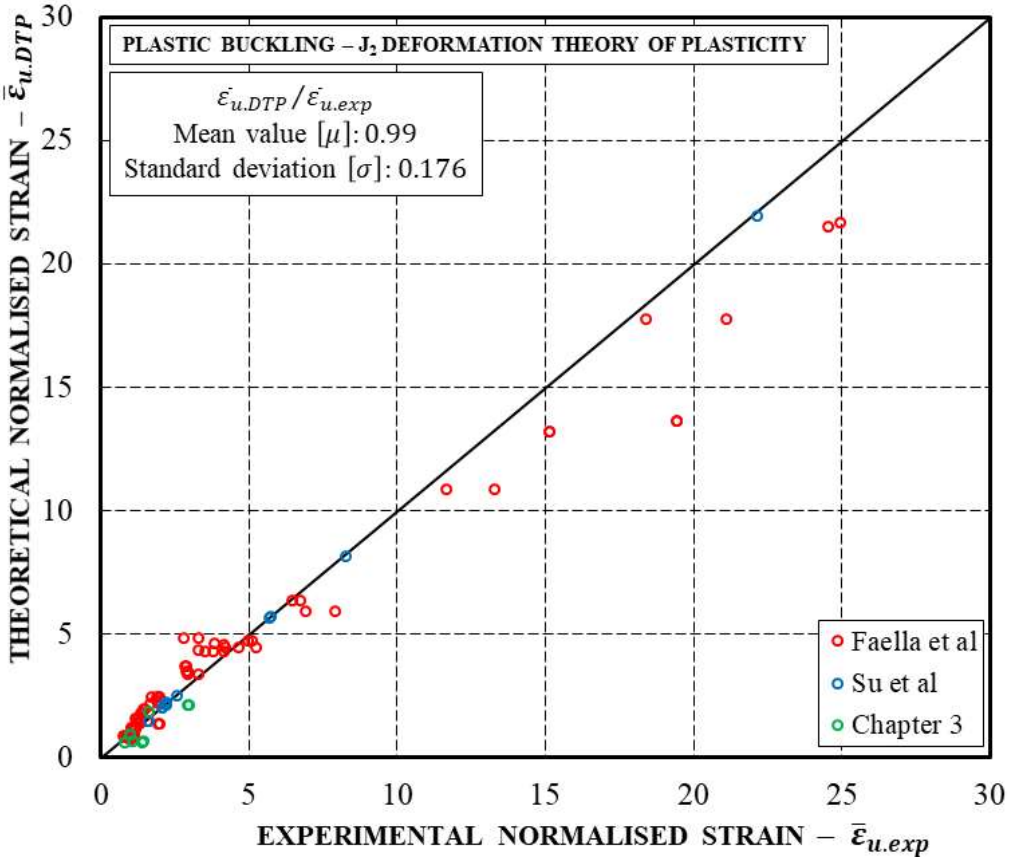

Figure 4.6. Comparison of the theoretical normalised strains with experimental results for box sections.

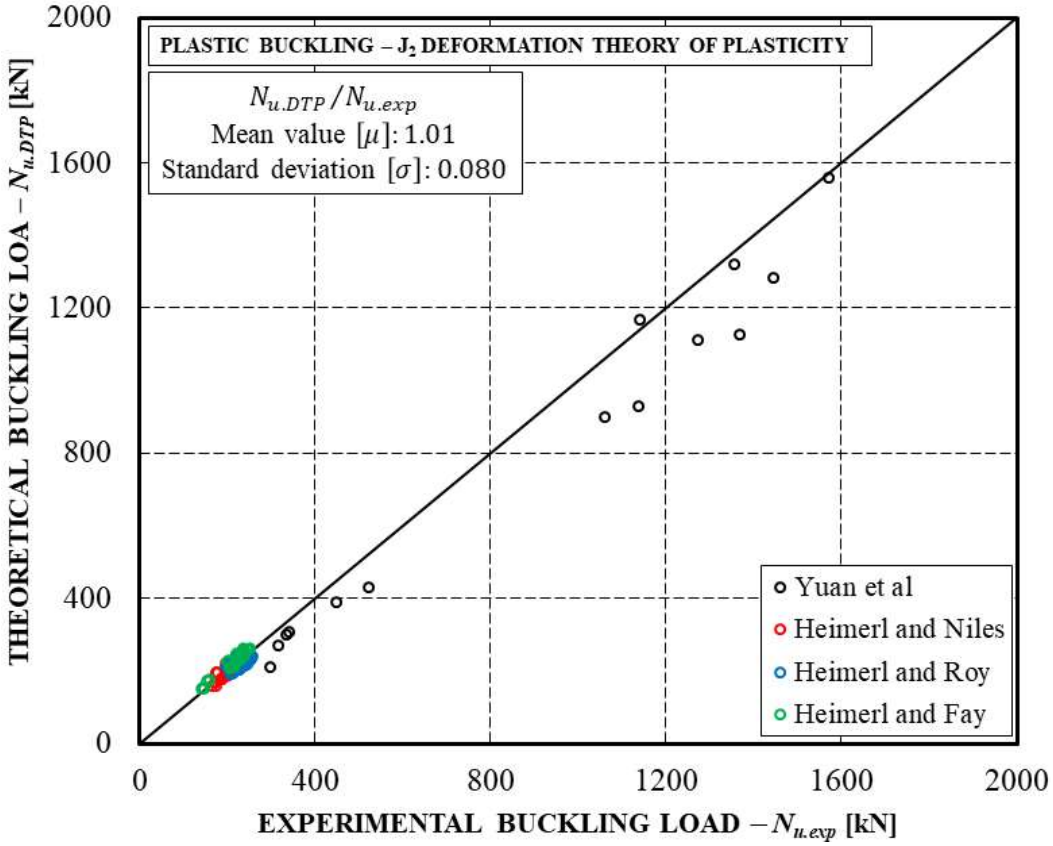

Figure 4.7. Comparison of the theoretical ultimate resistances with experimental results for H- sections.

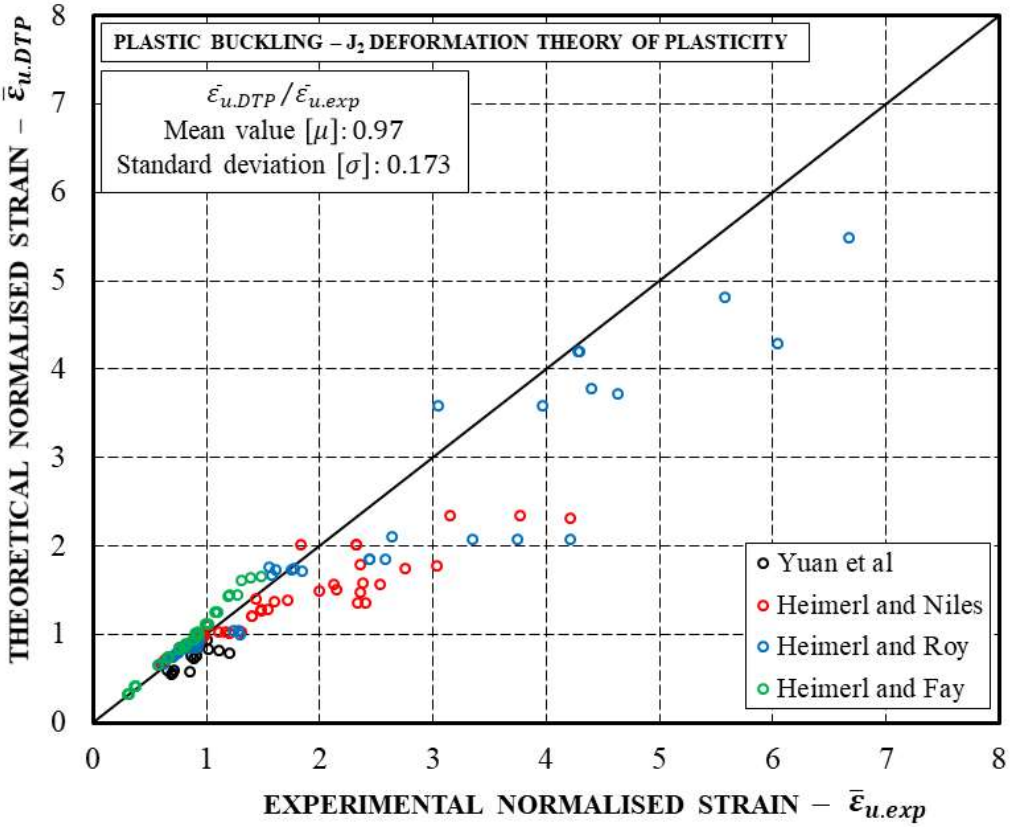

Figure 4.8. Comparison of the theoretical normalised strains with experimental results for H-sections.

4.5. References

[4.1] **EN 1993-1-1**: "Eurocode 3: Design of steel structures - Part 1-1: General rules and rules for buildings", European Committee for Standardization, 2005.

[4.2] **EN1999-1-1:** "Eurocode 9: Design of aluminium structures - Part 1-1: General structural rules", European Committee for Standardization, 2007.

[4.3] **M. Langseth, O.S. Hopperstad**: "Local Buckling of Square Thin-Walled Aluminium Extrusions", Thin-Walled Structures, 27(1), pp. 117-126, 1997.

[4.4] **O.S. Hopperstad, M. Langseth, L. Hanssen**: "Ultimate Compressive Strength of Plate Elements in Aluminium: Correlation of Finite Element Analyses and Tests", Thin-Walled Structures, 29, pp. 31-46, 1997.

[4.5] **G. De Matteis, R. Landolfo, M. Manganiello, F.M. Mazzolani:** "Inelastic behaviour of I-shaped aluminium beams: Numerical analysis and cross-sectional classification" Computers and Structures, 82, pp. 2157-2171, 2004.

[4.6] **L. Gardner, M. Ashraf:** "Structural design for non-linear metallic materials", Engineering Structures,28(6), pp.926–34, 2006.

[4.7] **M. Ashraf, B. Young:** "Design formulations for non-welded and welded aluminium columns using continuous strength method", Engineering Structures, 33(12), pp.3197–3207, 2011.

[4.8] **M.N. Su, B. Young, L. Gardner:** "The continuous strength method for the design of aluminium alloy structural elements", Engineering Structures, 122, pp.338–348, 2016.

[4.9] **NAS:** "North American specification for the design of cold-formed steel structural members", American Iron and Steel Institute, Washington, DC, 2001.

[4.10] **C.D. Moen and B.W. Schafer:** "Direct strength method for design of cold-formed steel columns with holes", Journal of Structural Engineering,137(5),559–570, 2011.

[4.11] **E. Georgantzia, M. Gkantou, G.S. Kamaris:** "Aluminium alloys as structural material: A review of research", Engineering Structures, 227, art. no. 111372, 2021.

[4.12] **C. Faella, F.M. Mazzolani, V. Piluso, G. Rizzano:** "Local buckling of aluminium members: testing and classification", Journal of Structural Engineering, ASCE 2000, 126 (3), pp.353–60, 2000.

[4.13] **G.J. Heimerl and D.E. Niles:** "Column and plate compressive strengths of aircraft structural materials extruded 14S-T aluminium alloys", NACA Technical Note L6c19, National Advisory Committee on Aeronautics, Washington, D.C., 1946.

[4.14] **G.J. Heimerl and J.A. Roy:** "Column and plate compressive strengths of aircraft structural materials extruded 75S-T aluminium alloys", NACA Technical Note L5F08a, National Advisory Committee on Aeronautics, Washington, D.C., 1945.

[4.15] **G.J. Heimerl and D.P. Fay:** "Column and plate compressive strengths of aircraft structural materials extruded R303S-T aluminium alloys", NACA Technical Note L5H04, National Advisory Committee on Aeronautics, Washington, D.C., 1945.

[4.16] **H.X. Yuan, Y.Q. Wang, T. Chang, X.X. Du, Y.D. Bu, Y.J. Shi:** "Local buckling and post buckling strength of extruded aluminium alloy stub columns with slender I-sections", Thin-Walled Structures, 90, pp.140-149, 2015.

[4.17] **MathWorks Inc.** "MATLAB-High Performance Numeric Computation and Visualization Software. User's Guide", Natick: MA, USA, 1997.

CHAPTER 5
INTERACTIVE LOCAL BUCKLING UNDER NON-UNIFORM BENDING

5.1. Introduction

The present Chapter is devoted to the study of the ultimate behaviour of aluminium beams under non-uniform bending moment. It is well known that, under seismic forces, structural members are often subjected to double curvature bending. This is the main reason why the ultimate behaviour and the plastic rotation capacity of metal members are usually investigated by referring either to a cantilever scheme or to the three-point bending testing scheme. In this way, the response under double curvature bending is interpreted considering the influence of the so-called shear length which is practically coincident with the distance between the point of zero moment and the section where the maximum bending moment occurs, i.e. the section where the development of the plastic hinge is expected.

As seen in the compressed members, even under bending actions, the occurrence of the instability phenomena, in the compressed parts of the member section influences the inelastic response of the beams. The behaviour obtained is dependent on the width-to-thickness ratio of the plate elements constituting the member section. Such phenomenon governs both the flexural resistance of metal members and their plastic deformation capacity.

Moreover, in the case of aluminium material, the strain-hardening plays a fundamental role both on the ultimate resistance and on the plastic rotation capacity. Strain hardening is related to the exponent n of the Ramberg-Osgood (R–O) constitutive law adopted in Eurocode 9 [5.1]. As higher is the coefficient n as lowest is the strain-hardening effect. So that, the attainment of a comprehensive knowledge of the ultimate behaviour of aluminium alloy beams, compared to the case of steel members, is even more difficult because of the great variety of aluminium alloys with different properties of the stress-strain constitutive law.

Naturally, in case of members subjected to non-uniform bending, plate elements are subjected to a strain gradient along the section and a longitudinal stress gradient due to the shear action. Moreover, the possibility of occurrence of lateral torsional buckling further complicates the ultimate behaviour of such members.

In modern codes, such as Eurocode 3 for steel structures [5.2] and Eurocode 9 [5.1] for aluminium structures, the computational methods are based on the section classification criterion and, in

particular, on the maximum slenderness parameter and the restraining conditions only. Conversely, neither mutual restraining conditions nor the longitudinal stress gradient due to shear is taken into account. Therefore, Eurocodes do not consider the interaction between the slenderness parameters of the plate elements constituting the member section. The influence of the so-called shear length is also neglected. The Japanese code for steel structures adopts a more sophisticated approach; in fact, the member classification accounts for slenderness interaction formulas [5.3].

Nowadays, there is still a substantial gap of knowledge regarding the ultimate behaviour of aluminium alloys beams which would require a large number of experimental tests because of the high variety of aluminium alloy tempers and section shapes. For this reason, many research activities aiming at the development of simplified procedures and formulas for evaluating the ultimate resistance and the rotation capacity of aluminium alloy beams subjected to local buckling under non-uniform bending have been planned.

It is evident that the study of aluminium beams is more complex than the aluminium columns and, consequently, a fully theoretical approach can not be carried out as made for aluminium members under uniform compression (Chapter 4). For this reason, in order to investigate the ultimate behaviour of hollow sections and H-shaped sections under bending moment, the finite element analyses have been performed on the four different aluminium alloys belonging to 6000 series, in order to evaluate the influence of the strain-hardening on the inelastic response of the aluminium beams. Obviously, the validation of FE models, adopted in the simulations, have been provided by comparing moment-rotation curves, obtained by the ABAQUS program [5.4],[5.5] with the experimental curves of the three point bending tests. In particular, in the case of box section, the reference is made to the experimental campaign described in Chapter 3; while for H-shaped section, the finite element curves are compared with the experimental curves provided by *Moen et al.* [5.6]. Subsequently, an extensive parametric analysis has been performed by varying the main mechanical and geometrical non-dimensional parameters: the flange slenderness and the flange-to-web slenderness ratio for taking into account the influence of the interactive local buckling; the ratio between the shear length and the width of section, in order to evaluate the influence of the moment gradient through the shear length. Finally, the empirical relationships are derived to estimate the flexural overstrength and the rotation capacity of aluminium beams in the post elastic range.

5.2. Finite Element Analysis

5.2.1. FE Model and its Validation

FEM simulations represent a practical tool to compensate the gap of knowledge due to the limited number of available experimental test results. In fact, many researchers have simulated the behaviour

of extruded aluminium beams subjected to gradient moment loading [5.7]-[5.10]. In particular, *De Matteis et al.* [5.11],[5.12] evaluated the influence of the main geometrical and mechanical parameters on the ultimate response of extruded beams subjected to the non-uniform bending moment, but they did not propose a formulation to predict the response parameters for practical applications. Also in this case, the attention is devoted to the rectangular and H-shaped sections.

The adopted FE model has been defined in Abaqus program and is similar to the one already proposed by *Moen et al.* [5.7] in a previous work. The scheme of the test set-up corresponds to the simply supported beam with a vertical load at mid-span (Figure 5.1), referred to as three-point bending test. However, the symmetry conditions of this structural scheme allow modelling only one half of the beam according to a cantilever scheme subjected to increasing displacement of a control node corresponding to the support location of the testing scheme. Moreover, the beam is transversely restrained to avoid the lateral displacements and the twist out of the vertical plane, which could generate flexural-torsional buckling. The choice of the partitions and the mesh discretization have been carried out according to the sensitivity analysis provided by *Moen et al.* [5.7] and *De Matteis et al.* [5.11],[5.12]. In particular, the mesh is based on the use of a 4-node shell element with reduced integration (S4R) with five integration points given through the thickness of the plate to guarantee that the spreading of plastic flow and the failure are adequately considered. The mesh density is not constant in the longitudinal direction. In particular, it increases close to the fixed end, where the maximum bending moment occurs. Figure 5.2 shows the partitions, the mesh discretization and the restraints of FE models adopted for box and H-shaped sections.

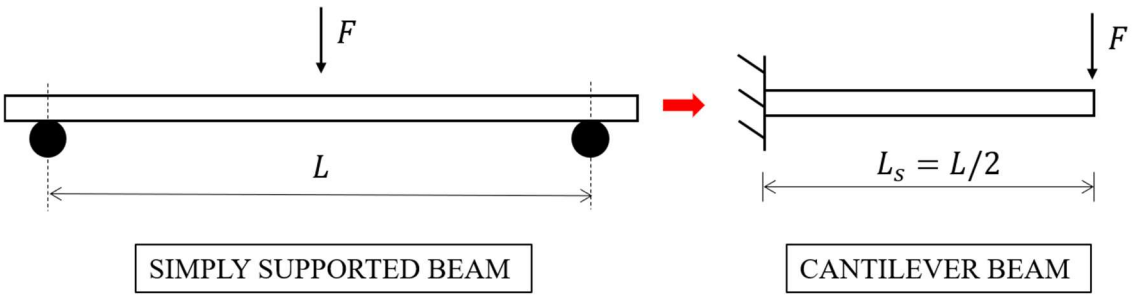

Figure 5.1. Geometrical scheme of FE model.

The numerical analyses have been carried out under displacement control, imposed on the cantilever section corresponding to the support of the testing scheme. In this section, a coupling constraint applied to all the points of section simulates a rigid diaphragm. Preliminarily, the influence of the geometrical imperfections on the ultimate behaviour has been investigated. To this scope, the buckling analysis has been performed and the lowest buckling mode characterised by a buckling shape corresponding to the local buckling of the flange in compression close to the fixed end is used for modelling initial geometrical imperfections. Such buckling mode is depicted in Figure 5.2 (down). The calibration of the magnitude of the corresponding eigenmode to be applied to the undeformed

model accounts for the initial geometrical imperfections. In particular, the scale factor of the eigenmode has been assumed equal to $b/500$, where b is the width of the base plates. The choice of the value of the initial imperfection is made according to the sensitivity analysis carried out by *Moen et al.* [5.7], which showed that the results obtained in the case of the moderate imperfection level are more coherent with the experimental results. The "Static, General" procedure has been performed by automatically increasing the step size. The input parameters imposed for the analysis are reported in the following table:

Table 5.1. The input parameters of static general analysis.

Static general Analysis			
Type:	Automatic		
Maximum Number of increments:	100		
Increment size:	Initial	Minimum	Maximum
	$1 \cdot 10^{-4}$	$1 \cdot 10^{-5}$	1

As the work herein presented is specifically devoted to the distribution of internal actions occurring in the three-point bending test (i.e. non uniform bending accompanied by shear), it is important to underline the differences occurring when four-point bending tests are carried out. In fact, in case of four-point bending tests, the part of the beam subjected to local buckling is under uniform bending so that there is no any longitudinal stress gradient in the plate elements of the bucked zone. Conversely, a stress gradient occurs in case of the three-point bending test so that the occurrence of local buckling is delayed. However, at the same time the length of the yielded zone in the four-point bending test is increased when compared to the three-point bending test. As a result of these effects, the beams subjected to four-point bending test exhibit a decrease of the flexural resistance and an increase of the plastic rotation supply when compared to the results of the three-point bending tests. According to Eurocode 9, the stress-strain relationship is provided in the form $\varepsilon = \varepsilon(\sigma)$ according to the Ramberg-Osgood model (R-O) and reported in Eq. (3.3). However, the experience in finite element analysis of aluminium alloy structures showed significant numerical difficulties and missing convergence drawbacks when using the Ramberg-Osgood model implemented in ABAQUS [5.7],[5.12]. For this reason, the use of the Hopperstad exponential model fitted on the Ramberg-Osgood curve is adopted as the material model. The following equation provides the uniaxial true-stress true-strain model used for the simulations:

$$\sigma = Y_0 + Q\left[1 - \exp(-C\varepsilon_p)\right] \tag{5.1}$$

where σ is the current stress, ε_p is the plastic strain, Y_0 is the conventional elastic limit strength equal to $f_{0.2}$, Q and C, are curve fitting parameters, whose values are presented below (Table 5.3).

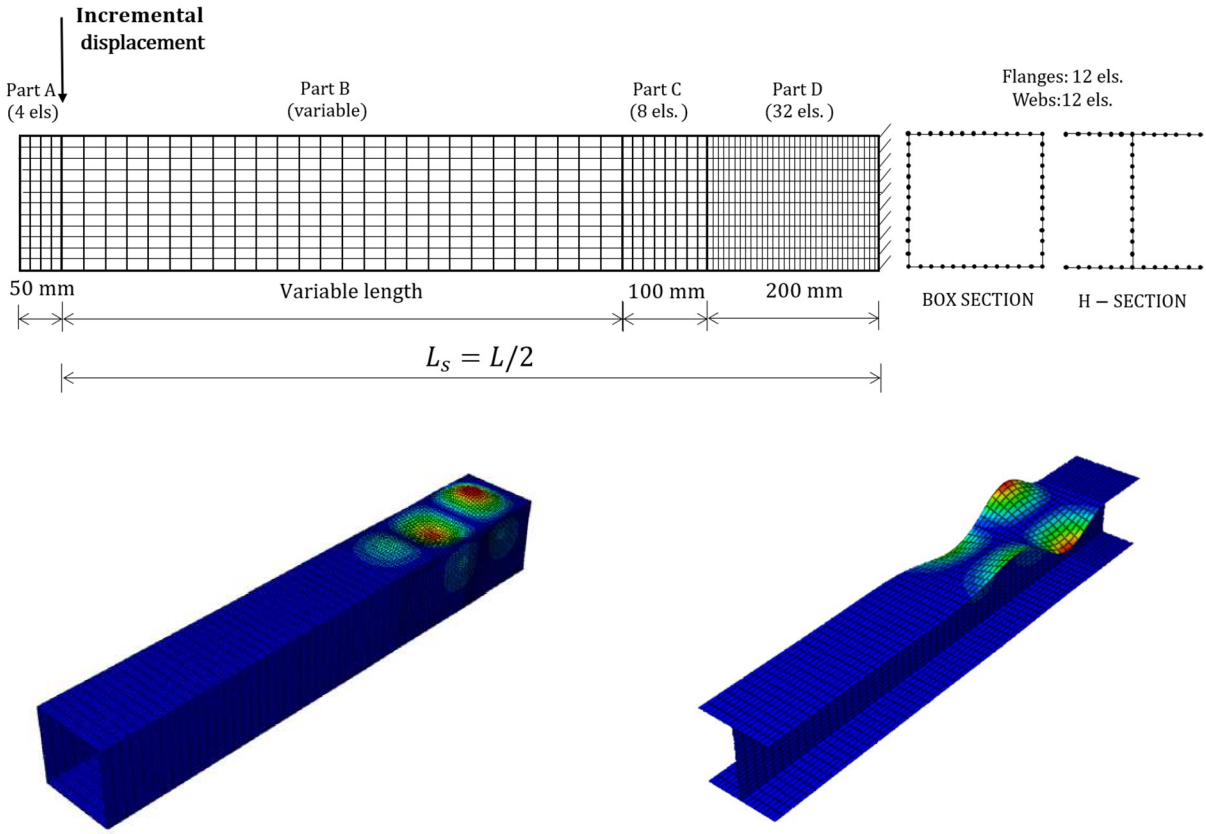

Figure 5.2. Finite element model: mesh discretization and partitions (top); buckling mode adopted to modelling initial imperfections(down).

According to Figure 5.3, the results of the Abaqus program are expressed as the normalised moment-rotation curves ($M/M_{0.2} - \theta/\theta_{0.2}$), which entirely describe the ultimate behaviour of aluminium alloy beams under non-uniform bending. In particular, M is the bending moment along the member length, occurring at the fixed end, θ is the rotation at the cantilever section where the displacement is imposed. As seen above, $M_{0.2}$ and $\theta_{0.2}$ are, respectively, the moment and the rotation corresponding to the achievement of the conventional yield stress $f_{0.2}$, consequently, according to Figure 5.4, it results:

$$M_{0.2} = W_e f_{0.2}$$
$$\theta_{0.2} = \frac{M_{0.2} L}{4EI} = \frac{f_{0.2} L_s}{Eh} \tag{5.2}$$

where W_e is the elastic section modulus, E is the Young's modulus of aluminium material, L is the total length of beam, L_s is the shear length and it is equal to $L/2$ and, finally, I is the inertia moment of section. However, in this case, the elastic section modulus evaluated with reference to the mid-thickness lines of the plate elements constituting the section. This choice is justified considering the use of shell elements for the development of the FE model, rather than the use of brick elements discretizing also the thickness of the plate elements. So that, according to the Figure 5.4, it results:

BOX SECTION	**H − SECTION**	
$W_e = b_f t_f h + \frac{t_w h^2}{3}$	$W_e = b_f t_f h + \frac{t_w h^2}{6}$	(5.3)

where b_f and t_f are, respectively, the width and thickness of the base plate and the h and t_w are the width and thickness of the web plate, referring to the thickness lines of the elements constituting the section (Figure 5.4).

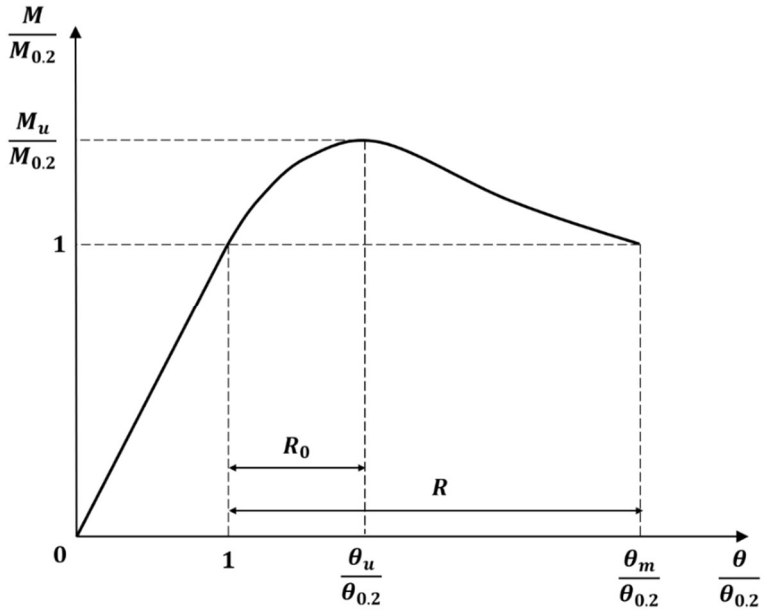

Figure 5.3. Scheme of normalized moment-rotation curve.

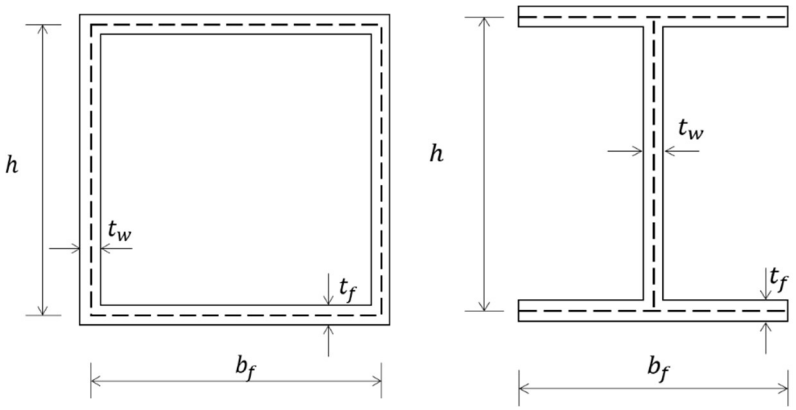

Figure 5.4. Schemes of geometric sections.

The accuracy of FE model has been checked against the available experimental tests presented in Chapter 3 and provided by *Moen et al.* [5.6]. In particular, for the box section, the results presented in Section 3.4 are compared with those obtined by the sofware program. While, in the case of H-section, the comparison is performed with the experimental results, referred to the specimens I_1 and I_2, obtained by *Moen*. The mechanical properties of aluminium alloys, considered for the model calibration, are reported in Table B.1 of Annex B. In the case of the hollow sections, only the beams, exceeding the yield region, have been reported for the comparison, specifically, the SHS40 and

SHS60 aluminium members. Figure 5.5 and Figure 5.6 show the comparison between the nomalised moment-rotation curves obtained by Abaqus and the corresponding experimental curves, respectively, for box sections and H-shaped sections.

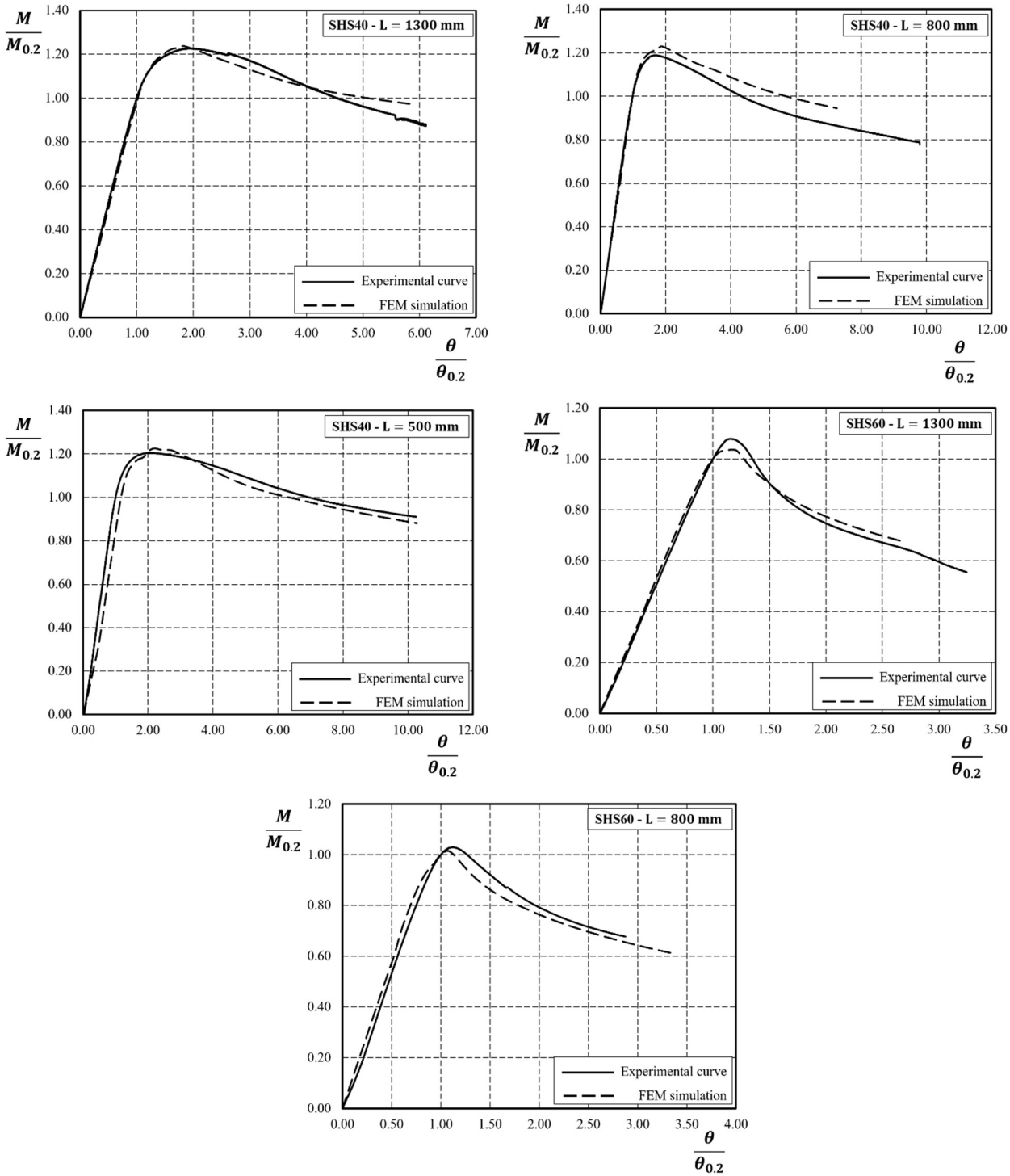

Figure 5.5. Comparison between FE numerical results and experimental test results for box section provided in Chapter 3.

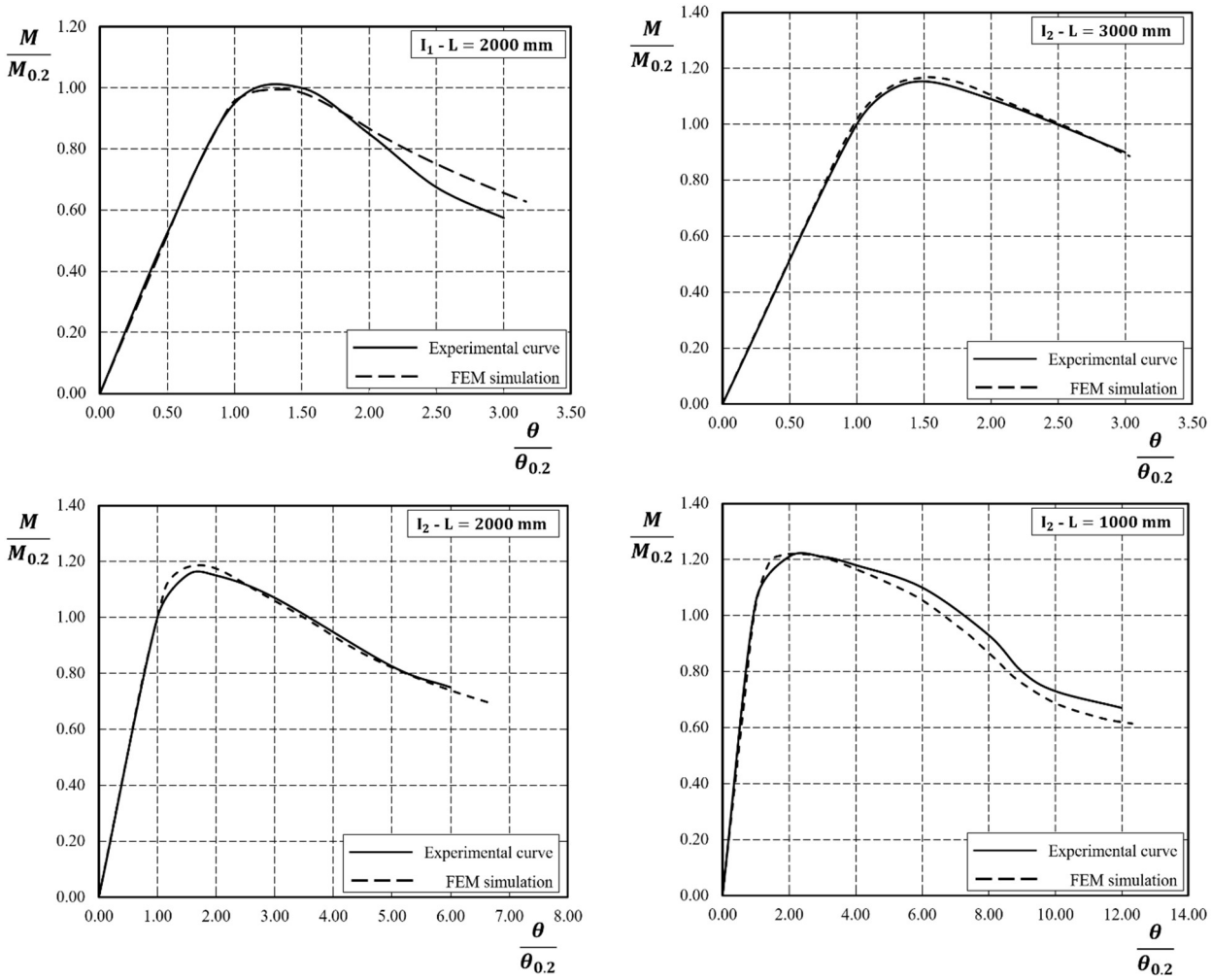

Figure 5.6. Comparison between FE numerical results and experimental test results for H-shaped section provided by Moen et al. [5.6].

5.2.2. Parametric Analysis

In order to investigate the ultimate behaviour of aluminium beams under non-uniform bending, a parametric analysis has been performed. The beams considered in this analysis are extruded profiles made of EN-AW6082 with temper T4 and T6 , EN-AW6063 T5 and, finally, EN-AW6061 T6. Temper T4 is a combination of solution process and natural ageing. After solution, followed by cooling, the material is not work hardened. In case of temper T5, the alloy is cooled after hot working and artificially aged. After the extrusion process, the material is rapidly cooled to obtain further hardening due to artificial ageing. Finally, temper T6 is the treatment it identifies a material artificially aged at a prescribed low temperature, as described in Section 3.2. Table 5.2 provides the nominal chemical composition of such alloys, while Table 5.3 presents the nominal mechanical properties and the values of the best fitting coefficients according to Hopperstad's model [Eq. (5.1)]. The comparison between the stress-strain curves provided by Ramberg-Osgood's law and those obtained by means of Hopperstad's model is reported in Figure 5.7.

Table 5.2. Chemical composition according to EN573-3 [5.13].

Alloy	Si	Fe	Cu	Mn	Mg	Cr	Zn	Ti	Others		Al
									Each	Total	
6082	0.70 -1.30	max 0.50	max 0.10	0.40 - 1.00	0.60 -1.20	max 0.25	max 0.20	max 0.10	max 0.05	max 0.15	rest
6063	0.20 -0.60	0.35	0.10	0.10	0.45 -0.90	0.10	0.10	0.10	max 0.05	max 0.15	rest
6061	0.40-0.80	0.70	0.15-0.40	0.15	0.80-1.20	0.04-0.35	0.25	0.15	max 0.05	max 0.15	rest

Table 5.3. Nominal mechanical material properties of aluminium alloys.

Alloy	***Temper***	$\boldsymbol{E}$ [MPa]	$\boldsymbol{n}$ [−]	$\boldsymbol{f_{0.2}}$ [MPa]	$\boldsymbol{f_u}$ [MPa]	$\boldsymbol{Y_0}$ [MPa]	$\boldsymbol{Q}$ [MPa]	$\boldsymbol{C}$ [−]
EN-AW6082	T4	70000	8	110	205	110	80	20
EN-AW6063	T5	70000	16	130	175	130	45	20
EN-AW6082	T6	70000	25	260	310	260	50	30
EN-AW6061	T6	70000	55	240	260	240	20	40

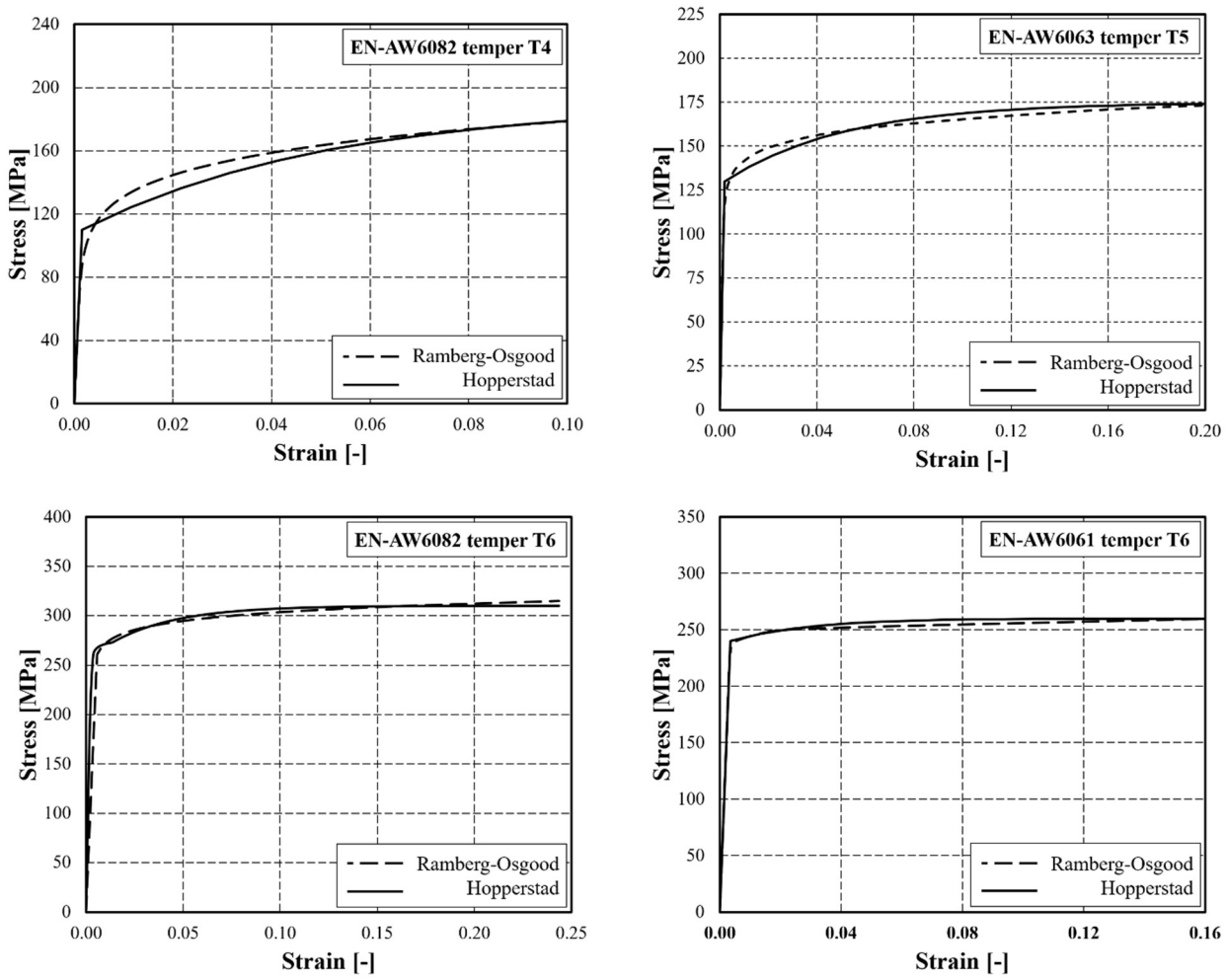

Figure 5.7. Comparison between the Ramberg-Osgood and the Hopperstad stress-strain curves.

According to Figure 5.2 and Figure 5.4, the parametric analysis investigated six parameters: the flange width b, the depth of the section h measured as the distance between the mid-thickness lines of flanges, the flange thickness t_f, the web thickness t_w and the shear length L_s and the Ramberg-Osgood coefficient n by considering four different aluminium alloys (Table 5.3). However, the case $t_f = t_w$ is assumed so that the main parameters reduce to five.

Three main non-dimensional parameters, which influence the non-linear response of H-shaped and box-shaped beams under non-uniform bending, are identified in the following table:

Table 5.4. The main non-dimensional parameters.

Non dimensional parameters	**BOX SECTION**	**H − SECTION**
Flange slenderness [$\boldsymbol{\lambda_f}$]	$\lambda_f = 0.52\frac{b_f}{t_f}\sqrt{\frac{f_{0.2}}{E}}$	$\lambda_f = 0.807\frac{b_f}{t_f}\sqrt{\frac{f_{0.2}}{E}}$
Flange to web slenderness ratio [$\boldsymbol{\alpha_s}$]	$\alpha_s = \frac{b_f t_w}{h t_f}$	$\alpha_s = \frac{b_f t_w}{2h t_f}$
Normalised shear length [$\boldsymbol{\bar{L}_s}$]	$\bar{L}_s = \frac{L_s}{b_f}$	$\bar{L}_s = \frac{L_s}{b_f}$

The slenderness parameters are considered to evaluate the influence of the geometrical properties of cross-section on the ultimate behaviour of beams, while the normalised shear length is introduced to take into account the influence of stress gradient along longitudinal direction. In the case of box-shaped section, 12 value of λ_f have been considered: 0.27, 0.29, 0.33, 0.37, 0.41, 0.44, 0.47, 0.50, 0.55, 0.60, 0.70 and 0.80. While the influence of the flange-to-web slenderness ratio α_s has been investigated by varying its value from 0.50 to 2.00 with a step size equal to 0.50, so that 4 values of have been analysed. Regarding the H-section, the flange slenderness varies λ_f its value from 0.52 to 1.24 with a step size equal to 0.08 for a total of 10 values. While the flange-to-web slenderness ratio α_s ranges from 0.20 to 0.50 with a step size equal to 0.10, so that 4 values of have been analysed.

Finally, concerning the ratio between the shear length and the flange width $\bar{L}_s$, three typical values have been considered for both section types: 6.25, 12.5 and 18.75. It is important to underline that the variation ranges of the investigated parameters are selected according to the commercial geometrical dimensions currently adopted in the structural applications. The number of analysed cases for each alloy is equal to 144 and 120, respectively, for the hollow section and H-shaped section, where only the material characteristics are constant, while the cross-section dimensions and the length of the tested beams change according to the ranges, mentioned above, of variation of the parameters investigated. It is useful to note that, even though minor difference in the definition of the non-dimensional parameters, the parametric analysis herein presented is similar to the one developed by

De Matteis et al. [5.11],[5.12] which gave rise to the background for the classification of cross sections according to Eurocode 9 [5.1]. The different approaches can be proposed for the definition of the slenderness parameter. In the present work, the simple definitions of slenderness parameters are adopted according to Eurocode purpose. Obviously, the disadvantage is that the interaction between the plate elements is not taken into account in the local slenderness definition.

A different approach has been proposed by other researchers where the slenderness is directly defined as the square root of the ratio between the yield and the critical stress [5.14],[5.15]. The main advantage of this approach is that the interaction between the plate elements can be directly taken into account as soon as the critical stress is numerically computed using programs such as CUFSM [5.16] or analytical expressions [5.17] .However, this approach gives rise to additional numerical or analytical work compared to the one herein adopted. The results of the finite element simulations are reported in Appendix D of the present Chapter. In particular, for each investigated aluminium alloy and for a fixed value of α_s and $\bar{L}_s$, the simulation curves are obtained by increasing the flange slenderness parameter λ_f.

5.3. Derivation of mathematical formulas

In this section, in order to evaluate the ultimate behaviour of aluminium members, the mathematical relationships are provided to compute the ultimate flexural resistance and the rotation capacity are presented. In particular, the obtained relations fitted the numerical results coming from FE simulations, previously described. According to Figure 5.3, Such relations provide the non-dimensional ultimate flexural resistance, the stable part of the rotation capacity and the total rotation capacity as functions of non-dimensional parameters presented in the previous section. These parameters are defined according to *Mazzolani and Piluso* [5.18], as also implemented by Eurocode 9. In particular, the flexural overstrength is defined as already shown in Eq. (3.9):

$$\bar{M}_u = \frac{M_u}{M_{0.2}} \tag{5.4}$$

While the capability of the plastic rotation is evaluated by means of two quantities: the stable part of rotation R_0, corresponding to the maximum bending moment and the total rotation capacity R, which includes the post-buckling behaviour. They are given by:

$$R_0 = \frac{\theta_u}{\theta_{0.2}} - 1 \tag{5.5}$$

and:

$$R = \frac{\theta_m}{\theta_{0.2}} - 1 \tag{5.6}$$

Aiming to develop a formula for predicting the non-dimensional ultimate flexural strength of aluminium beams subjected to non-uniform bending, it is necessary to study, preliminarily, the influence of the different non-dimensional geometrical parameters by graphical representations of the finite element model results. The aim is pointing out the role of each parameter, given all the others. From these curves, the first evident observation is that the maximum moment M_u and the ultimate rotation θ_m decrease for increasing values of the normalized slenderness parameter λ_f. In addition, it is evident that $M_u/M_{0.2}$, $\theta_u/\theta_{0.2}$, $\theta_m/\theta_{0.2}$ and, consequently, $\bar{M}_u$, R_0 and R reduce for increasing values of the non-dimensional shear length $\bar{L}_s$. Moreover, by analysing the results provided by FE simulations, it is immediate observing that the normalised flexural strength $\bar{M}_u$ decreases as the flange-to-web slenderness ratio α_s increases. In order to evaluate the trend between the normalised values of flexural capability and the non-dimensional parameters, the Figure 5.8-Figure 5.11 show these relations with reference to H-shaped beams made of EN-AW 6082 T4 aluminium alloy. In particular, Figure 5.8 and Figure 5.9 provide the normalised maximum bending moment $\bar{M}_u$ as a function of the slenderness parameters λ_f, α_s and the non-dimensional shear length $\bar{L}_s$. While the trend between the rotation capacity, in terms of stable rotation part R_0 and total rotational ability R, and the main non-dimensional parameters are reported in Figure 5.10 and Figure 5.11.

The strain-hardening behaviour of aluminium alloys, governed by the Ramberg-Osgood coefficient n, affects the ultimate response of the beams. In particular, it is evident that for each fixed value of λ_f, α_s and $\bar{L}_s$ the non-dimensional parameters $\bar{M}_u$, R_0 and R decreases when the R-O exponent n increases. This means that, even though aluminium alloys EN-AW6082 T6 and EN-AW6061 T6 are characterized by high yielding values, the plastic overstrength capacity is limited by the high values of the R-O exponent. Conversely, the opposite behaviour occurs for low yielding aluminium alloys EN-AW6082 T4 and EN-AW6063 T5. However, it is important to underline that these quantities are a measure of the ductile behaviour of the member, i.e. is the capacity of the aluminium beam of exhibiting a hardening behaviour and, therefore, a plastic capacity.

Taking into account the previous observations as well as the trend between the quantities involved, three multivariate regression are proposed for estimating the flexural overstrength and the rotational capacity of aluminium beams under non-uniform bending:

$$\bar{M}_u = \left\{[c_1\bar{L}_s + c_2\,]\alpha_s + (c_3 n^{c_4})(\bar{L}_s)^{[c_5 n + c_6]}\right\}\lambda_f^{\,[c_7 ln(n) + c_8]} \tag{5.7}$$

$$R_0 = \left(c_1\bar{L}_s^{\,c_2}\right)\exp\left[\alpha_s c_3\bar{L}_s^{\,c_4} - \alpha_s\lambda_f - \lambda_f(c_5 n^{c_6})\bar{L}_s^{\,c_7}\right] \tag{5.8}$$

$$R = \sqrt{\alpha_s}\left[(c_1 n^{c_2})\bar{L}_s^{\,c_3}\right]exp\left\{c_4\alpha_s - [c_5\bar{L}_s + c_6 ln(n) + c_7]\lambda_f\right\} \tag{5.9}$$

where c_i, with $i = 1 \dots 8$, are the regression coefficients and they are different for each formula. In Table 5.5 and Table 5.6 are reported the values of the regression coefficients, respectively, for box section and H-section. It is important to underline that The Eqns. (5.7),(5.8) and (5.9) are the outcomes of the fitting with numerical results obtained by advanced finite element simulations so that they should be used within the following ranges of the performed parametric analysis:

BOX SECTION	**H − SECTION**
$0.27 \leq \lambda_f \leq 0.80$	$0.52 \leq \lambda_f \leq 1.24$
$0.50 \leq \alpha_s \leq 2.00$	$0.20 \leq \alpha_s \leq 0.50$
$6.25 \leq \bar{L}_s \leq 18.75$	$6.25 \leq \bar{L}_s \leq 18.75$

(5.10)

The accuracy of the mathematical formulas is show in Figure 5.12, Figure 5.13 and Figure 5.14, providing the comparisons between the empirical results coming from the mathematical fitting models $[\bar{M}_{u.ER} - R_{0.ER} - R_{ER}]$ and the numerical results obtained by FE simulations $[\bar{M}_{u.FEM} - R_{0.FEM} - R_{FEM}]$. Moreover, in Table 5.7 the main statistical indices of the ratios between the values computed by Eqns. (5.8)-(5.10) and the corresponding results provided by FE simulations. From the comparison of the results, it is evident that the accuracy of the mathematical formula for estimating $\bar{M}_u$ is very high, as testified by the mean value of the empirical over numerical ratio equal to 1.00 while the corresponding standard deviation is equal to 0.02 for both section types. Conversely, in the estimation of the rotational capacity by means of Eqns. (5.8) and (5.9), the standard deviation assumes values higher than 0.15 and this indicates less accuracy in the prediction of R_0 and R. Therefore, to predict the rotation capacity of aluminium beams subjected to local buckling under non-uniform bending, it is suggested the use of Eqns. (5.8) and (5.9) with the corresponding model factors γ_{rd} evaluated according to prEN1993-1-14:2020 [5.19] and delivered in Table 5.7. In particular, the model factor γ_{rd} has been computed as corresponding to the 5% fractile of the ratio between the values resulting from mathematical formulas and the values obtained from FE simulations.

Table 5.5. Regression coefficients for evaluating $\bar{M}_u$, R_0 and R in the case of box-shaped beams.

	c_1	c_2	c_3	c_4	c_5	c_6	c_7	c_8
$\bar{M}_u$	-0.00076	-0.09282	1.0318	0.07255	-0.00059	-0.00383	0.08722	-0.4265
R_0	793.8	-0.9470	1.0318	-5.769	4.506	0.2414	-0.1445	/
R	117800	-1.3765	-0.9129	-0.8155	-0.00045	-2.0083	11.40	/

Table 5.6. Regression coefficients for evaluating $\bar{M}_u$, R_0 and R in the case of H-shaped beams.

	c_1	c_2	c_3	c_4	c_5	c_6	c_7	c_8
$\bar{M}_u$	0.0008	-0.3766	1.4982	-0.0149	0.0002	-0.0684	0.0843	-0.4719
R_0	82.83	-0.1663	1.4982	1.942	1.789	0.1656	0.2543	/
R	222100	-0.8908	-1.6453	-0.7752	-0.0036	-0.0005	4.560	/

Table 5.7. Summary of the comparison between the empirical regressions and the finite element simulations.

BOX SECTION				
	Mean $[\mu]$	Standard deviation $[\sigma]$	Coefficient of variation $[cov]$	Safety coefficient $[\gamma_{rd}]$
$\bar{M}_{u.ER}/\bar{M}_{u.FEM}$	1.00	0.02	0.02	1.03
$R_{0.ER}/R_{0.FEM}$	1.00	0.49	0.49	1.79
$R_{.ER}/R_{.FEM}$	1.05	0.30	0.29	1.55
H − SECTION				
	Mean $[\mu]$	Standard deviation $[\sigma]$	Coefficient of variation $[cov]$	Safety coefficient $[\gamma_{rd}]$
$\bar{M}_{u.ER}/\bar{M}_{u.FEM}$	1.00	0.02	0.02	1.03
$R_{0.ER}/R_{0.FEM}$	0.95	0.16	0.17	1.22
$R_{.ER}/R_{.FEM}$	1.00	0.15	0.15	1.21

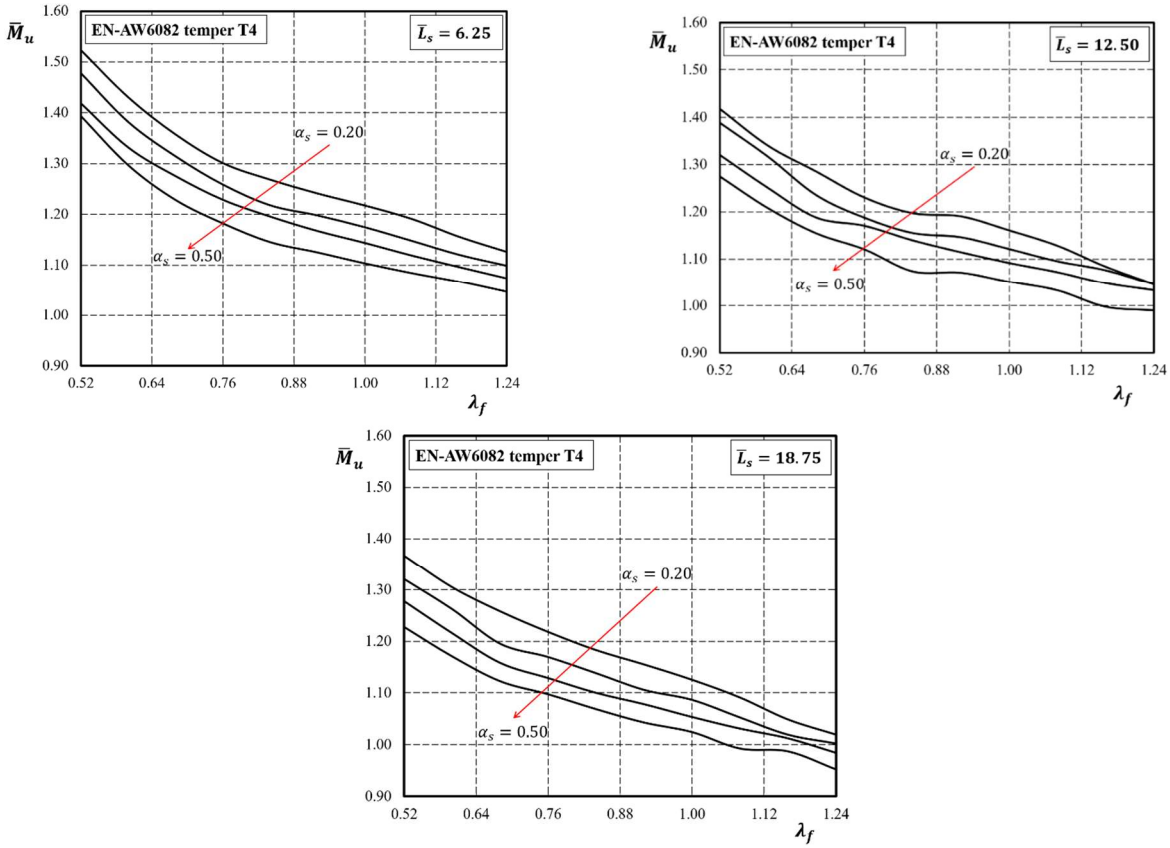

Figure 5.8. Influence of parameter α_s and λ_f on $\bar{M}_u$ for fixed value of $\bar{L}_s$.

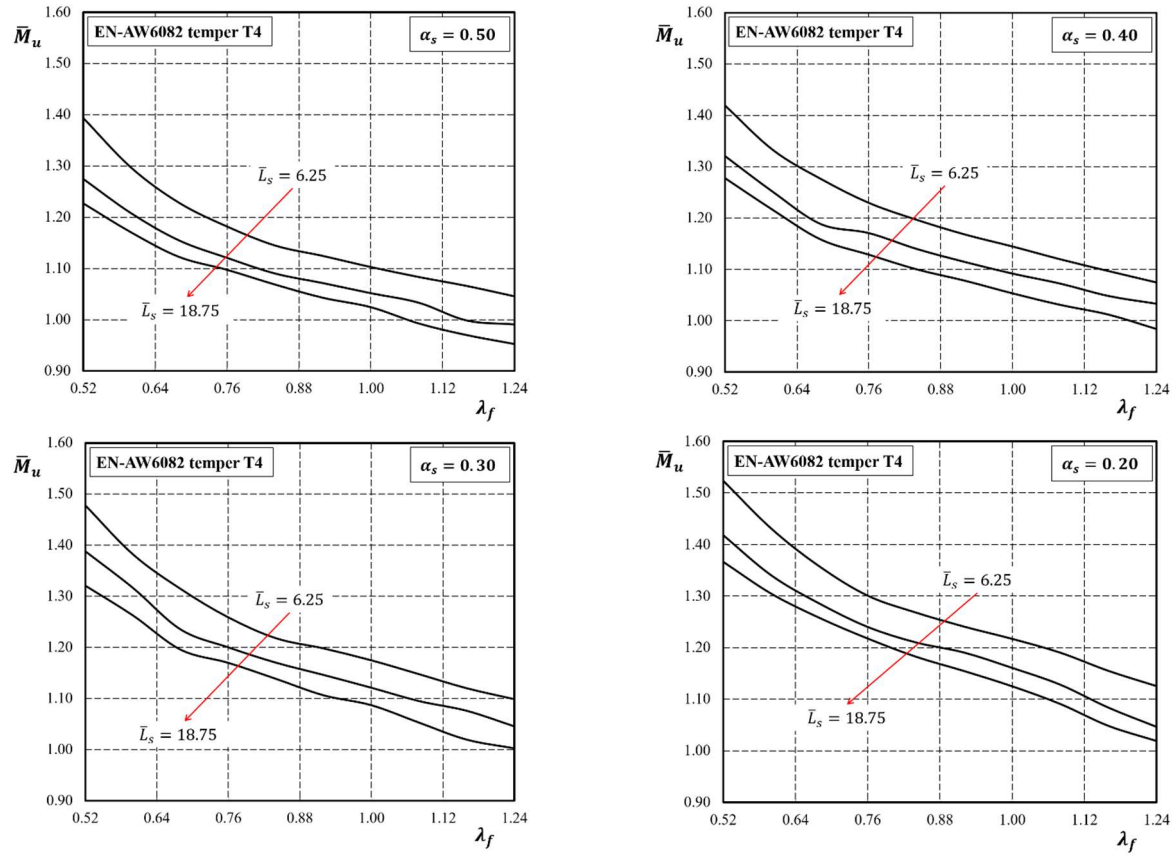

Figure 5.9. Influence of parameter $\bar{L}_s$ and λ_f on $\bar{M}_u$ for fixed value of α_s.

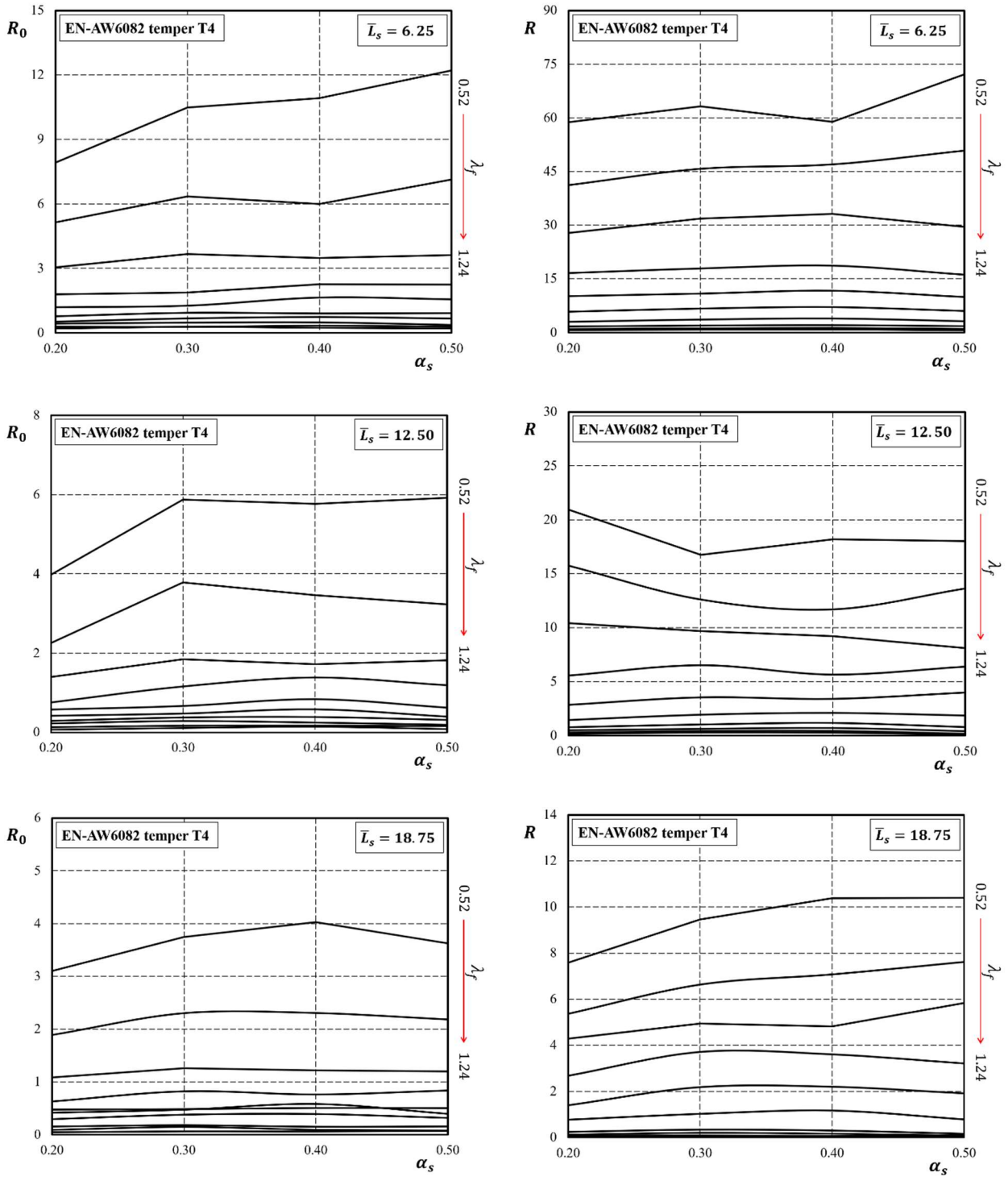

Figure 5.10. Influence of parameter α_s and λ_f on the rotational capacity for fixed value of $\bar{L}_s$.

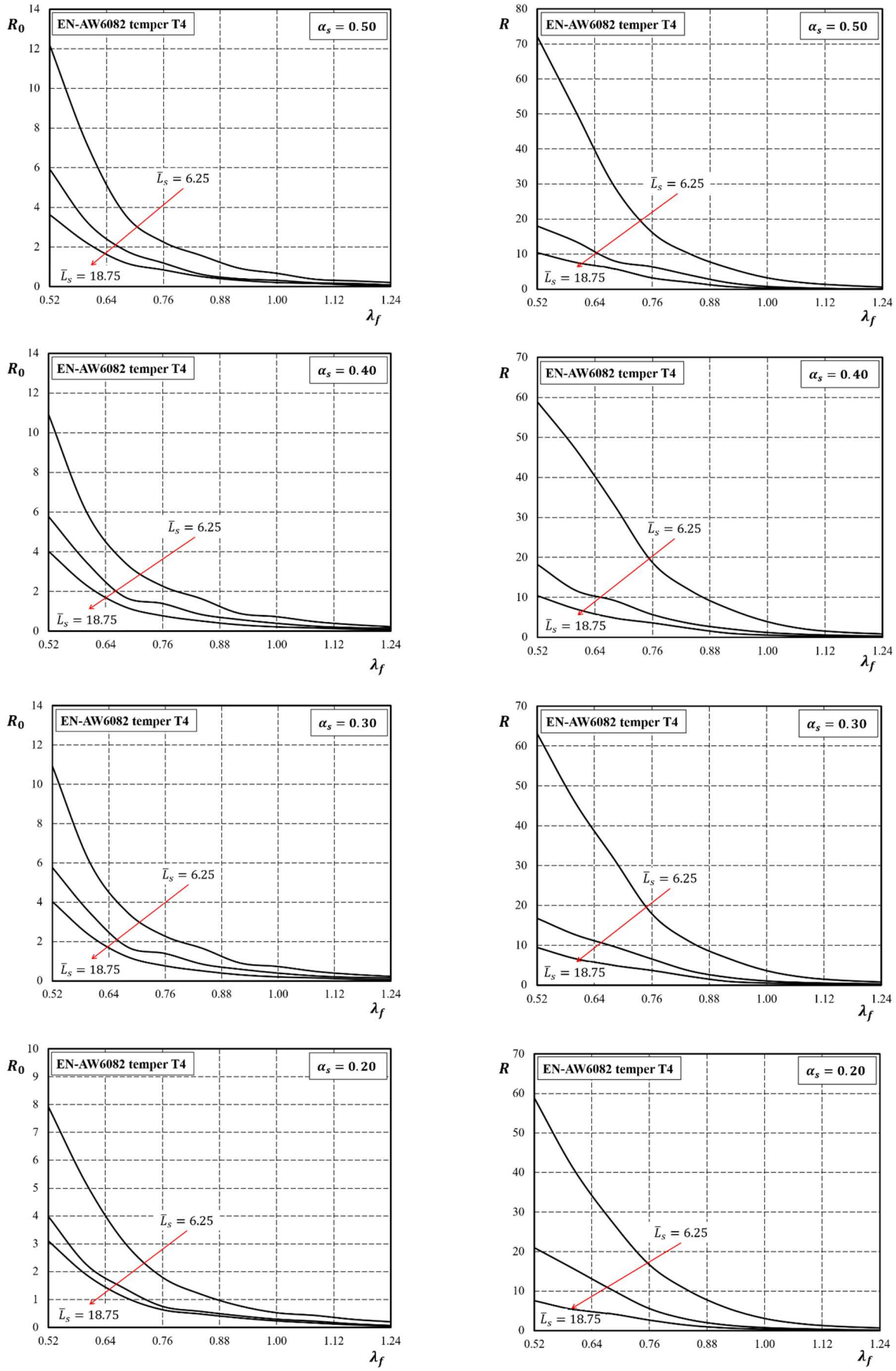

Figure 5.11. Influence of parameter $\bar{L}_s$ and λ_f on the rotational capacity for fixed value of α_s.

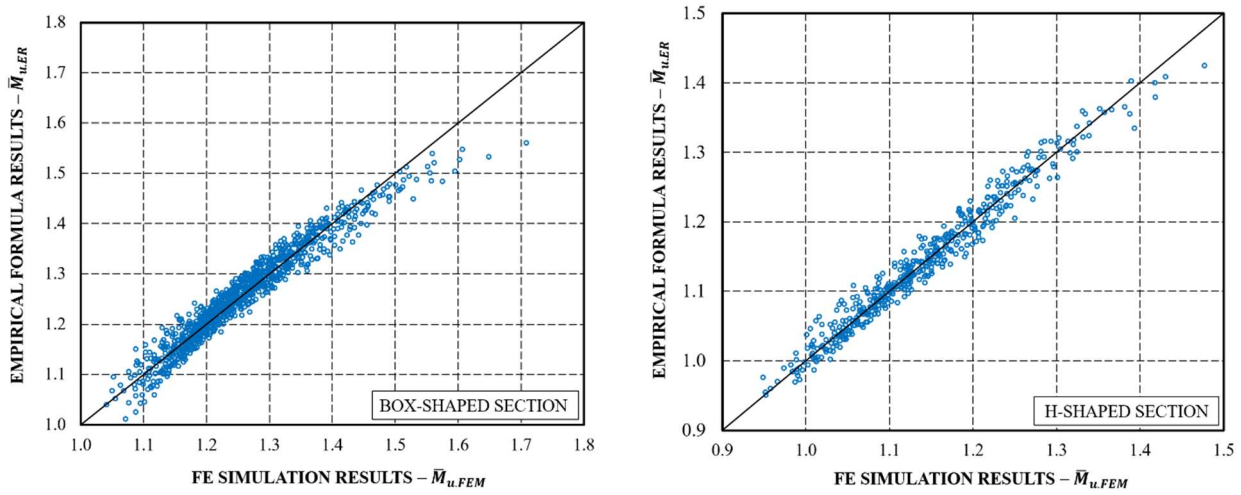

Figure 5.12. Accuracy of the mathematical fitting model for $\bar{M}_u$.

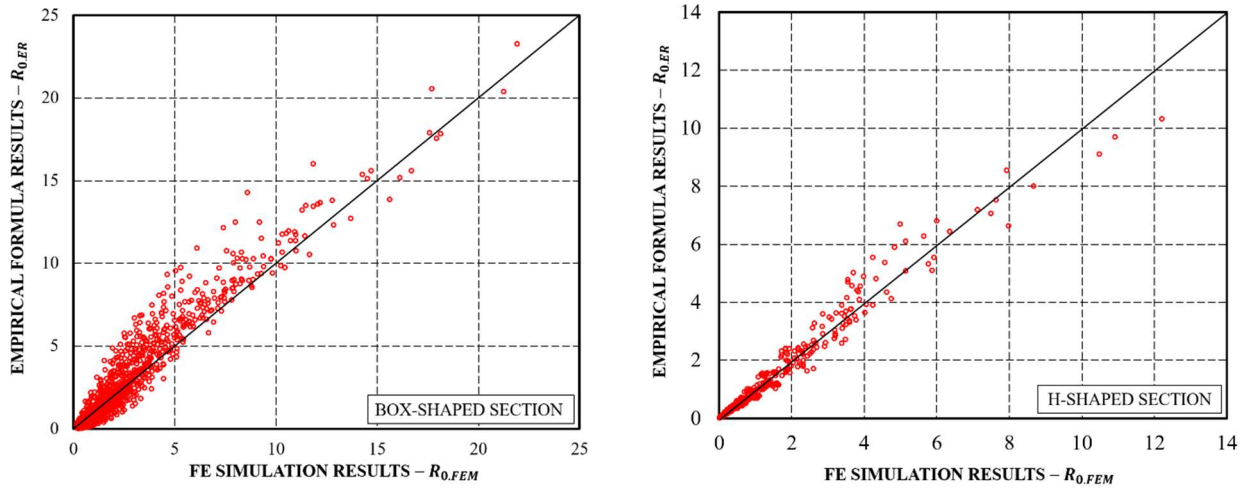

Figure 5.13. Accuracy of the mathematical fitting model for R_0

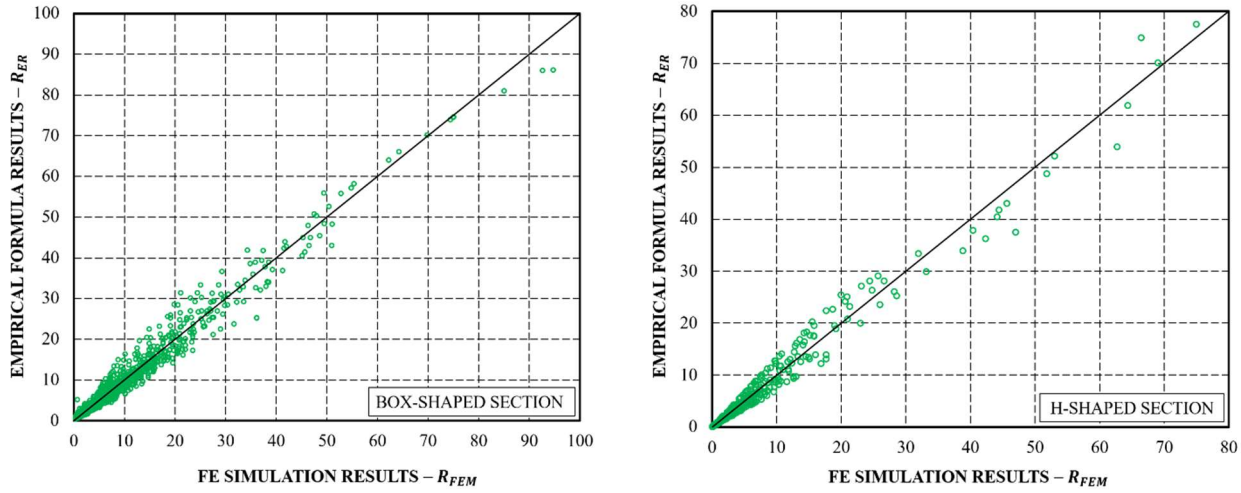

Figure 5.14. Accuracy of the mathematical fitting model for R.

5.4. Comparison with Bending Tests

In this section, the comparison between the results obtained by the previous methodology and the experimental results referring to the three point bending tests is provided. In particular, the empirical formulas, Eqns. (5.7) and (5.8), have been applied to evaluate the inelastic response of aluminium beams in terms of the maximum bending moment M_u and the corresponding non-dimensional rotation $\bar{\theta}_u$. For this reason, according to the definition provided in the previous section and considering the Eqns. (5.4) and (5.5), the maximum bending moment and the corresponding rotation can be computed as:

$$M_u = \bar{M}_{u.ER} \cdot M_{0.2} \tag{5.11}$$

and:

$$\bar{\theta}_u = \frac{\theta_u}{\theta_{0.2}} = 1 + R_{0.ER} \tag{5.12}$$

where $M_{0.2}$ and $\theta_{0.2}$ are, respectively, the bending moment and the rotation corresponding to the yielding region, while $\bar{M}_{u.ER}$ and $R_{0.ER}$ represent the flexural overstrength and the stable part of the rotation expressed as the empirical regressions in Eqns. (5.7) and (5.8).

For the comparison with the experimental results, the reference is made to the three point bending tests provided in Chapter 3 those performed by *Moen et al.* [5.6] at the Norwegian University of Science and Technology in 1999 and by *Su et al.* [5.14] at the University of Hong Kong in 2014. The experimental data are collected in the Section B.1 of Annex B.

Figure 5.15 shows the comparison between the values of the flexural resistance computed by Eq. (5.11) with those obtained by the experimental tests. The accuracy of the prediction of the ultimate behaviour of aluminium members is very high, especially, as regards the ultimate resistance. In fact, the average value of the ratio $M_{u.ER}/M_{u.exp}$ is equal to 1.02 with the standard deviation equal to 0.14. Instead, the prediction of the normalised rotational capacity is less accurate. In fact, the average value of the ratio $\bar{\theta}_{u.ER}/\bar{\theta}_{u.exp}$. is equal to 0.92, while the standard deviation is 0.15. However, the empirical approach is a safety procedure, because, in most cases, the experimental values are greater than those provided by empirical formula provided in Eq.(5.12). For the sake of completeness, the numerical results are given in Annex B. In cases where the experimental results are not reported, it means that they have not been presented by the authors. Moreover, in the comparison of the normalised rotations, some experimental tests are not considered because they did not exhibit a ductile behaviour being affected by the local buckling phenomena in the elastic range.

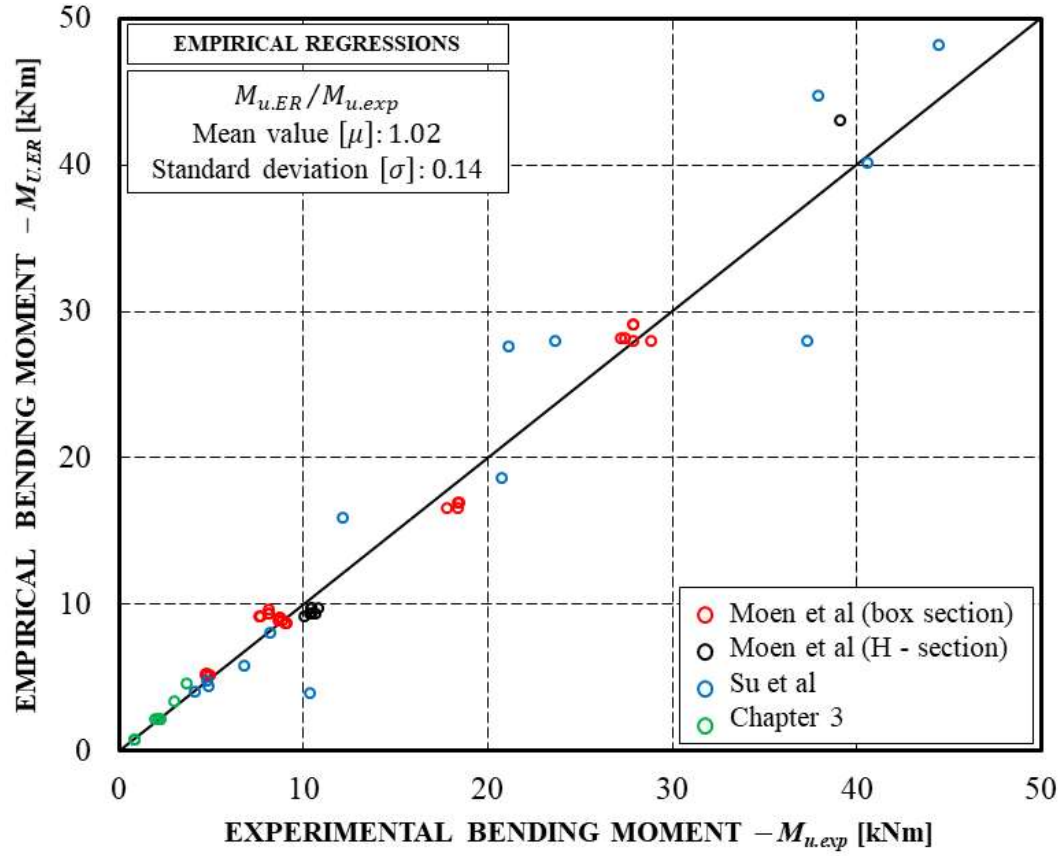

Figure 5.15. Comparison of the theoretical bending moments with experimental results.

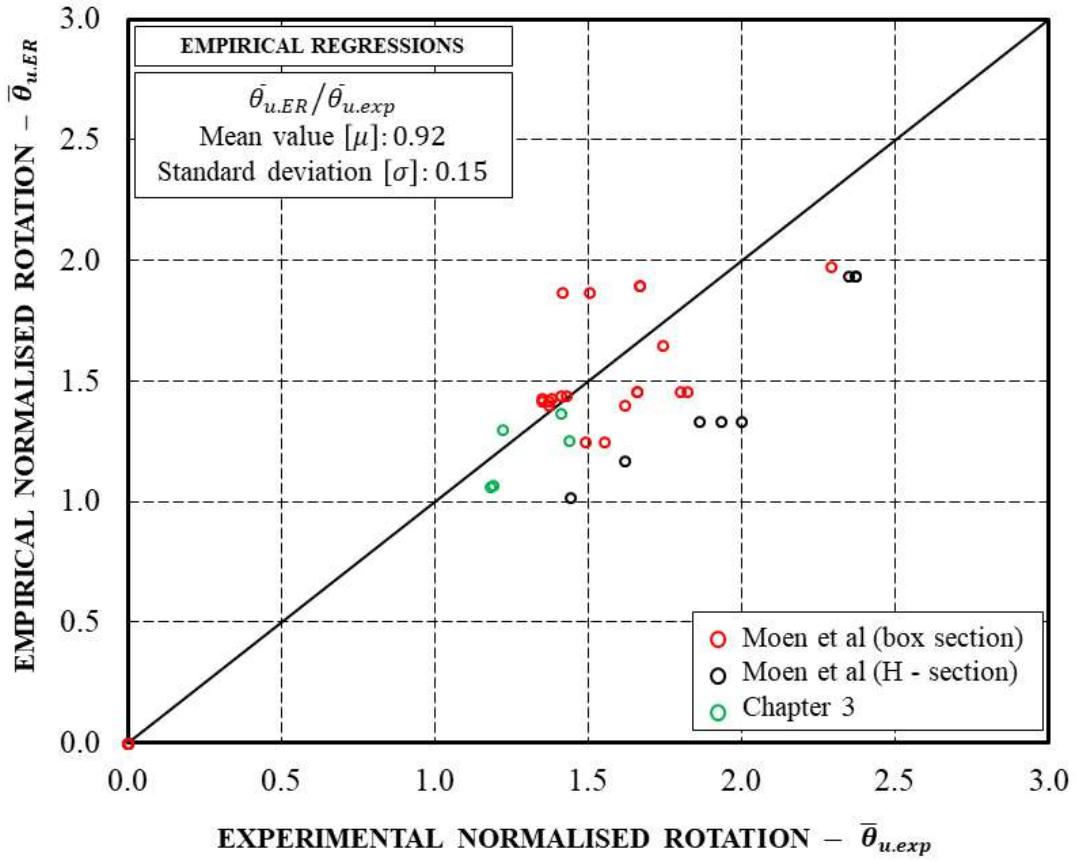

Figure 5.16. Comparison of the theoretical normalised rotations with experimental results.

5.5. References

[5.1] **EN1999-1-1:** "Eurocode 9: Design of aluminium structures - Part 1-1: General structural rules", European Committee for Standardization, 2007.

[5.2] **EN 1993-1-1**: "Eurocode 3: Design of steel structures - Part 1-1: General rules and rules for buildings", European Committee for Standardization, 2005.

[5.3] **B. Kato**: "Development and design of seismic-resistant steel structures in Japan", STESSA: Behaviour of Steel Structures in Seismic Areas, E&FN Spon, London, pp. 28–42, 1994.

[5.4] **ABAQUS**, User's Manual: Volume II: Materials, 2010.

[5.5] **ABAQUS**, User's Manual: Volume III: Elements, 2010.

[5.6] **L.A. Moen, O.S. Hopperstad, M. Langseth:** "Rotational capacity of aluminum beams under moment gradient. I: Experiments", Journal of Structural Engineering, 125 (8), pp. 910-920, 1999.

[5.7] **L.A. Moen, G. De Matteis, O.S. Hopperstad, M. Langseth, R. Landolfo, F.M. Mazzolani**: "Rotational capacity of aluminum beams under moment gradient. II: numerical simulation", Journal of Structural Engineering, 125 (8), pp. 921-929, 1999.

[5.8] **M. Cheng, Y. Shi, Y. Wang:** "Inelastic deformation analysis of aluminum bending members", Tsinghua Science and Technology, 11 (6), pp. 648-656, 2006.

[5.9] **P. Castaldo, E. Nastri, V. Piluso:** "FEM simulations and rotation capacity evaluation for RHS temper T4 aluminium alloy beams", Composites Part B: Engineering, 115, pp. 124-137, 2017.

[5.10] **P. Castaldo, E. Nastri, V. Piluso:** "Ultimate behaviour of RHS temper T6 aluminium alloy beams subjected to non-uniform bending: Parametric analysis", Thin-Walled Structures, 115, pp. 129-141, 2017.

[5.11] **G. De Matteis, L.A. Moen, M. Langseth, R. Landolfo, O.S. Hopperstad, F.M. Mazzolani**: "Cross-sectional classification for aluminium beams: a parametric study", Journal of Structural Engineering, 127 (3), pp. 271-279, 2001.

[5.12] **G. De Matteis, R. Landolfo, M. Manganiello, F.M. Mazzolani:** "Inelastic behaviour of I-shaped aluminium beams: Numerical analysis and cross-sectional classification", Computers and Structures, 82, pp. 2157-2171, 2004.

[5.13] **UNI-EN 573-3:** "Alluminio e leghe di alluminio - Composizione chimica e forma dei prodotti semilavorati - Parte 3: Composizione chimica e forma dei prodotti", European Standard, 2019.

[5.14] **M.N. Su, B. Young, L. Gardner:** "Deformation-based design of aluminum alloy beams" Engineering Structures, 80, pp. 339-349, 2014.

[5.15] **M.N. Su, B. Young, L. Gardner:** "The continuous strength method for the design of aluminium alloy structural elements", Engineering Structures, 122, pp.338–348, 2016.

[5.16] **Z. Li, B.W. Schafer:** "Buckling analysis of cold-formed steel members with general boundary conditions using CUFSM: Conventional and constrained finite strip methods", 20th International Specialty Conference on Cold-Formed Steel Structures, pp. 17-31, 2010.

[5.17] **M. Seif, B.W. Schafer:** "Local buckling of structural steel shapes", Journal of Constructional Steel Research, **66** (10), pp. 1232-1247, 2010.

[5.18] **F.M. Mazzolani, V. Piluso:** "Prediction of the rotation capacity of aluminium alloy beams", Thin-Walled Structures, **27** (1), pp. 103-116, 1997.

[5.19] **prEN 1993-1-14: Eurocode 3**: "Design of Steel Structures - Part 1-14: Design Assisted by Finite Element Analysis", Document CEN/TC 250/SC 9 N 867, 2020.

Appendix D

D.1. The Normalised Moment-Rotation Curves for Box-shaped Section

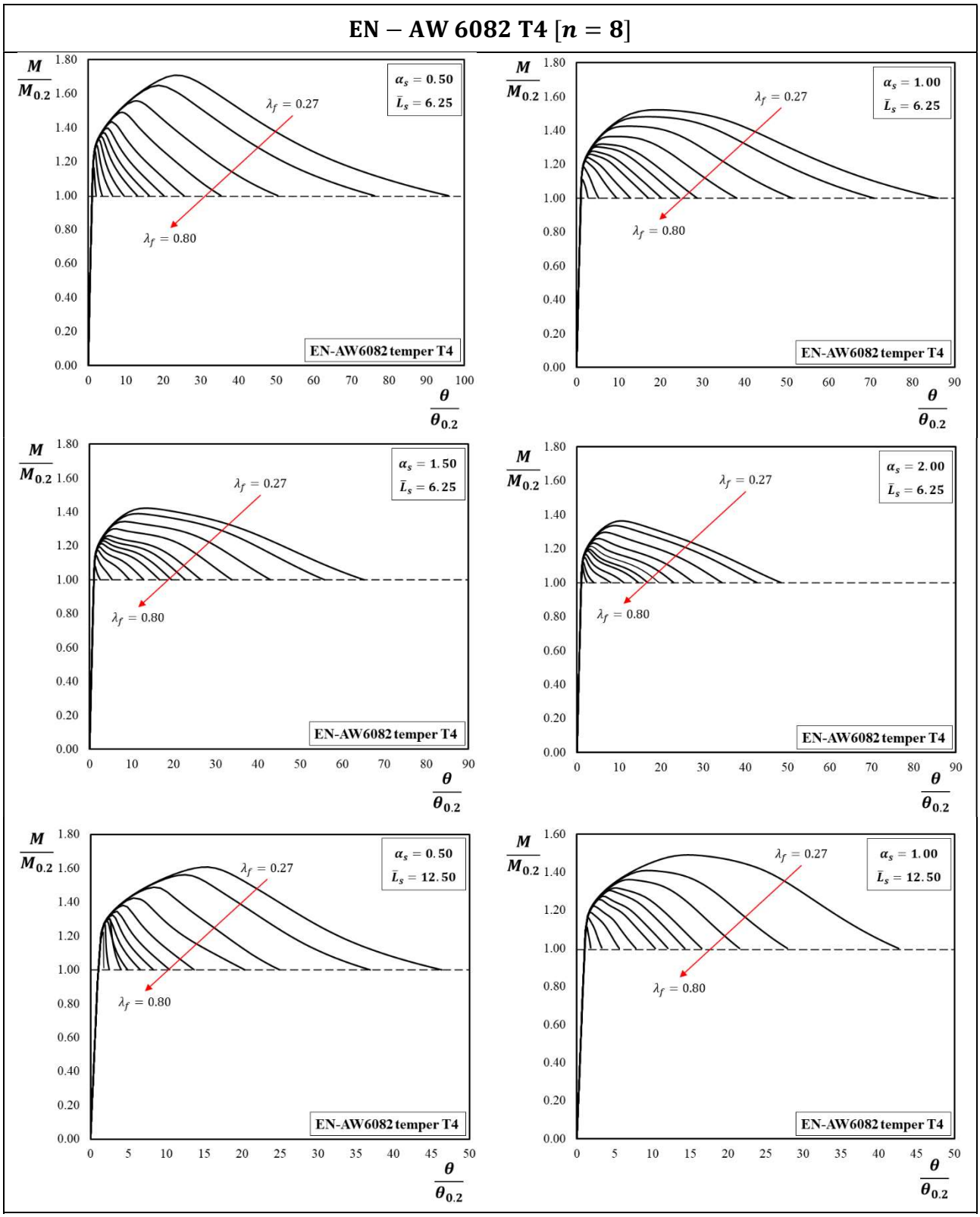

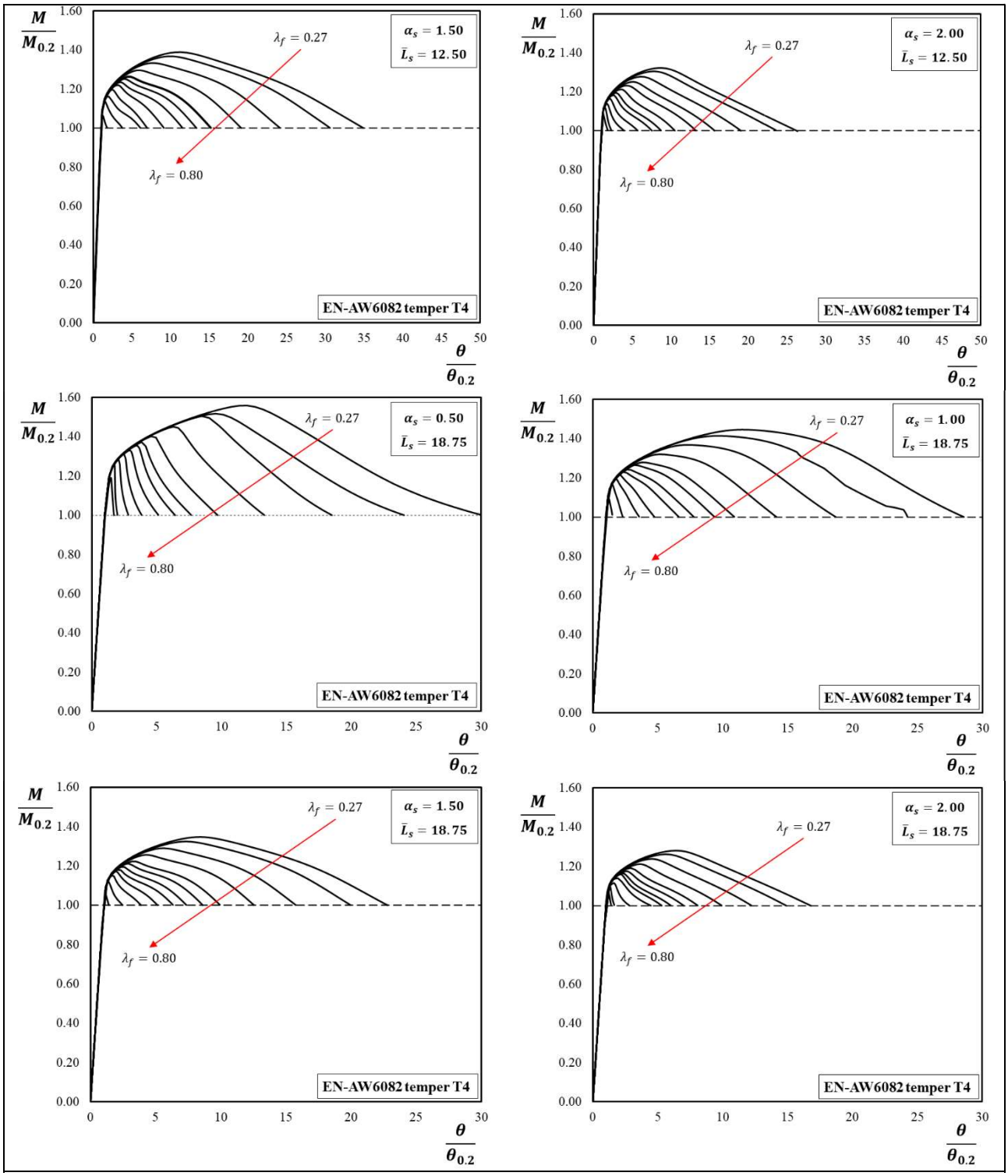
M / M0.2
θ / θ0.2
λf = 0.27
λf = 0.80
αs = 1.50
L̄s = 12.50
αs = 2.00
L̄s = 12.50
αs = 0.50
L̄s = 18.75
αs = 1.00
L̄s = 18.75
αs = 1.50
L̄s = 18.75
αs = 2.00
L̄s = 18.75
EN-AW6082 temper T4

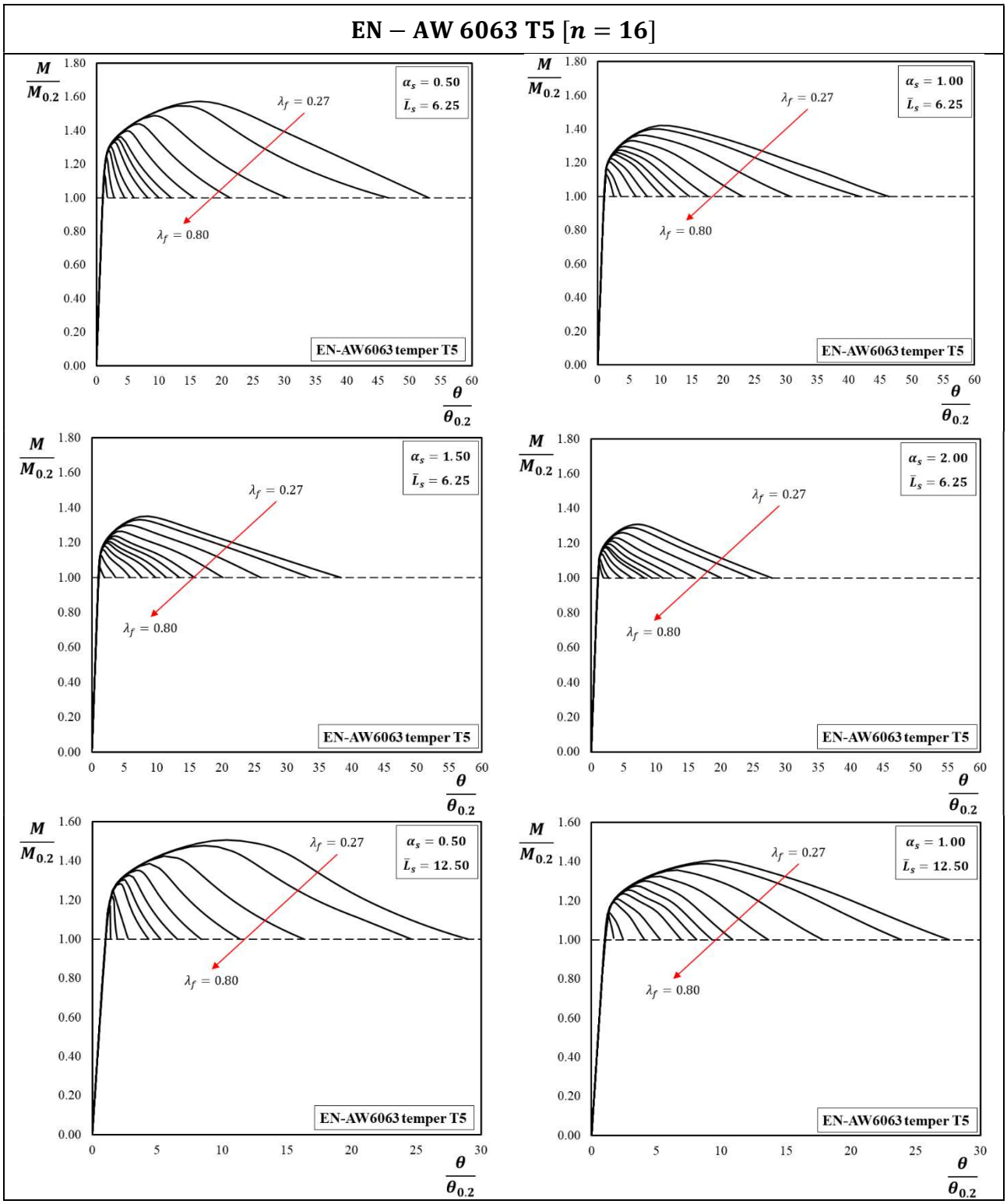
EN − AW 6063 T5 [n = 16]
M/M0.2
θ/θ0.2
αs = 0.50
L̄s = 6.25
αs = 1.00
L̄s = 6.25
αs = 1.50
L̄s = 6.25
αs = 2.00
L̄s = 6.25
αs = 0.50
L̄s = 12.50
αs = 1.00
L̄s = 12.50
λf = 0.27
λf = 0.80
EN-AW6063 temper T5

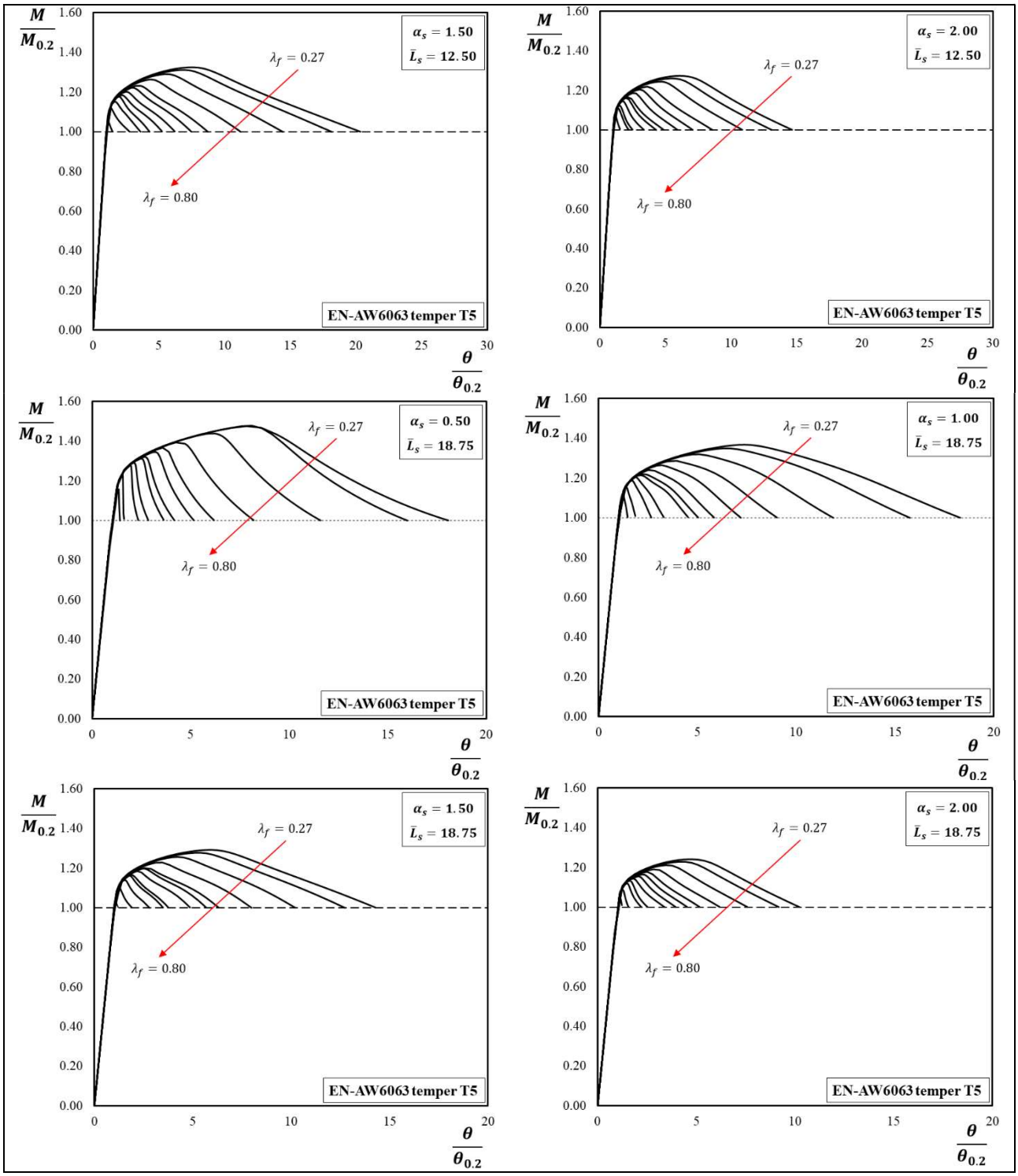
$\frac{M}{M_{0.2}}$
$\frac{\theta}{\theta_{0.2}}$
$\alpha_s = 1.50$
$\bar{L}_s = 12.50$
$\alpha_s = 2.00$
$\bar{L}_s = 12.50$
$\alpha_s = 0.50$
$\bar{L}_s = 18.75$
$\alpha_s = 1.00$
$\bar{L}_s = 18.75$
$\alpha_s = 1.50$
$\bar{L}_s = 18.75$
$\alpha_s = 2.00$
$\bar{L}_s = 18.75$
$\lambda_f = 0.27$
$\lambda_f = 0.80$
EN-AW6063 temper T5

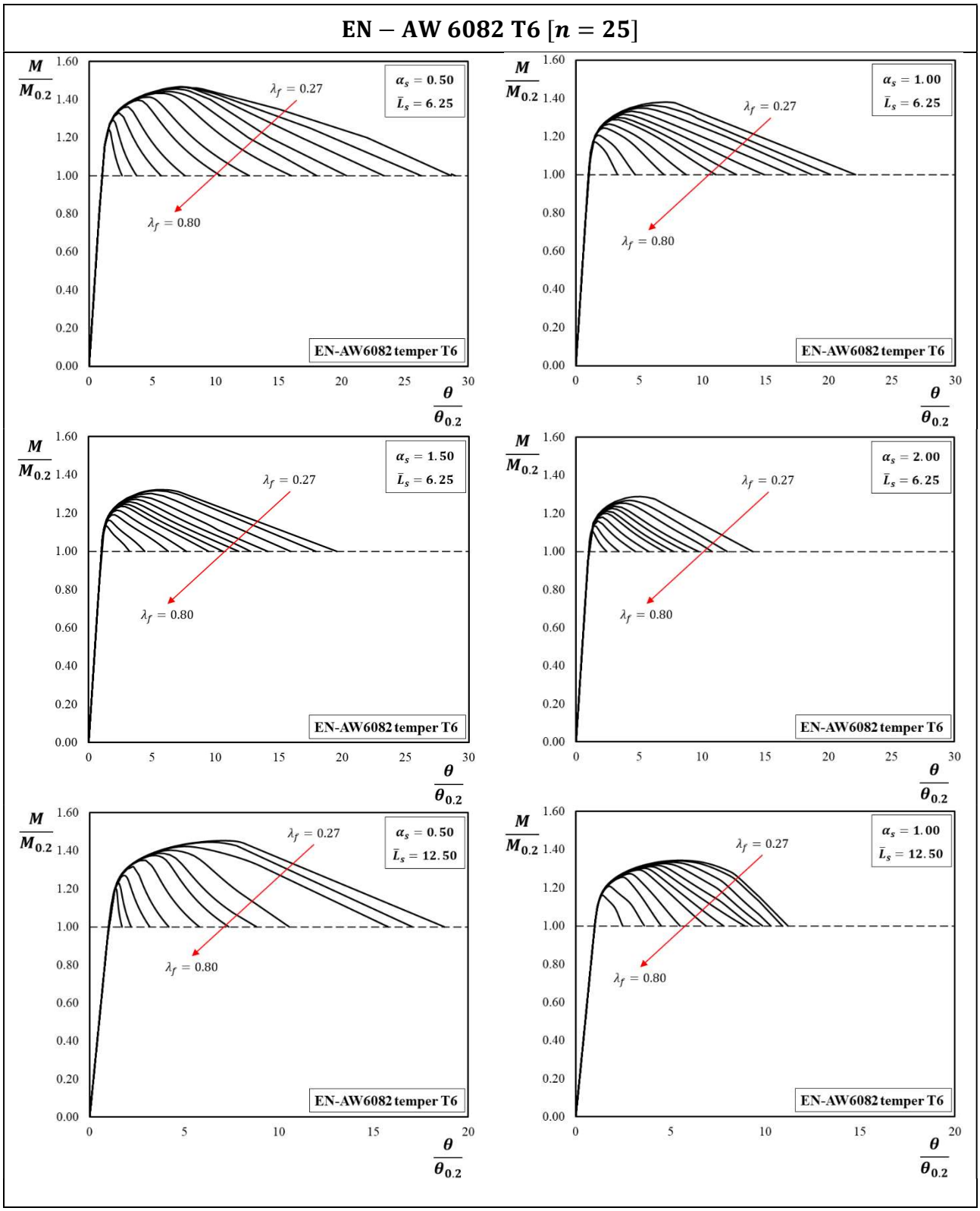
EN − AW 6082 T6 [n = 25]
M / M0.2
θ / θ0.2
λf = 0.27
λf = 0.80
αs = 0.50
L̄s = 6.25
αs = 1.00
L̄s = 6.25
αs = 1.50
L̄s = 6.25
αs = 2.00
L̄s = 6.25
αs = 0.50
L̄s = 12.50
αs = 1.00
L̄s = 12.50
EN-AW6082 temper T6

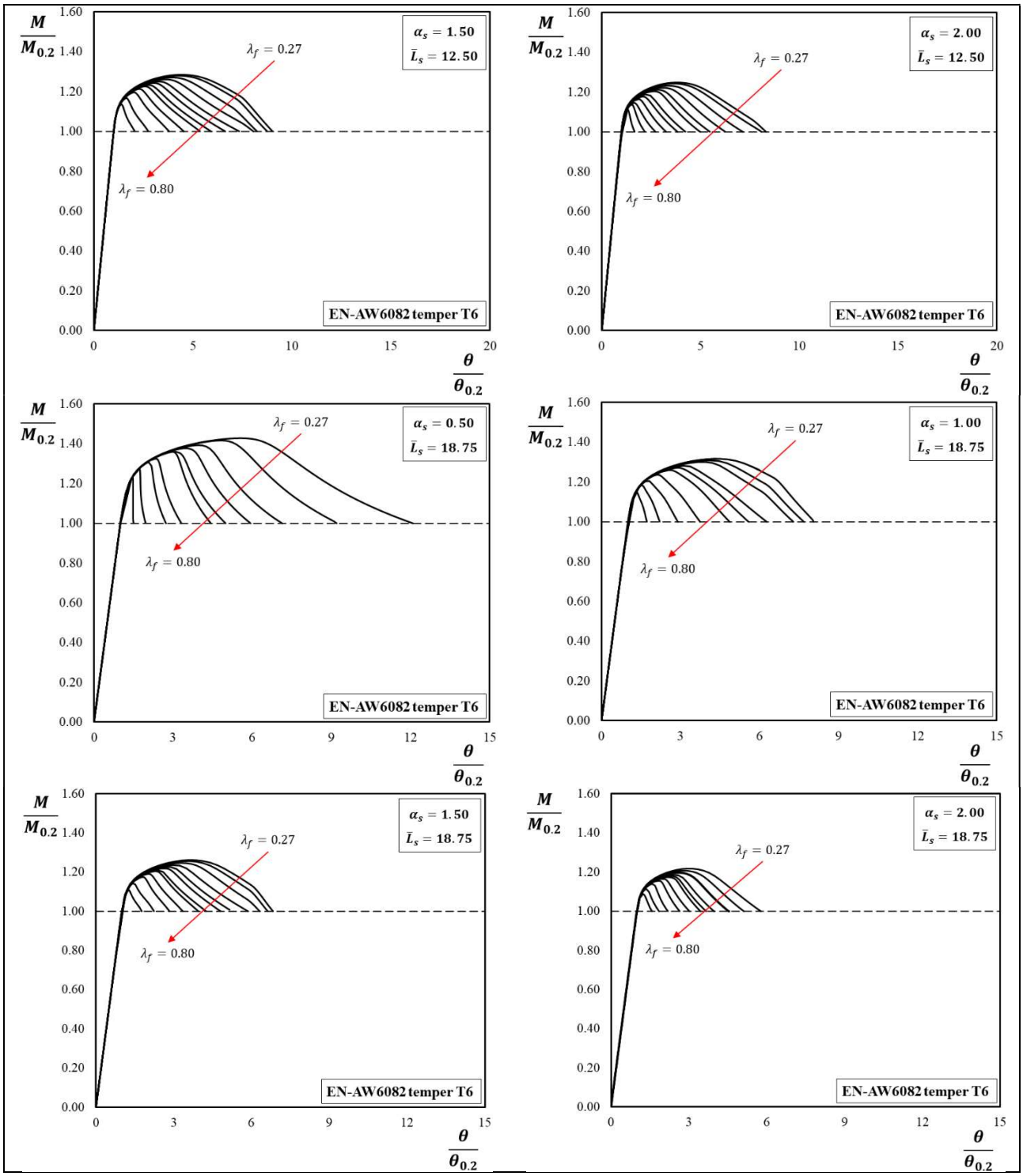
$\frac{M}{M_{0.2}}$
$\frac{\theta}{\theta_{0.2}}$
$\alpha_s = 1.50$
$\bar{L}_s = 12.50$
$\alpha_s = 2.00$
$\bar{L}_s = 12.50$
$\alpha_s = 0.50$
$\bar{L}_s = 18.75$
$\alpha_s = 1.00$
$\bar{L}_s = 18.75$
$\alpha_s = 1.50$
$\bar{L}_s = 18.75$
$\alpha_s = 2.00$
$\bar{L}_s = 18.75$
$\lambda_f = 0.27$
$\lambda_f = 0.80$
EN-AW6082 temper T6

EN − AW 6061 T6 [$n = 55$]

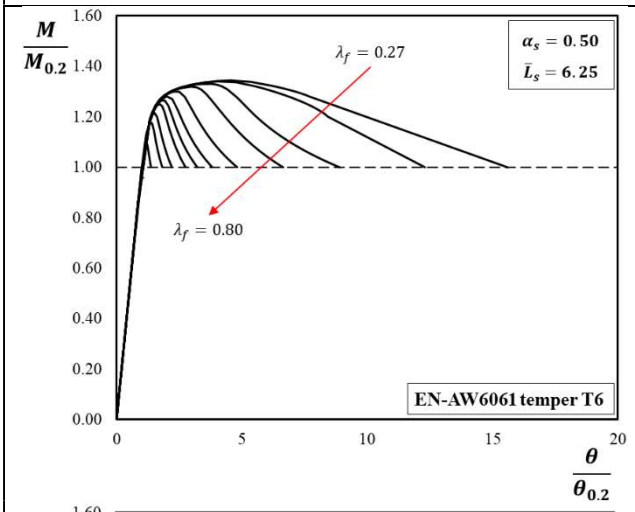

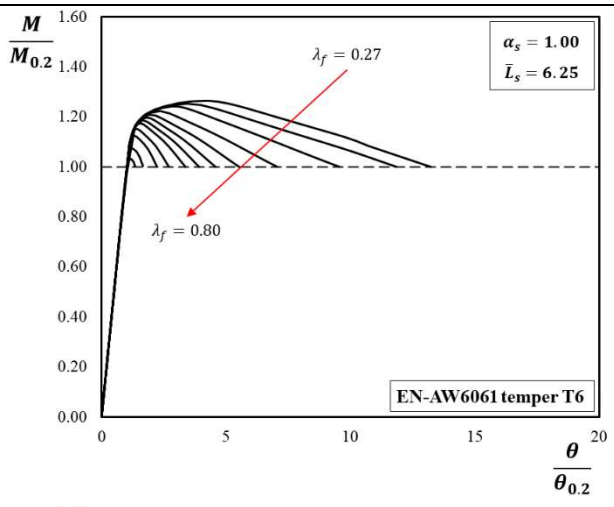

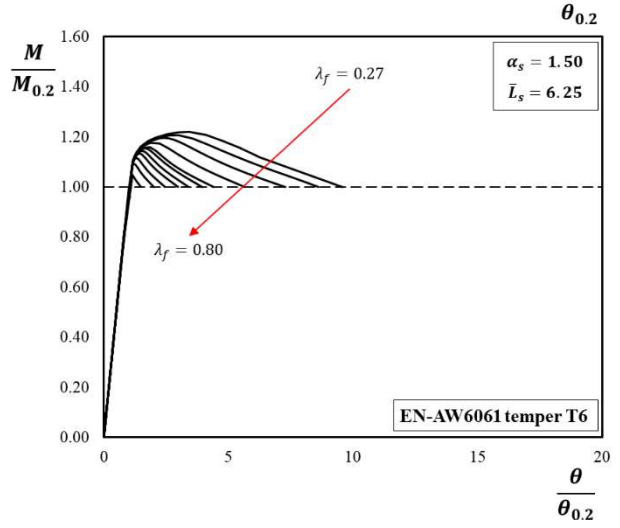

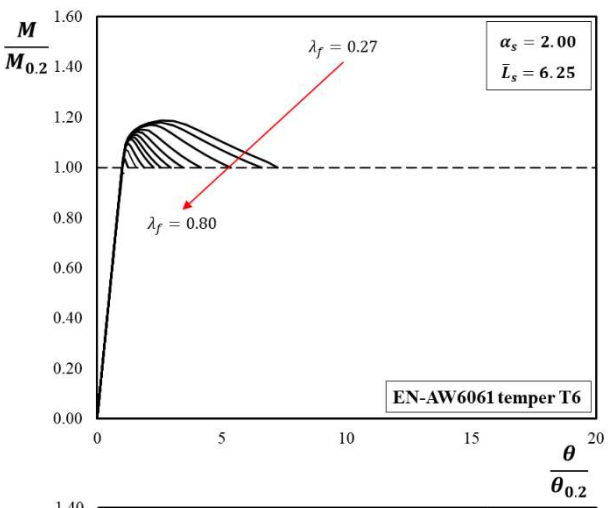

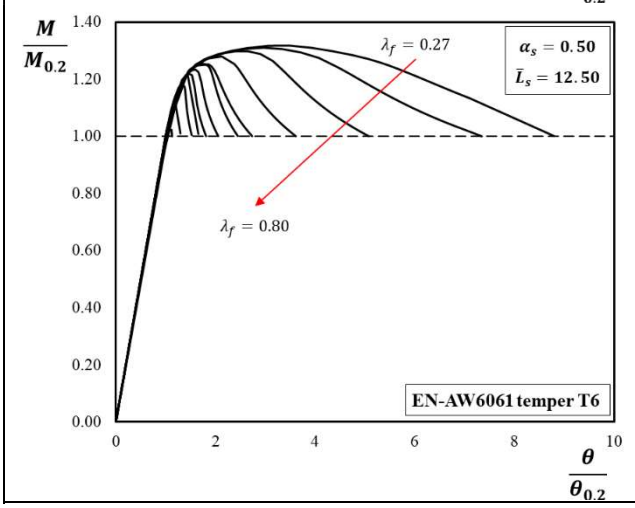

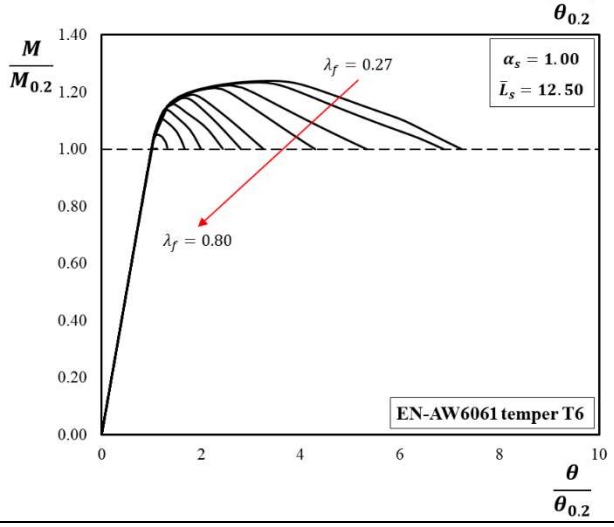

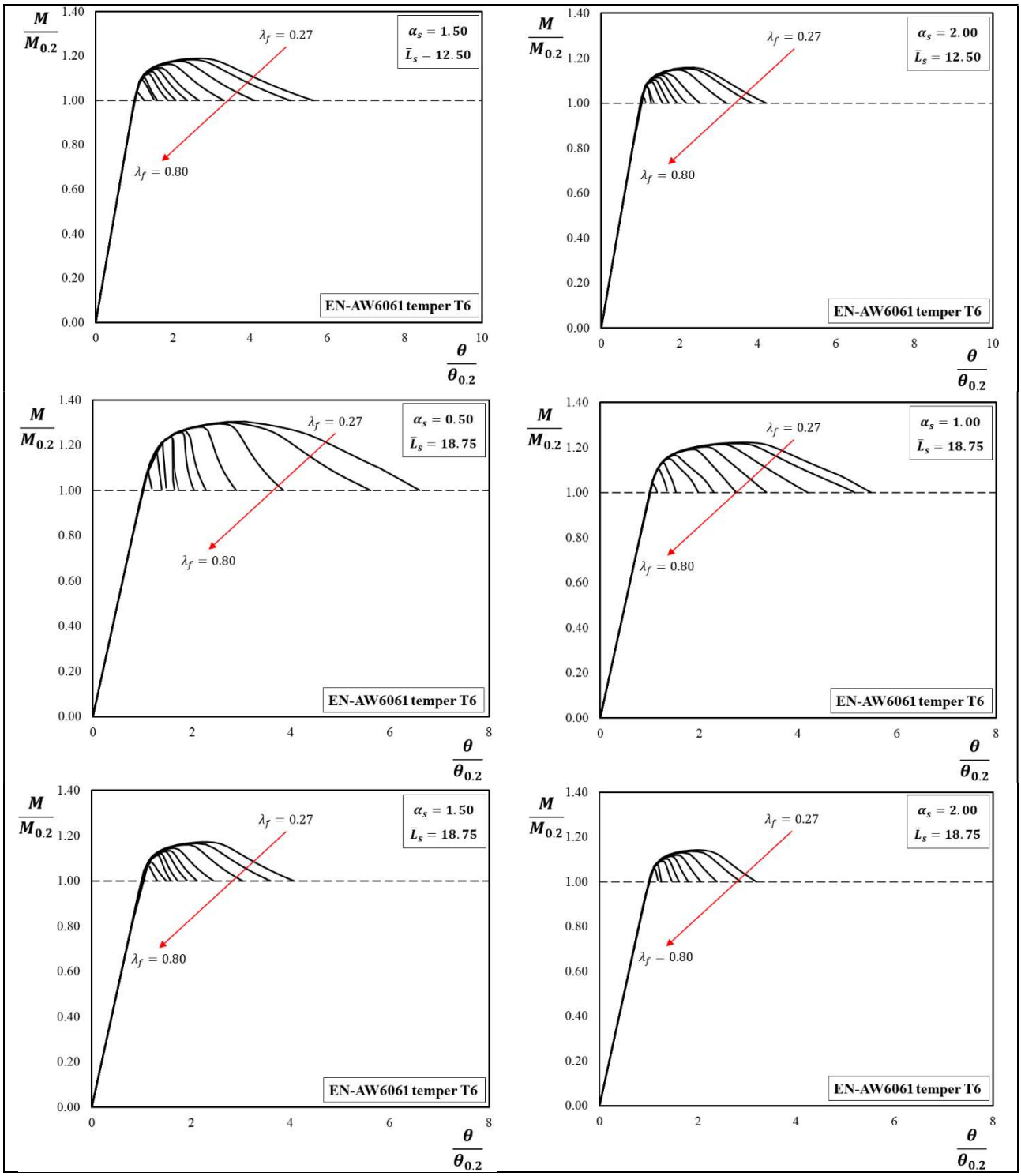
M / M0.2
θ / θ0.2
λf = 0.27
λf = 0.80
αs = 1.50
L̄s = 12.50
αs = 2.00
L̄s = 12.50
αs = 0.50
L̄s = 18.75
αs = 1.00
L̄s = 18.75
αs = 1.50
L̄s = 18.75
αs = 2.00
L̄s = 18.75
EN-AW6061 temper T6

D.2. The normalised Moment-Rotation Curves for H-shaped Section

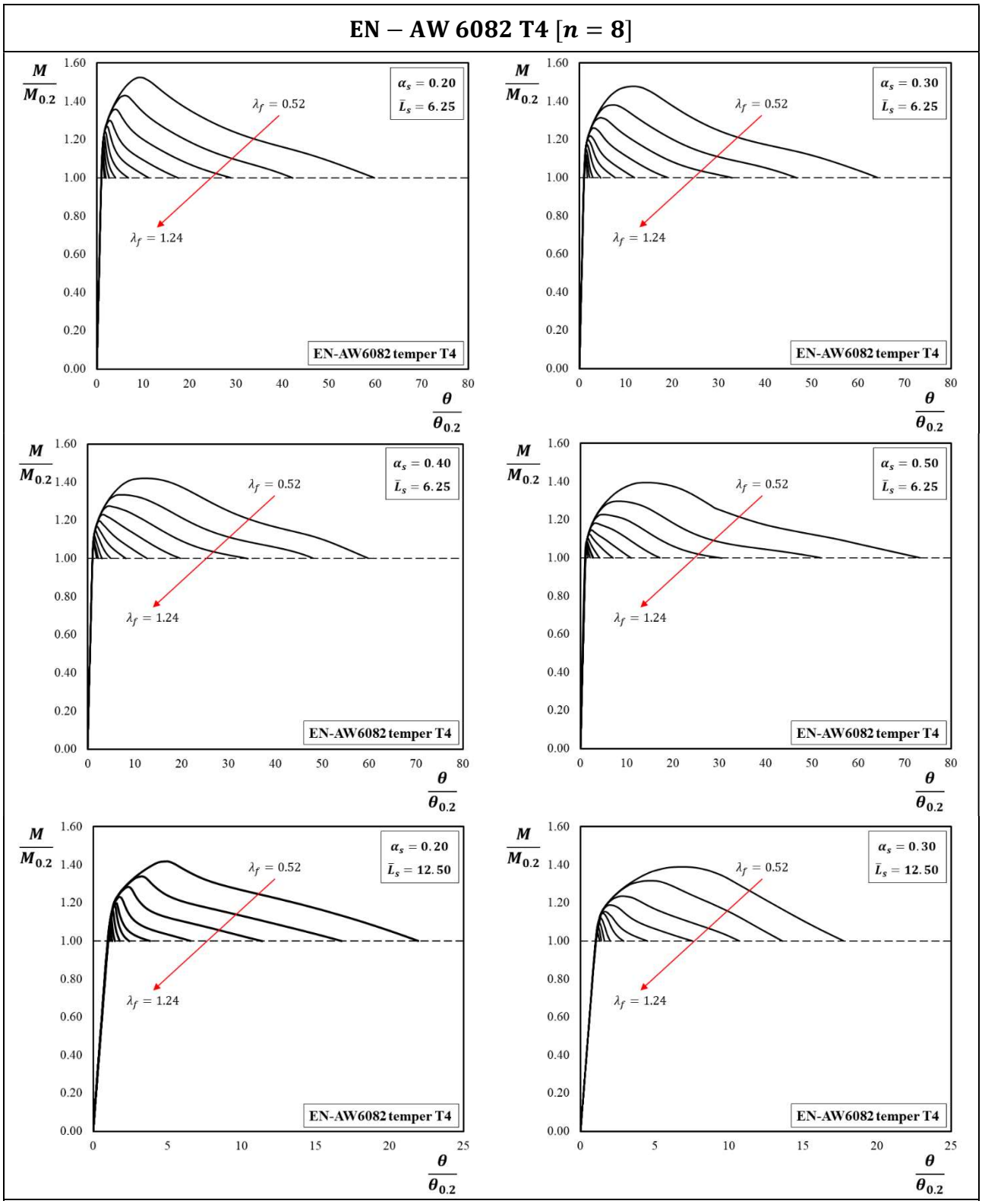

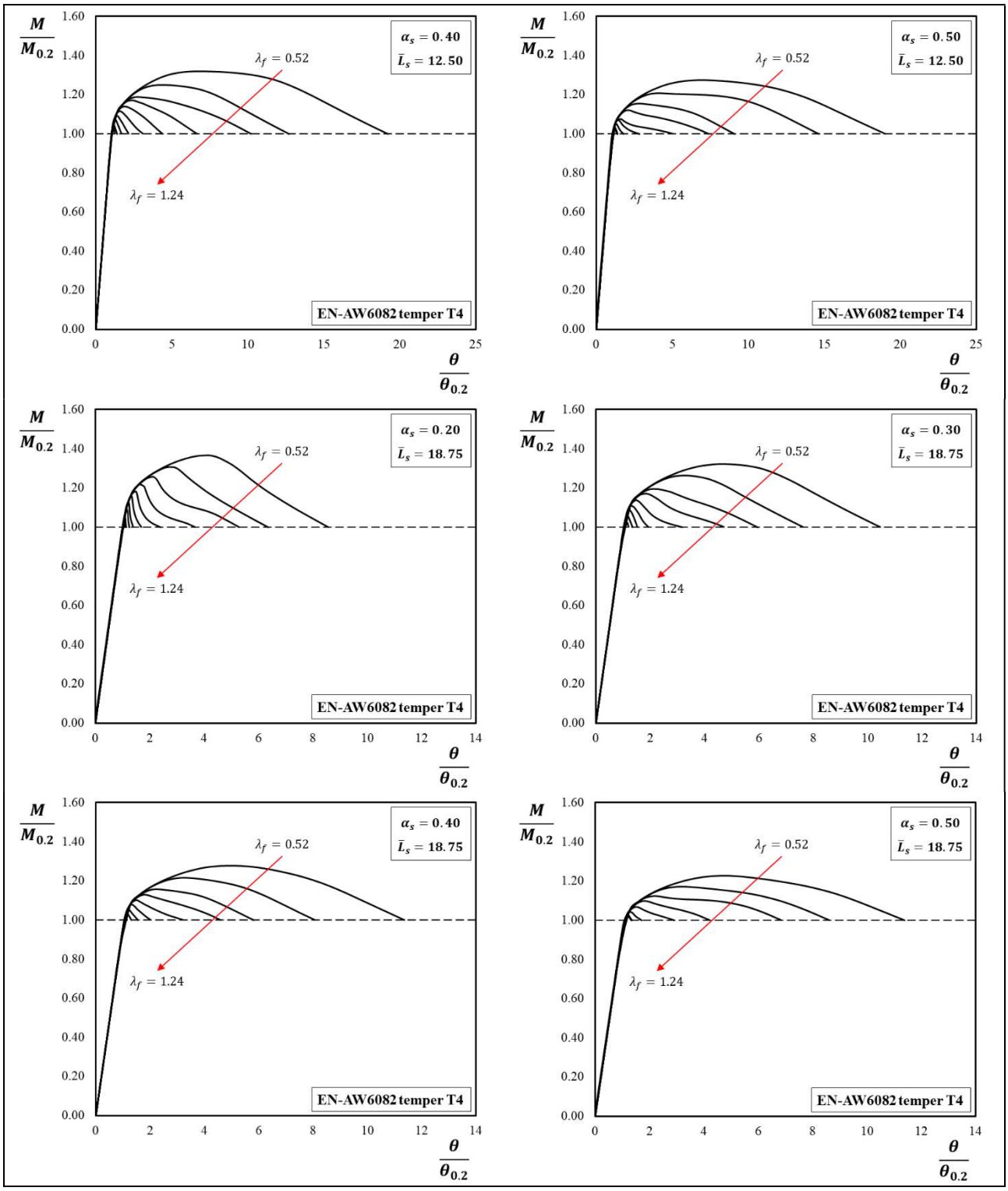
M/M0.2
θ/θ0.2
αs = 0.40
l̄s = 12.50
αs = 0.50
l̄s = 12.50
αs = 0.20
l̄s = 18.75
αs = 0.30
l̄s = 18.75
αs = 0.40
l̄s = 18.75
αs = 0.50
l̄s = 18.75
λf = 0.52
λf = 1.24
EN-AW6082 temper T4

EN − AW 6063 T5 [$n = 16$]

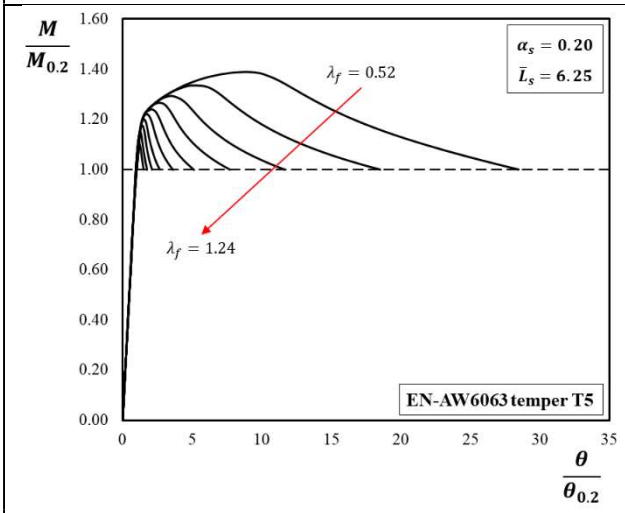

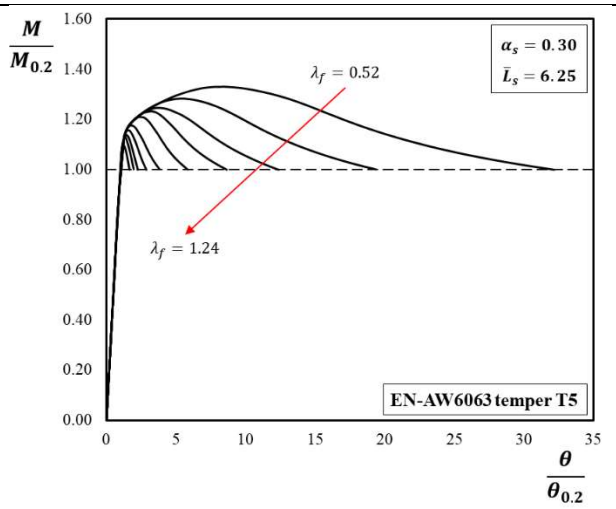

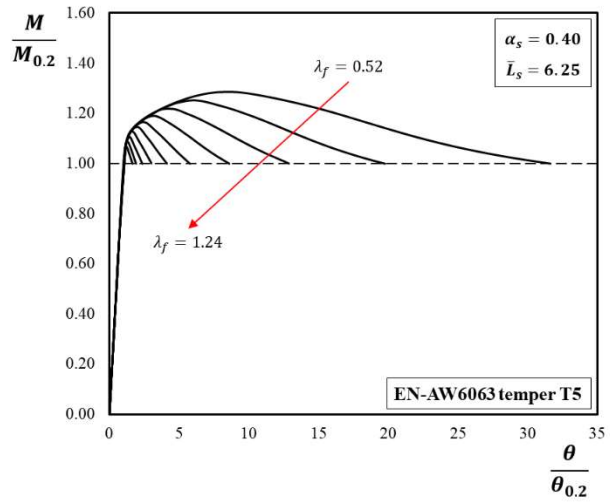

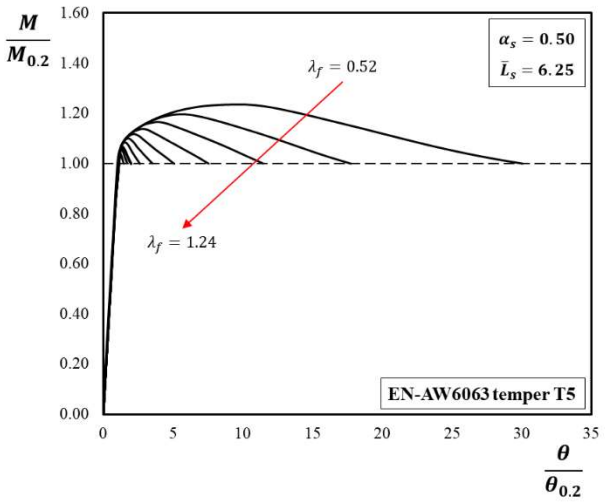

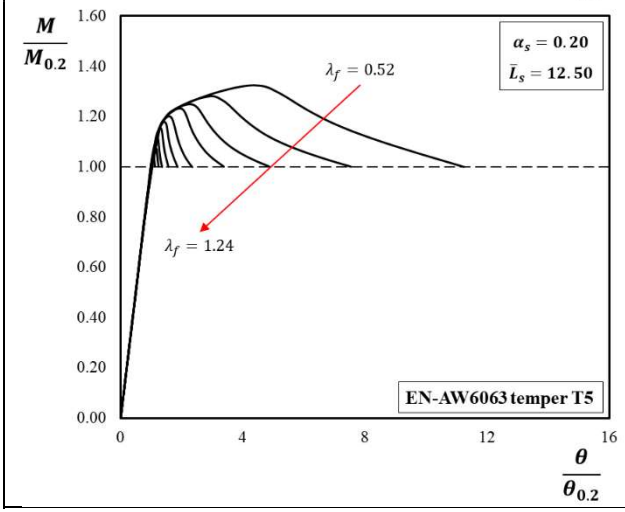

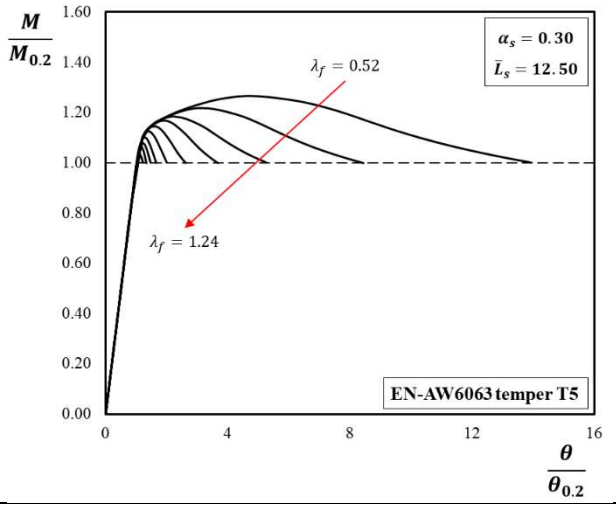

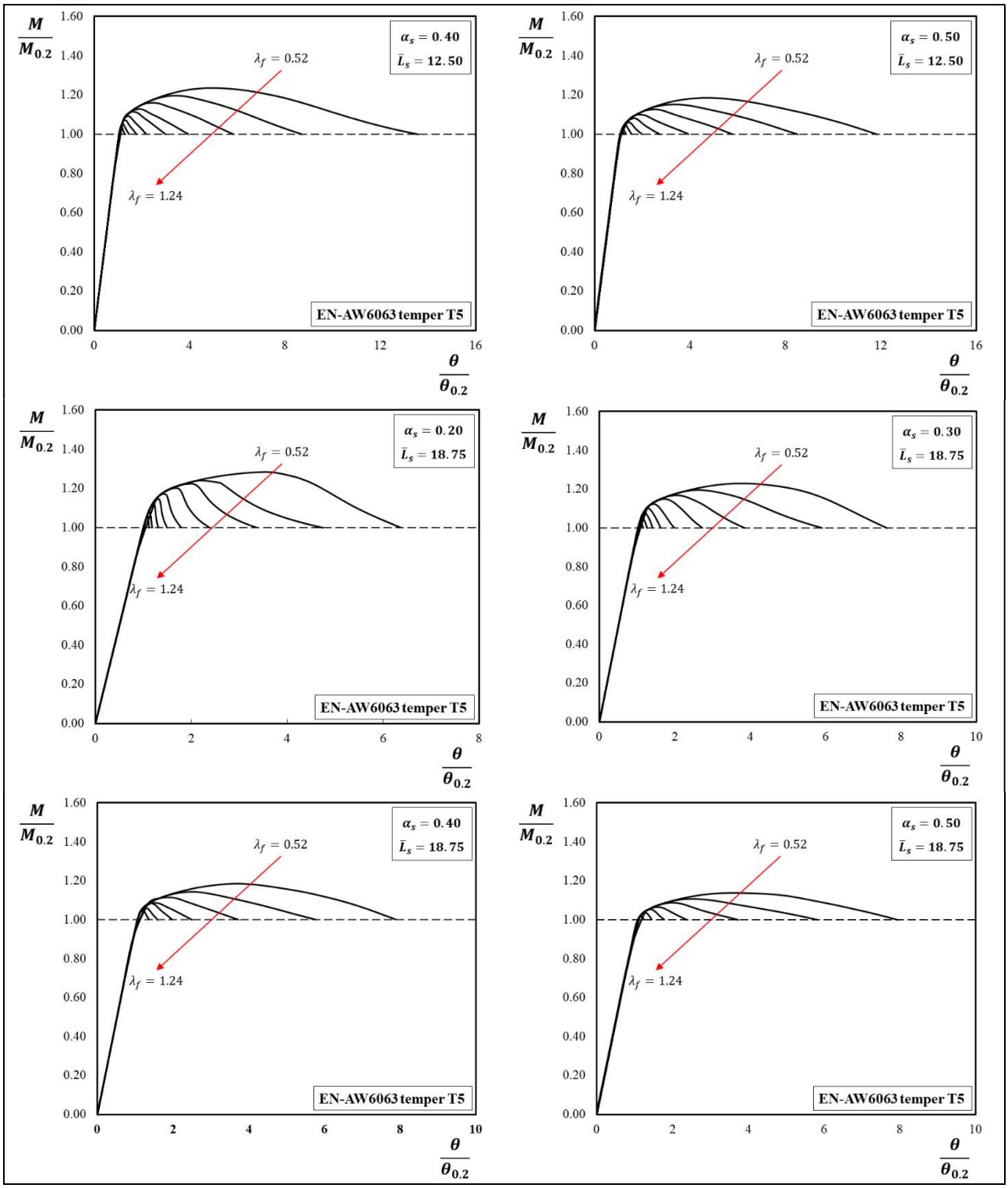
M / M0.2
θ / θ0.2
αs = 0.40
L̄s = 12.50
αs = 0.50
L̄s = 12.50
αs = 0.20
L̄s = 18.75
αs = 0.30
L̄s = 18.75
αs = 0.40
L̄s = 18.75
αs = 0.50
L̄s = 18.75
λf = 0.52
λf = 1.24
EN-AW6063 temper T5

EN − AW 6082 T6 [$n = 25$]

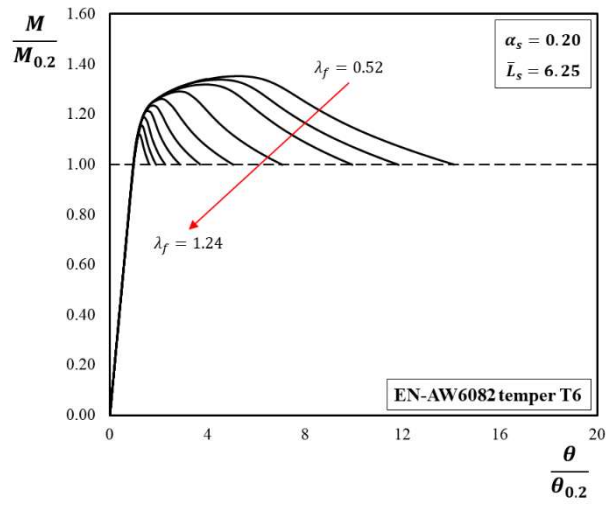

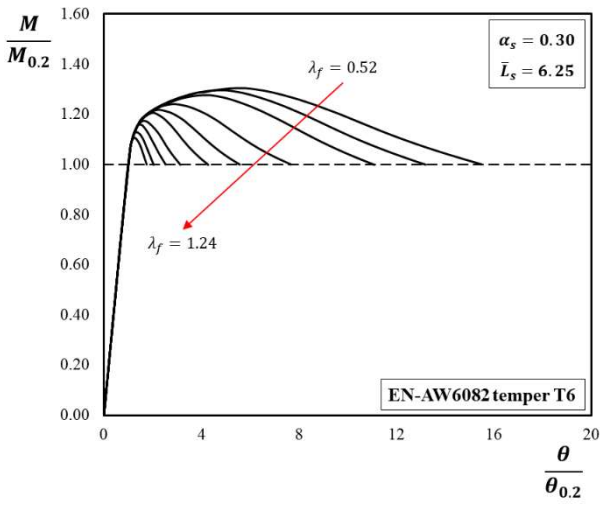

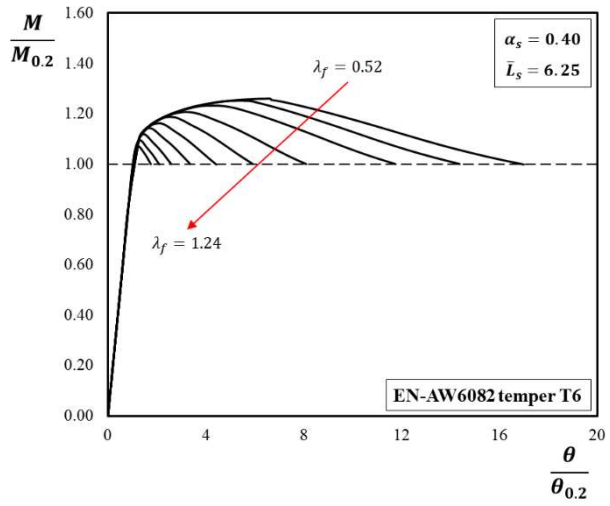

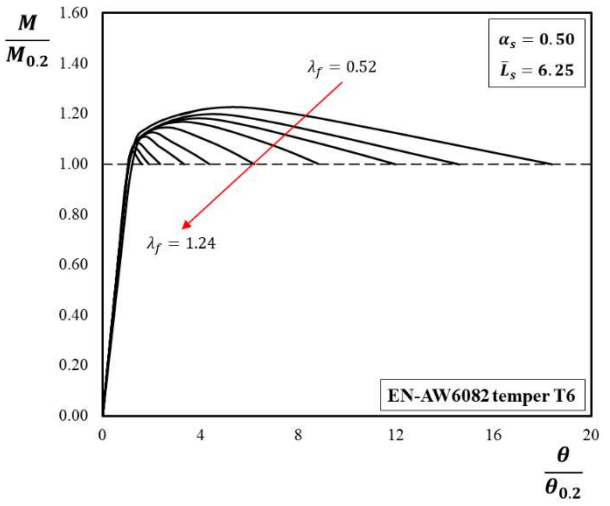

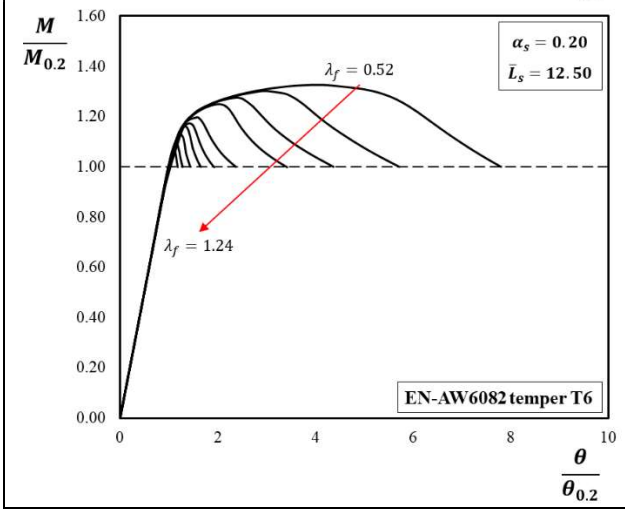

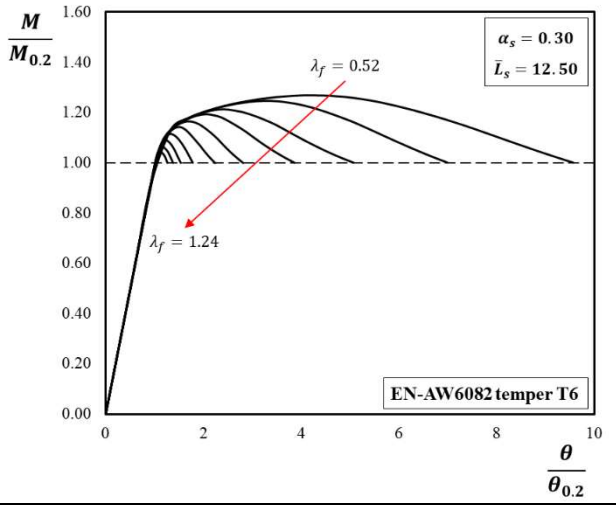

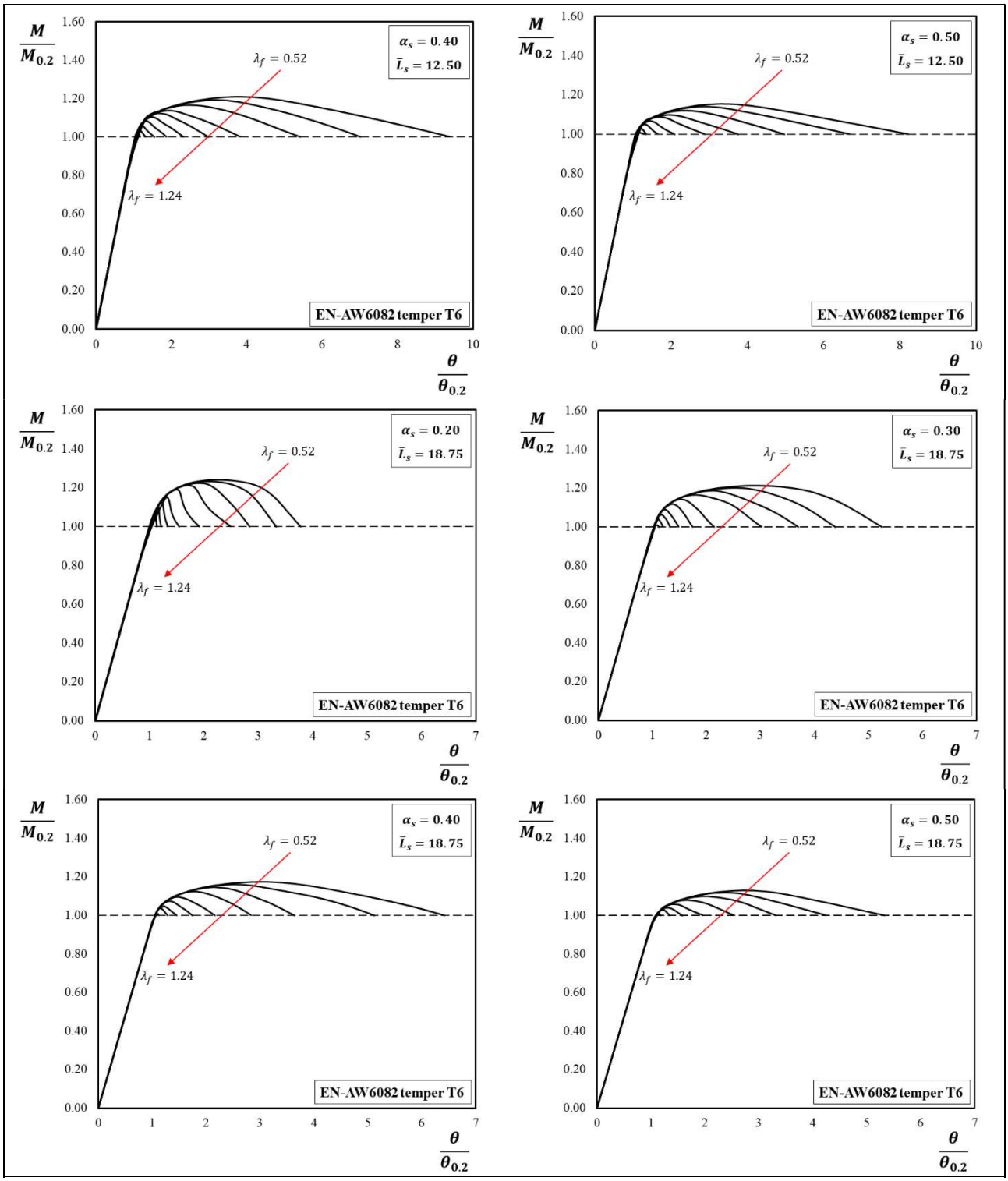
M/M0.2
θ/θ0.2
αs = 0.40
L̄s = 12.50
αs = 0.50
L̄s = 12.50
αs = 0.20
L̄s = 18.75
αs = 0.30
L̄s = 18.75
αs = 0.40
L̄s = 18.75
αs = 0.50
L̄s = 18.75
λf = 0.52
λf = 1.24
EN-AW6082 temper T6

EN − AW 6061 T6 [$n = 55$]

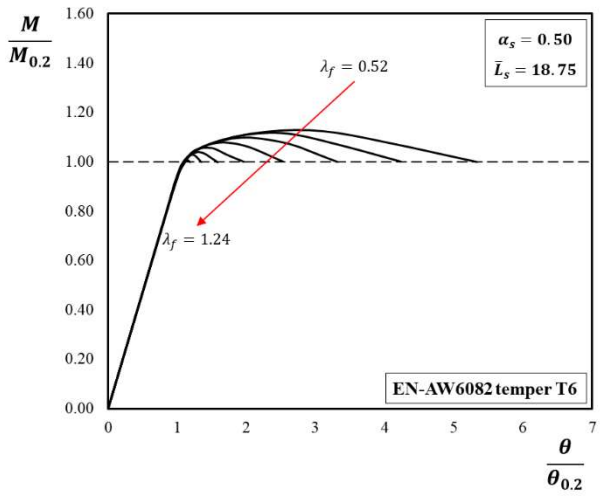

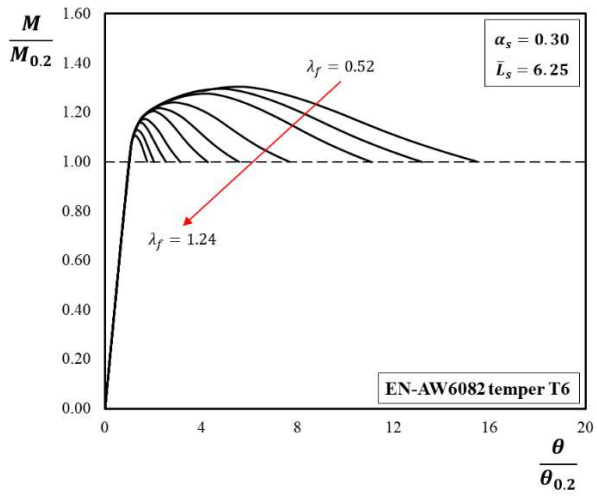

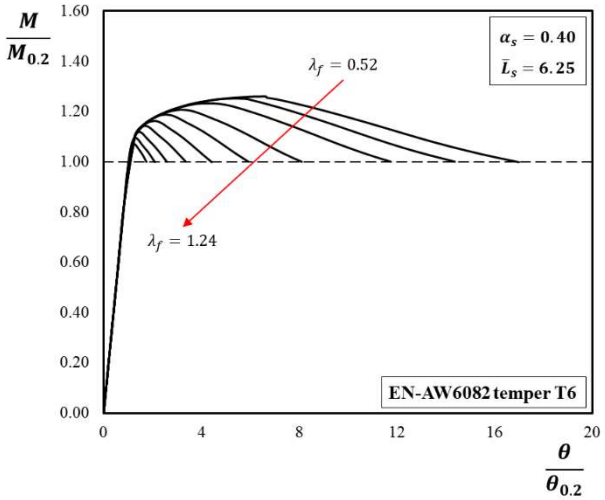

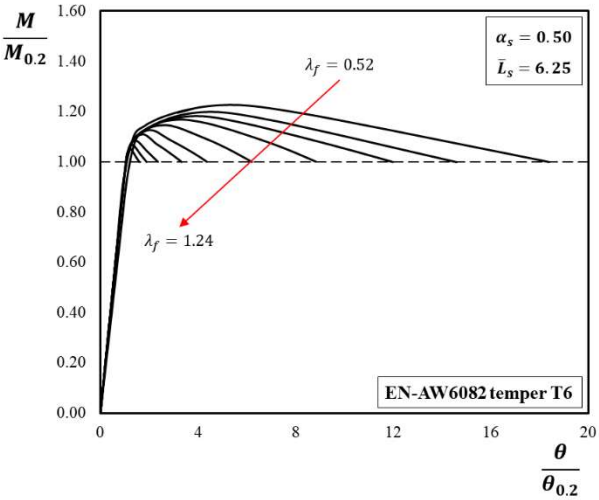

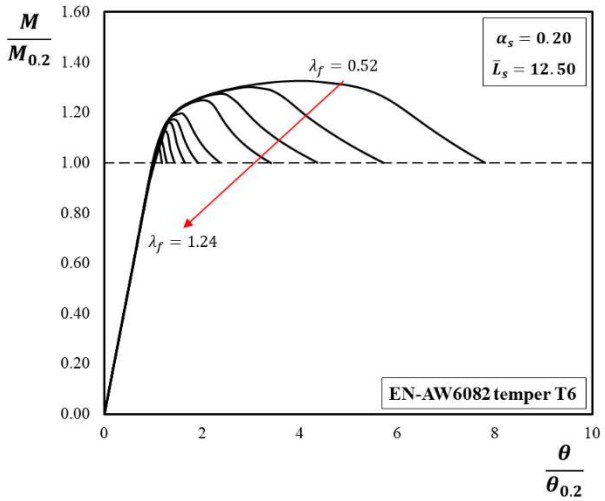

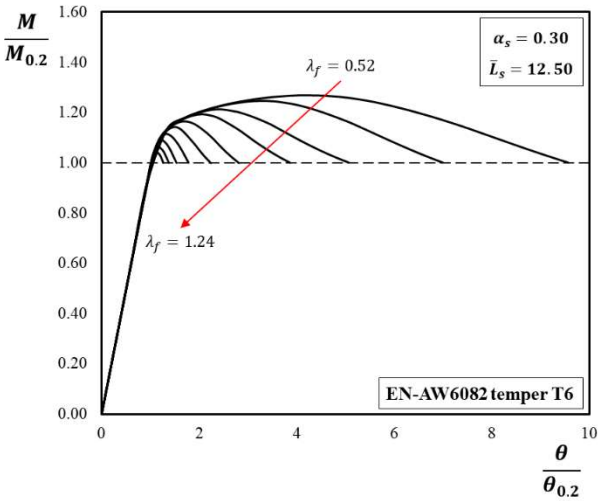

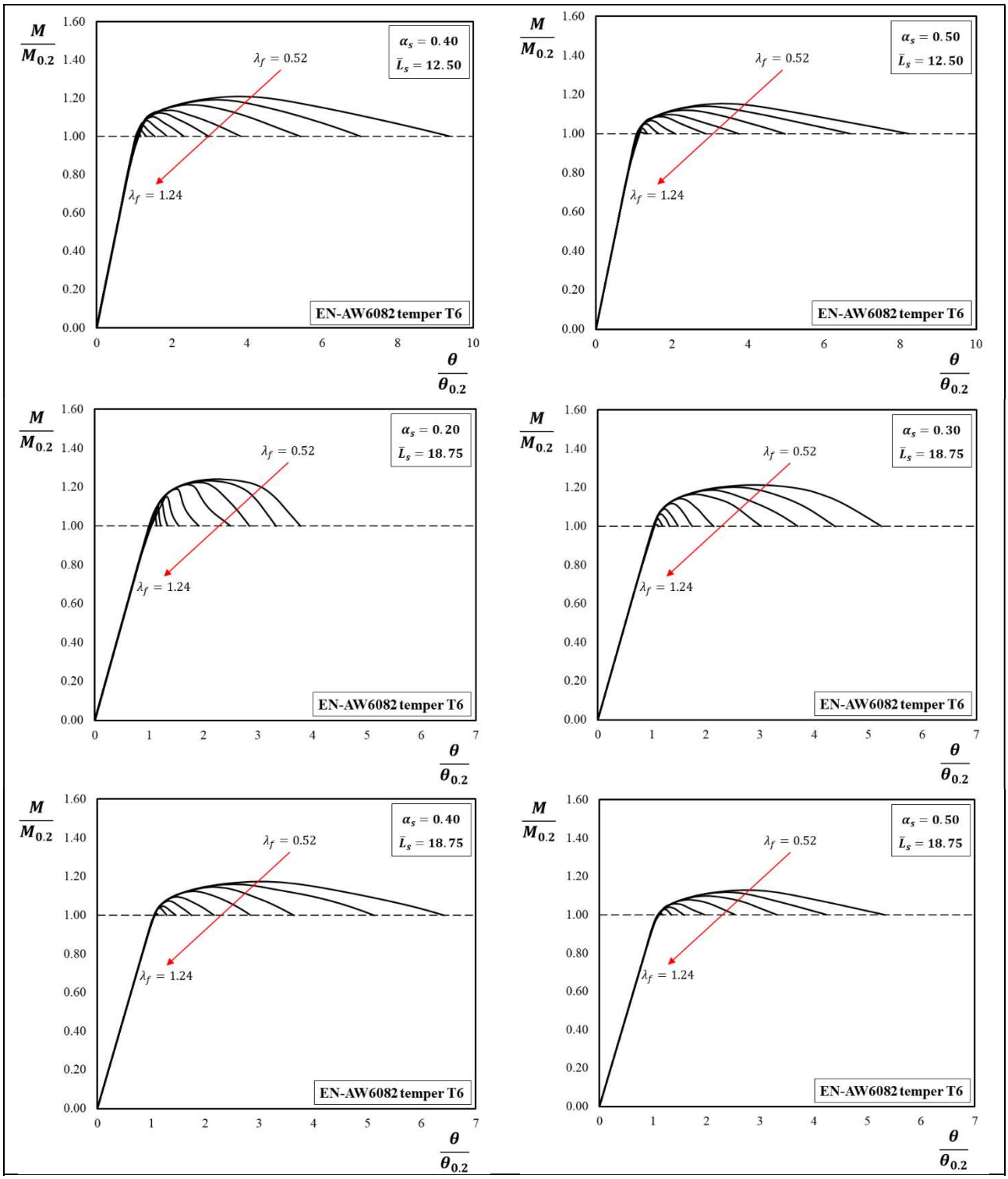
$\frac{M}{M_{0.2}}$
$\frac{\theta}{\theta_{0.2}}$
$\alpha_s = 0.40$
$\bar{L}_s = 12.50$
$\alpha_s = 0.50$
$\bar{L}_s = 12.50$
$\alpha_s = 0.20$
$\bar{L}_s = 18.75$
$\alpha_s = 0.30$
$\bar{L}_s = 18.75$
$\alpha_s = 0.40$
$\bar{L}_s = 18.75$
$\alpha_s = 0.50$
$\bar{L}_s = 18.75$
$\lambda_f = 0.52$
$\lambda_f = 1.24$
EN-AW6082 temper T6

CHAPTER 6
EFFECTIVE THICKNESS METHOD

6.1. Different Approaches in the Design of Aluminium Sections

In technical literature, there are different simplified methods to evaluate the behaviour of aluminium members under uniform and non-uniform compression, taking into account that the response of thin-walled sections is strongly affected by local instability phenomena which arise in the compressed part. The main approaches, codified and adopted by the European Eurocodes, are: 1) the width effective approach, 2) the reduced strength approach and 3) the effective thickness approach.

The first one is very well known, being codified for many years with particular reference to steel structures [6.1]. It was first introduced by *Von Kármán* in 1932 [6.2]. He stated that, for a fixed thickness, a fictitious plate with the width of b_{eff} would have the critical stress equal to the yield stress. If the actual plate has larger width, the capacity would be the same as that of the fictitious plate. In a plate the real stress distribution is approximated, or replaced, with two strips which describe the load carrying effective width of the plate. Consequently, this method is based on the reduction of the cross-section area in the parts affected by plate buckling.

The reduced stress method, used in the past in Aluminium Associated Code [6.3], checks at which stress level a plate part buckles, if a cross-section is built up from multiple plate parts the lowest stress is governing for the entire cross-section. So, it evaluates the capacities of a slender section by considering a reduced value of the limiting stress acting on the full section.

Finally, the effective thickness approach, firstly introduced in the British Code of Practice for Structural Aluminium [6.4], has been more recently introduced in EN1999-1-1 dealing with aluminium alloy structures [6.5]. It is based on replacing the true section by an effective one obtained to reduce the actual thickness of the compressed parts. The main advantage of the effective thickness approach is that it allows more easily to account for the influence of heat-affected zones in the case of cross-sections composed by welding. This is very important in the case of aluminium alloy structures where a significant reduction of the material properties arises in the heat-affected zones.

Figure 6.1 shows a qualitative comparison between the different design approaches for a generic box section subjected to non-uniform compression.

Nowadays, the currently European Code Provisions suggests the use of the effective width approach and the effective thickness method, respectively, for the steel and aluminium cross-section. In

particular, these methods are indirectly used to evaluate the behaviour of the slender sections, belonging to the class 4, affected by the local buckling occurring in the elastic region.

Moreover, as already mentioned in the previous chapters, in order to evaluate the ultimate behaviour of aluminium members, taking into account the interactive local buckling in the post elastic region, others simplified approaches have been recently been proposed as, for example, the continuous strength method (CSM) [6.6] or the direct strength method (DSM) [6.7] provided, respectively, by *Gardner* and *Schafer*. However, the current methodologies, aiming the evaluation the inelastic response of aluminium members, provide the predictional values of ultimate compressive resistance which are excessively conservative in comparison with the experimental results, presented in the technical literature.

In this Chapter, an extension of effective thickness method (ETM) is provided in order to take into account the interaction of the plate elements constituting the cross-sections and the strain-hardening behaviour of aluminium alloys.

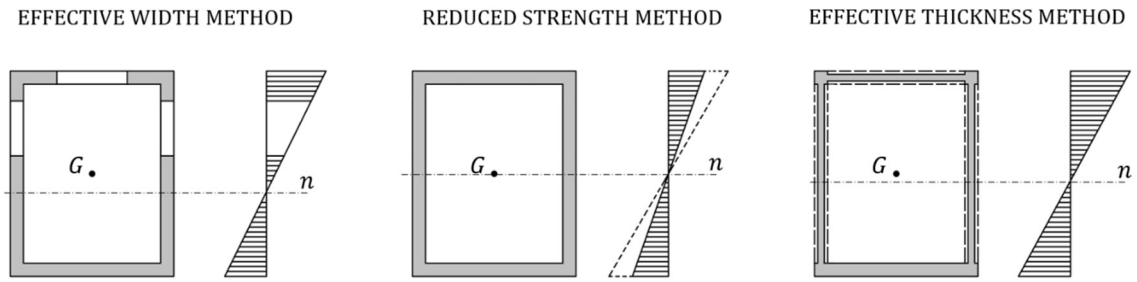

Figure 6.1. Comparison of the different design approaches for a rectangular section in bending.

6.2. Extension of the Effective Thickness Method (ETM)

The new version of the effective thickness approach properly modifies the simplified rules given in the general provisions of EN1991-1-1 [6.5] to account for the occurrence of buckling in the plastic range, as it occurs in the case of sections whose plate elements are characterised by small values of the width-to-thickness ratio.

As reported in Chapter 2 [Eq. (2.11)], the elastic buckling stress of an isolated plate element is given by:

$$\sigma_{cr.e} = k\frac{\pi^2 E}{12(1-\nu_e^2)(b/t)^2} \tag{6.1}$$

where E is the elastic modulus, ν_e is the Poisson's ratio in the elastic range, b is the plate width, t is the plate thickness and k is the buckling factor. The factor k accounts for the edge restraining conditions and the stress distribution along the loaded edges.

In the case of the plate elements constituting the section of a structural member, the occurrence of elastic buckling is also affected by the interaction between the plate elements constituting the member

section and by the longitudinal stress gradient. These effects can be taken into account by modifying Eq. (6.1) using two factors: ζ and α_{LS}. The factor ζ accounts for the interaction between the plate elements composing the section. The factor α_{LS} accounts for the influence of the longitudinal stress gradient occurring in structural members under non-uniform bending. Obviously, in the case of uniform compression, herein investigated, $\alpha_{LS} = 1.0$.

Therefore, including the effects of interactive buckling and longitudinal stress gradient, the elastic buckling stress can be expressed as:

$$\sigma_{cr.e} = \zeta\ \alpha_{LS} k \frac{\pi^2 E}{12(1-\nu_e^2)(b/t)^2} \tag{6.2}$$

The occurrence of buckling in the plastic range can be accounted for using a correction factor which depends on the non-linear behaviour of the material. By denoting with ξ such correction factor, the buckling stress in the plastic range $\sigma_{cr.p}$ is given by:

$$\sigma_{cr.p} = \xi\ \zeta\ \alpha_{LS} k \frac{\pi^2 E}{12(1-\nu^2)(b/t)^2} \tag{6.3}$$

where also the Poisson's ratio ν has to be evaluated accounting for the non-linear behaviour of the material. Regarding the ξ factor, many different expressions have been proposed in the technical literature for its evaluation. Some of them will be presented in the following discussion.

Concerning the Poisson's ratio in the yield region, as shown in Chapter 2, *Gerard and Wildhorn* [6.8] have studied the problem in the case of several aluminium alloys and have shown that it is seriously affected by the anisotropy of the material. In the case of materials exhibiting the same properties in the two directions orthogonal to the loading direction, they proposed Eq. (2.39). However, in the case of perfectly plastic material, the condition $\nu = \nu_p$ is reached only when the strain assumes infinite value ($\varepsilon \to \infty$) so that $E_s \to 0$. Therefore, within the framework of a simplified procedure like the effective thickness approach, an alternative relation can be proposed:

$$\nu = \nu_p - \frac{E_t}{E}\left(\nu_p - \nu_e\right) \tag{6.4}$$

which assures $\nu = \nu_e$ in the elastic range ($E_t = E$) and the condition $\nu = \nu_p$ when a plastic plateau is reached ($E_t = 0$). Eq. (6.3) can be written as follows:

$$E_s\ \varepsilon = \xi\ \zeta\ \alpha_{LS} k \frac{\pi^2 E}{12(1-\nu^2)(b/t)^2} \tag{6.5}$$

where ε is the strain corresponding to buckling. Consequently, the effective ratio b/t can be defined as a function of the strain level as:

$$\left(\frac{b}{t}\right)_{eff} = \sqrt{\frac{\xi E}{E_s}\,\zeta\,\alpha_{LS}k\,\frac{\pi^2}{12(1-\nu^2)}\,\frac{1}{\varepsilon}} \tag{6.6}$$

The effective thickness can be derived by noting that:

$$\left(\frac{t}{b}\right)_{eff} = \sqrt{\frac{E_s}{\xi E}\frac{1}{\zeta\,\alpha_{LS}k}\frac{12(1-\nu^2)}{\pi^2}\,\varepsilon} \tag{6.7}$$

and by introducing a parameter μ, which accounts for the non-linear behaviour of the material:

$$\mu = \frac{\xi E}{E_s}\frac{1}{1-\nu^2} \tag{6.8}$$

so that the following relation is obtained:

$$\frac{t_{eff}}{t} = \frac{b}{t}\sqrt{\frac{12}{\pi^2}\,\frac{1}{\mu}\,\frac{1}{\zeta\,\alpha_{LS}k}\,\varepsilon} \tag{6.9}$$

Remembering that:

$$\bar{\lambda}_p = \frac{t_{eff}}{t} \tag{6.10}$$

It means that the normalised slenderness in the non-linear range (elastic-plastic range), depending on the strain level, can be defined as:

$$\bar{\lambda}_p = \frac{b}{t}\sqrt{\frac{12}{\pi^2}\,\frac{1}{\mu}\,\frac{1}{\zeta\,\alpha_{LS}k}\,\varepsilon} \tag{6.11}$$

To use the buckling curves of EN1999-1-1 with the normalised slenderness corrected to account for the non-linearity depending on the strain level, it has to be considered that:

$$\bar{\lambda}_p = 0.03143\,\frac{\beta}{\epsilon_0} \tag{6.12}$$

where $\epsilon_0 = \sqrt{250/f_{0.2}}$, therefore:

$$\frac{\beta}{\epsilon_0} = \frac{\bar{\lambda}_p}{0.03143} = \frac{1}{0.03143}\sqrt{\frac{3}{\pi^2}\,\frac{\varepsilon}{\mu\,\zeta\,\alpha_{LS}}}\,\frac{2}{\sqrt{k}}\,\frac{b}{t} \tag{6.13}$$

Taking into account that, in EN1999-1-1, the factor accounting for the stress distribution along the loaded edge is:

$$\eta = \frac{2}{\sqrt{k}} \tag{6.14}$$

Eq. (6.12) provides:

$$\frac{\beta}{\epsilon_0} = 17.54\,\eta\,\frac{b}{t}\sqrt{\frac{\varepsilon}{\mu\,\zeta\,\alpha_{LS}}} \tag{6.15}$$

which is the final expression to compute the slenderness parameter of the plate element to be used, in combination with the buckling curves of EN1999-1-1. This allows computing the effective thickness in the non-linear range as a function of the strain level ε. In fact, according to EN1999-1-1, the reduction factor accounting for local buckling is computed as:

$$\rho_c = 1 \qquad if \qquad \frac{\beta}{\epsilon_0} \leq \frac{1}{2}\left(\mathrm{C}_1 + \sqrt{\mathrm{C}_1^2 - \mathrm{C}_2(3+\psi)}\right) \tag{6.16}$$

and:

$$\rho_c = \frac{\mathrm{C}_1}{\beta/\epsilon_0} - \frac{\mathrm{C}_2(3+\psi)}{4\,(\beta/\epsilon_0)^2} \qquad if \qquad \frac{\beta}{\epsilon_0} > \frac{1}{2}\left(\mathrm{C}_1 + \sqrt{\mathrm{C}_1^2 - \mathrm{C}_2(3+\psi)}\right) \tag{6.17}$$

The parameter ψ accounts for the strain distribution along the loaded edge of the plate. It is given by the ratio between the maximum compression strain at one end of the plate and the strain at the second end of the plate element. In the case of uniform compression, it results $\psi = 1$ while $\psi < 0$ when the second end of the plate element is subject to tension. While the coefficient C_1 and C_2 are reported in Eurocode 9 and they are defined according to the Buckling Curves:

Table 6.1. Values of the coefficients C_1 and C_2 reported in the Eurocode 9.

Buckling Curve	***Internal part***		***Outstand part***	
	$\mathbf{C_1}$	$\mathbf{C_2}$	$\mathbf{C_1}$	$\mathbf{C_2}$
A	32	220	10	24
B	30.5	209	9.5	22
C	29	198	9	20

Regarding the ξ factor needed in Eq. (6.8) as already stated, a variety of different formulations have been proposed in the technical literature [6.9]-[6.12].The most commonly used formulations are:

- *tangent modulus theory:* $\xi = \frac{E_t}{E}$
- *secant modulus theory:* $\xi = \frac{E_s}{E}$
- *Stowell (1948), Bijlaard (1949):* $\xi = \frac{E_s}{E}\left[\frac{1}{3} + \frac{2}{3}\sqrt{\frac{1}{4} + \frac{3}{4}\frac{E_t}{E_s}}\right]$
- *Li and Reid (1992):* $\xi = \frac{E_s}{E}\left[\frac{1}{2} + \frac{1}{2}\sqrt{\frac{1}{4} + \frac{3}{4}\frac{E_t}{E_s}}\right]$

The use of the tangent modulus theory provides the smallest value of the buckling load. Conversely, the secant modulus theory provides the greatest value of the buckling load. While the relationships provided by *Stowell-Bijlaard* and *Li-Reid* provide intermediate values. However, aiming to improve the accuracy of the results obtained when the effective thickness approach is applied to predict to ultimate resistance of aluminium members subjected to local buckling under compression and non-uniform bending, other two formulations are proposed. The first one derives by the theoretical results obtained in Chapter 2. In particular, as seen in Section 2.36, this is obtained by combining the Eqns. (2.108) and (2.109) derived by a single plate simply supported along four edges under uniform compression:

$$\xi = \left[0.42C_3 + 0.58\sqrt{C_1 C_5}\right]\left(\frac{1-\nu_e^2}{1-\nu^2}\right)\frac{E_s}{E} \tag{6.18}$$

where the expressions of the plastic coefficients C_i are reported in Eq.(2.76). It is possible to observe that this formulation is similar to the relations proposed by *Stowell-Bijlaard* and *Li-Reid,* however in this case the variability of Poisson's ratio is accounted. While, in the case of aluminium beams in bending, the following relationship is suggested:

$$\xi = \frac{E_s}{E}\left[\frac{n-8}{8} + \frac{8}{n}\sqrt{\frac{E_t}{E_s}}\right] \tag{6.19}$$

It can be recognised that Eq. (6.19) is a combination of the secant modulus theory with the *Gerard* formula. In particular, for small values of the Ramberg-Osgood exponent n, Eq. (6.19) tends to provide values close to those given by *Gerard*. Conversely, for high values of n, Eq. (6.19) tends to provide values close to the secant modulus theory. In the following, referring to the application of the effective thickness approach, Eqns. (6.18) and (6.19) are used.

Regarding the factor accounting for the influence of the longitudinal stress gradient, the following relations can be adopted [6.13],[6.14]:

- for a flat internal compression cross-section part:

$$\alpha_{LS} = 1 + \frac{1}{4}\frac{1.70}{\left(\frac{L_s}{b}\right)^{0.75} - 0.20} \tag{6.20}$$

- in case of flat outstand compression elements:

$$\alpha_{LS} = 1 + \frac{1}{0.425}\frac{1.70}{\left(\frac{L_s}{b}\right)^{0.95} - 0.60} \tag{6.21}$$

where L_s is the shear length and b is the plate width in compression. The shear length is defined as the distance between the point of zero bending moment and the section where the maximum bending moment occurs. In the case of uniform compression, $\alpha_{LS} = 1.0$.

The correction factor ζ for interactive buckling can be evaluated taking into account that it represents the ratio between the buckling factor k accounting for interactive buckling and the buckling factor k_0 evaluated for the isolated plate element, i.e. $\zeta = k/k_0$.

- in the case of plate elements, acting as flange, connected to webs on both edges (curve 1 of Figure 6.2)

$$\zeta = 1.75 - \frac{0.45\, b_2/b_1}{0.15 + b_2/b_1} - 0.02275(b_2/b_1)^3 \geq 1 \tag{6.22}$$

  which is derived from the expression of k given by BS5950-5 [6.15] considering that, in this case, $k_0 = 4$.

- in the case of plate elements, acting as flange, connected to the web on one edge and the lip on another edge (curve 2 of Figure 6.2)

$$\zeta = 1.35 - \frac{0.35\, b_2/b_1}{0.60 + b_2/b_1} - 0.005(b_2/b_1)^3 \geq 1 \tag{6.23}$$

  which is derived from the expression of k given by BS5950-5 [6.15] considering that, in this case, $k_0 = 4$.

- in the case of unstiffened elements, acting as a flange (Figure 6.2)

$$\zeta = 3.00 - \frac{1.882\, b_2/b_1}{2.0 + b_2/b_1} - 0.0059(b_2/b_1)^2 \geq 1 \tag{6.24}$$

  which is derived from the expression of k given by BS5950-5 [6.15] considering that, in this case, $k_0 = 0.425$.

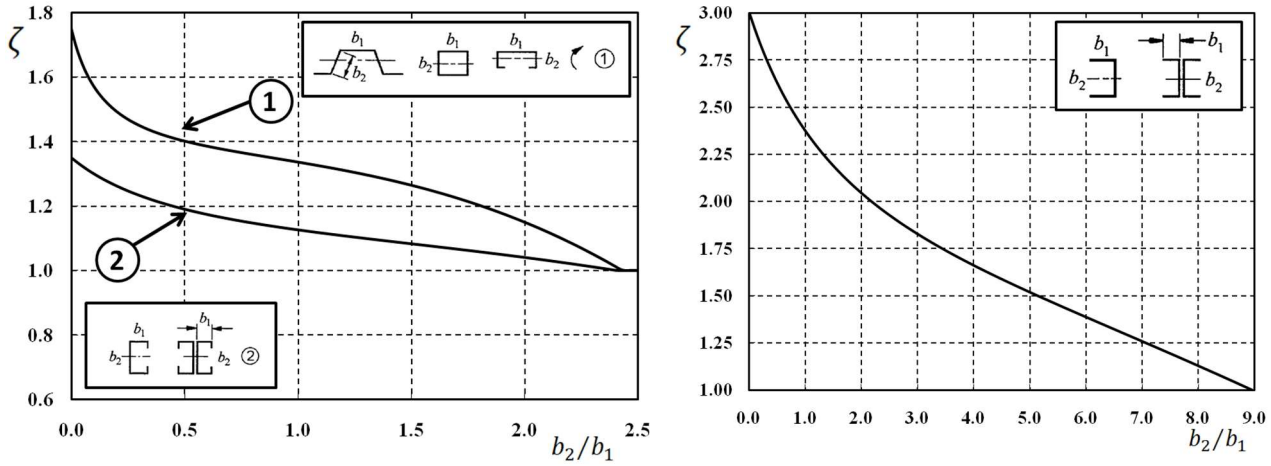

Figure 6.2. Correction factor for interactive buckling: for stiffened compression elements of beams (left) and unstiffened compression elements of beams (right)

6.3. Numerical Procedure under Displacement Control

The application of the effective thickness approach, as previously described, requires a procedure under displacement control. Regarding stub columns subjected to uniform compression, for increasing values of the axial displacement δ the corresponding average strain $\varepsilon = \delta/h$ is derived, being h the height of the specimen. Therefore, the slenderness parameter is given by Eq. (6.15) for increasing values of the strain level and computed for the plate elements constituting the member section. It increases for increasing values of ε. The appropriate buckling curve is used, according to EN1999-1-1, so that the effective thickness is computed for all the plate elements and the effective cross-section area A_{eff} is computed. The axial force corresponding to the axial displacement δ is obtained as $N = \sigma\, A_{eff}$ where σ is the stress level corresponding to ε, evaluated according to the constitutive stress-strain curve of the material, i.e., the Ramberg-Osgood model. The axial force versus axial displacement curve is thus obtained. The maximum value of this curve is the ultimate buckling resistance. The obtained curve includes also the softening branch due to the post-buckling behaviour. It occurs when the progressive reduction of the effective area is no more compensated by the increase of the stress due to the increase of the strain level (Figure 6.3).

In the case of beams under bending, the numerical procedure is more complicate than the previous case. In fact, after the strain level and, consequently, the corresponding stress σ, are not constant, but they vary along the section heigh. For this reason, it is not possible to apply a continuous relation, as depicted for the uniform compression, but a fiber model is used to evaluate the curvature χ as a function of the strain level ε. Finally, the bending moment M by means of the rotational equilibrium equation between the compression parts and the tension parts (Figure 6.3).

Moreover, according to Figure 6.4, the rotation θ corresponding to the attainment of the flexural resistance M has been calculated by integrating the curvature diagram χ along the shear length of the structural member:

$$\theta = \int_0^{L_s} \chi[M(x)]\, dx \tag{6.25}$$

Obviously, the rotation θ_u, can be estimated by means of Eq. (6.25) for $\chi[M(x)] = \chi_u$, i.e., the curvature corresponding to the maximum bending moment M_u. Instead, the maximum rotation θ_m, corresponding to the at the point where the moment resistance drops back below the conventional yield value $M_{0.2}$, can be computed as:

$$\theta_m = \theta_u + (\chi_m - \chi_u) L_p \tag{6.26}$$

where χ_m is the ultimate curvature and L_p is the length of the plastic hinge evaluated as the distance between the points where the conventional yield curvature $\chi_{0.2}$ and χ_m occur.

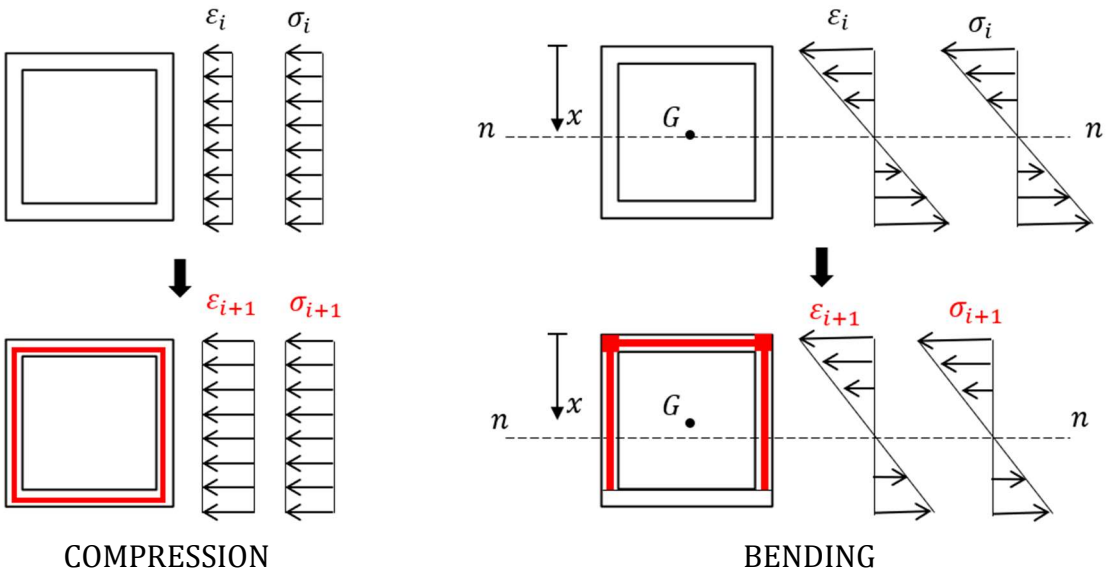

Figure 6.3.Scheme of a generic box section in compression (left) and in bending (right).

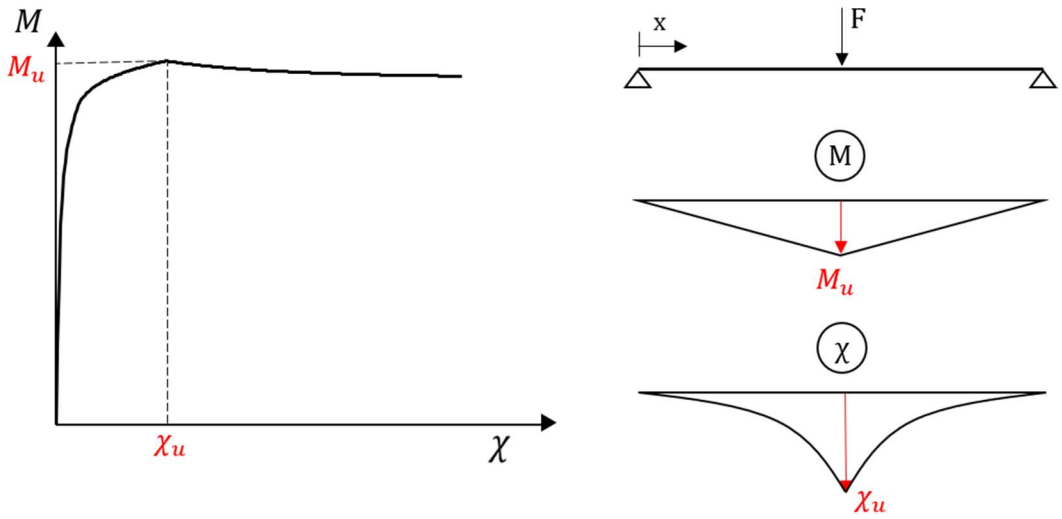

Figure 6.4. Moment and Curvature diagrams for a beam subjected to the concentrated load.

For the sake of completeness, the MATLAB scripts [6.24] of the numerical procedures, previously described, are given in Appendix E referring to a generic box section. Obviously, the same considerations can be assumed for the H-shaped sections. Finally, Figure 6.5 - Figure 6.8 show a comparison between the experimental curves, provided in Chapter 3, with those obtained by effective thickness approach. In particular, the stub column tests curves are compared with the compressive load- strain curves in Figure 6.5, while Figure 6.6-Figure 6.8 report the comparison between the three point bending tests and the moment-curvature curves. In the last cases, it is easy to recognize that the accuracy of the theoretical curves decreases for increasing the section width and when the length of beam decreases. Moreover, as already pointed out in Chapter 3, the experimental results of specimens

SHS80_L2, SHS80_L3, SHS100_L2 and SHS100_L3 are neglected, because they are not governed by the pure flexural behaviour, conversely, they are affected by the local instability phenomena due to the concentrated force.

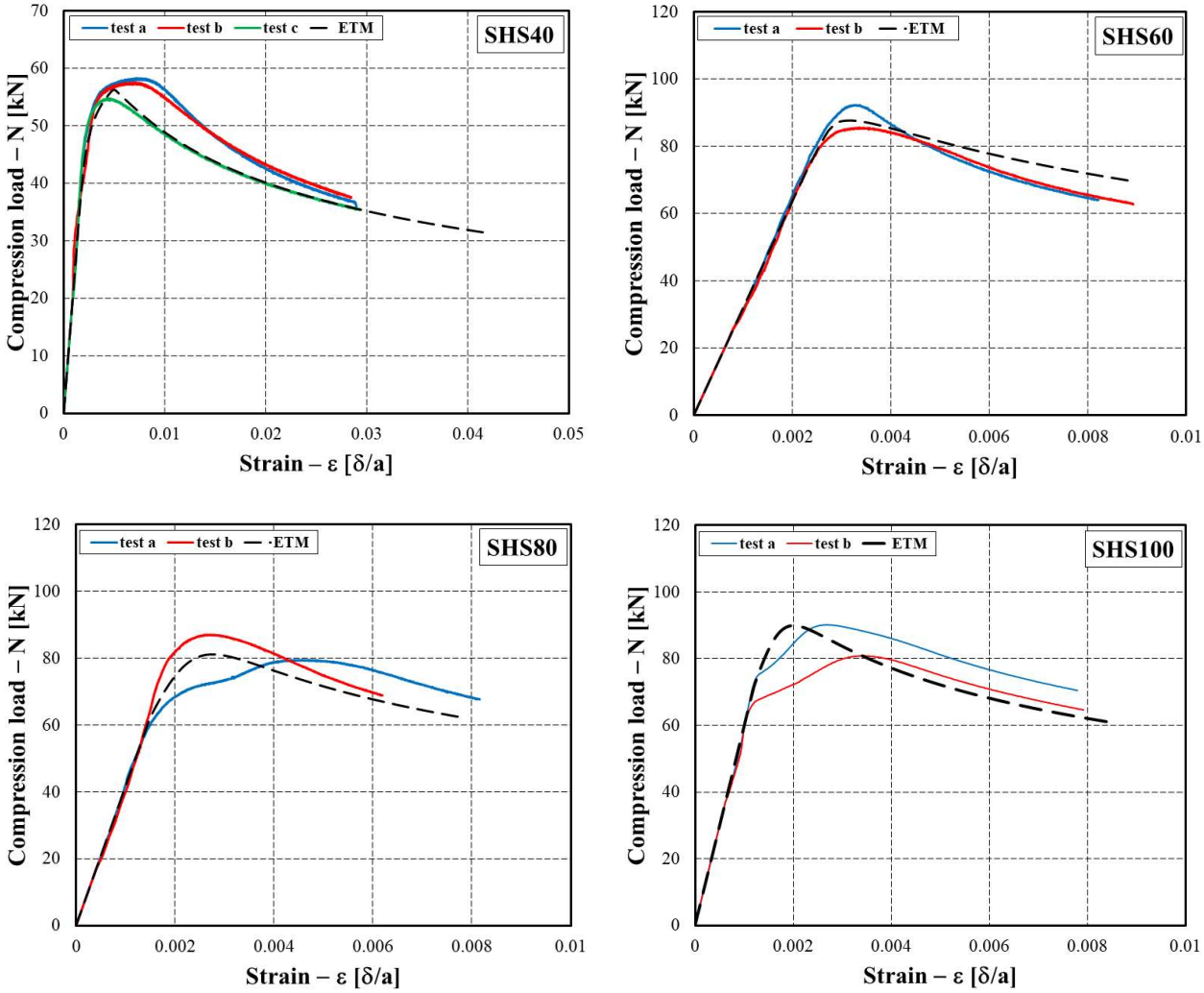

Figure 6.5. Comparison between stub test curves and compressive load-strain curves obtained by effective thickness method (ETM).

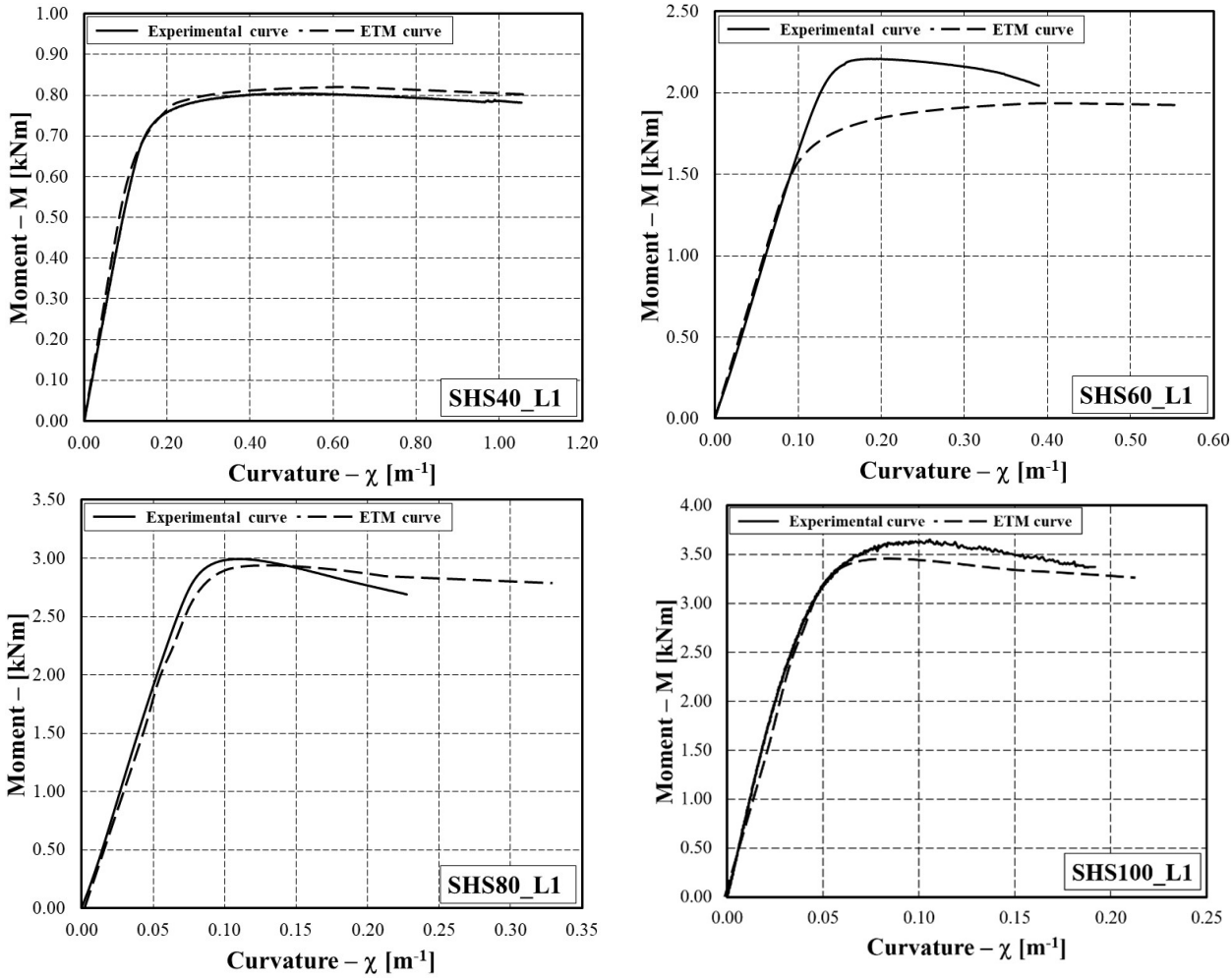

Figure 6.6. Comparison between experimental curves and moment-curvature curves obtained by effective thickness method (ETM) for length $L_1 = 1300\ mm$

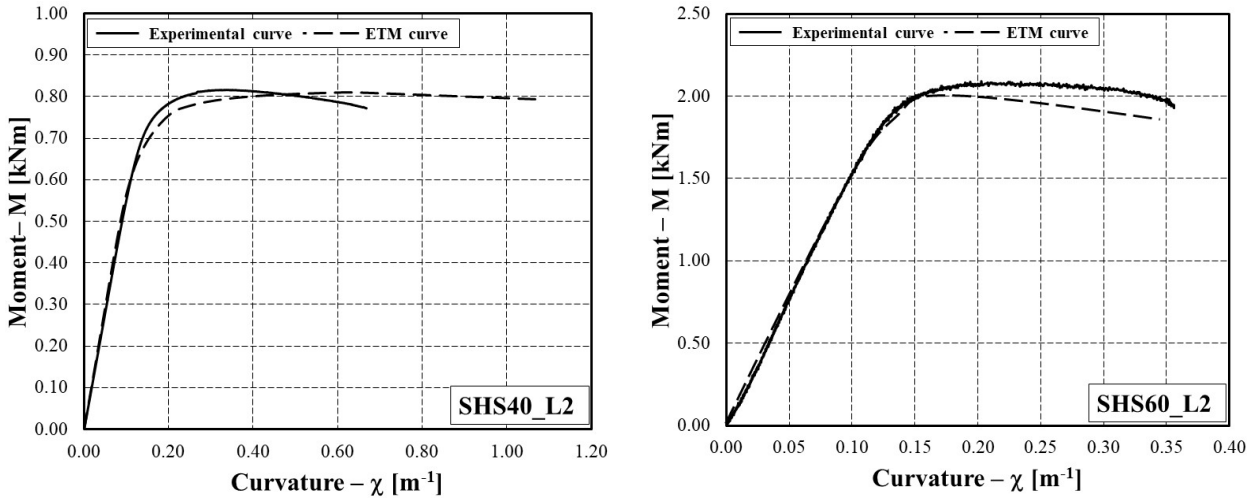

Figure 6.7. Comparison between experimental curves and moment-curvature curves obtained by effective thickness method (ETM) for length $L_2 = 800\ mm$

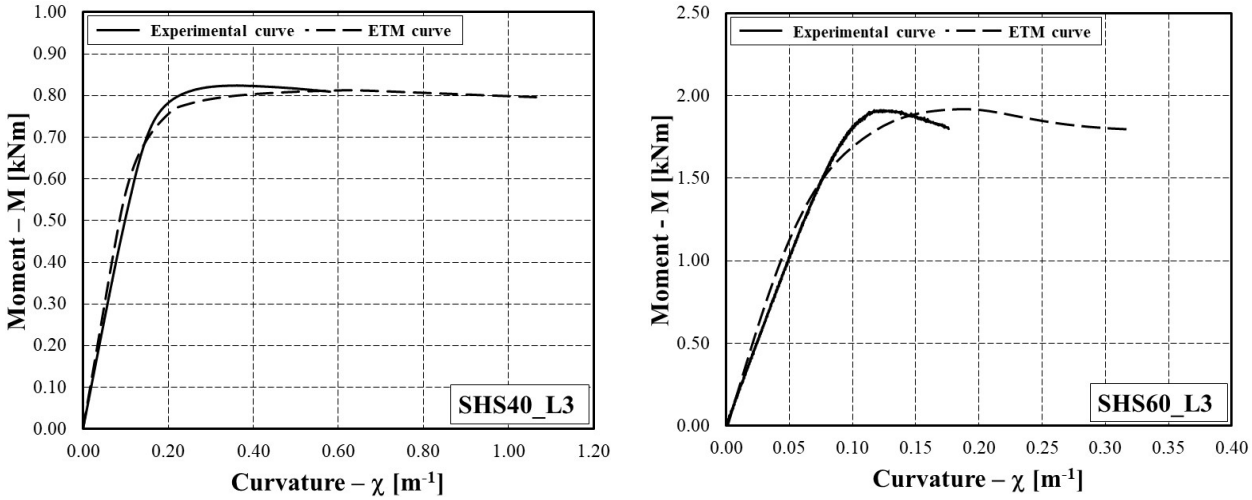

Figure 6.8. Comparison between experimental curves and moment-curvature curves obtained by effective thickness method (ETM) for length $L_3 = 500\ mm$

6.4. Comparison with Stub and Bending Tests

In this section, the accuracy of this methodology is evaluated in the prediction of the ultimate behaviour of aluminium members in compression and in bending. In particular, the same comparisons with experimental results, provided in Sections 4.4 and 5.4, respectively, for members in compression and in bending, have been proposed computing the theoretical values of the maximum resistances and the corresponding deformation capacities by means of the effective thickness method (ETM).

In the case of the uniform compression, Figure 6.9-Figure 6.12 show the comparison between the theoretical buckling loads $N_{u.ETM}$, and the normalised deformation $\bar{\varepsilon}_{u.ETM}$ with the corresponding experimental results reported in Chapter 3 and in scientific literature [6.16]-[6.21].The normalization of the strain, corresponding to the occurrence of local buckling, is defined according to Eq. (3.6). The prediction of the ultimate behaviour of aluminium members is accurate, especially, as regards the ultimate resistance. In fact, the average value of the ratio $N_{u.ETM}/N_{u.exp}$ is equal to 0.96 for hollow sections and 0.93 for H-shaped sections, while the standard deviation is, respectively, equal to 0.07 and 0.11. Instead, the prediction of the deformation capacity is less accurate. In fact, the average value of the ratio $\bar{\varepsilon}_{u.ETM}/\bar{\varepsilon}_{u.exp}$. is equal to 0.81 for hollow sections and 1.01 for H-shaped sections, while the standard deviation is, respectively, equal to 0.22 and 0.28. However, the theoretical approach is a safety procedure, because, in most cases, the experimental values are greater than those provided by the effective thickness method (ETM). The numerical results are given in Annex A.

In the case of aluminium beams in bending, the comparison refers to the three point bending tests presented in Chapter 3 and to the experimental results reported in scientific literature [6.22],[6.23]. Due to lack of lot of available experimental data, the results of the hollows sections and the H-shaped sections are not evaluated separately as for the case of compression. Figure 6.13 and Figure 6.14 shows the comparison between the results obtained by ETM method and those provided by the three point bending tests. There is a good accuracy in the prediction of the ultimate behaviour of aluminium members, especially, as regards the ultimate resistance. In fact, the average value of the ratio $M_{u.ETM}/M_{u.exp}$ is equal to 0.97 with the standard deviation equal to 0.15.

Instead, the prediction of the normalised rotational capacity is less accurate. In fact, the average value of the ratio $\bar{\theta}_{u.ETM}/\bar{\theta}_{u.exp}$ is equal to 0.90, while the standard deviation is 0.12. However, the effective thickness method can be applied in all cases without any limitations, instead the empirical regressions, although more accurate and simpler in the computation, can not be always used, but their application has to respect the limit the ranges provided in (5.10). The numerical results are given in Annex B.

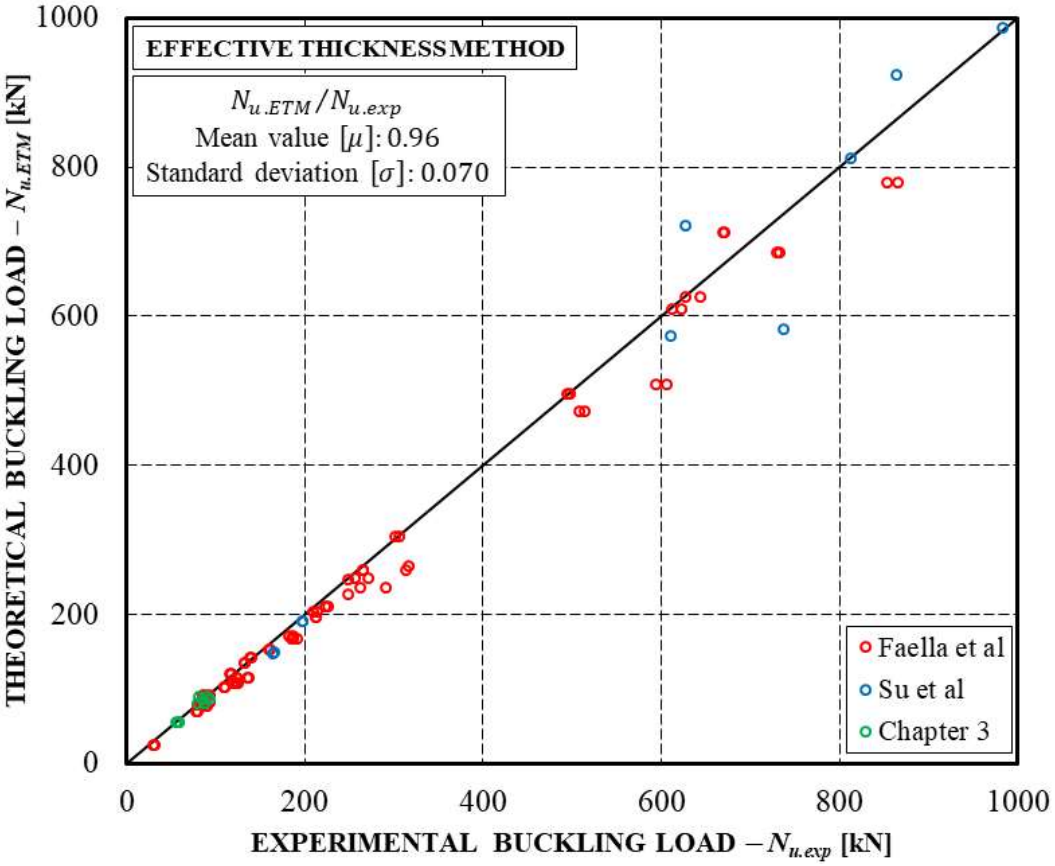

Figure 6.9. Comparison of the theoretical ultimate resistances with experimental results for box sections.

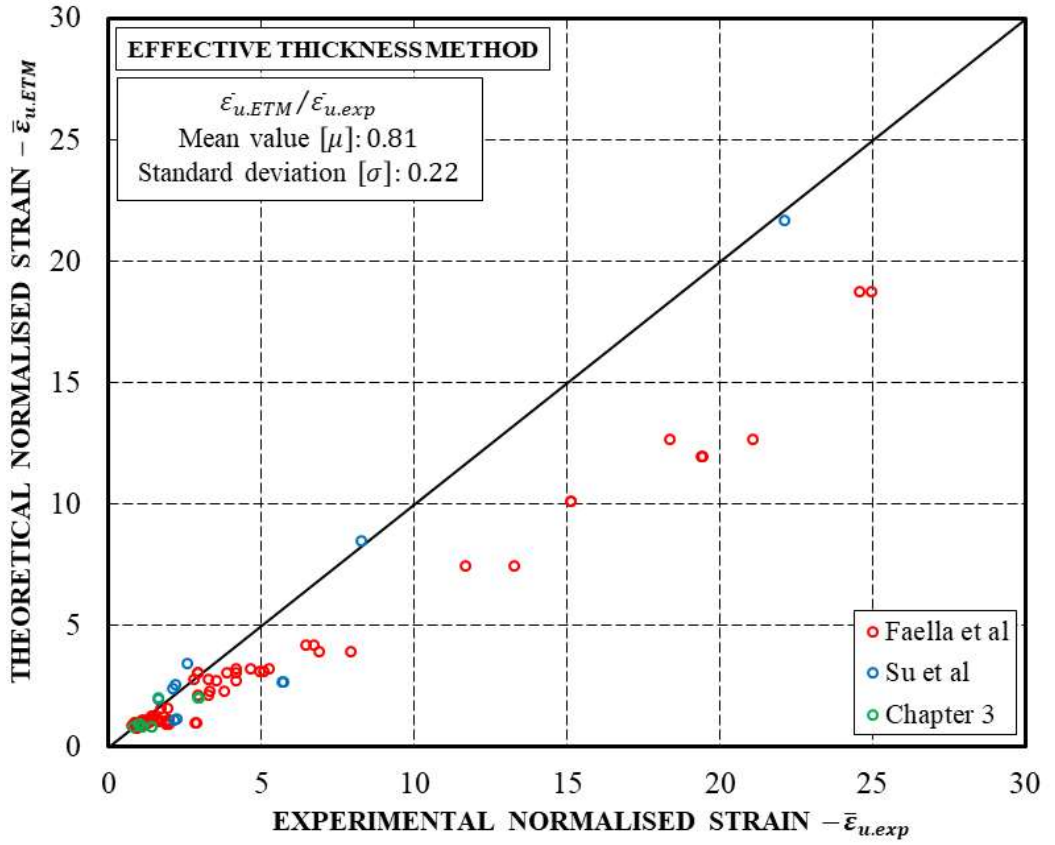

Figure 6.10. Comparison of the normalised strains with experimental results for box sections.

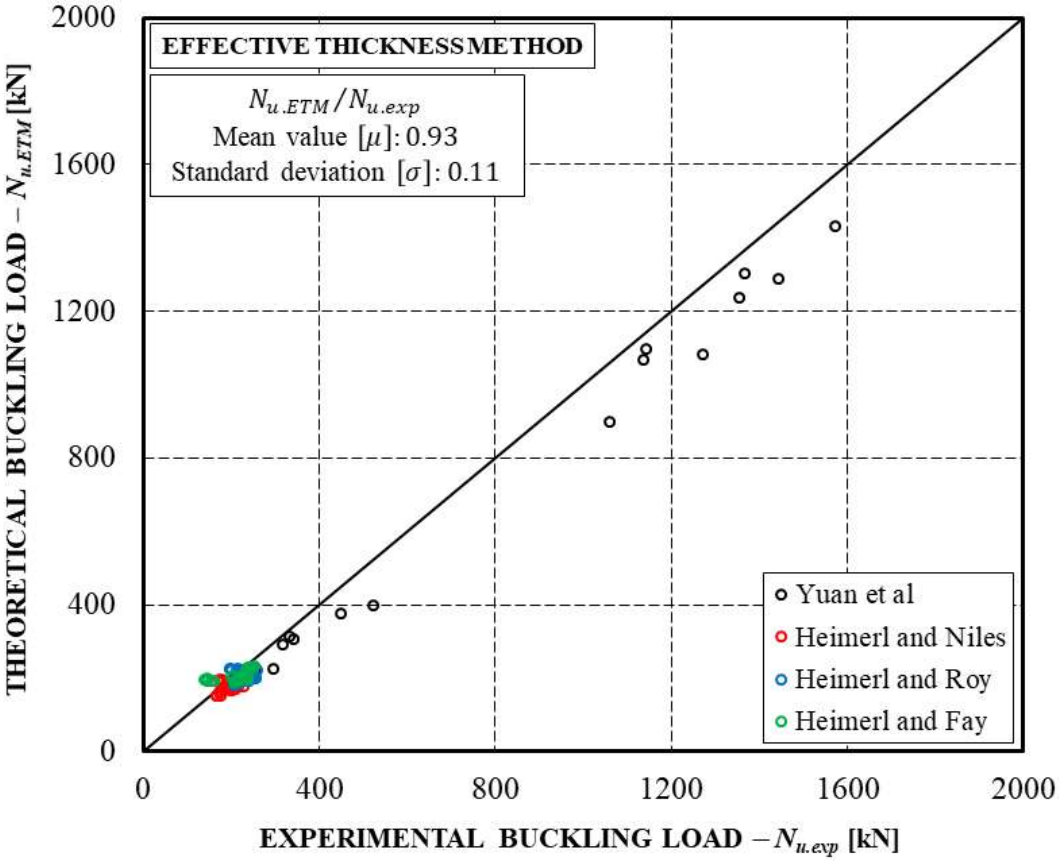

Figure 6.11. Comparison of the theoretical ultimate resistances with experimental results for H-sections.

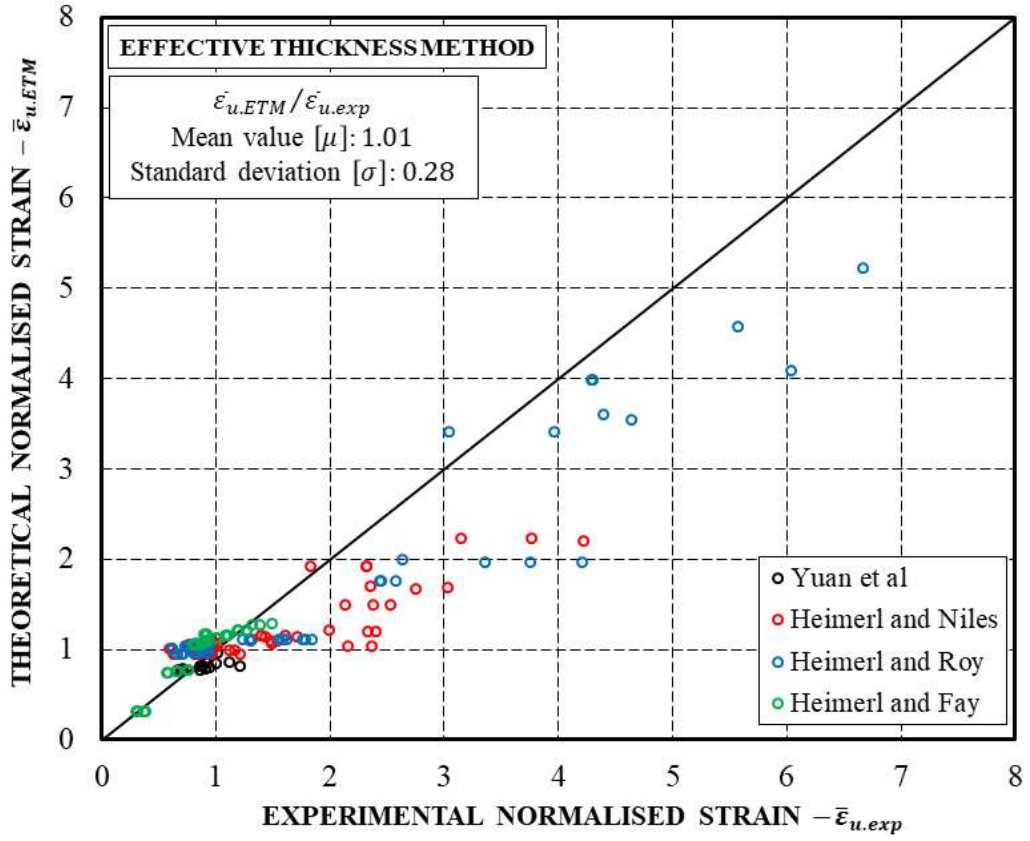

Figure 6.12. Comparison of the theoretical normalised strains with experimental results for H- sections.

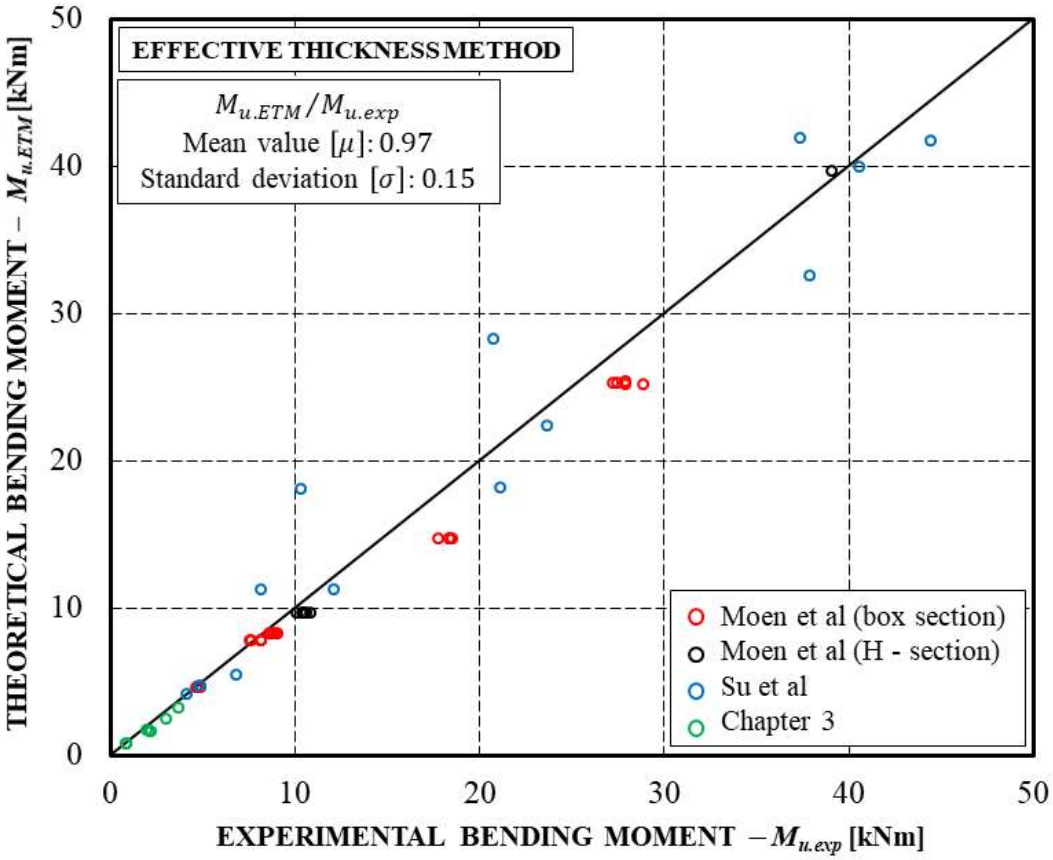

Figure 6.13. Comparison of the theoretical flexural resistances with experimental results.

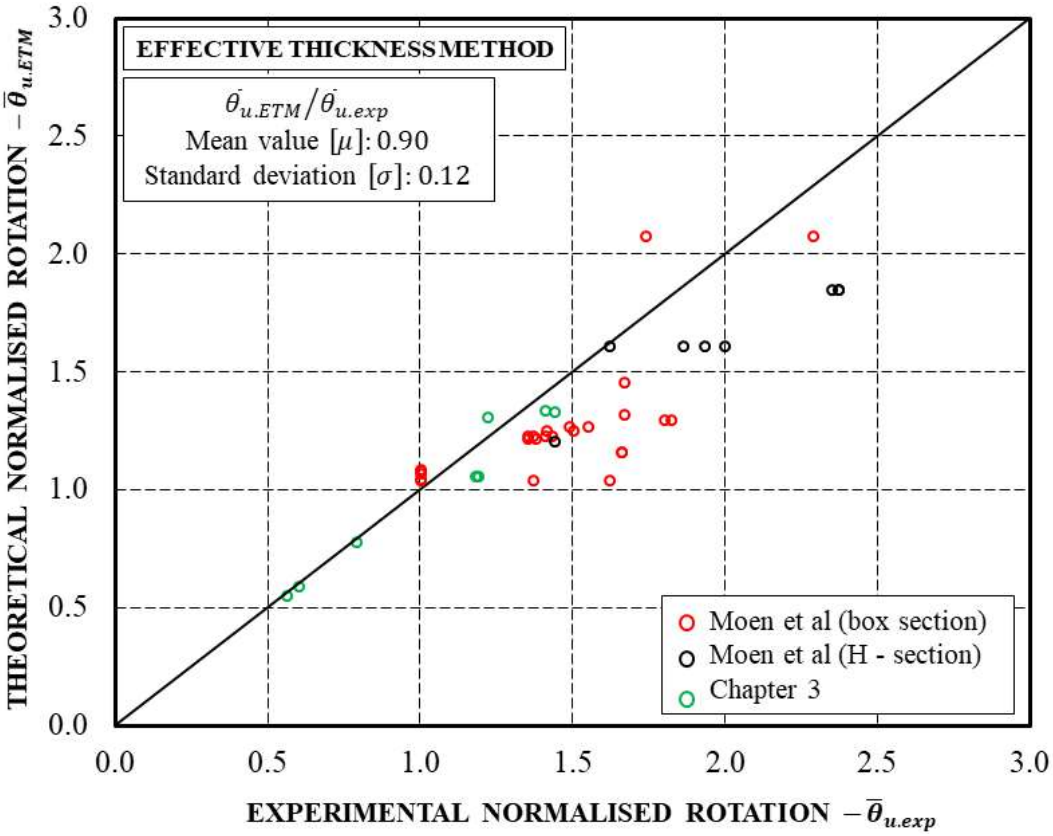

Figure 6.14. Comparison of the rotational capacities with experimental results.

6.5. References

[6.1] **EN 1993-1-1**: "Eurocode 3: Design of steel structures - Part 1-1: General rules and rules for buildings", European Committee for Standardization, 2005.

[6.2] **T. Von Kármán, E.E. Sechler, L.H. Donnell:** "The Strength of Thin Plate in Compression", Transactions A.S.M.E., Applied Mechanics, APM 54-5, pp. 53-58, 1932.

[6.3] **R. Landolfo and F.M. Mazzolani:** "Different Approaches in the Design of Slender Aluminium Alloy Sections", Thin-Walled Structures, 27(1), pp.85-102, 1997.

[6.4] **BS 8118-1:** "The Structural use of Aluminium", British Standard Institute, London, 1991.

[6.5] **EN1999-1-1:** "Eurocode 9: Design of aluminium structures - Part 1-1: General structural rules", European Committee for Standardization, 2007.

[6.6] **M.N. Su, B. Young, L. Gardner:** "The continuous strength method for the design of aluminium alloy structural elements", Engineering Structures, 122, pp.338–348, 2016.

[6.7] **B.W. Schafer and T. Peköz:** "Direct Strength prediction of cold-formed steel members using numerical elastic buckling solutions", International Specialty Conference on Cold-Formed Steel Structures: Recent Research and Developments in Cold-Formed Steel Design and Construction, pp. 69-76, 1998.

[6.8] **G. Gerard and S. Wildhorn:** "A Study of Poisson's Ratio in the Yield Region", NACA

[6.9] **E.Z. Stowell**: "A Unified Theory of Plastic Buckling of Columns and Plates", National Advisory Committee for Aeronautics, NACA Technical Note n. 1556, Washington, 1948.

[6.10] **A.A. Ilyushin:** "The Elasto-Plastic Stability of Plates", NACA Technical Memorandum 1188, National Advisory Committee on Aeronautics, Washington, D.C., 1946.

[6.11] **E.E. Lundquist and E.Z. Stowell**: "Critical Compressive Stress for Outstanding Flanges", National Advisory Committee for Aeronautics, NACA Technical Note n. 734, Washington, 1942.

[6.12] **E.E. Lundquist and E.Z. Stowell**: "Critical Compressive Stress for Flat Rectangular Plates Supported along All Edges and Elastically Restrained against Rotation along the Unloaded Edges", National Advisory Committee for Aeronautics, NACA Technical Note n. 733, Washington, 1942.

[6.13] **R. Rebiano, N. Silvestre, D. Camotim:** "GBT Formulation to Analyze the Buckling Behavior of Thin-Walled Members subjected to Non-Uniform Bending", International Journal of Structural Stability and Dynamics, 7(1), pp. 23-54, 2007.

[6.14] **C. Yu and B.W. Schafer:** "Effect of Longitudinal Stress Gradients on Elastic Buckling of Thin Plates", Journal of Engineering Mechanics, 133(4), pp. 452-463, 2007.

[6.15] **BS 5950-5:** "Structural use of steelwork in building - formed thin gauge sections Part 5: Code of practice for design of cold formed thin gauge sections", Steel Construction Institute, Silwood Park, Ascot, Berkshire SL5 7QN, 1998.

[6.16] **M.N. Su, B. Young, L. Gardner:** "The continuous strength method for the design of aluminium alloy structural elements", Engineering Structures, 122, pp.338–348, 2016.

[6.17] **C. Faella, F.M. Mazzolani, V. Piluso, G. Rizzano:** "Local buckling of aluminium members: testing and classification", Journal of Structural Engineering, ASCE 2000, 126 (3), pp.353–60, 2000.

[6.18] **G.J. Heimerl and D.E. Niles:** "Column and plate compressive strengths of aircraft structural materials extruded 14S-T aluminium alloys", NACA Technical Note L6c19, National Advisory Committee on Aeronautics, Washington, D.C., 1946.

[6.19] **G.J. Heimerl and J.A. Roy:** "Column and plate compressive strengths of aircraft structural materials extruded 75S-T aluminium alloys", NACA Technical Note L5F08a, National Advisory Committee on Aeronautics, Washington, D.C., 1945.

[6.20] **G.J. Heimerl and D.P. Fay:** "Column and plate compressive strengths of aircraft structural materials extruded R303S-T aluminium alloys", NACA Technical Note L5H04, National Advisory Committee on Aeronautics, Washington, D.C., 1945.

[6.21] **H.X. Yuan, Y.Q. Wang, T. Chang, X.X. Du, Y.D. Bu, Y.J. Shi:** "Local buckling and post buckling strength of extruded aluminium alloy stub columns with slender I-sections", Thin-Walled Structures, 90, pp.140-149, 2015.

[6.22] **L.A. Moen, O.S. Hopperstad, M. Langseth:** "Rotational capacity of aluminum beams under moment gradient. I: Experiments", Journal of Structural Engineering, 125 (8), pp. 910-920, 1999.

[6.23] **M.N. Su, B. Young, L. Gardner:** "Deformation-based design of aluminum alloy beams" Engineering Structures, 80, pp. 339-349, 2014.

[6.24] **MathWorks Inc.** "MATLAB-High Performance Numeric Computation and Visualization Software. User's Guide", Natick: MA, USA, 1997.

Appendix E

E.1. Script for Box Section in Compression

```
%EFFECTIVE THICKNESS METHOD FOR UNIFORM COMPRESSION

clear all
close all
clc
%% DATA
%%MECHANICAL PROPERTIES
E=71770; %Young's Modulus [MPa]
n=11.8; %Ramberg-Osgood coefficient
f02=168; %Yield stress [MPa]
fu=201.4; %Ultimate stress [MPa]
csi=3; %Plastic coefficient
%GEOMETRIC PROPERTIES
a=180; %Height of column [mm]
B1=40; % Width of plate 1 [mm]
B2=40; % Width of plate 2 [mm]
B3=B1;
B4=B2;
t1=2.197; % Thickness of plate 1 [mm]
t2=2.085; % Thickness of plate 2 [mm]
t3=1.99; % Thickness of plate 3 [mm]
t4=1.997; % Thickness of plate 4 [mm]
b1=B1-(t2+t4);
b2=B2-(t1+t3);
b3=b1;
b4=b2;
%% STRESS-STRAIN CURVE-SECANT AND TANGENT MODULI-POISSON'S RATIO
s=1:fu; %Stress vector
e =s./E+0.002*(s./f02).^n; %Strain vector
ne=0.33; %Elastic Poison's ratio
np=0.5;   %Plastic Poison's ratio
for i=2:length(e)
Es(i)=s(i)./e(i); %Secant Modulus vector
Et(i)=(s(i)-s(i-1))./(e(i)-e(i-1)); %Tangent Modulus vector
ni(i)=np-(Es(i)./E)*(np-ne); %Poisson ratios vector
end

%% DEFINITION OF CSI,ZETA,ALPHA
 z=1.35-(0.35*(B2/B1)/(0.60+B2/B1))-0.005*(B2/B1)^3; %ZETA FACTOR
a1=1+0.25*(1.7/((h/b1)^0.75-0.20)); %ALPHA FACTOR FOR PLATE 1 AND 3
a2=1+0.25*(1.7/((h/b2)^0.75-0.20)); %ALPHA FACTOR FOR PLATE 2 AND 4

if csi==1;
x=Et/E; % theory of tangent modulus
end
if csi==2;
x=Es/E; % theory of Secant modulus
end
if csi==3;
x=Es/E.*(1/3+(2/3)*sqrt(0.25+0.75*(Et./Es))); %Theory of Stowell
end
if csi==4;
x=Es/E.*(1/3+(2/3)*sqrt(0.5+0.5*(Et./Es))); %Theory of Li and Reid
end
if csi==5;
x=Es/E.*((n-8)/n+(8/n)*sqrt(Et./Es)); %Piluso&Pisapia
```

```
end
if csi==6;
x=Es/E.*((n-5)/n+(5/n)*sqrt(Et./Es)); % Piluso&Pisapia
end
m=(x*E)./(Es.*(1-ni.^2));

%% DEFINITION OF BETA
 b_1=17.54*(b1/t1)*sqrt(e./(m.*z.*a1)); %Beta plate 1
b_3=17.54*(b3/t3)*sqrt(e./(m.*z.*a1)); %Beta plate 2
b_2=17.54*(b2/t2)*sqrt(e./(m.*z.*a2)); %Beta plate 3
b_4=17.54*(b4/t4)*sqrt(e./(m.*z.*a2)); %Beta plate 4
%% DEFINITION OF RO FACTORS
C1=32;
C2=220;
%plate 1
for i=1:length(b_1);
   if b_1(i)<=0.5*(C1+sqrt(C1^2-4*C2));
      r_1(i)=1;
   else
      r_1(i)=C1/b_1(i)-C2/((b_1(i))^2);
   end
end
%plate 2
for i=1:length(b_2);
   if b_2(i)<=0.5*(C1+sqrt(C1^2-4*C2));
      r_2(i)=1;
   else
      r_2(i)=C1/b_2(i)-C2/((b_2(i))^2);
   end
end
%plate 3
for i=1:length(b_3);
   if b_3(i)<=0.5*(C1+sqrt(C1^2-4*C2));
      r_3(i)=1;
   else
      r_3(i)=C1/b_3(i)-C2/((b_3(i))^2);
   end
end
%plate 4
for i=1:length(b_4);
   if b_4(i)<=0.5*(C1+sqrt(C1^2-4*C2));
      r_4(i)=1;
   else
      r_4(i)=C1/b_4(i)-C2/((b_4(i))^2);
   end
end

%% N-e Curve
A1=(b1+t2)*t1*r_1;
A2=(b2+t3)*t2*r_2;
A3=(b3+t4)*t3*r_3;
A4=(b4+t1)*t4*r_4;
A=A1+A2+A3+A4;

N=A.*s;
 plot(e,N);
```

E.2. Script for Box section in Bending

```
%EFFECTIVE THICKNESS METHOD FOR NON-UNIFORM BENDING
clear all
close all
clc
%% DATA
%%MECHANICAL PROPERTIES
E=71770; %Young's Modulus [MPa]
n=11; %Ramberg-Osgood coefficient
f02=171; %Yield stress [MPa]
fu=201.36; %Ultimate stress [MPa]
BC='A'; %Buckling curve
csi=7; %plastic coefficient

%%GEOMETRIC PROPERTIES
B1=40.11; %section width
B2=40.18; %section height
L=650; %shear length
t1=2.09;
t2=2.085;
t3=t1;
t4=t2;

B3=B1;
B4=B2;
bf=B1-(t2+t4);
bw=B2-(t1+t3);
%% BUCKLING CURVE
if BC=='A';
C1=32;
C2=220;
end
if BC=='B';
C1=30.5;
C2=209;
end
if BC=='C'
C1=29;
C2=198;
end
%% SECTION CLASSIFICATION
e_0=sqrt(250/f02);

%Internal part
if BC=='A'
   beta1=11;
   beta2=16;
   beta3=22;
end
if BC=='B'
   beta1=12;
   beta2=16;
   beta3=20;
end
if BC=='C'
   beta1=13;
   beta2=16;
   beta3=18;
end
```

```
%flanges
betaf_1=(bf/t1)/e_0;
betaf_3=(bf/t3)/e_0;
if betaf_1<beta2
   S_f_1=1;
end
if betaf_1>=beta2&betaf_1<=beta3
   S_f_1=3;
end
if betaf_1>beta3
   S_f_1=4;
end

if betaf_3<beta2
   S_f_3=1;
end
if betaf_3>=beta2&betaf_3<=beta3
   S_f_3=3;
end
if betaf_3>beta3
   S_f_3=4;
end

%webs
betaw_2=0.4*(bw/t2)/e_0;
betaw_4=0.4*(bw/t4)/e_0;
if betaw_2<beta2
   S_w_2=1;
end
if betaw_2>=beta2&betaw_2<=beta3
   S_w_2=3;
end
if betaw_2>beta3
   S_w_2=4;
end

if betaw_4<beta2
   S_w_4=1;
end
if betaw_4>=beta2&betaw_4<=beta3
   S_w_4=3;
end
if betaw_4>beta3
   S_w_4=4;
end

S=max([S_f_1,S_f_3,S_w_2,S_w_4]); %class section
%% STRESS-STRAIN CURVE-SECANT AND TANGENT MODULI-POISSON'S RATIO
s=0:fu; %stress vector
e =s./E+0.002*(s./f02).^n; %strain vector
ne=0.33; %elastic Poison's ratio
np=0.5;   %plastic Poison's ratio
for i=2:length(e)
   Es(i)=s(i)./e(i); %Secant Modulus Vector
   Et(i)=(s(i)-s(i-1))./(e(i)-e(i-1)); %Tangent Modulus Vector
   ni(i)=np-(Es(i)./E)*(np-ne); %Poisson coefficient
   H(i)=1+(((1-2*ni(i)).^2)./4*(1-ni(i).^2)).*(1-Et(i)./Es(i));%Interactive elastic-plastic coefficients
   c1(i)=1-(((2-ni(i)).^2)./(4*H(i).*(1-ni(i).^2))).*(1-Et(i)./Es(i));
   c3(i)=1+(((1-2*ni(i)).*(2-ni(i)))./(4*H(i).*(1-ni(i).^2))).*(1-Et(i)./Es(i));
```

```
   c5(i)=1-(((1-2*ni(i)).^2)./(4*H(i).*(1-ni(i).^2))).*(1-Et(i)./Es(i));
end
%% DEFINITION OF PLASTIC COEFFICIENT "CSI"

if csi==1;
x=Et/E; % theory of tangent modulus
end
if csi==2;
x=Es/E; % theory of Secant modulus
end
if csi==3;
x=Es/E.*(1/3+(2/3)*sqrt(0.25+0.75*(Et./Es))); %Theory of Stowell
end
if csi==4;
x=Es/E.*(1/3+(2/3)*sqrt(0.5+0.5*(Et./Es))); %Theory of Li and Reid
end
if csi==5;
x=Es/E.*((n-8)/n+(8/n)*sqrt(Et./Es)); %Piluso&Pisapia
end
if csi==6;
x=Es/E.*(1-ne^2)./(1-ni.^2).*(0.58*sqrt(c1.*c5)+0.42*c3); % Piluso&Pisapia
end
m=(x*E)./(Es.*(1-ni.^2)); %Influence of plastic coefficient
%% DEFINITION OF ZETA AND ALPHA FACTORS
z=1.35-(0.35*(B2/B1)/(0.60+B2/B1))-0.005*(B2/B1)^3; %Influence of plate interaction
af=1+0.25*(1.7/((L/bf)^0.75-0.20)); %Influence of stress gradient along the length of flange plate
aw=1+0.25*(1.7/((L/bw)^0.75-0.20)); %Influence of stress gradient along the length of web plate
%% DEFINITION OF BETA
b_f=17.54*(bf/t3)*sqrt(e./(m.*z.*af)); %Beta for upper flange
%flange
for i=1:length(b_f);
   if b_f(i)<=0.5*(C1+sqrt(C1^2-4*C2));
      r_f(i)=1;
   else
      r_f(i)=C1/b_f(i)-C2/((b_f(i))^2);
   end
end

t_3=r_f*t3;

%webs
Aeff=B1*t1+bw*t2+bw*t4+bf*t3+t3*(t2+t4);
Sx=(B1*t1^2)/2+bf*t3*(B2-0.5*t3)+0.5*bw*B2*(t2+t4)+t3*(t2+t4)*(B2-0.5*t3);
Yg=Sx/Aeff;

for i=2:length(e);
   e_i(i)=Yg*e(i)/(B2-Yg);
   psi(i)=-e_i(i)/e(i);
   eta(i)=0.70+0.30*psi(i);
   b_2(i)=17.54*eta(i)*(bw/t2)*sqrt(e(i)/(m(i)*z*aw)); %Beta for web flange 2
   b_4(i)=17.54*eta(i)*(bw/t4)*sqrt(e(i)/(m(i)*z*aw)); %Beta for web flange 4
   if b_2(i)<=0.5*(C1+sqrt(C1^2-C2*(3+psi(i))))
      r_2(i)=1;
   else
      r_2(i)=C1/b_2(i)-C2*(3+psi(i))/(4*(b_2(i))^2);%coefficient "ro" 2
   end
   if b_4(i)<=0.5*(C1+sqrt(C1^2-C2*(3+psi(i))))
      r_4(i)=1;
   else
      r_4(i)=C1/b_4(i)-C2*(3+psi(i))/(4*(b_4(i))^2);%coefficient "ro" 4
```

```
    end
t_2(i)=r_2(i)*t2;
t_4(i)=r_4(i)*t4;
Aeff(i)=B1*t1+bw*t_2(i)+bw*t_4(i)+bf*t_3(i)+t3*(t2+t4);
Sx(i)=(B1*t1^2)/2+bf*t_3(i)*(B2-0.5*t3)+0.5*bw*B2*(t_2(i)+t_4(i))+t3*(t2+t4)*(B2-0.5*t3);
Yg(i)=Sx(i)/Aeff(i);
end

Ieff=(B1*(t1^3))/12+B1*t1.*(Yg-0.5*t1).^2+(t_2+t_4).*((bw^3)/12+bw.*(Yg-
0.5.*bw).^2)+(bf.*(t_3.^3))/12+bf.*t_3.*(B2-Yg-0.5.*t_3).^2+(t2+t4).*((t3^3)/12+t3.*(B2-Yg-0.50*t3).^2);
chi=e./(B2-Yg);

M02=f02*(Ieff(2)/Yg(2)); %Bending moment correponding to f0.2
chi02=M02/(E*Ieff(2));   %curvature corresponding to M0.2
%% MOMENT-CURVATURE

% Section 1-2-3
% web in tension_compression
nw=100;
for i=1:length(e)
   for j=1:nw
      chi_s(i)=e(i)/(B2-Yg(i));
      bw_s(i)=B2-t1-Yg(i);
      br_sup(i,j)=bw_s(i)-(bw_s(i)/nw)*j+bw_s(i)/(2*nw);
      e_sup(i,j)=chi_s(i)*(bw_s(i)-(bw_s(i)/nw)*j+bw_s(i)/(2*nw));
   end
end
e_sup=e_sup';
br_sup=br_sup'
for i=1:length(e)
   for j=1:nw
      bw_i(i)=Yg(i)-t1;
      br_inf(i,j)=bw_i(i)-(bw_i(i)/nw)*j+bw_i(i)/(2*nw);
      e_inf(i,j)=chi_s(i)*(bw_i(i)-(bw_i(i)/nw)*j+bw_i(i)/(2*nw));
   end
end
e_inf=e_inf';
br_inf=br_inf';
for i=1:nw
   for j=1:length(e)
      if e_sup(i,j)<f02/E
         s_sup(i,j)=E*e_sup(i,j);
      else
         s_sup(i,j)=(((e_sup(i,j)-f02/E)/0.002)^(1/n))*f02;
      end
   end
end
for i=1:nw
   for j=1:length(e)
      if e_inf(i,j)<f02/E
         s_inf(i,j)=-E*e_inf(i,j);
      else
         s_inf(i,j)=-(((e_inf(i,j)-f02/E)/0.002)^(1/n))*f02;
      end
   end
end

m_sup=t_2.*(bw_s/nw).*s_sup.*br_sup+t_4.*(bw_s/nw).*s_sup.*br_sup;

m_inf=t_2.*(bw_i/nw).*s_inf.*br_inf+t_4.*(bw_i/nw).*s_inf.*br_inf;
```

```
M_web=sum(m_sup-m_inf);
%flanges

%flange 3 in compression

B_3=(B2-Yg-0.50*t3);
M_f_s=t_3*(B3-t2-t4).*s.*B_3+t2*t3.*s.*B_3+t4*t3.*s.*B_3;

%flange 1 in tension
nf=100;
for j=1:nf;
for i=1:length(e)
  e_1(i,j)=(e_i(i)/Yg(i))*(Yg(i)-(t1/nf)*j+0.50*(t1/nf));
  B_1(i,j)=Yg(i)-0.50*t1;
end
end
e_1=e_1';
B_1=B_1';

for i=1:nf
   for j=1:length(e)
      if e_1(i,j)<f02/E
         s_1(i,j)=E*e_1(i,j);
      else
         s_1(i,j)=(((e_1(i,j)-f02/E)/0.002)^(1/n))*f02;
      end
   end
end

m_1=B1*(t1/nf).*s_1.*B_1;

M_f_i=sum(m_1);

M=M_f_s+M_f_i+M_web;
end

Mmax=max(M)/10^6 % MAXIMUM BENDING MOMENT
chi_max=chi(find(M==max(M)));%CURVATURE CORRESPONDING TO MAXIMUM BENDING MOMENT
%title('Moment-Curvature')
%hold on


%% ULTIMATE ROTATION AND ROTATION CORRESPONDING TO MAXIMUM BENDING MOMENT
L_u=(L/length(chi))*(1:length(chi));
CHI_0=chi(1:find(chi==chi_max));
L_0=(L/length(CHI_0))*(1:length(CHI_0));

teta_0=sum(CHI_0*(L/length(CHI_0)));
teta_u=sum(chi*(L/length(chi)));

figure;
plot(chi/chi02,(M/M02)/10^6);

figure;
plot(L_0,-CHI_0,'b');
hold on
plot(L_u,-chi,'r');
```

CHAPTER 7
CONCLUSIONS

The present research work was addressed to the study of the influence of the local buckling phenomena on the behaviour of aluminium members in compression or in bending. So that, starting from the main results on the theories of the plate stability in the elastic, the theory of plastic buckling has been developed according to the J_2 deformation theory of plasticity to define the plate differential equation by introducing the variability of Poisson's ratio as a function of the stress level. Subsequently, the stub column tests and the three point bending tests, carried out on the same SHS aluminium members, have been presented.

Starting from the theoretical and experimental results, previously described, different methodologies have been proposed to evaluate the ultimate behaviour of aluminium members under uniform compression and the beams under moment gradient.

In particular, the plate differential equation at the onset of buckling has been integrated referring to plates under uniform compression and applied to analyse the interactive buckling occurring in the case of box sections, like SHS and RHS, and of H-shaped sections. The boundary conditions accounting for plate elements interaction have been properly derived and the buckling criterion has been defined by imposing the conditions assuring a non-trivial solution of the relevant equation system, so that a fully theoretical approach has been proposed to evaluate the behaviour of columns under uniform compression.

The non-linear behaviour of aluminium alloy beams subject to non-uniform bending has been investigated by means of a finite element model including both geometrical and mechanical non-linearity and initial geometrical imperfections. In particular, a wide parametric analysis has been carried out by varying the non-dimensional geometrical parameters describing the structural scheme and the accuracy of the finite element model, carried out using ABAQUS software. Moreover, in order to evaluate the influence of the strain-hardening, the parametric analysis has been performed with reference to four different alloys: EN-AW6082 temper T4 and T6, EN-AW6063 temper T5 and EN-AW6061 temper T6. The numerical results derived by finite element simulations have allowed the development of mathematical formulations for estimating the non-dimensional ultimate flexural resistance and the rotational capability of box-shaped and H-shaped beams.

Finally, the effective thickness approach, currently adopted in the Eurocode 9 for evaluating the ultimate resistance of the fourth-class sections affected by the local buckling, has been extended accounting for the mechanical non-linearity of aluminium material and the interaction of the plate elements constituting the cross sections. In particular, a simplified procedure under displacement control has been performed to determine the inelastic response of the box-shaped sections and H-shaped sections in compression or in bending.

To evaluate the accuracy of the previous methodologies, the experimental results presented in this work and provided in the technical literature have been compared with those obtained by the theoretical and empirical procedures. The comparison of these methodologies is summarised in Table 7.1 and Table 7.2. In the case of members under compression, both the theoretical approach (DTP) and the effective thickness method (ETM) accurately estimate the maximum compressive load. Instead, as regard the estimated of the normalised deformation, the ETM method represents a very conservative approach, although simpler to apply than the DTP method.

As for the beams under non-uniform bending, the empirical formulas provide the results closer to the experimental one in comparison to the effective thickness method and their applications are very simple. However, the mathematical formulas can not be applied to evaluate the behaviour of aluminium beams in the elastic region and, generally, they have to be applied according to specific ranges of validity of the non-dimensional parameters, previously mentioned. The prediction of the rotational capacity, corresponding to the maximum bending moment, is more conservative than the values obtained by the three point bending tests. Furthermore, high values of standard deviations σ suggest the scattering and thus the rotational predictions are considerate of low reliability in relation to the low number of cases analysed.

For the sake of completeness, the comparison has been carried out also with the values of the resistance obtained by the Eurocode 9. In particular, the maximum compressive strength is computed according to Section 6.2.4 of EN 1999-1-1, as depicted in Eq. (1.1), while the maximum flexural strength is evaluated according to Section 6.2.5 of EN 1999-1-1, as provided in Eqns. (1.2) and (1.3). The safety coefficient γ_{M2} is assumed equal to 1.00 for both cases, because the estimation is carried out from the point of view of maximum resistance prediction not from that of the safety control as reported in the design code provisions. The values computed according to Eurocode 9 are, respectively, reported in Annex A and in Annex B. From the comparison of the results, it is evident that the ultimate strength values computed according to the design code approach are more conservative than others, including the experimental ones.

Moreover, it is worth to underline that the mathematical relationships and the extension of effective thickness approach are currently adopted in the new proposed informative Annex L of EN1999-1-1.

They have been proposed within the framework of the activities of the project teams of CEN/TC250/SC9 encharged of the revision of Eurocode 9.

Finally, the following future developments can be suggested. The fully theoretical procedure, developed for the box-shaped and H-shaped sections, could easily be extended to the other aluminium cross-section (channel section, angle section stiffened rectangular section, ecc).

In reference to the study of the ultimate behaviour of beams in bending, there is still a substantial gap of knowledge, especially, regarding the H-shaped sections. So that, an extensive experimental campaign could be carried out on the H-shaped beams, by varying the width-to-thickness ratios, the shear length and the aluminium alloy. Moreover, for extending the validation of the proposed mathematical formula, the parametric analysis, developed in Chapter 5, could be performed on the other different aluminium alloys possibly belonging to the 5000 and 7000 series. Another aspect that might be worth investigating is related to evaluate accurately the maximum rotational capacity. In fact, the estimation by means of Eq. (6.26) provided very different values respect to the experimental results and for this reason, they have not been depicted. One reason could be related to the inaccurate assessment of the length of the plastic hinge. So that, a future study could be devoted to improving the evaluation of the plastic length through the experimental tests and finite element analysis.

Table 7.1. Comparison between the deformation theoretical procedure (DTP) and the effective thickness method (ETM).

SECTION	**Design Code EN 1999-1-1**	**Deformation Theoretical Procedure (DTP)**		**Effective Thickness Method (ETM)**	
SHS, RHS	$\frac{N_{u.EC9}}{N_{u.exp}}$	$\frac{N_{u.DTP}}{N_{u.exp}}$	$\frac{\bar{\varepsilon}_{u.DTP}}{\bar{\varepsilon}_{u.exp}}$	$\frac{N_{u.ETM}}{N_{u.exp}}$	$\frac{\bar{\varepsilon}_{u.ETM}}{\bar{\varepsilon}_{u.exp}}$
Mean [μ]	0.93	1.02	0.99	0.96	0.81
Standard deviation [σ]	0.09	0.09	0.18	0.07	0.22

SECTION	**Design Code EN 1999-1-1**	**Deformation Theoretical Procedure (DTP)**		**Effective Thickness Method (ETM)**	
I, H	$\frac{N_{u.EC9}}{N_{u.exp}}$	$\frac{N_{u.DTP}}{N_{u.exp}}$	$\frac{\bar{\varepsilon}_{u.DTP}}{\bar{\varepsilon}_{u.exp}}$	$\frac{N_{u.ETM}}{N_{u.exp}}$	$\frac{\bar{\varepsilon}_{u.ETM}}{\bar{\varepsilon}_{u.exp}}$
Mean [μ]	0.90	1.01	0.97	0.93	0.97
Standard deviation [σ]	0.14	0.08	0.17	0.11	0.28

Table 7.2. Comparison between the empirical regressions (ER) and the effective thickness method (ETM).

SECTION	**Design Code EN 1999-1-1**	**Empirical Regressions (ER)**		**Effective Thickness Method (ETM)**	
SHS, RHS, I, H	$\frac{M_{u.EC9}}{M_{u.exp}}$	$\frac{M_{u.ER}}{M_{u.exp}}$	$\frac{\bar{\theta}_{u.ER}}{\bar{\theta}_{u.exp}}$	$\frac{M_{u.ETM}}{M_{u.exp}}$	$\frac{\bar{\theta}_{u.ETM}}{\bar{\theta}_{u.exp}}$
Mean [μ]	0.91	1.02	0.92	0.97	0.90
Standard deviation [σ]	0.06	0.14	0.15	0.15	0.12

ANNEX A

A.1. Geometrical and Mechanical Properties of Experimental Tests

In this section, the main experimental properties of the stub column test, presented in the technical literature, are reported according to the following geometric schemes:

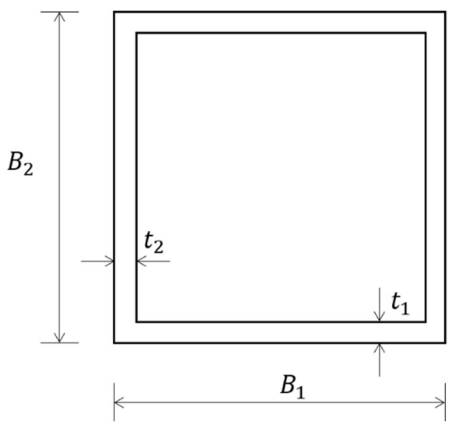

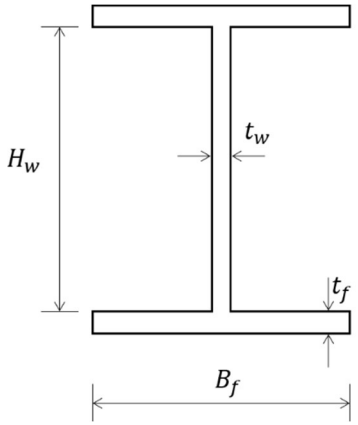

Table A.1. Geometrical and mechanical properties of tested hollow sections provided in Chapter 3.

Specimen		***Alloy***	B_1 [mm]	t_1 [mm]	B_2 [mm]	t_2 [mm]	a [mm]	A [mm^2]	E [MPa]	$f_{0.2}$ [MPa]	f_u [MPa]	n [-]
SHS40	A	6060 T6	40.11	2.097	40.18	2.038	120.05	314.90	71770	176.00	201.36	11.85
	B	6060 T6	40.11	2.097	40.18	2.038	120.12	314.90	71770	176.00	201.36	11.85
	C	6061 T6	40.11	2.097	40.18	2.038	130.43	314.90	71770	176.00	201.36	11.85
SHS60	A	6060 T6	60.31	2.000	60.40	2.123	181.10	480.71	66219	225.07	249.32	13.45
	B	6060 T6	60.31	2.000	60.40	2.123	180.80	480.71	66219	225.07	249.32	13.45
SHS80	A	6060 T6	80.06	1.950	80.17	1.940	240.12	608.16	68539	225.80	252.14	8.49
	B	6060 T6	80.06	1.950	80.17	1.940	240.32	608.16	68539	225.80	252.14	8.49
SHS100	A	6060 T6	100.30	2.180	100.30	2.200	300.10	859.44	69558	168.15	201.80	10.43
	B	6060 T6	100.30	2.180	100.30	2.200	299.00	859.44	69558	168.15	201.80	10.43

Table A.2. Geometrical and mechanical properties of tested hollow sections provided by Faella et al [4.12].

Specimen		***Alloy***	B_1 [mm]	t_1 [mm]	B_2 [mm]	t_2 [mm]	a [mm]	A [mm^2]	E [MPa]	$f_{0.2}$ [MPa]	f_u [MPa]	n [-]
SHS1	A	6060 T6	15.00	1.910	15.00	1.910	44.50	100.01	67520	214.4	241.3	22.4
	B	6060 T6	15.00	1.910	15.00	1.910	46.00	100.01	67520	214.4	241.3	22.4
SHS2	A	6060 T6	40.10	4.100	40.05	4.075	115.70	588.40	72265	223.6	244.3	19.1
	B	6060 T6	40.10	4.100	40.05	4.075	120.00	588.40	72265	223.6	244.3	19.1
SHS3	A	6060 T6	50.40	3.100	50.35	3.100	149.40	586.21	64863	222.5	244.8	28.9
	B	6060 T6	50.40	3.100	50.35	3.100	149.40	586.21	64863	222.5	244.8	28.9
SHS4	A	6060 T6	50.40	4.275	50.35	4.250	149.40	786.22	64090	202.6	225.2	30.6
	B	6060 T6	50.40	4.275	50.35	4.250	149.30	786.22	64090	202.6	225.2	30.6
SHS5	A	6060 T6	70.15	4.150	70.10	4.100	209.50	1089.01	70211	175.7	202.9	20.6
	B	6060 T6	70.15	4.150	70.10	4.100	209.50	1089.01	70211	175.7	202.9	20.6
SHS6	A	6060 T6	80.40	4.240	80.20	4.275	239.00	1295.00	71733	194.2	220.3	26.8
	B	6060 T6	80.40	4.240	80.20	4.275	239.00	1295.00	71733	194.2	220.3	26.8
SHS7	A	6060 T6	100.00	3.950	99.80	3.900	296.00	1506.82	70757	209.8	228.3	28.4

Specimen		*Alloy*	B_1 [mm]	t_1 [mm]	B_2 [mm]	t_2 [mm]	a [mm]	A [mm^2]	E [MPa]	$f_{0.2}$ [MPa]	f_u [MPa]	n [-]
SHS7	B	6060 T6	100.00	3.950	99.80	3.900	299.00	1506.82	70757	209.8	228.3	28.4
SHS8	A	6060 T6	60.40	2.275	60.35	2.250	179.00	525.92	71963	158.2	186.6	12
	B	6060 T6	60.40	2.275	60.35	2.250	179.00	525.92	71963	158.2	186.6	12
SHS9	A	6060 T6	80.40	2.100	80.20	2.050	239.00	649.28	65125	186.7	203.9	27.5
	B	6060 T6	80.40	2.100	80.20	2.050	239.00	649.28	65125	186.7	203.9	27.5
SHS10	A	6060 T6	100.30	5.975	99.90	6.050	303.00	2262.78	65321	293.5	323.7	26.9
	B	6060 T6	100.30	5.975	99.90	6.050	303.00	2262.78	65321	293.5	323.7	26.9
SHS11	A	6060 T6	150.20	4.975	150.10	4.850	437.00	2853.95	75250	208.9	252.1	11.3
	B	6060 T6	150.20	4.975	150.10	4.850	451.00	2853.95	75250	208.9	252.1	11.3
SHS12	A	6082 T6	149.90	5.100	149.90	5.125	451.50	2960.91	68368	258.4	300.1	13.4
	B	6082 T6	149.90	5.100	149.90	5.125	452.00	2960.91	68368	258.4	300.1	13.4
RHS1	A	6060 T6	34.00	3.000	20.00	3.000	46.80	288.00	62814	218.7	250.9	23.6
	B	6060 T6	34.00	3.000	20.00	3.000	46.80	288.00	62814	218.7	250.9	23.6
RHS2	A	6060 T6	39.90	4.000	29.90	4.000	73.60	494.40	69750	202	214.3	31.1
	B	6060 T6	39.90	4.000	29.90	4.000	120.40	494.40	69750	202	214.3	31.1
RHS3	A	6060 T6	50.10	4.050	20.00	4.150	52.30	504.58	68439	210.7	233.3	26.5
	B	6060 T6	50.10	4.050	20.00	4.150	52.30	504.58	68439	210.7	233.3	26.5
RHS4	A	6060 T6	50.00	3.025	30.25	3.075	80.70	451.33	70873	217.4	242.5	19.5
	B	6060 T6	50.00	3.025	30.25	3.075	149.00	451.33	70873	217.4	242.5	19.5
RHS5	A	6060 T6	50.25	2.700	40.30	2.700	104.50	459.81	69695	221.6	244.5	48.4
	B	6060 T6	50.00	2.700	40.00	2.700	211.00	456.84	69695	221.6	244.5	48.4
RHS6	A	6060 T6	60.20	3.000	34.10	3.000	88.80	529.80	77760	212.5	235	18.6
	B	6060 T6	60.20	3.000	34.10	3.000	179.00	529.80	77760	212.5	235	18.6
RHS7	A	6060 T6	60.20	2.550	40.10	2.550	179.50	485.52	62761	234.6	258.9	31.3
	B	6060 T6	60.20	2.550	40.10	2.550	176.00	485.52	62761	234.6	258.9	31.3
RHS8	A	6060 T6	80.25	4.000	40.10	3.900	234.50	892.38	63508	222	258.6	26.6
	B	6060 T6	80.25	4.000	40.10	3.900	233.50	892.38	63508	222	258.6	26.6
RHS9	A	6060 T6	99.80	4.000	40.10	3.950	236.00	1051.99	70203	216.6	242.2	45.2
	B	6060 T6	99.80	4.000	40.10	3.950	236.00	1051.99	70203	216.6	242.2	45.2
RHS10	A	6060 T6	120.30	4.150	50.60	4.275	361.00	1360.16	68945	215.8	227.3	24.7
	B	6060 T6	120.30	4.150	50.60	4.275	361.00	1360.16	68945	215.8	227.3	24.7
RHS11	A	6060 T6	150.50	4.100	40.80	4.050	225.00	1498.16	68796	224.6	255.5	13.5
	B	6060 T6	150.50	4.100	40.80	4.050	225.00	1498.16	68796	224.6	255.5	13.5
RHS12	A	6060 T6	181.20	4.200	40.80	4.100	242.00	1787.76	74543	212.3	246.8	18.7
	B	6060 T6	181.20	4.200	40.80	4.100	237.00	1787.76	74543	212.3	246.8	18.7
RHS13	A	6060 T6	100.10	3.950	50.25	3.950	299.00	1125.36	68504	216	236.6	33.3
	B	6060 T6	100.10	3.950	50.25	3.950	299.00	1125.36	68504	216	236.6	33.3
RHS14	A	6060	60.10	2.150	40.10	2.050	181.00	405.21	62446	219.6	242.8	34.7
	B	6060	60.10	2.150	40.10	2.050	178.00	405.21	62446	219.6	242.8	34.7
	C	6060	60.10	2.150	40.10	2.050	176.00	405.21	62446	219.6	242.8	34.7
RHS15	A	6060	79.90	3.950	40.00	3.900	234.50	881.59	69329	188.9	212.4	26.8
	B	6060	79.90	3.950	40.00	3.900	235.50	881.59	69329	188.9	212.4	26.8
	C	6060	79.90	3.950	40.00	3.900	233.90	881.59	69329	188.9	212.4	26.8
RHS16	A	6060	80.20	2.075	40.25	2.075	239.00	482.65	60000	225.4	260.5	53
	B	6060	80.20	2.075	40.25	2.075	238.00	482.65	60000	225.4	260.5	53
RHS17	A	6060 T6	59.90	1.950	40.00	2.000	180.00	378.01	69263	234.3	253.3	37.5
	B	6060 T6	59.90	1.950	40.00	2.000	178.00	378.01	69263	234.3	253.3	37.5

Specimen		Alloy	B_1 [mm]	t_1 [mm]	B_2 [mm]	t_2 [mm]	a [mm]	A [mm^2]	E [MPa]	$f_{0.2}$ [MPa]	f_u [MPa]	n [-]
RHS18	A	6082	100.30	2.300	25.70	2.300	125.00	558.44	68037	264.8	285	27.8
	B	6082	100.30	2.300	25.70	2.300	127.00	558.44	68037	264.8	285	27.8
RHS19	A	6060	119.90	2.700	61.00	2.600	359.00	936.58	69318	209.7	229.4	33.7
	B	6060	119.90	2.700	61.00	2.600	355.00	936.58	69318	209.7	229.4	33.7
RHS20	A	6060	200.00	4.850	99.90	4.900	601.00	2823.96	65234	235.2	282.8	14.6
	B	6060	200.00	4.850	99.90	4.900	601.00	2823.96	65234	235.2	282.8	14.6
RHS21	A	6082	47.00	2.875	40.00	2.875	140.00	467.19	67488	251.3	276.9	32.9
	B	6082	47.00	2.875	40.00	2.875	140.00	467.19	67488	251.3	276.9	32.9
RHS22	A	6082 T6	179.50	4.575	70.00	4.650	540.00	2208.33	72038	320	353.4	83.7
	B	6082 T6	179.50	4.575	70.00	4.650	540.00	2208.33	72038	320	353.4	83.7
RHS23	A	6082 TF	153.00	4.850	71.60	6.850	411.00	2309.00	71850	309.2	329.9	90.7
	B	6082 TF	153.00	4.850	71.60	6.850	411.00	2309.00	71850	309.2	329.9	90.7
RHS24	A	6082 T6	200.50	15.300	179.20	9.225	531.20	8660.00	71360	340	362.1	77.4
	B	6082 T6	200.50	15.300	179.20	9.225	535.00	8660.00	71360	340	362.1	77.4
RHS25	A	6082 TF	120.50	4.750	100.35	6.775	361.00	2268.00	68841	323	342.8	30.3
	B	6082 TF	120.50	4.750	100.35	6.775	361.00	2268.00	68841	323	342.8	30.3
RHS26	A	6082	201.00	6.100	181.50	6.100	601.00	4373.00	71601	185	220	84.4
	B	6082	201.00	6.100	181.50	6.100	601.00	4373.00	71601	185	220	84.4

Table A.3. Geometrical and mechanical properties of tested hollow sections provided by Su et al [4.8].

Specimen		Alloy	B_1 [mm]	t_1 [mm]	B_2 [mm]	t_2 [mm]	a [mm]	A [mm^2]	E [MPa]	$f_{0.2}$ [MPa]	f_u [MPa]	n [-]
H64x64x3	A	6061 T6	63.90	2.810	63.90	2.810	191.10	686.65	66000	234	248	12
	B	6061 T6	63.90	2.850	63.90	2.850	191.50	695.97	66000	234	248	12
H70x55x4.2	A	6061 T6	69.90	4.080	54.90	4.080	209.80	951.78	65000	193	207	22
	B	6061 T6	69.90	4.090	54.90	4.090	209.90	953.95	65000	193	207	22
H95x50x10.5	A	6061 T6	94.80	10.360	49.70	10.360	284.90	2564.72	71000	229	242	11
H120x70x10.5	A	6061 T6	119.90	10.390	69.90	10.390	360.00	3512.24	69000	226	238	10
H120x120x9	A	6061 T6	120.00	8.910	120.00	8.910	360.20	3959.25	65000	225	234	13
N95x50x10.5	A	6063 T5	94.90	10.370	49.70	10.370	285.20	2568.86	69000	179	220	10
N120x70x10.5	A	6063 T5	119.90	10.450	69.80	10.450	360.90	3527.92	71000	139	194	9
N120x120x9	A	6063 T5	120.00	8.920	120.00	8.920	361.30	3963.33	69000	181	228	9

Table A.4. Geometrical and mechanical properties of tested H-shaped sections provided by Heimerl and Niles [4.13].

Specimen		Alloy	B_f [mm]	t_f [mm]	H_w [mm]	t_w [mm]	a [mm]	A [mm]	E [MPa]	$f_{0.2}$ [MPa]	f_u [MPa]	n [-]
H1	A	2014 T6	41.15	3.277	47.45	3.18	163.58	420.30	72395	370	415	30
	B	2014 T6	41.15	3.226	47.35	3.18	165.61	415.79	72395	370	415	30
	C	2014 T6	41.15	3.226	47.09	3.20	165.10	416.18	72395	370	415	30
H2	A	2014 T6	45.72	3.277	47.70	3.15	192.53	449.85	72395	370	415	30
	B	2014 T6	45.72	3.277	47.70	3.15	193.04	449.85	72395	370	415	30
	C	2014 T6	45.72	3.277	47.70	3.15	190.50	449.85	72395	370	415	30
H3	A	2014 T6	49.78	3.277	47.70	3.15	221.49	476.48	72395	370	415	30
	B	2014 T6	49.78	3.302	47.75	3.15	220.98	479.17	72395	370	415	30
	C	2014 T6	49.78	3.251	47.65	3.15	226.57	473.80	72395	370	415	30
H4	A	2014 T6	53.85	3.277	47.45	3.15	230.89	502.32	72395	370	415	30
	B	2014 T6	53.85	3.277	47.70	3.15	231.14	503.12	72395	370	415	30
	C	2014 T6	53.85	3.302	47.75	3.15	230.63	506.01	72395	370	415	30
H5	A	2014 T6	57.91	3.302	47.75	3.15	238.25	532.85	72395	370	415	30

Specimen		Alloy	B_f [mm]	t_f [mm]	H_w [mm]	t_w [mm]	a [mm]	A [mm]	E [MPa]	$f_{0.2}$ [MPa]	f_u [MPa]	n [-]
H5	B	2014 T6	57.91	3.277	47.70	3.15	239.78	529.75	72395	370	415	30
H6	A	2014 T6	61.47	3.302	47.75	3.18	244.35	557.55	72395	370	415	30
	B	2014 T6	61.47	3.302	48.01	3.18	245.87	558.35	72395	370	415	30
	C	2014 T6	61.47	3.277	47.96	3.15	245.36	553.85	72395	370	415	30
H7	A	2014 T6	68.07	3.30	47.50	3.15	257.56	599.15	72395	370	415	30
	B	2014 T6	68.07	3.30	47.75	3.18	256.54	601.16	72395	370	415	30
	C	2014 T6	68.07	3.30	47.75	3.15	258.06	599.95	72395	370	415	30
H8	A	2014 T6	45.72	3.18	62.99	3.07	226.57	483.92	72395	370	415	30
	B	2014 T6	45.72	3.18	63.25	3.05	227.08	483.10	72395	370	415	30
	C	2014 T6	45.72	3.15	63.20	3.05	226.06	480.62	72395	370	415	30
H9	A	2014 T6	51.31	3.18	63.25	3.05	274.32	518.58	72395	370	415	30
	B	2014 T6	51.31	3.18	63.25	3.05	256.03	518.58	72395	370	415	30
	C	2014 T6	51.31	3.15	62.94	3.07	255.52	516.64	72395	370	415	30
H10	A	2014 T6	57.40	3.18	63.25	3.05	285.24	557.29	72395	370	415	30
	B	2014 T6	57.40	3.18	63.25	3.05	286.00	557.29	72395	370	415	30
	C	2014 T6	66.04	3.18	63.25	3.05	286.00	612.13	72395	370	415	30
H11	A	2014 T6	68.58	3.15	63.45	3.05	307.85	625.39	72395	370	415	30
	B	2014 T6	68.58	3.15	63.20	3.05	308.36	624.62	72395	370	415	30
	C	2014 T6	68.58	3.15	63.20	3.05	309.12	624.62	72395	370	415	30
H12	A	2014 T6	80.26	3.18	62.99	3.07	328.68	703.28	72395	370	415	30
	B	2014 T6	80.26	3.18	63.25	3.05	329.18	702.45	72395	370	415	30
	C	2014 T6	80.26	3.18	62.99	3.07	328.68	703.28	72395	370	415	30
H13	A	2014 T6	92.96	3.18	62.99	3.07	357.63	783.92	72395	370	415	30
	B	2014 T6	92.96	3.18	62.99	3.07	360.68	783.92	72395	370	415	30
H14	A	2014 T6	55.88	3.07	75.49	3.00	319.02	569.74	72395	370	415	30
	B	2014 T6	55.88	3.05	75.44	3.00	318.52	566.75	72395	370	415	30
	C	2014 T6	55.88	3.05	75.69	2.97	318.52	565.59	72395	370	415	30
H15	A	2014 T6	62.99	3.05	75.44	3.02	334.26	612.02	72395	370	415	30
	B	2014 T6	62.99	3.07	75.23	3.02	332.23	614.60	72395	370	415	30
	C	2014 T6	62.99	3.07	75.49	3.02	335.79	615.37	72395	370	415	30
H16	A	2014 T6	69.60	3.05	75.69	3.00	346.46	651.12	72395	370	415	30
	B	2014 T6	69.60	3.05	75.69	3.00	345.19	651.12	72395	370	415	30
	C	2014 T6	69.60	3.05	75.69	3.00	352.04	651.12	72395	370	415	30
H17	A	2014 T6	84.33	3.07	75.74	3.02	373.38	747.29	72395	370	415	30
	B	2014 T6	83.82	3.07	75.74	3.00	374.90	742.24	72395	370	415	30

Table A.5. Geometrical and mechanical properties of tested H-shaped sections provided by Heimerl and Roy [4.14].

Specimen		Alloy	B_f [mm]	t_f [mm]	H_w [mm]	t_w [mm]	a [mm]	A [mm]	E [MPa]	$f_{0.2}$ [MPa]	f_u [MPa]	n [-]
H1	A	7075 T6	41.66	3.20	47.29	3.05	154.94	410.79	72395	460	530	24
	B	7075 T6	40.64	3.20	47.29	3.05	154.94	404.28	72395	460	530	24
	C	7075 T6	41.66	3.18	47.50	3.05	154.94	409.29	72395	460	530	24
H2	A	7075 T6	45.72	3.20	47.29	3.05	153.67	436.80	72395	460	530	24
	B	7075 T6	45.72	3.20	47.55	3.05	154.18	437.57	72395	460	530	24
	C	7075 T6	49.78	3.20	47.55	3.05	154.94	463.59	72395	460	530	24
H3	B	7075 T6	50.29	3.20	47.55	3.05	154.43	466.84	72395	460	530	24
H4	A	7075 T6	50.29	3.07	47.29	3.05	222.25	453.29	72395	460	530	24

Specimen		Alloy	B_f [mm]	t_f [mm]	H_w [mm]	t_w [mm]	a [mm]	A [mm]	E [MPa]	$f_{0.2}$ [MPa]	f_u [MPa]	n [-]
H4	B	7075 T6	50.29	3.07	47.29	3.05	222.25	453.29	72395	460	530	24
	C	7075 T6	50.29	3.07	47.29	3.05	222.25	453.29	72395	460	530	24
H5	A	7075 T6	52.32	3.20	47.55	3.05	164.85	479.84	72395	460	530	24
	B	7075 T6	52.32	3.20	47.55	3.05	165.61	479.84	72395	460	530	24
	C	7075 T6	52.32	3.20	47.55	3.05	164.08	479.84	72395	460	530	24
H6	A	7075 T6	54.86	3.07	47.29	3.05	222.25	481.39	72395	460	530	24
	B	7075 T6	55.37	3.10	47.35	3.05	222.50	487.48	72395	460	530	24
	C	7075 T6	54.86	3.07	47.29	3.05	222.50	481.39	72395	460	530	24
H7	A	7075 T6	58.93	3.20	47.55	3.05	176.02	522.12	72395	460	530	24
	B	7075 T6	59.44	3.20	47.55	3.05	177.80	525.37	72395	460	530	24
	C	7075 T6	59.94	3.20	47.55	3.05	178.05	528.62	72395	460	530	24
H8	A	7075 T6	58.93	3.20	47.29	3.05	198.63	521.34	72395	460	530	24
	B	7075 T6	59.44	3.20	47.55	3.05	198.12	525.37	72395	460	530	24
H9	A	7075 T6	59.44	3.07	47.29	3.05	256.54	509.50	72395	460	530	24
	B	7075 T6	59.44	3.07	47.29	3.05	256.54	509.50	72395	460	530	24
	C	7075T6	59.44	3.07	47.29	3.05	256.54	509.50	72395	460	530	24
H10	A	7075 T6	63.50	3.20	47.55	3.05	198.63	551.38	72395	460	530	24
H11	A	7075 T6	68.07	3.23	47.35	3.05	221.49	583.48	72395	460	530	24
	B	7075 T6	68.07	3.23	47.35	3.05	221.23	583.48	72395	460	530	24
	C	7075 T6	68.07	3.23	47.35	3.05	221.23	583.48	72395	460	530	24
H12	A	7075 T6	68.07	3.10	47.35	3.07	273.05	567.39	72395	460	530	24
	B	7075 T6	68.07	3.07	47.29	3.05	274.32	562.58	72395	460	530	24
	C	7075 T6	68.07	3.10	47.35	3.05	274.32	566.19	72395	460	530	24
H13	A	7075 T6	64.01	3.12	62.89	3.05	295.15	591.64	72395	460	530	24
	B	7075 T6	64.01	3.12	62.89	3.02	294.89	590.04	72395	460	530	24
	C	7075 T6	64.01	3.12	62.89	3.02	294.64	590.04	72395	460	530	24
H14	A	7075 T6	69.09	3.12	63.14	3.02	319.79	622.55	72395	460	530	24
	B	7075 T6	69.60	3.12	62.89	3.02	320.80	624.96	72395	460	530	24
	C	7075 T6	69.09	3.12	62.89	3.02	320.80	621.78	72395	460	530	24
H15	A	7075 T6	72.64	3.12	63.14	3.02	337.82	644.77	72395	460	530	24
	B	7075 T6	72.64	3.12	62.89	3.02	337.82	644.00	72395	460	530	24
	C	7075 T6	72.64	3.12	62.89	3.02	338.07	644.00	72395	460	530	24
H16	A	7075 T6	81.28	3.12	62.89	3.02	351.03	697.96	72395	460	530	24
	B	7075 T6	80.77	3.12	62.89	3.02	351.28	694.79	72395	460	530	24
	C	7075 T6	80.77	3.12	62.89	3.02	350.77	694.79	72395	460	530	24
H18	A	7075 T6	58.93	3.07	75.74	3.12	291.85	598.85	72395	460	530	24
	B	7075 T6	62.99	3.07	76.25	3.12	291.85	625.42	72395	460	530	24
H19	A	7075 T6	62.99	3.073	75.74	3.10	329.69	621.91	72395	460	530	24
	B	7075 T6	62.99	3.073	75.49	3.12	330.20	623.04	72395	460	530	24
	C	7075 T6	61.98	3.048	75.44	3.10	330.45	611.57	72395	460	530	24
H20	A	7075 T6	69.60	3.023	75.64	3.10	365.76	655.12	72395	460	530	24
	B	7075 T6	69.60	3.048	75.69	3.10	366.01	658.81	72395	460	530	24
	C	7075 T6	70.10	3.048	75.69	3.10	365.76	661.91	72395	460	530	24

Table A.6. Geometrical and mechanical properties of tested H-shaped sections provided by Heimerl and Fay [4.15].

Specimen		**Alloy**	B_f [mm]	t_f [mm]	H_w [mm]	t_w [mm]	a [mm]	A [mm]	E [MPa]	$f_{0.2}$ [MPa]	f_u [MPa]	n [-]
H1	A	7178 T6	42.16	3.18	48.01	3.15	151.89	418.94	72395	495	565	25
	B	7178 T6	42.16	3.15	47.70	3.15	154.94	415.84	72395	495	565	25
	C	7178 T6	42.16	3.10	47.85	3.15	153.16	412.04	72395	495	565	25
H2	A	7178 T6	45.72	3.10	47.60	3.15	176.53	433.27	72395	495	565	25
	B	7178 T6	45.72	3.10	47.85	3.15	177.80	434.07	72395	495	565	25
	C	7178 T6	45.72	3.10	47.60	3.12	177.80	432.06	72395	495	565	25
H3	A	7178 T6	50.29	3.10	47.85	3.12	201.17	461.19	72395	495	565	25
	B	7178 T6	50.29	3.10	47.85	3.15	199.14	462.41	72395	495	565	25
	C	7178 T6	50.29	3.10	47.85	3.12	199.90	461.19	72395	495	565	25
H4	A	7178 T6	54.86	3.10	47.85	3.15	221.49	490.74	72395	495	565	25
	B	7178 T6	54.86	3.10	48.11	3.15	221.49	491.54	72395	495	565	25
	C	7178 T6	54.86	3.12	47.90	3.15	222.25	493.69	72395	495	565	25
H5	A	7178 T6	59.94	3.07	48.06	3.12	256.03	518.60	72395	495	565	25
	B	7178 T6	59.94	3.10	48.36	3.12	256.03	522.60	72395	495	565	25
	C	7178 T6	59.94	3.10	48.36	3.12	255.52	522.60	72395	495	565	25
H6	A	7178 T6	64.01	3.10	47.85	3.15	264.16	547.42	72395	495	565	25
	B	7178 T6	64.01	3.10	47.85	3.12	264.16	546.20	72395	495	565	25
	C	7178 T6	64.01	3.10	48.11	3.15	264.16	548.22	72395	495	565	25
H7	A	7178 T6	69.09	3.12	47.90	3.15	274.32	582.57	72395	495	565	25
	B	7178 T6	69.09	3.10	47.85	3.15	274.32	578.90	72395	495	565	25
	C	7178 T6	69.09	3.07	48.06	3.12	274.57	574.81	72395	495	565	25
H8	A	7178 T6	56.90	3.10	62.84	3.30	271.53	560.12	72395	495	565	25
	B	7178 T6	56.90	3.10	63.09	3.30	271.27	560.95	72395	495	565	25
	C	7178 T6	56.90	3.12	62.89	3.30	268.99	563.17	72395	495	565	25
H9	A	7178 T6	62.99	3.10	63.60	3.12	292.10	589.10	72395	495	565	25
	B	7178 T6	62.99	3.10	63.60	3.12	294.13	589.10	72395	495	565	25
H10	A	7178 T6	68.58	3.10	62.84	3.30	319.53	632.53	72395	495	565	25
	B	7178 T6	69.09	3.07	63.55	3.28	318.52	632.90	72395	495	565	25
	C	7178 T6	69.09	3.07	63.55	3.28	318.77	632.90	72395	495	565	25
H11	A	7178 T6	74.68	3.10	63.35	3.30	336.80	671.99	72395	495	565	25
	B	7178 T6	75.18	3.07	63.30	3.28	337.31	669.54	72395	495	565	25
	C	7178 T6	75.18	3.10	63.60	3.30	339.09	675.97	72395	495	565	25
H12	A	7178 T6	81.28	3.10	63.35	3.30	350.52	712.91	72395	495	565	25
	B	7178 T6	80.77	3.07	63.55	3.30	351.54	706.33	72395	495	565	25
H18	A	7178 T6	99.57	3.07	76.25	3.12	422.91	850.25	72395	495	565	25
	B	7178 T6	99.57	3.10	76.30	3.10	422.40	853.53	72395	495	565	25
	C	7178 T6	99.57	3.10	76.56	3.07	420.62	852.37	72395	495	565	25
H19	A	7178 T6	114.81	3.07	76.25	3.12	451.36	943.92	72395	495	565	25
	B	7178 T6	114.81	3.10	76.30	3.10	450.85	947.98	72395	495	565	25
	C	7178 T6	114.81	3.10	76.30	3.15	450.60	951.85	72395	495	565	25

Table A.7. Geometrical and mechanical properties of tested H-shaped sections provided by Yuan et al [4.16].

Specimen		**Alloy**	B_f [mm]	t_f [mm]	H_w [mm]	t_w [mm]	a [mm^2]	A [mm^2]	E [MPa]	$f_{0.2}$ [MPa]	f_u [MPa]	n [-]
H1	A	6061 T6	149.40	10.89	278.30	7.79	897.90	5421.89	69500	269	293	27
H2	A	6061 T6	199.20	10.87	278.30	7.67	899.40	6465.17	69500	269	293	27
H3	A	6061 T6	159.40	9.90	259.70	6.94	839.80	4958.44	71300	264	295	26

Specimen		Alloy	B_f [mm]	t_f [mm]	H_w [mm]	t_w [mm]	a [mm²]	A [mm²]	E [MPa]	$f_{0.2}$ [MPa]	f_u [MPa]	n [-]
H4	A	6061 T6	111.00	10.06	329.10	7.72	1052.90	4773.97	71650	256	292	26
H5	A	6061 T6	149.90	10.01	330.60	7.95	1049.40	5629.27	71650	256	292	26
H6	A	6061 T6	199.80	10.00	330.60	7.93	1049.80	6617.66	71650	256	292	26
H7	A	6061 T6	147.40	10.21	429.10	8.40	1351.50	6614.35	69100	250	276	24
H8	A	6061 T6	199.70	10.50	428.90	8.64	1348.10	7899.40	69100	250	276	24
H9	A	6063 T5	74.70	6.96	225.80	4.44	719.60	2042.38	65250	149	193	15
H10	A	6063 T5	117.30	6.90	226.00	4.35	720.30	2601.84	65250	149	193	15
H11	A	6063 T5	168.70	7.00	225.20	4.25	720.30	3318.90	65250	149	193	15
H12	A	6063 T5	206.90	6.92	225.20	4.11	719.60	3789.07	65250	149	193	15
H13	A	6063 T5	100.30	5.96	257.20	3.59	809.10	2118.92	64150	169	217	17
H14	A	6063 T5	144.50	5.96	257.30	3.64	808.60	2659.01	64150	169	217	17
H15	A	6063 T5	178.00	5.83	257.20	3.63	809.00	3009.12	64150	169	217	17

A.2. Collection of Numerical Results

A.2.1. Box Sections

Table A.8. Comparison between the theoretical ultimate loads with the experimental results provided by Faella et al [4.12].

Specimen		$N_{u.exp}$ [kN]	$N_{u.EC9}$ [kN]	$N_{u.DTP}$ [kN]	$N_{u.ETM}$ [kN]	Specimen		$N_{u.exp}$ [kN]	$N_{u.EC9}$ [kN]	$N_{u.DTP}$ [kN]	$N_{u.ETM}$ [kN]
SHS1	A	30.6	21.44	25.47	25.05	RHS8	B	212	198.11	209.29	197.37
	B	29.7	21.44	25.47	25.05	RHS9	A	222.6	227.86	232.03	212.50
SHS2	A	158.4	131.57	155.94	152.98		B	224.9	227.86	232.03	212.50
	B	160.8	131.57	155.95	152.98	RHS10	A	271.2	279.03	296.30	250.31
SHS3	A	132.4	130.43	139.00	136.29		B	255.6	279.03	296.30	250.31
	B	131.3	130.43	139.00	136.29	RHS11	A	290.8	275.92	312.79	236.38
SHS4	A	186.6	159.29	174.22	171.79		B	261.2	250.83	312.79	236.38
	B	180.9	159.29	174.22	171.79	RHS12	A	313.2	250.83	336.21	260.00
SHS5	A	213.8	191.34	208.81	203.64		B	315.6	284.01	335.99	265.00
	B	208.7	191.34	208.81	203.64	RHS13	A	248.1	243.08	248.44	248.00
SHS6	A	264.4	251.49	265.75	259.65		B	248.2	243.08	248.44	228.33
	B	263.8	251.49	265.75	259.65	RHS14	A	85.1	85.90	89.02	80.50
SHS7	A	300.2	316.13	320.23	305.19		B	79.1	85.90	89.02	80.50
	B	304.8	316.13	320.25	305.19		C	79.7	85.90	89.02	80.50
SHS8	A	82.7	83.20	86.49	80.53	RHS15	A	185.7	166.53	176.42	168.19
	B	83.3	83.20	86.49	80.53		B	190.7	166.53	176.42	168.19
SHS9	A	84.7	81.03	107.85	92.33		C	185.2	166.53	176.41	168.19
	B	84.6	81.03	107.85	92.33	RHS16	A	92.5	90.14	99.49	83.03
SHS10	A	728.5	664.13	706.27	686.75		B	92.8	90.14	99.49	83.03

Specimen		$N_{u.exp}$ [kN]	$N_{u.EC9}$ [kN]	$N_{u.DTP}$ [kN]	$N_{u.ETM}$ [kN]	Specimen		$N_{u.exp}$ [kN]	$N_{u.EC9}$ [kN]	$N_{u.DTP}$ [kN]	$N_{u.ETM}$ [kN]
SHS10	B	731.5	664.13	706.27	686.75	RHS17	A	89.4	81.80	87.67	78.14
SHS11	A	605.5	540.06	577.65	509.27		B	88.6	81.80	87.67	78.14
	B	592.5	540.06	577.55	509.27	RHS18	A	92.7	94.92	116.27	92.35
SHS12	A	626.5	605.82	721.78	626.40		B	89.4	87.00	115.72	92.35
	B	643.5	605.82	721.77	626.40	RHS19	A	137.7	132.00	166.64	143.78
RHS1	A	78.7	62.99	71.77	70.00		B	139.6	132.00	166.78	143.78
	B	77.5	62.99	71.77	70.00	RHS20	A	513.5	529.34	535.33	474.27
RHS2	A	124.3	99.87	111.39	109.26		B	506.5	529.34	535.33	474.27
	B	122.4	99.87	111.36	109.26	RHS21	A	115.3	117.40	124.58	121.58
RHS3	A	134.8	106.32	118.72	116.00		B	116.5	117.40	124.58	121.58
	B	136.8	106.32	118.72	115.50	RHS22	A	493	525.32	571.11	496.62
RHS4	A	109.8	98.12	109.19	104.19		B	497	525.32	571.11	496.62
	B	109.2	98.12	109.22	104.19	RHS23	A	621.5	631.77	708.55	611.11
RHS5	A	108.5	101.89	105.45	103.46		B	612	631.77	708.55	611.11
	B	109.1	101.24	104.78	103.46	RHS24	A	2939.4	2743.00	3016.10	2929.40
RHS6	A	122.4	112.58	122.53	115.24		B	2934	2743.00	3016.12	2929.40
	B	122.9	112.58	122.47	115.24	RHS25	A	669	664.00	748.64	714.22
RHS7	A	120.6	113.90	116.88	108.88		B	670.5	672.07	748.64	714.22
	B	118.7	113.90	116.87	108.88	RHS26	A	865	771.97	802.70	780.13
RHS8	A	212	198.11	209.30	197.37		B	852	771.97	802.70	780.13

Table A.9. Comparison between the theoretical ultimate loads with the experimental results reported in the Chapter 3 and provided by Su et al [4.8].

Specimen		$N_{u.exp}$ [kN]	$N_{u.EC9}$ [kN]	$N_{u.DTP}$ [kN]	$N_{u.ETM}$ [kN]	Specimen		$N_{u.exp}$ [kN]	$N_{u.EC9}$ [kN]	$N_{u.DTP}$ [kN]	$N_{u.ETM}$ [kN]
SHS40	A	58.3	50.38	56.82	56.21	H64x64x3	A	164.2	160.68	170.16	148.13
	B	57.53	50.38	56.82	56.09		B	165.4	162.86	173.28	150.54
	C	55.55	50.38	55.00	56.09	H70x55x4.2	A	196.2	183.69	200.46	191.31
SHS60	A	92.26	89.62	94.38	87.65		B	196.9	184.11	200.98	191.74
	B	85.62	89.62	94.38	87.65	H95x50x10.5	A	626.2	587.32	613.59	722.86
SHS80	A	79.5	88.11	85.12	81.21	H120x70x10.5	A	862.5	793.77	840.28	924.23
	B	87.18	88.11	85.12	81.21	H120x120x9	A	981.5	890.83	882.53	987.83
SHS100	A	90.22	78.70	96.12	89.86	N95x50x10.5	A	609.8	459.83	572.61	574.76
	B	80.85	78.70	96.12	89.86	N120x70x10.5	A	736.9	490.38	684.69	583.69
						N120x120x9	A	811.1	717.36	769.20	812.48

Table A.10. Comparison between the theoretical normalised strains with the experimental results provided by Faella et al [4.12].

Specimen		$\bar{\varepsilon}_{u.exp}$ [-]	$\bar{\varepsilon}_{u.DTP}$ [-]	$\bar{\varepsilon}_{u.ETM}$ [-]	***Specimen***		$\bar{\varepsilon}_{u.exp}$ [-]	$\bar{\varepsilon}_{u.DTP}$ [-]	$\bar{\varepsilon}_{u.ETM}$ [-]
SHS1	A	30.04	31.00	21.73	RHS8	B	2.88	3.52	3.10
	B	32.51	30.95	21.73	RHS9	A	1.95	2.49	0.98
SHS2	A	18.36	17.80	12.69		B	1.88	2.49	0.98
	B	21.07	17.81	12.69	RHS10	A	1.60	1.82	1.06
SHS3	A	4.94	4.73	3.12		B	1.35	1.20	1.06
	B	5.07	4.73	3.12	RHS11	A	1.09	1.16	1.14
SHS4	A	11.65	10.92	7.46		B	1.09	1.16	1.14
	B	13.26	10.92	7.46	RHS12	A	1.04	0.96	0.99
SHS5	A	6.88	5.93	3.95		B	0.99	0.96	0.99
	B	7.89	5.93	3.95	RHS13	A	1.95	2.33	1.06
SHS6	A	3.52	4.30	2.77		B	1.88	2.00	1.06
	B	4.13	4.30	2.77	RHS14	A	1.24	1.27	1.05
SHS7	A	1.43	1.99	1.23		B	1.26	1.20	1.05
	B	1.47	1.99	1.23		C	1.15	1.58	1.05
SHS8	A	1.90	2.49	1.60	RHS15	A	4.64	4.50	3.21
	B	1.71	2.49	1.60		B	4.16	4.50	3.21
SHS9	A	0.81	0.70	0.91		C	5.21	4.50	3.21
	B	0.76	0.70	0.91	RHS16	A	1.12	0.92	0.95
SHS10	A	2.91	3.39	2.13		B	1.08	0.92	0.95
	B	3.26	3.39	2.13	RHS17	A	1.24	1.39	1.03
SHS11	A	1.56	1.47	1.17		B	1.28	1.39	1.03
	B	1.29	1.47	1.17	RHS18	A	0.98	0.79	0.95
SHS12	A	1.13	1.19	1.07		B	1.02	0.78	0.95
	B	1.06	1.19	1.07	RHS19	A	0.83	0.85	0.99
RHS1	A	19.41	13.64	11.98		B	0.83	0.85	0.99
	B	19.39	13.64	11.98	RHS20	A	0.89	0.83	0.80
RHS2	A	24.93	21.69	18.76		B	0.93	0.83	0.80
	B	24.54	21.56	18.76	RHS21	A	2.77	2.00	2.79
RHS3	A	15.10	13.21	10.11		B	3.26	3.00	2.79
	B	15.12	13.21	10.14	RHS22	A	0.97	0.81	0.95
RHS4	A	6.70	6.36	4.20		B	0.92	0.81	0.95
	B	6.45	6.39	4.20	RHS23	A	1.00	1.00	0.96

Specimen		$\bar{\varepsilon}_{u.exp}$ [-]	$\bar{\varepsilon}_{u.DTP}$ [-]	$\bar{\varepsilon}_{u.ETM}$ [-]	Specimen		$\bar{\varepsilon}_{u.exp}$ [-]	$\bar{\varepsilon}_{u.DTP}$ [-]	$\bar{\varepsilon}_{u.ETM}$ [-]
RHS5	A	3.75	4.34	2.33	RHS23	B	0.99	0.98	0.96
	B	3.28	4.36	2.33	RHS24	A	2.83	2.83	1.01
RHS6	A	3.83	4.62	3.05		B	2.85	2.70	1.01
	B	4.15	4.59	3.05	RHS25	A	1.37	1.37	1.26
RHS7	A	1.94	1.50	1.13		B	1.39	1.37	1.26
	B	1.63	1.50	1.13	RHS26	A	1.95	1.39	1.13
RHS8	A	2.90	3.52	3.10		B	1.92	1.39	1.13

Table A.11. Comparison between the theoretical normalised strains with the experimental results reported in the Chapter 3 and provided by Su et al [4.8].

Specimen		$\bar{\varepsilon}_{u.exp}$ [-]	$\bar{\varepsilon}_{u.DTP}$ [-]	$\bar{\varepsilon}_{u.ETM}$ [-]	Specimen		$\bar{\varepsilon}_{u.exp}$ [-]	$\bar{\varepsilon}_{u.DTP}$ [-]	$\bar{\varepsilon}_{u.ETM}$ [-]
SHS40	A	2.94	2.96	2.05	H64x64x3	A	2.14	2.18	1.14
	B	2.90	2.92	2.05		B	2.20	2.25	1.15
	C	1.60	1.60	2.05	H70x55x4.2	A	5.67	5.69	2.69
SHS60	A	0.97	0.96	0.93		B	5.70	5.72	2.69
	B	0.99	0.99	0.93	H95x50x10.5	A	2.07	2.05	2.43
SHS80	A	1.38	0.76	0.84	H120x70x10.5	A	2.17	2.14	2.60
	B	0.80	0.81	0.84	H120x120x9	A	1.61	1.50	2.00
SHS100	A	1.08	0.58	0.83	N95x50x10.5	A	8.24	8.16	8.51
	B	1.41	0.75	0.83	N120x70x10.5	A	22.11	22.00	21.70
					N120x120x9	A	2.56	2.50	3.47

A.2.2. H-shaped Sections

Table A.12. Comparison between the theoretical ultimate loads with the experimental results provided by Heimerl and Niles [4.13].

Specimen		$N_{u.exp}$ [kN]	$N_{u.EC9}$ [kN]	$N_{u.DTP}$ [kN]	$N_{u.ETM}$ [kN]	Specimen		$N_{u.exp}$ [kN]	$N_{u.EC9}$ [kN]	$N_{u.DTP}$ [kN]	$N_{u.ETM}$ [kN]
H1	A	3.15	161.91	2.35	2.24	H9	B	2.40	191.49	1.37	1.20
	B	4.21	160.04	2.32	2.21		C	1.60	190.88	1.37	1.16
	C	3.76	160.29	2.35	2.23	H10	A	1.39	202.56	1.21	1.16
H2	A	2.31	171.69	2.02	1.93		B	1.39	202.55	1.21	1.16
	B	1.82	171.70	2.03	1.93		C	1.30	214.96	1.03	1.11
	C	2.31	171.68	2.02	1.93	H11	A	0.95	216.15	0.98	1.11
H3	A	3.03	180.20	1.78	1.69		B	0.97	215.97	0.99	1.07
	B	2.35	181.34	1.79	1.71		C	0.95	215.97	0.99	1.06
	C	2.75	179.05	1.76	1.68	H12	A	0.75	223.20	0.86	1.06
H4	A	2.12	188.08	1.57	1.50		B	0.78	221.70	0.86	1.06
	B	2.53	188.36	1.57	1.49		C	0.76	223.20	0.86	1.02

Specimen		$N_{u.exp}$ [kN]	$N_{u.EC9}$ [kN]	$N_{u.DTP}$ [kN]	$N_{u.ETM}$ [kN]	Specimen		$N_{u.exp}$ [kN]	$N_{u.EC9}$ [kN]	$N_{u.DTP}$ [kN]	$N_{u.ETM}$ [kN]
H4	C	2.38	189.61	1.58	1.51	H13	A	0.59	196.31	0.68	1.02
H5	A	1.43	197.49	1.41	1.14		B	0.61	196.52	0.68	1.02
	B	1.71	196.13	1.40	1.14	H14	A	1.11	200.34	1.04	0.99
H6	A	1.48	204.49	1.29	1.10		B	1.16	199.06	1.03	0.99
	B	1.53	204.78	1.29	1.10		C	1.20	197.96	1.02	0.96
	C	1.48	202.76	1.27	1.07	H15	A	0.93	209.37	0.96	0.96
H7	A	1.01	214.14	1.10	1.07		B	0.94	210.89	0.97	0.96
	B	1.00	214.99	1.11	1.07		C	0.96	210.98	0.97	0.96
	C	1.01	214.39	1.10	1.04	H16	A	0.80	212.55	0.89	0.96
H8	A	2.15	180.60	1.52	1.04		B	0.84	212.59	0.89	0.96
	B	1.99	180.03	1.49	1.22		C	0.84	212.43	0.89	0.96
	C	2.36	179.02	1.48	1.04	H17	A	0.63	199.39	0.72	0.96
H9	A	2.33	191.40	1.36	1.20		B	0.63	198.61	0.72	0.96

Table A.13. Comparison between the theoretical ultimate loads with the experimental results provided by Heimerl and Roy [4.14].

Specimen		$N_{u.exp}$ [kN]	$N_{u.EC9}$ [kN]	$N_{u.DTP}$ [kN]	$N_{u.ETM}$ [kN]	Specimen		$N_{u.exp}$ [kN]	$N_{u.EC9}$ [kN]	$N_{u.DTP}$ [kN]	$N_{u.ETM}$ [kN]
H1	A	213.93	172.24	195.96	186.63	H11	A	241.02	188.21	243.39	211.16
	B	204.81	171.26	193.36	184.15		B	239.46	188.21	243.39	211.16
	C	210.24	171.20	195.04	185.76		C	242.57	188.21	243.39	211.16
H2	A	226.43	175.66	205.80	196.00	H12	A	234.03	180.34	233.20	202.04
	B	225.70	176.02	206.11	196.29		B	231.73	178.01	229.83	199.50
	C	235.15	178.80	215.06	204.82		C	230.94	179.75	232.25	201.47
H3	B	237.48	179.11	216.12	205.83	H13	A	234.90	189.86	244.23	217.95
H4	A	225.01	171.31	208.62	198.68		B	235.10	188.76	242.94	217.17
	B	228.61	171.31	208.62	198.68		C	235.88	188.76	242.95	217.17
	C	222.91	171.31	208.62	198.68	H14	A	221.42	190.38	241.94	221.15
H5	A	241.22	180.29	220.29	209.80		B	221.89	190.42	241.45	221.21
	B	239.63	180.29	220.30	209.81		C	220.73	190.28	241.82	220.86
	C	242.80	180.29	220.28	209.79	H15	A	217.06	191.30	236.10	223.48
H6	A	236.37	173.50	216.54	206.23		B	219.81	191.20	236.10	223.20
	B	238.44	175.34	219.05	208.62		C	216.79	191.20	236.08	223.20
	C	235.42	173.50	216.54	206.23	H16	A	196.18	193.08	216.03	228.23
H7	A	248.81	183.49	231.71	201.63		B	196.19	192.98	217.08	227.96
	B	250.07	183.70	232.46	202.11		C	195.26	192.98	217.15	227.96
	C	252.73	183.91	233.19	202.58	H18	A	246.99	192.71	243.35	218.02
H8	A	244.97	183.13	231.79	202.11		B	255.80	194.25	243.70	222.49
	B	247.98	183.70	232.73	201.34	H19	A	228.20	192.89	241.58	221.15
H9	A	239.90	175.32	223.11	192.93		B	233.98	194.03	243.85	222.38
	B	233.47	175.32	223.11	192.93		C	239.05	190.86	239.34	218.32
	C	231.78	175.32	223.11	192.93	H20	A	199.20	191.41	227.97	223.58
H10	A	253.03	185.27	237.59	205.74		B	213.10	193.08	230.96	225.45
							C	211.03	193.21	230.09	225.87

Table A.14. Comparison between the theoretical ultimate loads with the experimental results provided by Heimerl and Fay [4.15].

Specimen		$N_{u.exp}$ [kN]	$N_{u.EC9}$ [kN]	$N_{u.DTP}$ [kN]	$N_{u.ETM}$ [kN]	**Specimen**		$N_{u.exp}$ [kN]	$N_{u.EC9}$ [kN]	$N_{u.DTP}$ [kN]	$N_{u.ETM}$ [kN]
H1	A	211.25	185.59	213.90	195.32	H7	C	227.93	191.40	244.62	217.47
	B	207.78	183.68	212.16	193.45	H8	A	244.45	206.38	262.55	231.80
	C	204.33	181.07	209.86	190.72		B	247.07	206.51	262.76	232.14
H2	A	213.67	183.29	217.93	195.15		C	250.25	208.06	264.47	233.67
	B	212.08	183.69	218.27	195.48	H9	A	236.48	200.57	258.13	231.97
	C	210.57	182.65	217.15	194.51		B	237.66	200.57	258.04	231.97
H3	A	220.25	185.79	227.34	200.28	H10	A	235.48	210.19	265.55	200.78
	B	220.17	186.43	228.13	200.91		B	234.90	207.72	260.15	199.52
	C	220.86	185.79	227.33	200.28		C	235.32	207.72	260.14	199.52
H4	A	227.10	188.65	236.46	205.69	H11	A	218.76	211.91	250.95	204.60
	B	227.81	189.05	236.78	206.02		B	214.92	209.00	243.60	202.38
	C	230.08	190.37	238.32	207.55		C	218.75	212.15	249.35	205.14
H5	A	230.70	188.67	240.78	208.11	H12	A	201.95	213.23	231.25	207.69
	B	233.86	190.82	243.19	210.38		B	198.66	211.40	228.75	205.89
	C	229.35	190.82	243.19	210.38	H18	A	152.41	210.18	176.33	194.56
H6	A	235.49	192.04	247.08	213.71		B	155.89	210.83	178.06	193.97
	B	236.47	191.39	246.12	213.09		C	158.00	209.62	176.91	192.53
	C	233.66	192.43	247.36	214.03	H19	A	137.72	211.69	152.39	197.76
H7	A	233.64	195.33	251.32	219.59		B	144.72	212.37	153.45	201.37
	B	229.86	193.48	248.44	215.06		C	142.06	214.93	156.12	195.47

Table A.15. Comparison between the theoretical ultimate loads with the experimental results provided by Yuan et al [4.16].

Specimen		$N_{u.exp}$ [kN]	$N_{u.EC9}$ [kN]	$N_{u.DTP}$ [kN]	$N_{u.ETM}$ [kN]	**Specimen**		$N_{u.exp}$ [kN]	$N_{u.EC9}$ [kN]	$N_{u.DTP}$ [kN]	$N_{u.ETM}$ [kN]
H1	A	1353.00	1246.15	1323.66	1237.92	H9	A	254.10	254.71	243.86	227.10
H2	A	1569.50	1338.97	1560.49	1434.29	H10	A	340.20	332.81	310.04	307.18
H3	A	1139.60	1059.20	1171.13	1098.97	H11	A	446.80	377.41	392.22	378.41
H4	A	1057.80	978.58	901.32	899.80	H12	A	520.60	383.80	433.17	401.37
H5	A	1271.00	1141.88	1112.96	1085.68	H13	A	295.10	269.14	212.33	226.93
H6	A	1442.00	1220.58	1286.30	1290.41	H14	A	315.60	302.78	271.05	293.16
H7	A	1135.70	1204.20	929.62	1069.41	H15	A	332.00	306.36	303.54	314.66
H8	A	1365.10	1362.86	1127.52	1305.92						

Table A.16. Comparison between the theoretical normalised strains with the experimental results provided by Heimerl and Niles [4.13].

Specimen		$\bar{\varepsilon}_{u.exp}$ [-]	$\bar{\varepsilon}_{u.DTP}$ [-]	$\bar{\varepsilon}_{u.ETM}$ [-]	**Specimen**		$\bar{\varepsilon}_{u.exp}$ [-]	$\bar{\varepsilon}_{u.DTP}$ [-]	$\bar{\varepsilon}_{u.ETM}$ [-]
H1	A	3.15	2.35	2.24	H9	B	2.40	1.37	1.20
	B	4.21	2.32	2.21		C	1.60	1.37	1.16
	C	3.76	2.35	2.23	H10	A	1.39	1.21	1.16
H2	A	2.31	2.02	1.93		B	1.39	1.21	1.16
	B	1.82	2.03	1.93		C	1.30	1.03	1.11
	C	2.31	2.02	1.93	H11	A	0.95	0.98	1.11
H3	A	3.03	1.78	1.69		B	0.97	0.99	1.07
	B	2.35	1.79	1.71		C	0.95	0.99	1.06
	C	2.75	1.76	1.68	H12	A	0.75	0.86	1.06
H4	A	2.12	1.57	1.50		B	0.78	0.86	1.06
	B	2.53	1.57	1.49		C	0.76	0.86	1.02
	C	2.38	1.58	1.51	H13	A	0.59	0.68	1.02
H5	A	1.43	1.41	1.14		B	0.61	0.68	1.02
	B	1.71	1.40	1.14	H14	A	1.11	1.04	0.99
H6	A	1.48	1.29	1.10		B	1.16	1.03	0.99
	B	1.53	1.29	1.10		C	1.20	1.02	0.96
	C	1.48	1.27	1.07	H15	A	0.93	0.96	0.96
H7	A	1.01	1.10	1.07		B	0.94	0.97	0.96
	B	1.00	1.11	1.07		C	0.96	0.97	0.96
	C	1.01	1.10	1.04	H16	A	0.80	0.89	0.96
H8	A	2.15	1.52	1.04		B	0.84	0.89	0.96
	B	1.99	1.49	1.22		C	0.84	0.89	0.96
	C	2.36	1.48	1.04	H17	A	0.63	0.72	0.96
H9	A	2.33	1.36	1.20		B	0.63	0.72	0.96

Table A.17. Comparison between the theoretical normalised strains with the experimental results provided by Heimerl and Roy [4.14].

Specimen		$\bar{\varepsilon}_{u.exp}$ [-]	$\bar{\varepsilon}_{u.DTP}$ [-]	$\bar{\varepsilon}_{u.ETM}$ [-]	**Specimen**		$\bar{\varepsilon}_{u.exp}$ [-]	$\bar{\varepsilon}_{u.DTP}$ [-]	$\bar{\varepsilon}_{u.ETM}$ [-]
H1	A	4.28	4.20	4.00	H11	A	0.92	0.94	1.02
	B	4.29	4.20	4.00		B	0.91	0.94	1.02
	C	5.57	4.82	4.59		C	0.93	0.94	1.02
H2	A	6.67	5.50	5.24	H12	A	0.92	0.91	1.02
	B	6.03	4.30	4.09		B	0.92	0.91	1.02
	C	4.39	3.79	3.61		C	0.90	0.91	1.02
H3	B	4.63	3.73	3.56	H13	A	0.87	0.92	1.08
H4	A	3.04	3.59	3.42		B	0.88	0.92	1.06
	B	3.96	3.59	3.42		C	0.88	0.92	1.06
	C	2.63	2.11	2.01	H14	A	0.77	0.85	1.06
H5	A	3.74	2.08	1.98		B	0.77	0.84	1.06
	B	3.35	2.08	1.98		C	0.77	0.85	1.06
	C	4.20	2.08	1.98	H15	A	0.73	0.80	1.05
H6	A	2.57	1.86	1.77		B	0.74	0.80	1.04
	B	2.44	1.85	1.76		C	0.73	0.80	1.04

Specimen		$\bar{\varepsilon}_{u.exp}$ [-]	$\bar{\varepsilon}_{u.DTP}$ [-]	$\bar{\varepsilon}_{u.ETM}$ [-]	Specimen		$\bar{\varepsilon}_{u.exp}$ [-]	$\bar{\varepsilon}_{u.DTP}$ [-]	$\bar{\varepsilon}_{u.ETM}$ [-]
H6	C	2.43	1.86	1.77	H16	A	0.61	0.67	1.02
H7	A	1.77	1.76	1.12		B	0.61	0.68	1.02
	B	1.75	1.74	1.12		C	0.61	0.68	1.02
	C	1.83	1.72	1.12	H18	A	0.92	0.90	0.97
H8	A	1.55	1.77	1.12		B	0.91	0.85	0.97
	B	1.61	1.74	1.12	H19	A	0.80	0.85	0.97
H9	A	1.57	1.68	1.12		B	0.82	0.86	0.97
	B	1.28	1.05	1.12		C	0.86	0.86	0.97
	C	1.23	1.05	1.12	H20	A	0.66	0.76	0.96
H10	A	1.29	1.00	1.10		B	0.70	0.76	0.96
						C	0.69	0.76	0.96

Table A.18. Comparison between the theoretical normalised strains with the experimental results provided by Heimerl and Fay [4.15].

Specimen		$\bar{\varepsilon}_{u.exp}$ [-]	$\bar{\varepsilon}_{u.DTP}$ [-]	$\bar{\varepsilon}_{u.ETM}$ [-]	Specimen		$\bar{\varepsilon}_{u.exp}$ [-]	$\bar{\varepsilon}_{u.DTP}$ [-]	$\bar{\varepsilon}_{u.ETM}$ [-]
H1	A	1.48	1.67	1.29	H7	C	0.80	0.87	1.06
	B	1.38	1.65	1.28	H8	A	0.89	1.02	1.18
	C	1.31	1.63	1.28		B	0.91	1.02	1.17
H2	A	1.26	1.45	1.22		C	0.92	1.03	1.18
	B	1.20	1.45	1.22	H9	A	0.81	0.90	1.07
	C	1.18	1.44	1.22		B	0.82	0.90	1.07
H3	A	1.08	1.26	1.17	H10	A	0.75	0.85	0.77
	B	1.07	1.27	1.17		B	0.75	0.83	0.77
	C	1.10	1.26	1.17		C	0.75	0.83	0.77
H4	A	0.99	1.12	1.13	H11	A	0.66	0.75	0.76
	B	0.99	1.12	1.13		B	0.65	0.74	0.76
	C	1.01	1.13	1.13		C	0.65	0.75	0.76
H5	A	0.92	1.00	1.11	H12	A	0.57	0.66	0.75
	B	0.93	1.00	1.11		B	0.57	0.65	0.75
	C	0.90	1.00	1.11	H18	A	0.36	0.42	0.32
H6	A	0.88	0.94	1.08		B	0.37	0.42	0.32
	B	0.88	0.94	1.08		C	0.37	0.42	0.32
	C	0.87	0.94	1.08	H19	A	0.29	0.33	0.32
H7	A	0.81	0.88	1.06		B	0.31	0.33	0.32
	B	0.80	0.88	1.06		C	0.30	0.33	0.32

Table A.19. Comparison between the theoretical normalised strains with the experimental results provided by Yuan et al [4.16].

Specimen		$\bar{\varepsilon}_{u.exp}$ [-]	$\bar{\varepsilon}_{u.DTP}$ [-]	$\bar{\varepsilon}_{u.ETM}$ [-]	Specimen		$\bar{\varepsilon}_{u.exp}$ [-]	$\bar{\varepsilon}_{u.DTP}$ [-]	$\bar{\varepsilon}_{u.ETM}$ [-]
H1	A	1.00	0.95	0.85	H9	A	0.90	0.84	0.88
H2	A	0.94	0.93	0.80	H10	A	1.01	0.84	0.97
H3	A	0.88	0.92	0.82	H11	A	1.11	0.82	0.87
H4	A	0.88	0.74	0.97	H12	A	1.20	0.79	0.82
H5	A	0.90	0.77	0.80	H13	A	0.85	0.59	0.83
H6	A	0.86	0.76	0.78	H14	A	0.70	0.60	0.80
H7	A	0.69	0.56	0.78	H15	A	0.65	0.60	0.78
H8	A	0.69	0.57	0.77					

ANNEX B

B.1. Geometrical and Mechanical Properties of Experimental Tests

In this section, the main experimental properties of the three point bending tests, presented in the technical literature, are reported according to the following geometric schemes:

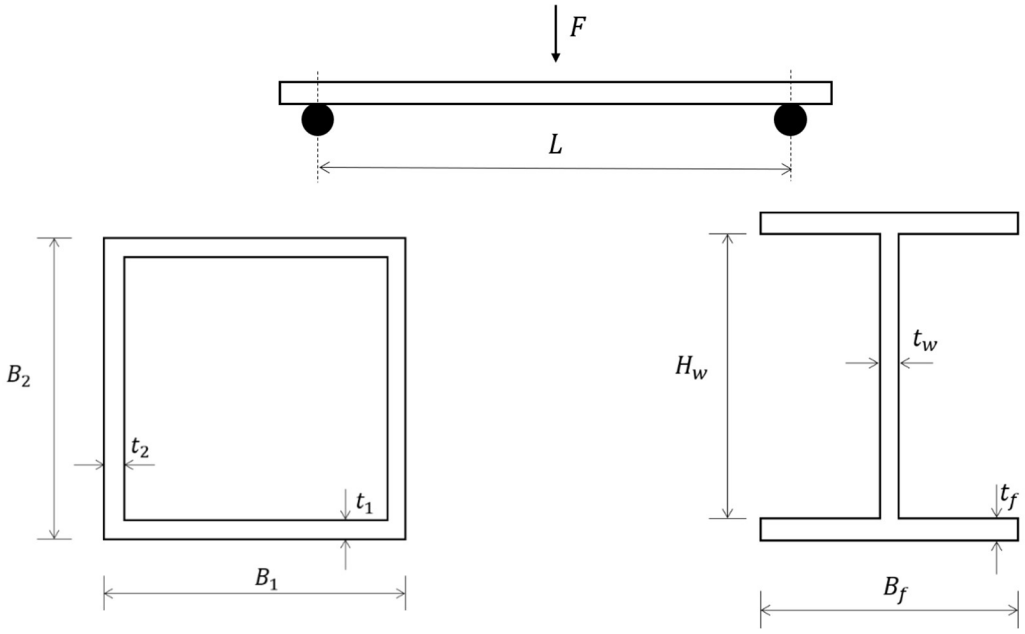

Table B.1. Geometrical and mechanical properties of tested hollow sections provided in Chapter 3.

Specimen	***Alloy***	B_1 [mm]	t_1 [mm]	B_2 [mm]	t_2 [mm]	L [mm]	A [mm^2]	E [MPa]	$f_{0.2}$ [MPa]	f_u [MPa]	n [-]
SHS40_L1	6060 T6	40.11	2.097	40.18	2.038	1300	314.90	71770	176.00	201.36	11.85
SHS40_L2	6060 T6	40.11	2.097	40.18	2.038	800	314.90	71770	176.00	201.36	11.85
SHS40_L3	6061 T6	40.11	2.097	40.18	2.038	500	314.90	71770	176.00	201.36	11.85
SHS60_L1	6060 T6	60.31	2.000	60.40	2.123	1300	480.71	66219	225.07	249.32	13.45
SHS60_L2	6060 T6	60.31	2.000	60.40	2.123	800	480.71	66219	225.07	249.32	13.45
SHS60_L3	6060 T6	60.31	2.000	60.40	2.123	500	480.71	66219	225.07	249.32	13.45
SHS80_L1	6060 T6	80.06	1.950	80.17	1.940	1300	608.16	68539	225.80	252.14	8.49
SHS80_L2	6060 T6	80.06	1.950	80.17	1.940	800	608.16	68539	225.80	252.14	8.49
SHS80_L3	6060 T6	80.06	1.950	80.17	1.940	500	608.16	68539	225.80	252.14	8.49
SHS100_L1	6060 T6	100.30	2.180	100.30	2.200	1300	859.44	69558	168.15	201.80	10.43
SHS100_L2	6060 T6	100.30	2.180	100.30	2.200	800	859.44	69558	168.15	201.80	10.43
SHS100_L3	6060 T6	100.30	2.180	100.30	2.200	500	859.44	69558	168.15	201.80	10.43

Table B.2. Geometrical and mechanical properties of tested hollow sections provided by Moen et al [5.6].

Specimen	***Alloy***	B_1 [mm]	t_1 [mm]	B_2 [mm]	t_2 [mm]	L [mm]	A [mm^2]	E [MPa]	$f_{0.2}$ [MPa]	f_u [MPa]	n [-]
Q1-1m-1	6082 T6	99.60	5.94	100.30	5.89	1000	2224	68886	315.50	323.50	64.0
Q1-1m-2	6082 T6	99.60	5.94	100.30	5.89	1000	2224	68886	315.50	323.50	64.0
Q1-2m-1	6082 T6	99.60	5.94	100.30	5.89	2000	2224	68886	315.50	323.50	64.0
Q1-2m-3	6082 T6	99.60	5.94	100.30	5.89	2000	2224	68886	315.50	323.50	64.0
Q2-1m-1	6082 T4	100.00	5.95	100.00	5.88	1000	2225	66868	176.60	283.40	38.0

Specimen	*Alloy*	B_1 [mm]	t_1 [mm]	B_2 [mm]	t_2 [mm]	L [mm]	A [mm^2]	E [MPa]	$f_{0.2}$ [MPa]	f_u [MPa]	n [-]
Q2-1m-2	6082 T4	100.00	5.95	100.00	5.88	1000	2225	66868	176.60	283.40	38.0
Q2-2m-1	6082 T4	100.00	5.95	100.00	5.88	2000	2225	66868	176.60	283.40	38.0
Q2-2m-2	6082 T4	100.00	5.95	100.00	5.88	2000	2225	66868	176.60	283.40	38.0
Q3-1m-1	6082 T4	100.00	2.89	99.70	2.83	1000	1110	66853	120.10	221.00	26.0
Q3-1m-3	6082 T4	100.00	2.89	99.70	2.83	1000	1110	66853	120.10	221.00	26.0
Q3-2m-1	6082 T4	100.00	2.89	99.70	2.83	2000	1110	66853	120.10	221.00	26.0
Q3-2m-2	6082 T4	100.00	2.89	99.70	2.83	2000	1110	66853	120.10	221.00	26.0
Q4-2m-1	7108-T7	100.10	5.94	100.00	5.98	2000	2243	66880	314.00	333.40	65.0
Q4-2m-2	7108-T7	100.10	5.94	100.00	5.98	2000	2243	66880	314.00	333.40	65.0
R1-1m-1	6082 T6	60.00	2.29	119.40	2.58	1000	867	66577	288.50	302.30	51.0
R1-2m-1	6082 T6	60.00	2.29	119.40	2.58	2000	867	66577	288.50	302.30	51.0
R1-2m-2	6082 T6	60.00	2.29	119.40	2.58	2000	867	66577	288.50	302.30	51.0
R1-3m-1	6082 T6	60.00	2.29	119.40	2.58	3000	867	66577	288.50	302.30	51.0
R1-3m-2	6082 T6	60.00	2.29	119.40	2.58	3000	867	66577	288.50	302.30	51.0
R2-1m-1	6082 T6	60.10	2.94	100.00	2.94	1000	906	66225	281.40	290.40	45.0
R2-1m-2	6082 T6	60.10	2.94	100.00	2.94	1000	906	66225	281.40	290.40	45.0
R2-2m-1	6082 T6	60.10	2.94	100.00	2.94	2000	906	66225	281.40	290.40	45.0
R2-2m-2	6082 T6	60.10	2.94	100.00	2.94	2000	906	66225	281.40	290.40	45.0
R2-3m-1	6082 T6	60.10	2.94	100.00	2.94	3000	906	66225	281.40	290.40	45.0
R2-3m-2	6082 T6	60.10	2.94	100.00	2.94	3000	906	66225	281.40	290.40	45.0

Table B.3. Geometrical and mechanical properties of tested hollow sections provided by Su et al [5.14].

Specimen	*Alloy*	B_1 [mm]	t_1 [mm]	B_2 [mm]	t_2 [mm]	L [mm]	A [mm^2]	E [MPa]	$f_{0.2}$ [MPa]	f_u [MPa]	n [-]
H70x55x4B3	6061 T6	69.80	4.09	55.20	4.09	695	906	67000	207.00	222.00	16.0
H55x70x4B3	6061 T6	54.70	4.09	69.80	4.09	693	956	67000	207.00	222.00	16.0
H95x50x10B3	6061 T6	94.70	10.34	49.60	10.34	695	951	68000	229.00	242.00	11.0
H50x95x10B3	6061 T6	49.50	10.34	94.60	10.34	693	2556	68000	229.00	242.00	11.0
H64x64x3B3	6061 T6	63.90	2.89	63.80	2.89	693	2552	67000	232.00	245.00	10.0
H120x120x9xB3	6061 T6	120.00	8.90	119.90	8.90	691	705	65000	225.00	234.00	13.0
H120x70x10xB3	6061 T6	119.80	10.28	69.80	10.28	691	3953	68000	226.00	238.00	10.0
H70x120x10xB4	6061 T6	69.80	10.26	119.80	10.26	692	3475	68000	226.00	238.00	10.0
H70x55x4B3-R	6061 T6	69.80	4.07	54.80	4.07	694	3470	65000	193.00	207.00	22.0
H50x95x10B3-R	6061 T6	49.50	10.33	94.70	10.33	693	948	68000	229.00	242.00	11.0
H64x64x3B3-R	6061 T6	63.90	2.83	63.90	2.83	696	2552	67000	232.00	245.00	10.0
N120x70x10B3	6063 T5	120.00	10.40	69.90	10.40	689	691	71000	139.00	194.00	9.0
N70x120x10B3	6063 T5	69.90	10.40	119.90	10.40	688	3517	71000	139.00	194.00	9.0
N120x120x9B3	6063 T5	119.90	8.90	119.90	8.90	693	3515	69000	181.00	228.00	9.0

Table B.4. Geometrical and mechanical properties of tested H-shaped sections provided by Moen et al [5.6].

Specimen	*Alloy*	B_f [mm]	t_f [mm]	H_w [mm]	t_w [mm]	L [mm]	A [mm^2]	E [MPa]	$f_{0.2}$ [MPa]	f_u [MPa]	n [-]
I1-2m-1	6061 T6	119.90	7.96	120.20	7.98	2000	2438	66716	312.20	324.20	74
I2-1m-1	6082 T6	70.00	4.94	80.35	4.95	1000	1042	66874	279.40	300.70	62
I2-1m-2	6082 T6	70.00	4.94	80.35	4.95	1000	1042	66874	279.40	300.70	62
I2-1m-3	6082 T6	70.00	4.94	80.35	4.95	1000	1042	66874	279.40	300.70	62
I2-2m-1	6082 T6	70.00	4.94	80.35	4.95	2000	1042	66874	279.40	300.70	62
I2-2m-2	6082 T6	70.00	4.94	80.35	4.95	2000	1042	66874	279.40	300.70	62
I2-2m-3	6082 T6	70.00	4.94	80.35	4.95	2000	1042	66874	279.40	300.70	62
I2-3m-1	6082 T6	70.00	4.94	80.35	4.95	3000	1042	66874	279.40	300.70	62

B.2. Collection of Numerical Results

Table B.5. Comparison between the theoretical ultimate bending moments with the experimental results provided by Moen et al [5.6]

Specimen	$M_{u.exp}$ [kNm]	$M_{u.EC9}$ [kNm]	$M_{u.ER}$ [kNm]	$M_{u.ETM}$ [kNm]	***Specimen***	$M_{u.exp}$ [kNm]	$M_{u.EC9}$ [kNm]	$M_{u.ER}$ [kNm]	$M_{u.ETM}$ [kNm]
Q1-1m-1	27.87	22.42	29.18	25.44	R1-3m-1	7.62	7.53	9.27	7.85
Q1-1m-2	27.87	22.42	29.18	25.44	R1-3m-2	7.54	7.53	9.27	7.85
Q1-2m-1	27.15	22.42	28.20	25.32	R2-1m-1	8.65	7.22	9.19	8.35
Q1-2m-3	27.39	22.42	28.20	25.32	R2-1m-2	8.65	7.22	9.19	8.35
Q2-1m-1	18.43	12.55	17.00	14.78	R2-2m-1	8.58	7.22	8.96	8.33
Q2-1m-2	18.30	12.55	17.00	14.78	R2-2m-2	8.80	7.22	8.96	8.33
Q2-2m-1	17.76	12.55	16.61	14.78	R2-3m-1	9.03	7.22	8.82	8.33
Q2-2m-2	18.30	12.55	16.61	14.78	R2-3m-2	8.95	7.22	8.82	8.33
Q3-1m-1	4.78	4.30	5.33	4.67	I1-2m-1	39.04	32.24	43.07	39.76
Q3-1m-3	4.69	4.30	5.33	4.67	I2-1m-1	10.76	8.03	9.85	9.69
Q3-2m-1	4.64	4.30	5.24	4.65	I2-1m-2	10.40	8.03	9.85	9.69
Q3-2m-2	4.87	4.30	5.24	4.65	I2-1m-3	10.40	8.03	9.85	9.69
Q4-2m-1	28.81	22.39	28.06	25.22	I2-2m-1	10.32	8.03	9.45	9.69
Q4-2m-2	27.85	22.39	28.06	25.22	I2-2m-2	10.40	8.03	9.45	9.69
R1-1m-1	8.10	7.53	9.69	7.90	I2-2m-3	10.58	8.03	9.45	9.69
R1-2m-1	8.10	7.53	9.43	7.86	I2-3m-1	10.05	8.03	9.22	9.69
R1-2m-2	8.10	7.53	9.43	7.86					

Table B.6. Comparison between the theoretical ultimate bending moments with the experimental results reported in Chapter 3 provided by Su et [5.14].

Specimen	$M_{u.exp}$ [kNm]	$M_{u.EC9}$ [kNm]	$M_{u.ER}$ [kNm]	$M_{u.ETM}$ [kNm]	***Specimen***	$M_{u.exp}$ [kNm]	$M_{u.EC9}$ [kNm]	$M_{u.ER}$ [kNm]	$M_{u.ETM}$ [kNm]
H70x55x4.2B3	4.75	4.16	4.88	4.75	N120x70x10.5B3	20.72	14.30	18.69	18.17
H55x70x4.2B3	6.76	4.63	5.89	5.56	N70x120x10.5B3	37.30	18.43	28.00	28.36
H95x50x10.5B3	12.09	12.68	15.95	11.33	N120x120x9.0B3	40.53	30.93	40.14	42.01
H50x95x10.5B3	21.09	17.05	27.67	18.25	SHS40_L1	0.81	0.70	0.84	0.82
H64x64x3.0B3	4.10	3.72	4.14	4.17	SHS40_L2	0.81	0.69	0.84	0.81
H120x120x9.0xB3	44.42	38.47	48.22	41.79	SHS40_L3	0.82	0.69	0.84	0.81
H120x70x10.50xB3	23.59	22.92	28.05	22.41	SHS60_L1	2.18	1.89	2.20	1.95
H70x120x10.50xB4	37.86	29.53	44.74	32.63	SHS60_L2	2.08	1.89	2.23	1.95
H70x55x4.2B3-R	4.82	3.83	4.49	4.75	SHS60_L3	1.91	1.89	2.23	1.93
H64x64x3.0B3-R	10.28	3.65	4.04	11.33	SHS80_L1	2.98	2.79	3.48	2.93
					SHS100_L1	3.65	3.76	4.71	3.32

Table B.7. Comparison between the theoretical normalised rotations with the experimental results provided by Moen et al [5.6].

Specimen	$\overline{\theta}_{u.exp}$ [-]	$\overline{\theta}_{u.ER}$ [-]	$\overline{\theta}_{u.ETM}$ [-]	***Specimen***	$\overline{\theta}_{u.exp}$ [-]	$\overline{\theta}_{u.ER}$ [-]	$\overline{\theta}_{u.ETM}$ [-]
Q1-1m-1	1.80	1.46	1.30	R1-3m-1	1.00	-	1.04
Q1-1m-2	1.82	1.46	1.30	R1-3m-2	1.00	-	1.08
Q1-2m-1	1.49	1.25	1.27	R2-1m-1	1.43	1.44	1.23
Q1-2m-3	1.55	1.25	1.27	R2-1m-2	1.41	1.44	1.23
Q2-1m-1	1.67	1.90	1.46	R2-2m-1	1.35	1.43	1.22
Q2-1m-2	1.67	1.90	1.32	R2-2m-2	1.38	1.43	1.22
Q2-2m-1	1.41	1.87	1.25	R2-3m-1	1.37	1.42	1.23
Q2-2m-2	1.50	1.87	1.25	R2-3m-2	1.35	1.42	1.23
Q3-1m-1	2.29	1.98	2.08	I1-2m-1	1.44	1.02	1.21
Q3-1m-3	1.74	1.65	2.08	I2-1m-1	2.35	1.93	1.85
Q3-2m-1	1.37	1.40	1.04	I2-1m-2	2.37	1.93	1.85
Q3-2m-2	1.62	1.40	1.04	I2-1m-3	2.37	1.93	1.85
Q4-2m-1	1.66	1.46	1.16	I2-2m-1	1.93	1.33	1.61
Q4-2m-2	1.66	1.46	1.16	I2-2m-2	2.00	1.33	1.61
R1-1m-1	1.00	-	1.07	I2-2m-3	1.86	1.33	1.61
R1-2m-1	1.00	-	1.05	I2-3m-1	1.62	1.17	1.61
R1-2m-2	1.00	-	1.09				

Table B.8. Comparison between the theoretical normalised rotations with the experimental results reported in Chapter 3 provided by Su et al [5.14].

Specimen	$\overline{\theta}_{u.exp}$ [-]	$\overline{\theta}_{u.ER}$ [-]	$\overline{\theta}_{u.ETM}$ [-]	***Specimen***	$\overline{\theta}_{u.exp}$ [-]	$\overline{\theta}_{u.ER}$ [-]	$\overline{\theta}_{u.ETM}$ [-]
H70x55x4.2B3	-	2.03	1.27	N120x70x10.5B3	-	4.47	5.18
H55x70x4.2B3	-	2.45	1.29	N70x120x10.5B3	-	5.31	5.43
H95x50x10.5B3	-	2.61	1.12	N120x120x9.0B3	-	2.17	2.29
H50x95x10.5B3	-	2.36	1.19	SHS40_L1	1.44	1.26	1.33
H64x64x3.0B3	-	1.46	1.12	SHS40_L2	1.22	1.30	1.31
H120x70x10.50xB3	-	2.65	1.16	SHS40_L3	1.41	1.37	1.34
H70x120x10.50xB4	-	2.67	1.20	SHS60_L1	1.19	1.07	1.06
H70x55x4.2B3-R	-	1.83	1.27	SHS60_L2	1.18	1.06	1.06
H50x95x10.5B3-R	-	2.40	1.29	SHS60_L3	0.79	-	0.78
H64x64x3.0B3-R	-	1.46	1.12	SHS80_L1	0.56	-	0.55
				SHS100_L1	0.60	-	0.59